Reactivity of metallacycles of palladium: Experimental and computational Studies

by

Daniel M. E. van Niekerk

Dissertation for the degree

of

MASTER OF SCIENCE IN CHEMISTRY

at the

UNIVERSITY OF STELLENBOSCH

Supervisor: Prof. S. F. Mapolie

Co-supervisor: Prof. J. L. M. Dillen

March 2012

Declaration

By submitting this dissertation electronically, I declare that the work contained therein is my own, original work and that I have not previously in its entirety or in part submitted it at any university for a degree.

March 2012

Acknowledgements

I would like to acknowledge and thank the following people for their contributions to my studies:

My supervisor, Prof. Mapolie, for being an excellent study leader and for the support, guidance and motivation throughout this research work.

My co-supervisor, Prof. Dillen, for the guidance and inspiration and for always being available for discussion.

All the students that have been a part of the Organometallic research group over the past two years namely Andrew Swarts, Hennie Kotze, Wallace Manning, Jane Mugo, Rehana Malgas-Enus, Drs Gangadhar Bagihalli and Douglas Onyancha, Corli Joubert, Derik Wilbers and Angelique Viret, for their input towards my research work.

Elsa Malherbe and Dr Vincent Smith for their assistance with NMR spectroscopy and X-ray diffraction analyses respectively.

Conference contributions

Poster Presentations

Reactivity of Palladacycles: Experimental and Computational Studies, D. M. E. Van Niekerk, S. F. Mapolie and J. L. M. Dillen, SACI Convention, WITS University, Johannesburg, South Africa, 2011.

Reactivity of Palladacycles: Experimental and Computational Studies, D. M. E. Van Niekerk, S. F. Mapolie and J. L. M. Dillen, CATSA Conference, Misty Hills Country Hotel & Spa, Muldersdrift, South Africa, 2011.

Oral Presentation

Reactivity of Palladacycles: Experimental and Computational Studies, SACI Student Symposium, Western Cape Section, 2011.

Abstract

Schiff base imine ligands (2-chlorophenyl-2,6-diisopropylphenyl) imine (**L1**), (2-bromophenyl-2,6-diisopropylphenyl) imine (**L2**), (phenyl-2,6-diisopropylphenyl) imine (**L3**), (2-methylphenyl-2,6-diisopropylphenyl) imine (**L4**) and (4-methylphenyl-2,6-diisopropylphenyl) imine (**L5**) were prepared by the Schiff base condensation reaction of 2,6-diisopropylaniline and the respective mono-substituted aromatic aldehydes in a 1:1 molar ratio. The ligands were characterised by FT-IR spectroscopy, ^{1}H- and ^{13}C $\{^{1}$H$\}$-NMR spectroscopy, ESI-MS and microanalysis.

μ-Cl binuclear cyclopalladated complexes **C1 – C5** of the type [PdCl(R-C_6H_3)CH=N-{2,6-(i-Pr)$_2$-C_6H_3}]$_2$ (R = *o*-Cl, *o*-Br, H, *o*-Me and *p*-Me) were prepared by the electrophilic C_{aryl}-H bond activation reaction of the prepared Schiff base imine ligands **L1 – L5** and *bis*(acetonitrile) dichloropalladium(II) in a 1:1 molar ratio in the presence of sodium acetate. The complexes were characterised by FT-IR, ^{1}H- and ^{13}C $\{^{1}$H$\}$-NMR spectroscopy.

Cleavage of the prepared μ-Cl binuclear cyclopalladated complexes **C1 – C5** with two mol equivalents of triphenylphosphine yielded mononuclear, neutral, cyclopalladated complexes **C6 – C10** of the type PdClPPh$_3$(R-C_6H_3)CH=N-{2,6-(i-Pr)$_2$-C_6H_3} (R = *o*-Cl, *o*-Br, H, *o*-Me and *p*-Me), which were characterised by FT-IR spectroscopy, ^{1}H-, ^{13}C $\{^{1}$H$\}$-, and ^{31}P $\{^{1}$H$\}$-NMR spectroscopy, ESI-MS and microanalysis. Single crystal X-ray diffraction analysis of complex **C9** confirms the distorted square planar geometry of the palladium atom and that the chloride ligand that remains bound to the palladium after the cleavage reaction is situated *trans* to the Pd-C bond.

Mononuclear, neutral, non-cyclopalladated complexes **C11 – C15** of the type PdCl(PMe$_3$)$_2$(R-C_6H_3)CH=N-{2,6-(i-Pr)$_2$-C_6H_3} (R = *o*-Cl, *o*-Br, H, *o*-Me and *p*-Me) were prepared by the cleavage of the prepared μ-Cl binuclear cyclopalladated complexes **C1 – C5**

with excess trimethylphosphine. The complexes were characterised by FT-IR spectroscopy, ^{1}H-, ^{13}C {^{1}H}- and ^{31}P {^{1}H}-NMR spectroscopy, ESI-MS and microanalysis. Single crystal X-ray diffraction analysis of complex **C14** confirms that the geometry of the palladium atom is only slightly distorted square planar since it is no longer subject to ring strain imposed on it when a member of a five-membered palladacycle as was the case for complex **C9**. The two trimethylphosphine ligands are situated *trans* to one another, as the chloride is *trans* to the Pd-C bond.

Cationic cyclopalladated complexes **C16 – C20** of the type $[Pd(CH_3CN)PPh_3(R\text{-}C_6H_3)CH{=}N\text{-}\{2,6\text{-}(i\text{-}Pr)_2\text{-}C_6H_3\}]^+[B(Ar)_4]^-$ (R = *o*-Cl, *o*-Br, H, *o*-Me and *p*-Me) were prepared by the abstraction of the chloride ligand of the prepared neutral cyclopalladated complexes **C6 – C10** in the presence of acetonitrile using sodium tetrakis [3,5-*bis*(trifluoromethyl)phenyl] borate in a 1:1 molar ratio. The complexes were characterised by FT-IR spectroscopy, ^{1}H-, ^{13}C {^{1}H}- and ^{31}P {^{1}H}-NMR spectroscopy, ESI-MS and microanalysis. Single crystal X-ray diffraction analysis of complex **C19** confirms the distorted square planar geometry of the palladium atom in a similar manner to that of complex **C9** and that the acetonitrile ligand is situated *trans* to the Pd-C bond.

Cationic cyclopalladated complexes **C21 – C25** of the type $[Pd(C_5H_5N)PPh_3(R\text{-}C_6H_3)CH{=}N\text{-}\{2,6\text{-}(i\text{-}Pr)_2\text{-}C_6H_3\}]^+[B(Ar)_4]^-$ (R = *o*-Cl, *o*-Br, H, *o*-Me and *p*-Me) were prepared by the abstraction of the chloride ligand of the prepared neutral cyclopalladated complexes **C6 – C10** in the presence of pyridine using sodium tetrakis [3,5-*bis*(trifluoromethyl)phenyl] borate in a 1:1 molar ratio. The complexes were characterised by FT-IR spectroscopy, ^{1}H-, ^{13}C {^{1}H}- and ^{31}P {^{1}H}-NMR spectroscopy, ESI-MS and microanalysis. Single crystal X-ray diffraction analysis of complex **C24** confirms the distorted square planar geometry of the palladium atom in a similar manner to that of complexes **C9** and **C19** and that the pyridine ligand is situated *trans* to the Pd-C bond.

Cationic cyclopalladated complexes **C26 – C30** of the type $[Pd(PMe_3)_2(R\text{-}C_6H_3)CH{=}N\text{-}\{2,6\text{-}(i\text{-}Pr)_2\text{-}C_6H_3\}]^+[B(Ar)_4]^-$ (R = *o*-Cl, *o*-Br, H, *o*-Me and *p*-Me) were prepared by the abstraction of the chloride ligand of the prepared neutral non-cyclopalladated complexes **C11 – C15** using sodium tetrakis [3,5-*bis*(trifluoromethyl)phenyl] borate in a 1:1 molar ratio. Cationic non-cyclopalladated complex $[Pd(PMe_3)_3(Cl\text{-}C_6H_3)CH{=}N\text{-}\{2,6\text{-}(i\text{-}Pr)_2\text{-}C_6H_3\}]^+[B(Ar)_4]^-$ (**C31**) was prepared by the abstraction of the chloride ligand of the prepared *ortho*-Cl neutral non-cyclopalladated complex **C11** in the presence of excess trimethylphosphine using sodium tetrakis [3,5-*bis*(trifluoromethyl)phenyl] borate in a 1:1 molar ratio. All the complexes were characterised by FT-IR spectroscopy, ^{1}H-, ^{13}C $\{^1H\}$- and ^{31}P $\{^1H\}$-NMR spectroscopy and ESI-MS. Single crystal X-ray diffraction analysis of complex **C31** confirms the distorted square planar geometry of the palladium atom, which is dissimilar to that of the starting material, complex **C11**, and that the chloride ligand is displaced by trimethylphosphine.

The thermodynamically most stable conformations of the Schiff base imine ligands **L1**, **L3** and **L4** and the μ-Cl binuclear cyclopalladated complexes **C1**, **C3** and **C4** were determined computationally. The calculated $\nu_{C=N}$ absorption bands corresponding to the imine are consistent with the experimentally obtained $\nu_{C=N}$ absorption bands for all compounds. The calculated five-membered chelate product, complex **C4**, which forms via C_{aryl}-H bond activation is thermodynamically more stable than the six-membered chelate product, complex **C4i**, which would form via C_{allyl}-H bond activation.

The thermodynamically most stable conformations of the mononuclear, neutral cyclopalladated complexes **C6**, **C8** and **C9** and the mononuclear, neutral non-cyclopalladated complexes **C11**, **C13** and **C14** were determined computationally. Predictive calculations of cleaved compounds that bear analogous phosphines were also determined. Subsequent bond dissociation energies of the various phosphine ligands were calculated and compared.

Calculations that confirm the energetically favourable formation of non-cyclopalladated complexes bearing two trimethylphosphine ligands and the non-formation of non-cyclopalladated complexes bearing two triphenylphosphine ligands were performed. Predictive calculations indicate that triphenylphosphine is not basic enough to displace the imine nitrogen to generate non-cyclopalladated complexes. The calculated structural parameters of complexes **C9**, **C10**, **C11** and **C14** were compared to the crystallographically determined parameters. The calculated $\nu_{C=N}$ absorption bands corresponding to the imine are consistent with the experimentally obtained $\nu_{C=N}$ absorption bands for all compounds.

The thermodynamically most stable conformations of the cationic complexes of acetonitrile **C16**, **C18** and **C19** and the cationic complexes of pyridine **C21**, **C23** and **C24** were determined computationally. Predictive calculations of cationic compounds that bear analogous phosphines were also done. Subsequent bond dissociation energies of the various phosphine ligands and donor ligands were calculated and compared. The calculated structural parameters of complexes **C19** and **C24** were compared to the crystallographically determined parameters. The calculated $\nu_{C=N}$ absorption bands corresponding to the imine are consistent with the experimentally obtained $\nu_{C=N}$ absorption bands for all compounds.

Opsomming

Schiff-basis imien ligande (2-chloorfeniel-2,6-diisopropielfeniel) imien (**L1**), (2-broomfeniel-2,6-diisopropielfeniel) imien (**L2**), (feniel-2,6-diisopropielfeniel) imien (**L3**), (2-metielfeniel-2,6-diisopropielfeniel) imien (**L4**) en (4-metielfeniel-2,6-diisopropielfeniel) imien (**L5**) is deur middel van die Schiff-basis kondensasie reaksie van 2,6-diisopropielanilien en verskeie aromatiese aldehiede in ’n 1:1 molêre verhouding berei. Die ligande is volledig met FT-IR spektroskopie, ^{1}H- en ^{13}C {^{1}H}-KMR spektroskopie, ESI-massa spektrometrie en mikroanalise gekarakteriseer.

μ-Cl tweekernige palladasikliese komplekse **C1 – C5** van die tipe [PdCl(R-C_6H_3)CH=N-{2,6-(*i*-Pr)$_2$-C_6H_3}]$_2$ (R = *o*-Cl, *o*-Br, H, *o*-Me and *p*-Me) is deur middel van die elektrofiliese C_{ariel}-H binding aktivering van die Schiff-basis imien ligande **L1 – L5** en *bis*(asetonitriel) dichloorpalladium(II) in ’n 1:1 molêre verhouding in die teenwoordigheid van natriumasetaat berei. Die komplekse is met FT-IR, ^{1}H- en ^{13}C {^{1}H}-KMR spektroskopie gekarakteriseer.

Splitsing van die bereide μ-Cl tweekernige palladasikliese komplekse **C1 – C5** met twee mol trifenielfosfien lewer eenkernige, neutrale, palladasikliese komplekse **C6 – C10** van die tipe PdClPPh$_3$(R-C_6H_3)CH=N-{2,6-(*i*-Pr)$_2$-C_6H_3} (R = *o*-Cl, *o*-Br, H, *o*-Me and *p*-Me) wat daarna met FT-IR spektroskopie, ^{1}H-, ^{13}C {^{1}H}-, en ^{31}P {^{1}H}-KMR spektroskopie, ESI-massa spektrometrie en mikroanalise gekarakteriseer is. Enkelkristal X-straaldiffraksie-analise van kompleks **C9** bevestig die verwronge vierkantvlakkige geometrie van die palladium atoom en dat die chloor ligand wat aan die palladium gebind bly na die splitsing reaksie *trans* teenoor die Pd-C binding is.

Eenkernige, neutrale, nie-palladasikliese komplekse **C11 – C15** van die tipe PdCl(PMe$_3$)$_2$(R-C_6H_3)CH=N-{2,6-(*i*-Pr)$_2$-C_6H_3} (R = *o*-Cl, *o*-Br, H, *o*-Me and *p*-Me) is deur middel van die splitsing van die μ-Cl tweekernige palladasikliese komplekse met oormaat

trimetielfosfien berei. Die komplekse is met FT-IR spektroskopie, ^{1}H-, ^{13}C {^{1}H}-, en ^{31}P {^{1}H}-KMR spektroskopie, ESI-massa spektrometrie en mikroanalise gekarakteriseer. Enkelkristal X-straaldiffraksie-analise van kompleks **C14** bevestig dat die geometrie van die palladium atoom slegs effens verwronge vierkantvlakkig is. Dit is omdat dit nie meer blootgestel is aan die ringspanning wat betrokke is wanneer dit deel van ’n vyf-lid palladasikliese sisteem is nie, soos in die geval van kompleks **C9**. Die twee trimetielfosfien ligande is *trans* teenoor mekaar terwyl die chloor *trans* teenoor die Pd-C binding is.

Kationiese palladasikliese komplekse **C16 – C20** van die tipe [Pd(CH_3CN)PPh_3(R-C_6H_3)CH=N-{2,6-(*i*-Pr)$_2$-C_6H_3}]$^{+}$[B(Ar)$_4$]$^{-}$ (R = *o*-Cl, *o*-Br, H, *o*-Me and *p*-Me) is deur middel van die abstraksie van die chloor ligand van die neutrale palladasikliese komplekse **C6 – C10** in die teenwoordigheid van asetonitriel met natrium [3,5-*bis*(trifluoormetiel)feniel] boraat in ’n 1:1 molêre verhouding berei. Die komplekse is met FT-IR spektroskopie, ^{1}H-, ^{13}C {^{1}H}-, en ^{31}P {^{1}H}-KMR spektroskopie, ESI-massa spektrometrie en mikroanalise gekarakteriseer. Enkelkristal X-straaldiffraksie-analise van kompleks **C19** bevestig die verwronge vierkantvlakkige geometrie van die palladium atoom in ’n soortgelyke wyse as die van kompleks **C9** en dat die asetonitriel ligand *trans* teenoor die Pd-C binding is.

Kationiese palladasikliese komplekse **C21 – C25** van die tipe [Pd(C_5H_5N)PPh_3(R-C_6H_3)CH=N-{2,6-(*i*-Pr)$_2$-C_6H_3}]$^{+}$[B(Ar)$_4$]$^{-}$ (R = *o*-Cl, *o*-Br, H, *o*-Me and *p*-Me) is deur middel van die abstraksie van die chloor ligand van die neutrale palladasikliese komplekse **C6 – C10** in die teenwoordigheid van piridien met natrium [3,5-*bis*(trifluoormetiel)feniel] boraat in ’n 1:1 molêre verhouding berei. Die komplekse is met FT-IR spektroskopie, ^{1}H-, ^{13}C {^{1}H}-, en ^{31}P {^{1}H}-KMR spektroskopie, ESI-massa spektrometrie en mikroanalise gekarakteriseer. Enkelkristal X-straaldiffraksie-analise van kompleks **C24** bevestig die verwronge vierkantvlakkige geometrie van die palladium atoom in ’n soortgelyke wyse as die van komplekse **C9** en **C19** en dat die piridien ligand *trans* teenoor die Pd-C binding is.

Kationiese palladasikliese komplekse **C26 – C30** van die tipe $[Pd(PMe_3)_2(R\text{-}C_6H_3)CH{=}N\text{-}\{2,6\text{-}(i\text{-}Pr)_2\text{-}C_6H_3\}]^+[B(Ar)_4]^-$ (R = *o*-Cl, *o*-Br, H, *o*-Me and *p*-Me) is deur middel van die abstraksie van die chloor ligand van die nie-palladasikliese komplekse **C11 – C15** met natrium [3,5-*bis*(trifluoormetiel)feniel] boraat in 'n 1:1 molêre verhouding berei. Kationiese nie-palladasikliese kompleks $[Pd(PMe_3)_3(Cl\text{-}C_6H_3)CH{=}N\text{-}\{2,6\text{-}(i\text{-}Pr)_2\text{-}C_6H_3\}]^+[B(Ar)_4]^-$ (**C31**) is deur middel van die abstraksie van die chloor ligand van die *orto*-Cl, neutrale, nie-palladasikliese kompleks **C11** in die teenwoordigheid van oormaat trimetielfosfien met natrium [3,5-*bis*(trifluoormetiel)feniel] boraat in 'n 1:1 molêre verhouding berei. Al die komplekse is met FT-IR spektroskopie, ^{1}H-, ^{13}C $\{^1H\}$-, en ^{31}P $\{^1H\}$-KMR spektroskopie en ESI-massa spektrometrie gekarakteriseer. Enkelkristal X-straaldiffraksie-analise van kompleks **C31** bevestig die verwronge vierkantvlakkige geometrie van die palladium atoom, wat verskil van die uitgangstof, kompleks **C11**, en dat die chloor ligand deur die trimetielfosfien vervang is.

Die termodinamies mees stabiele konformasies van die Schiff-basis imien ligande **L1**, **L3** en **L4** en die μ-Cl tweekernige palladasikliese komplekse **C1, C3** en **C4** is bereken. Die berekende $\nu_{C=N}$ absorpsiebande wat korreleer met die imien is konsekwent met die eksperimenteel verkreë absorpsiebande vir alle verbindings. Die berekende vyf-lid chelaat produk, kompleks **C4**, wat deur middel van C_{ariel}-H binding aktivering verkry word, is termodinamies meer stabiel as die berekende ses-lid chelaat produk wat deur middel van C_{alliel}-H binding aktivering verkry sou word.

Die termodinamies mees stabiele konformasies van die eenkernige, neutrale, palladasikliese komplekse **C6**, **C8** en **C9** en die eenkernige, neutrale, nie-palladasikliese komplekse **C11, C13** en **C14** is bereken. Voorspellende berekeninge van die gesplete verbindings met soortgelyke fosfien ligande is ook bepaal. Daaropvolgende bindingsdissosiasie-energieë van die verskeie fosfien ligande is bereken en met mekaar

vergelyk. Bevestiging van die energeties gunstige vorming van nie-palladasikliese komplekse met twee trimetielfosfien ligande en die nie-vorming van nie-palladasikliese komplekse met twee trifenielfosfien ligande is gedoen. Voorspellende berekeninge dui daarop dat trifenielfosfien nie basies genoeg is om die imien stikstof te vervang om vervolgens nie-palladasikliese komplekse te genereer nie. Die berekende strukturele parameters van komplekse **C9**, **C10**, **C11** en **C14** is met die kristallografies bepaalde parameters vergelyk. Die berekende $\nu_{C=N}$ absorpsiebande wat korreleer met die imien is konsekwent met die eksperimenteel verkreë absorpsiebande vir alle verbindings.

Die termodinamies mees stabiele konformasies van die kationiese palladasikliese komplekse van asetonitriel **C16**, **C18** en **C19** en die kationiese palladasikliese komplekse van piridien **C21, C23** en **24** is bereken. Voorspellende berekeninge van kationiese verbindings met soortgelyke fosfien ligande is ook bepaal. Daaropvolgende bindingsdissosiasie-energieë van die verskeie fosfien ligande en donor ligande is bereken en met mekaar vergelyk. Die berekende strukturele parameters van komplekse **C19** en **C24** is met die kristallografies bepaalde parameters vergelyk. Die berekende $\nu_{C=N}$ absorpsiebande wat korreleer met die imien is konsekwent met die eksperimenteel verkreë absorpsiebande vir alle verbindings.

Table of Contents

List of Figures

Chapter 1 - General introduction

Chapter 2 - The synthesis of neutral cyclopalladated and non-cyclopalladated complexes derived from Schiff base imine ligands

Chapter 3 - The synthesis of cationic cyclopalladated complexes derived from neutral cyclopalladated and non-cyclopalladated complexes

List of Schemes

Chapter 1 - General introduction

Chapter 2 - The synthesis of neutral cyclopalladated and non-cyclopalladated complexes derived from Schiff base imine ligands

Chapter 3 - The synthesis of cationic cyclopalladated complexes derived from neutral cyclopalladated and non-cyclopalladated complexes

Chapter 4 - Density functional theory (DFT) studies relating to the reactivity and physical properties of the prepared cyclopalladated complexes

List of Tables

Chapter 2 - The synthesis of neutral cyclopalladated and non-cyclopalladated complexes derived from Schiff base imine ligands

Chapter 3 - The synthesis of cationic cyclopalladated complexes derived from neutral cyclopalladated and non-cyclopalladated complexes

List of Abbreviations

MeCN	Acetonitrile
OAc	Acetate
Å	Angström (10^{-10} m)
Ar	aryl
ATR	Attenuated Total Reflectance
BDE	bond dissociation energy
br.	broad
δ	chemical shift
J	coupling constant
DFT	Density Functional Theory
$CDCl_3$	deuterated chloroform
dba	dibenzylideneacetone
DCM	dichloromethane
d	doublet
dd	doublet of doublets
ESI-MS	Electron Spray Ionisation Mass Spectrometry
EtOH	ethanol
FT-IR	Fourier Transform Infra Red

ν	frequency
Hz	hertz
hr(s)	hour(s)
i-Pr	isopropyl
m/z	mass to charge ratio
MHz	megahertz
Me	methyl
mg	milligram
ml	millilitres
mmol	millimole
m	multiplet
NMR	Nuclear Magnetic Resonance
Ph	C_6H_5
ppm	parts per million
py	pyridine
q	quartet
qq	quartet of quartets
rt	room temperature
sep	septet

SCD	Single Crystal X-Ray Diffraction
s	singlet
THF	Tetrahydrofuran
TGA	Thermogravimetric Analysis
t	triplet

Chapter 1

General introduction

1.1 Metallacycles and cyclometallated complexes of transition metals

A metallacycle is "a carbocyclic system with one or more carbons replaced by a transition metal".[1] The definition implies that these compounds have a transition metal atom incorporated into a ring by two metal-carbon σ-bonds (**Figure 1-1.**), excluding those compounds that contain chelating P^P ligands, N^N ligands, cyclometallated complexes or any other cyclic compounds in which the metal is bound to a heteroatom.

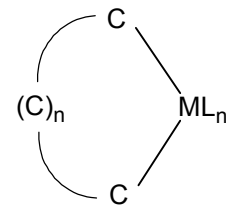

M = Transition metal

L = Ligand(s)

Figure 1-1. General structure of a metallacycle.

It was in 1955 that Tipper[2] prepared the first metallacyclic complex. Hexachloroplatinic acid was treated with cyclopropane in acetic anhydride to isolate a substance with the empirical formula $[Cl_2Pt(C_3H_6)]_n$ (**Scheme 1-1.**). It was initially suggested that the product was a dimeric structure analogous to Zeise's dimer, but was later found to be a chloride-bridged tetramer,[3] in which platinum had inserted into the cyclopropane ring.

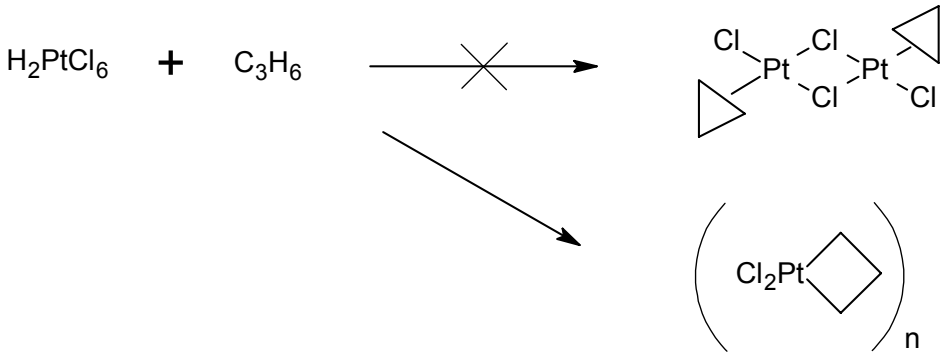

Scheme 1-1. The synthesis of the first metallacyclic complex, polymeric platina(IV)cyclobutane (below) by Tipper[2] and the expected product (above).

Despite the discovery of such metallacyclic compounds in the mid-fifties, it was only after the discovery of their role as potential catalysts that the field became intensively studied. Since this discovery there has been enormous growth in metallacyclic chemistry of transition metals, both as a scientific discipline as well as for their applications in industry, as it was recognised that they were playing an important role in a number of catalytic reactions, including alkene metathesis,[4] isomerisation of strained carbocyclic rings,[5] cycloaddition of alkenes,[6] oligomerisation of dienes[7] and various polymerisation reactions.[8]

Cyclometallated complexes are compounds which contain a metal-carbon bond which is intra-molecularly stabilised by at least one other heteronuclear atom, such as N, P or S, that is directly bound to the metal centre as a two electron donor (**Figure 1-2.**).[9] The two electron donor is typically a Lewis base in such chelate ring systems that generally comprise of between three to seven atoms, with five-membered ring systems being the most prevalent due to their stability and freedom from angular strain.

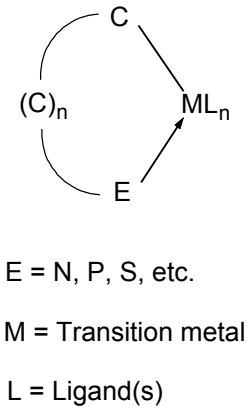

Figure 1-2. General structure of a cyclometallated complex.

The first cyclometallated complexes were prepared by Cope *et al.*[10,11] in the mid 1960's, when aromatic azo compounds were reacted with potassium tetrachloroplatinate(II) or palladium(II) dichloride metal precursors. Dubeck *et al.*[12] had obtained a cyclopentadienyl nickel compound with a similar azobenzene ligand two years earlier, but they incorrectly proposed that the N=N double bond was π-coordinated to the nickel centre, when in fact it was directly bound in a five-membered cyclometallated ring system (**Scheme 1-2.**). The first observation of a metal insertion into a C-H bond was made in the case of a *bis* (dimethylphosphinoethane) complex of ruthenium [Ru(dmpe)$_2$] which yielded the complex [HRu($CH_2PMe(CH_2)_2PMe_2$)(dmpe)].[13]

Cyclometallation reactions under C-H activation have been known and studied for more than thirty years[14-16] and is one of the best developed subjects in organometallic chemistry today. Despite this, it was only after almost two decades that L. Lewis[17] reported the discovery of cycloruthenated compounds that displayed great catalytic activity. From this, an *ortho*-ruthenated phosphite complex was used for olefin hydrogenation[18] and the double alkylation of phenol with ethylene selectively in the *ortho* positions.

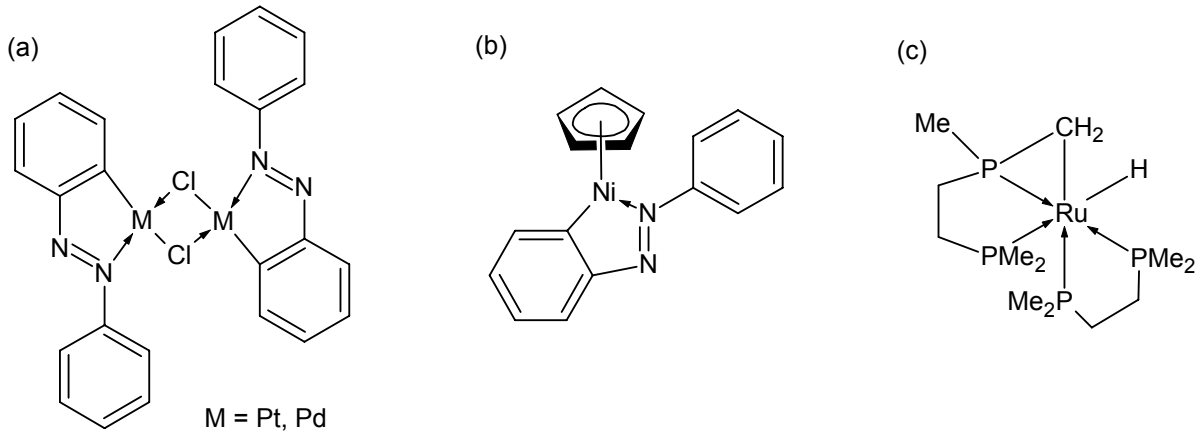

Scheme 1-2. (a) Cyclometallated complexes of Cope *et al.*[10,11] (b) A cyclopentadienyl azobenzene nickel complex of Dubeck *et al.*[12] (c) First reported cycloruthenated complex derived from a C-H insertion of a methyl group of the coordinated ligand.[13]

The field of cyclometallation chemistry is still an area of growing importance today. There has been a remarkable growth in the synthetic and structural aspects of cyclometallation, as well as in their use in organometallic catalysis and new molecular materials.[19,20]

1.2 Palladacycles

Palladacycles have a very rich chemistry and are amongst the most readily available and easily prepared and handled of the plethora of known transition-metal complexes.[19] They are often air and moisture stable, easily prepared through a C-H bond activation process, and once catalytically active (usually above 100°C), they can attain high turnover numbers.[21]

The two main types of cyclopalladated compounds are the bidentate, anionic four-electron donor, and the tridentate, anionic six-electron donor, ligand complexes (**Figure 1-3.**

(a)). Most reported compounds are either one of these two. Bidentate complexes usually exist as halogen- or acetate-bridged dimers that can have either a *transoid* or *cisoid* conformation (**Figure 1-3.** (b)). They can be neutral (monomeric,[22] dimeric,[23] or *bis*-cyclopalladated[24])[22], cationic,[25] or anionic,[26] depending on the nature of the other ligands. The metallated carbon is usually an aromatic sp^2 hybridised carbon and less commonly an sp^3 hybridised carbon (aliphatic or benzylic) or an sp^2 hybridised vinylic carbon.[27] Examples of donor atoms sources are azobenzenes,[23,28] amines,[29,30] imines,[31,32] pyridines,[33,34] thioketones,[35] amides,[36-38] amidines,[39] oxazolines, phosphorous and arsine(III) containing ligands,[40] thioethers,[41] and ethers.

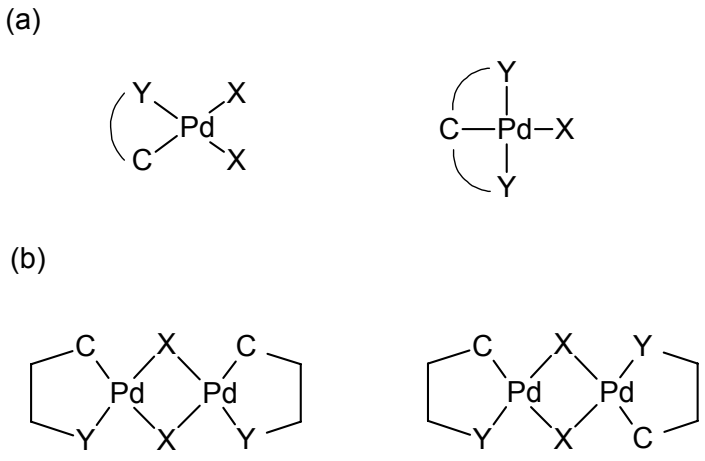

Figure 1-3. (a) Anionic four-electron donor (left) and anionic six-electron donor (right) cyclopalladated compounds. (b) Halogen or acetate *cisoid*- (left) and *transoid*- (right) palladacycle geometric isomers. (Y = N, P, S, etc. and X = Cl, Br, I, OAc, etc.)

There are several different known methods for the generation of palladacycles. A variety of mechanisms are employed with the three major pathways including electrophilic C-H bond activation, oxidative addition and transmetallation. Their synthesis is generally facile and it is possible to modulate both their electronic and steric properties by varying the size of the

palladacyclic ring(s), the nature of the palladated carbon (aromatic, aliphatic, vinylic, etc.), the type of donor group Y (N-, P-, S-, etc.) and it's substituents (alkyl, aryl, etc.), or the nature of the ligand(s), X (halides, polar donor solvents, etc.). Together, these factors will determine whether the complex is dimeric, monomeric, neutral or cationic. This flexibility in synthetic methodology together with the ease of preparation is responsible for the plethora of potential applications of palladacycle complexes.

1.2.1 Electrophilic C-H bond activation

The most simple and direct method for the generation of palladacycles is by a direct chelation assisted palladation of C-H bonds.[41] This can be achieved by using either some palladation agent, eg. tetrachloropalladated salts, with a suitable base,[42] or palladium acetate in acetic acid or benzene. A third method involves a ligand exchange process using another palladacycle, known as transcyclopalladation.[43]

Electrophilic bond activation pathways are generally observed with electron-poor late transition metals. The C_{aryl}-H bond activation mediated by palladium(II), renowned for its electrophilic character, is a classic example of this process. An accelaration of C_{aryl}-H bond activation has been observed upon the insertion of an electron-donating substituent on the aromatic ring, analagous to that of organic electrophilic aromatic substitution reactions.[44] This analogy is reinforced by the fact that many organic aromatic substitution reactions are facilitated in the presence of a transition metal catalyst. The organic model, then, of electrophilic aromatic substitution[45] involves two intermediates, firstly the formation of a π-complex followed by the formation of a σ-complex, which is an arenium intermediate (**Scheme 1-3. B**). Organometallic analogues of the σ-complex have been observed previously in platinum-mediated C-C and C-H bond making and breaking processes in a N^C^N pincer

scaffold.[46] There has been no evidence thus far for the existence of the π-complex as the preceeding intermediate.

The formation of π-complex intermediates is insignificant if the metal precursor contains a directing and templating ligand such as acetate (AcO^-) or carbonate (CO_3^{2-} or $M'CO_3^-$). In the transition state, these anions serve to act as a ligand, a hydrogen bond acceptor and also a proton scavenger during the bond activation process. This process involving agostic interactions does therefore not proceed via a preceeding π-complex intermediate, but is initiated by direct formation of a σ-complex assisted by an exogenous bifunctional ligand (**Scheme 1-3. C**).

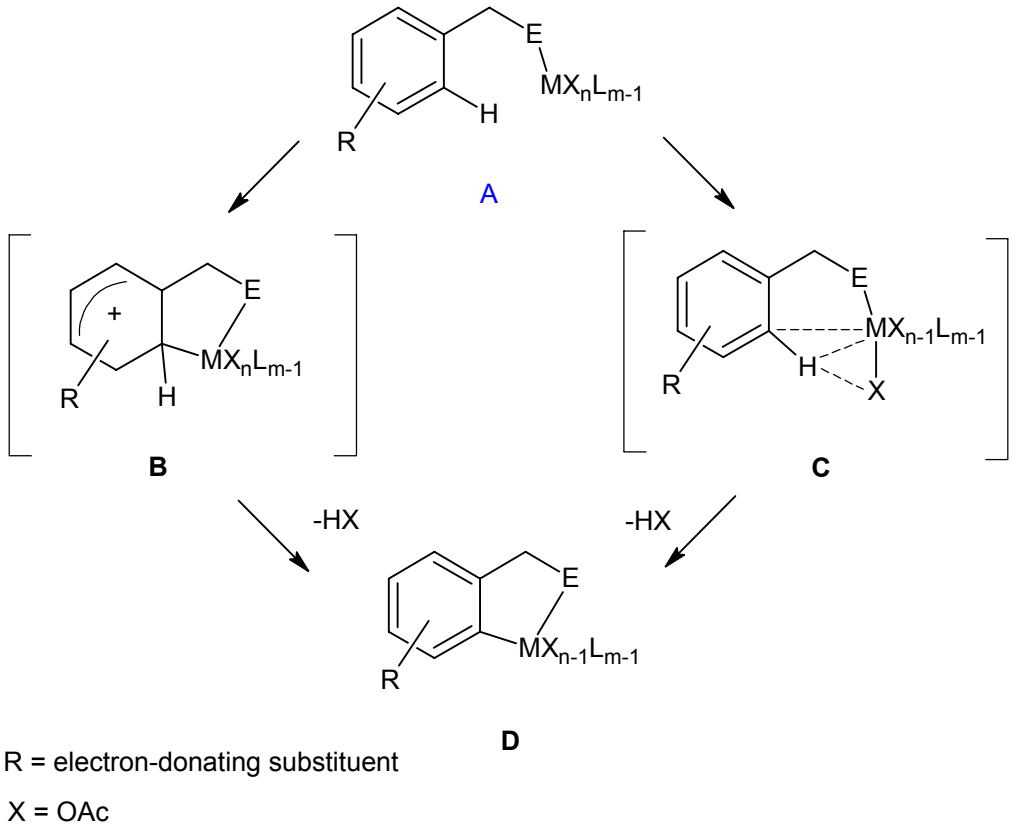

Scheme 1-3. C-H bond activation via formation of an arenium σ-complex **B** in electrophilic aromatic substitution and via agostic interactions, **C**.

Theoretical considerations that predict agostic interactions at the initial stage of the bond activation process have been investigated.[47] As seen in **Scheme 1-3.**, intermediate **C** features a hydrogen-metal interaction and a weak carbon-metal interaction. Stabilisation of the intermediate has been postulated to occur predominantly via AcO···H-C_{aryl} hydrogen bonding. According to calculations, the rate-limiting step of the mechanism is the displacement of one oxygen donor of the κ^2-bound acetate ligand in the metal coordination sphere with the C-H bond. The subsequent steps that complete the reaction, i.e. the C-H bond cleavage followed by metallacycle formation, have been calculated along a virtually barrierless reaction coordinate.

The characteristics that emphasise the differences between these two mechanisms are related to the distinct geometric parameters of the arenium intermediate **B** as compared to the agostic intermediate **C**. In the arenium intermediate the Pd···H distance is expected to be large and the Pd-C-H bond angle is expected to be wide, while in the agostic intermediate the Pd···H contact is short and the C-H bond is elongated due to the hydrogen bonding. The distribution of charge is also different. In the arenium intermediate a partial positive charge extends to all the conjugated carbons, while in the agostic intermediate calculated atomic charges show alterations at only the activated C-H bond.

It is suggested that the straightforward differentiation between pathways involving either intermediate **B** or **C** is possible by correlating the rate-dependence of the cyclometallation with the electron donor ability of the aromatic substituents.[47] According to this speculation, a strong correlation, i.e. a large slope in the Hammett plot, would suggest development via an arenium intermediate, while a weak correlation would suggest development via the agostic activation process.

1.2.2 Oxidative addition

The oxidative addition of aryl halides or alkyl halides (less common) that possess a two-electron donor in close proximity, with an appropriate palladium starting material, is another useful method for the generation of palladacycles. Examples of commonly used palladium starting materials are $Pd(dba)_2$ (dba = dibenzylideneacetone) or $Pd_2(dba)_3$ or $Pd(PPh_3)_4$. Oxidative addition is generally used to generate various palladacycles that cannot be accessed by the direct C-H bond activation methodology, i.e. the synthesis of three- and four-membered ring cyclopalladated compounds (**Scheme 1-4.** (a)).

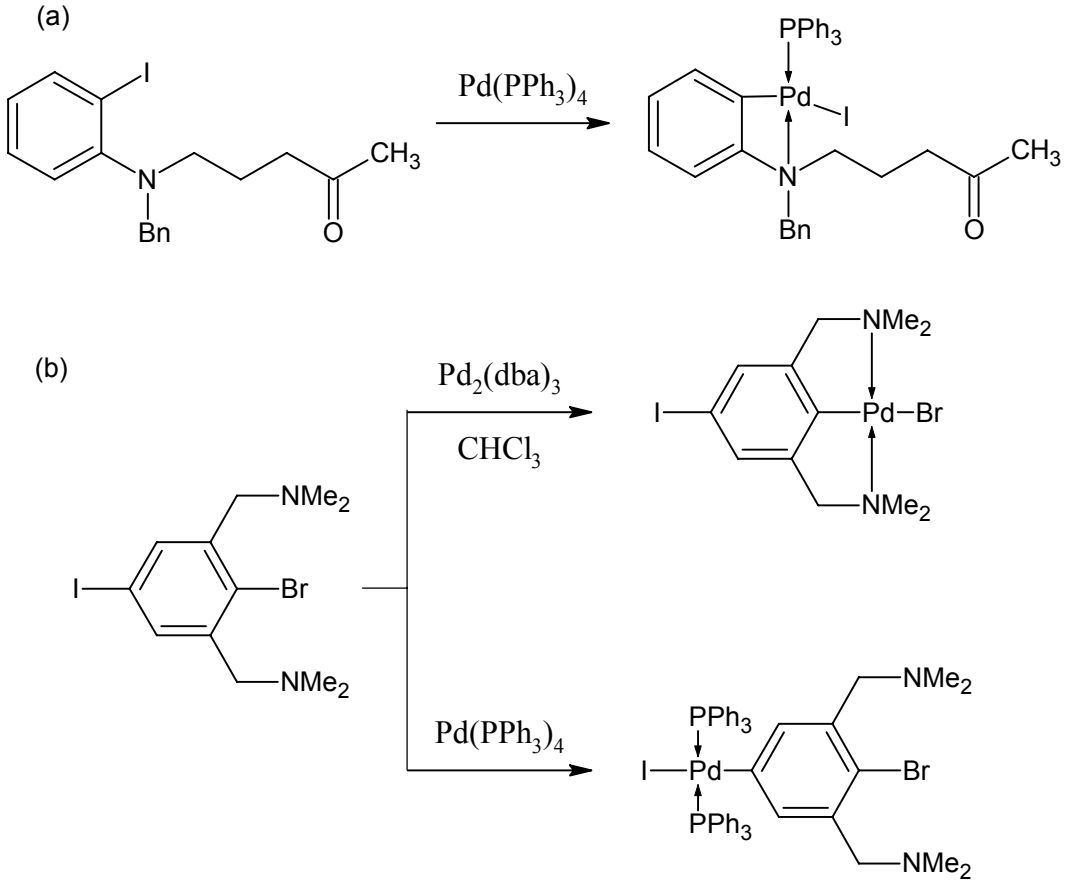

Scheme 1-4. Oxidative addition used to generate (a) an unfavourable four-membered cyclopalladated complex[48] and (b) chemoselective palladation of the bifunctional pincer N^C^N ligand.[49] (Bn = Benzyl group)

Oxidative addition is important for the generation of palladacycles that have reactive functionalities, with the intention that the palladated product can be utilised for further transformations such as for the synthesis of heterobimetallic systems or dendrimers.[49] Van Koten achieved chemoselective palladation on a pincer ligand at C_{aryl}-I or C_{aryl}-Br bonds (**Scheme 1-4.** (b)).[49] One major drawback of the oxidative addition synthetic methodology is the accessibility of the halo starting material, which often requires a multistep procedure to prepare.

1.2.3 Transmetallation reaction

The transmetallation reaction is an important method for the generation of palladacycles and is often used for the preparation of *bis*cyclopalladated complexes. Like oxidative addition it is often used to generate those cyclopalladated complexes that are not accessible by the direct C-H bond activation methodology. Commonly used transmetallating agents are organolithium, which is easily prepared directly by selective lithiation of the ligand or by Li/halogen exchange, or organomercurial reagents.

*Bis*cyclopalladated complexes are easily prepared by a transmetallation reaction of organolithium or organomercurial N- and O- containing ligands with halogen dimer palladacycles (**Scheme 1-5.**).[35,50] Organomercurial reagents are useful for the generation of planar chiral cyclopalladated complexes containing the $Cr(CO)_3$ moiety.[51-53]

In both the transmetallation and oxidative addition synthetic procedures, it is possible that the initial step does not involve the donor group coordination to the metal, and the presence of a substituent in the *ortho* position has been shown to decelerate such an addition through both steric and electronic effects.[54]

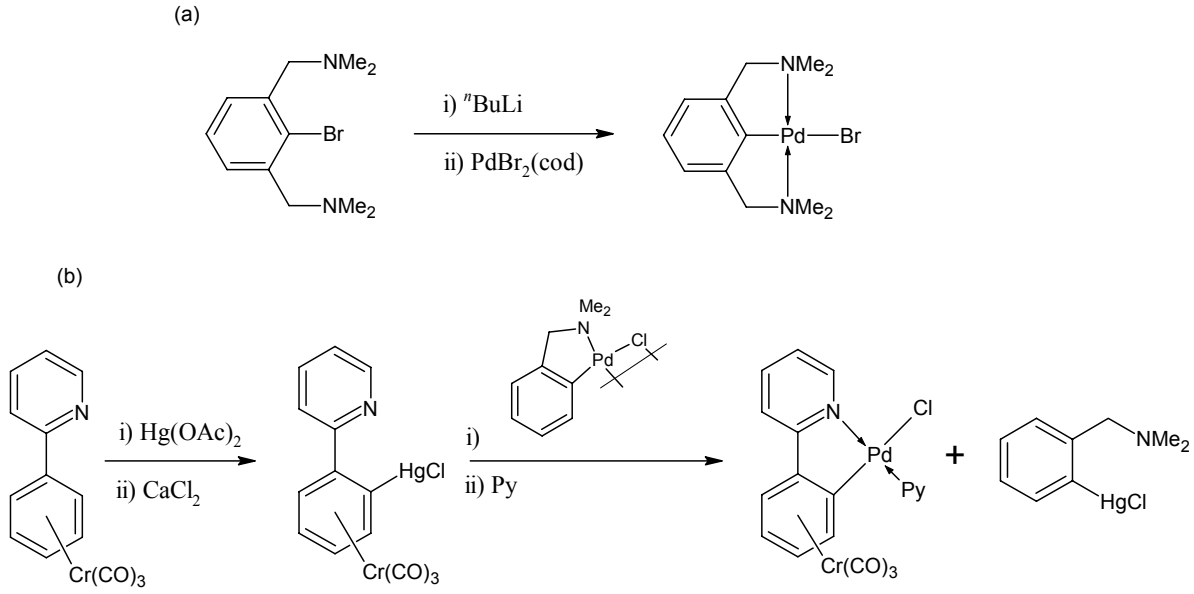

Scheme 1-5. (a) Transmetallation via lithiation of an N^C^N pincer ligand and (b) the synthesis of a chiral planar palladacycle by the transmetallation of the *ortho*-mercurated 2-[tricarbonyl(η^6-phenyl) chromium] pyridine.[53]

1.3 Palladacycles and Cyclopalladated Compounds in Catalysis

It was in the mid 1980's that the first applications of palladacycles as catalyst precursors were reported. After the hydrogenation of C=C double bonds with a cyclopalladated triphenyl phosphite complex[55] followed the use of cyclopalladated azobenzenes, hydrazobenzenes and *N*,*N*-dimethylbenzylamine in the selective reduction of nitro-aromatic compounds, nitro-alkenes, nitriles, alkynes, alkenes and aromatic carbonyl compounds.[56] But it was only after the first report on the synthesis and applications in catalytic C-C coupling reactions using a palladacycle derived from the cyclopalladation of *tris*-*o*-tolylphosphine,[57] known as the Herrmann-Beller palladacycle (**Figure 1-4.**),[58] that renewed interest in these organo-palladium compounds was awakened.

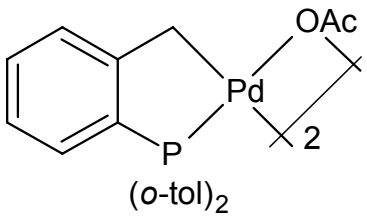

Figure 1-4. Herrmann-Beller palladacycle.[58]

Palladacycles are amongst the most active catalysts in the Heck-type carbon-carbon bond formation as well as other related carbon-heteroatom bond forming reactions.[59] They have recently emerged as showing the highest activity in the Suzuki coupling of electronically challenging aryl chloride substrates. Their ease of synthesis, facile modification and comparative stability all add to enhance their appeal. They serve to supply catalytically active Pd(0) species in the vast majority of reported C-C coupling reactions,[60] particularly the Heck- (**Scheme 1-6.**) and Suzuki-type reactions. The ability of the metal-centre to undergo redox-interchange between the stable Pd(II)/Pd(0) oxidation states makes organopalladium compounds ideal for these catalytic processes.

The Heck (or Mizoroki-Heck) reaction, which involves the catalytic arylation and alkenylation of olefinic substrates to form substituted alkenes, is named after Tsutumo Mizoroki[61] and Richard F. Heck[62]. The formation of the Pd(0) catalytically active species from palladacycles most probably results from an olefin insertion into the Pd-C bond of the palladacycle, followed by β-hydride elimination and reductive elimination (**Scheme 1-6.**).

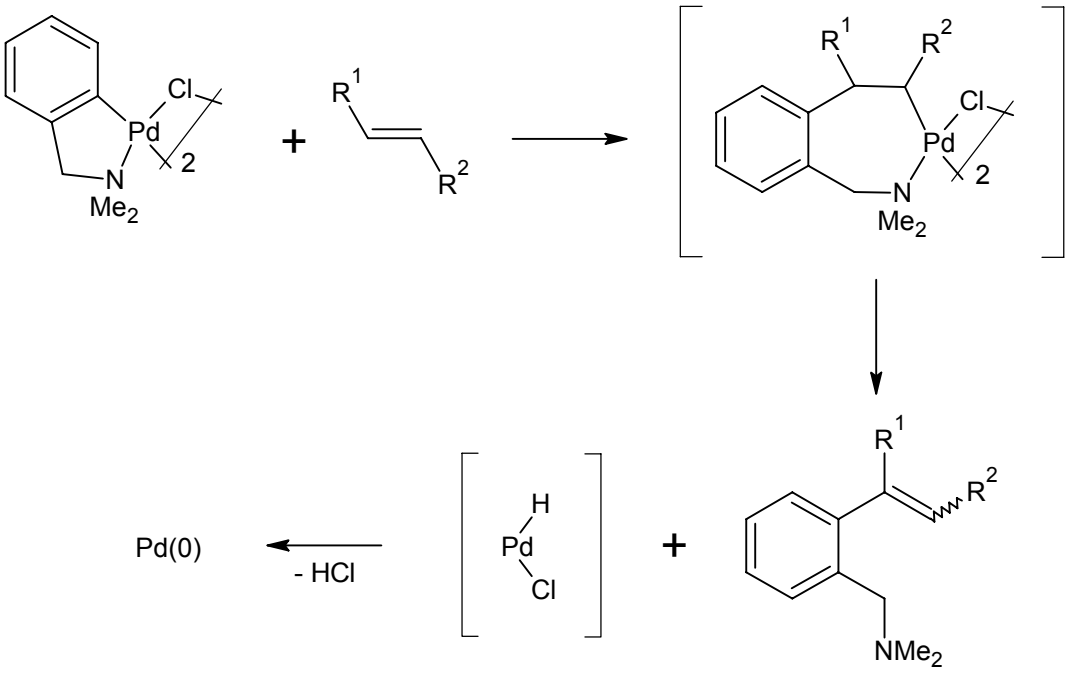

Scheme 1-6. An example of the formation of a catalytically active Pd(0) species in the Heck reaction.

Scientific and industrial applications of the Heck reactions catalysed by the palladacycle **1a**[63] (**Figure 1-5.**) have been reported for the synthesis of the anti-leukaemia alkaloid caphalotoxin.[64] The vinylation of 2-bromo-6-methoxynaphthalene with ethylene to a single product has been applied on the plant scale for Naproxen synthesis (**Scheme 1-7.**).[65]

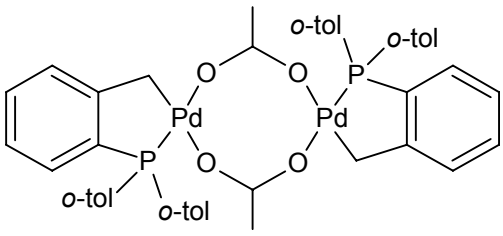

Figure 1-5. *trans*-di(*μ*-acetato)-*bis*[*o*-(di-*o*-tolylphosphino)benzyl]dipalladium(II) (**1a**).[63]

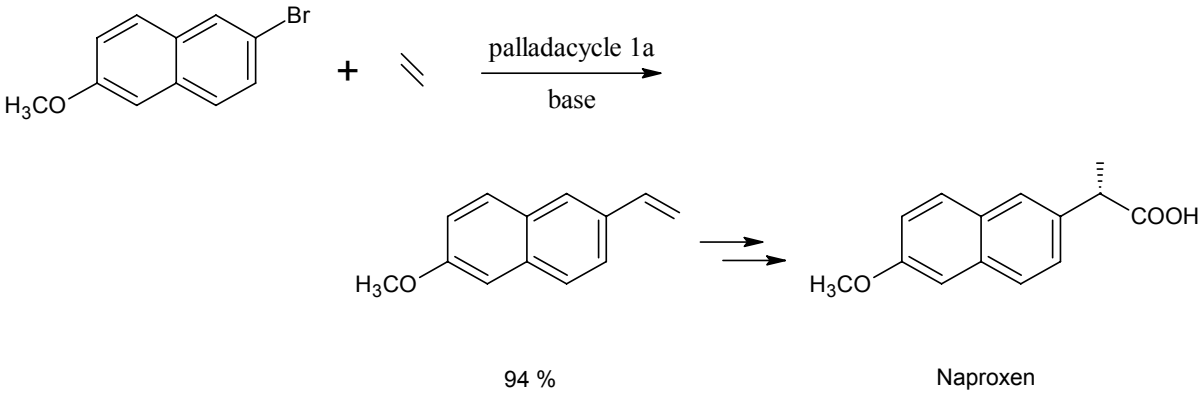

Scheme 1-7. An industrially feasible Heck reaction with palladacycle **1a**.[65]

The Suzuki cross-coupling reaction involves the coupling of an aryl or vinyl boronic acid with an aryl or vinyl halide or triflate in the presence of a base (**Scheme 1-8.**). It is named after Akira Suzuki following a series of articles reporting the development of the method.[66-69]

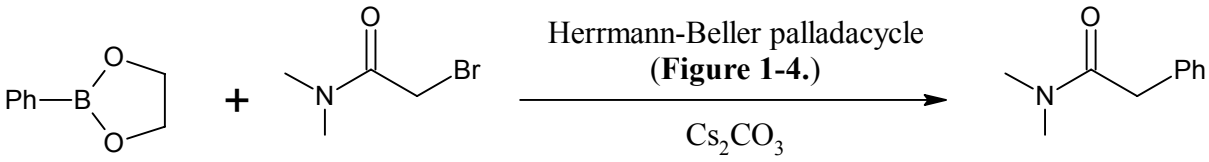

Scheme 1-8. Suzuki cross-coupling reaction employing the Herrmann-Beller palladacycle precursor.

Bedford employed a C-N palladacycle that bears a tricyclohexylphosphine ligand as a catalyst precursor for the Suzuki coupling of aryl chlorides and phenylboronic acid (**Figure 1-6.**).[59] The palladacycle, which was generated *in-situ* due to the extreme lability of the

tricyclohexylphosphine ligand, achieved TON's comparable to the most active previously reported aryl chloride coupling catalysts.

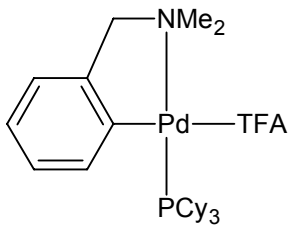

Figure 1-6. C-N palladacycle employed by Bedford in the Suzuki coupling of aryl chlorides and phenylboronic acid.[59]

1.3.1 *α*-olefin oligomerisation and phenyl acetylene polymerisation reactions

Recently our group has applied palladacycles as catalyst precursors in *α*-olefin oligomerisation and phenyl acetylene polymerisation reactions.[70] The initial objective of the catalysis was to synthesise oligomers and/or polymers without using an activating compound as co-catalyst based on similar results where neutral salicylaldimine nickel complexes produced high molecular weight polymers in the absence of an activating compound.[71-73] The proposed mechanism is that a triphenylphosphine ligand dissociates from the metal centre in solution creating a vacant coordination site to which the *α*-olefin first coordinates and then inserts into the Pd-C bond where polymerisation takes place until eventual chain termination, forming the desired products. No oligomerisation or polymerisation took place in the absence of an activator (**Scheme 1-9.**).

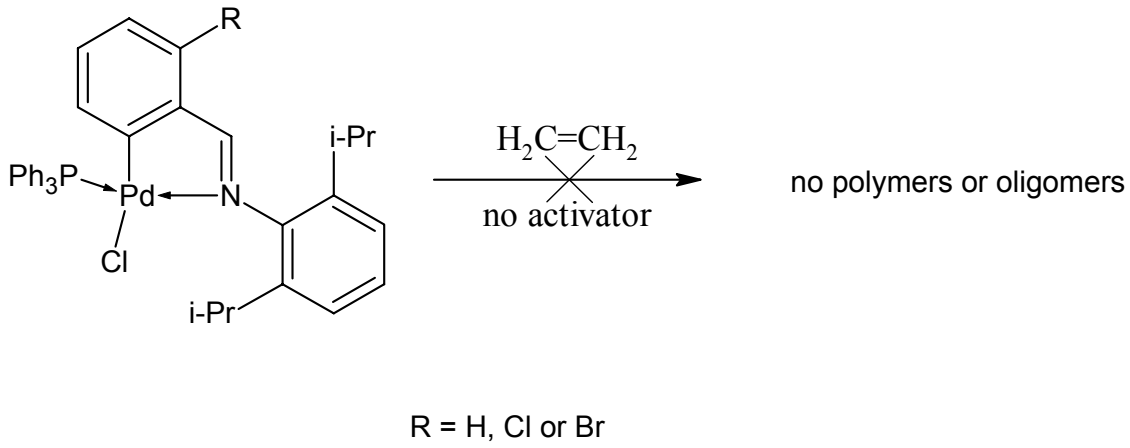

Scheme 1-9. The attempted ethylene oligomerisation reactions in the absence of an activator.

Aluminium containing co-catalysts have been extensively employed in ethylene oligomerisation reactions achieving very high activities. The attempted ethylene oligomerisation reactions (**Scheme 1-9.**) were repeated with the introduction of a suitable aluminium containing co-catalyst.[70] Modified methylaluminoxane (MMAO) was chosen to activate the catalyst precursors resulting in the selective formation of C8, C12, C14 and C16 olefins.

The polymerisation of phenylacetylene using the cyclopalladated, catalyst precursors was performed while varying a number of important factors that impact on the activity and selectivity of the products such as the concentration of the monomer, i.e. the nature of the employed co-catalyst, the reaction temperature and the time dependance.[70] Different silver salts [$Ag(OTf)_2$ and $AgBF_4$] were employed as activators for the neutral catalyst precursors. The use of a suitable co-catalyst or activator is crucial for the performance of a catalytic procedure. It is responsible for creating a vacant coordination site on the precatalyst, forming an *in-situ* active catalyst so that the monomer substrate can coordinate. The drawback with *in-situ* activation is that the nature of the actual active species is not fully known. Therefore

cationic cyclopalladated complexes synthesised from $NaB(Ar)_4$ were investigated as catalyst precursors for the same phenylacetylene polymerisation reactions in order to determine whether or not the cationic complex is the active species (**Figure 1-7.**).

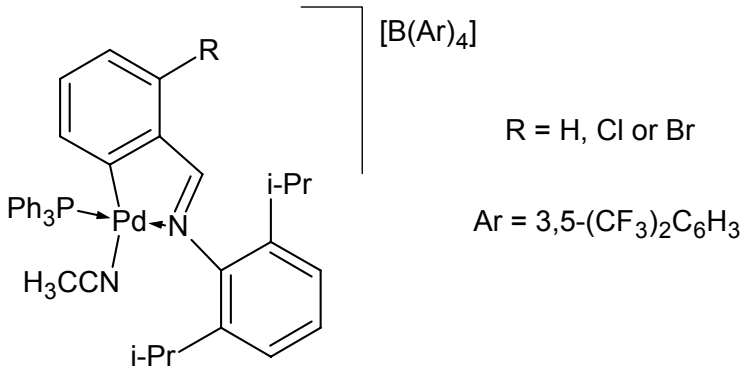

Figure 1-7. Cationic cyclopalladated complexes employed as catalyst precursors in phenylacetylene polymerisation.

The polymerisation with the cationic complexes (**Figure 1-7.**) was performed by reacting the complex with phenylacetylene in dichloromethane and they were observed to be more active than the *in-situ* generated cyclopalladated cationic species using the silver salts as activators.[70]

From the results obtained for the polymerisation of phenylacetylene[70] it is envisaged that the products formed from the alkene oligomerisation proceed via a cationic metallacycle intermediate after activation of the pre-catalyst with aluminium alkyls. Further investigation into the reactivity and physical properties of cyclopalladated cationic species that were employed as well as analagous examples thereof is required. The nature and behaviour of the ligands surrounding the metal centre can be investigated by means of computer modelling.

1.3.2 Pd(II) based catalysts for polymerisation of ethylene and *α*-olefins

The catalytic copolymerisation of polar vinyl monomers (eg. acrylates and methacrylates) is an area of great current interest. For electronic reasons, acrylates have a strong preference for 2,1-insertion into metal-carbon bonds.[74-76] When methacrylate inserts in a 2,1 fashion, the ensuing alkyl bears both an ester functionality and a methyl group on the *α*-carbon, resulting in extreme steric congestion, which strongly disfavours further monomer insertion. The cationic Pd(II) di-imine based system reported by Brookhart and coworkers is among the very few systems that copolymerize acrylates via an insertion mechanism (**Figure 1-8.**).[77,78] The inclusion of bulky 2,6 disubstituted aryl sidegroups hinders the chain transfer/termination steps, resulting in the formation of high molecular weight polymers.

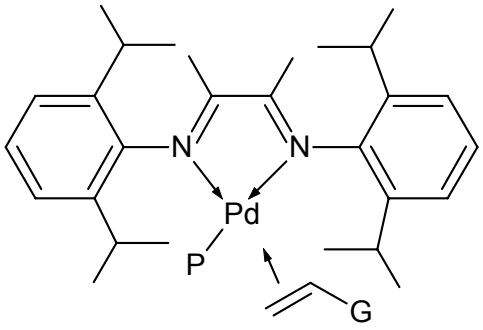

Figure 1-8. The prototype Brookhart Pd di-imine catalyst. P represents the growing polymer and G represents either H or a polar group.

Density functional methods have been applied in studies of transition metal compounds in order to understand and predict their properties and have been used to investigate isomerisation reactions in ethylene/methyl acrylate copolymerization catalyzed by Pd-dimine and Ni-dimine complexes.[79]

1.4 Aim and outline of thesis

The main aim of the research presented in this thesis is to synthesise and characterise representative examples of neutral and cationic metallacycles of palladium together with the investigation of their reactivity with small molecules. Where applicable, the use of density functional theory calculations is employed to gain further insight into the properties relating to the prepared complexes. This combination of experimental and computational studies aims to clarify an understanding into the characteristics of important intermediates in some of the catalytic cycles mediated by palladacycles.

Chapter 1 describes the fundamental aspects of palladacycles and cyclopalladated compounds, including the various methods that are employed for their preparation as well as their numerous catalytic applications. This introduction to the history and development of the field of palladacycle chemistry highlights their suitability to be employed as catalyst precursors, particularly for carbon-carbon coupling reactions but also for polymerisation reactions that have previously been completed in our research group.

The synthesis and characterisation of a range of μ-Cl binuclear cyclopalladated complexes derived from monofunctional Schiff base imine ligands are presented in **Chapter 2**. The subsequent cleavage of the μ-Cl binuclear cyclopalladated complexes with triphenylphosphine or trimethylphosphine to form neutral cyclopalladated and non-cyclopalladated complexes respectively are described in detail.

Chapter 3 details the synthesis and characterisation of cationic cyclopalladated complexes derived from the prepared neutral cyclopalladated and non-cyclopalladated complexes that are discussed in **Chapter 2**. The complexes are prepared by abstraction of the chloride ligand in the absence or in the presence of a weakly coordinating donor ligand which serves to stabilise the cationic compounds.

A comprehensive understanding of the experimental work as described in **Chapter 2** and **Chapter 3** is achieved with computer modelling, which is described in **Chapter 4**. The computational studies provide further insight into the reactivity and physical properties of the prepared cyclopalladated and non-cyclopalladated palladium complexes.

The final chapter in this thesis, **Chapter 5**, summarises the conclusions from the experimental and computational results. Following the conclusions are some suggestions with regards to future research work which would complement and expand on the topics that were studied and presented in this thesis.

References

1. J. P. Collman, L. S. Hegedus, J. R. Norton and R. G. Finke, *Principles and Applications of Organotransition Metal Chemistry*, University Science Books, Mill Valley, 1987.

2. C. F. H. Tipper, *J. Chem. Soc.*, 1955, 2045.

3. S. E. Binns, R. H. Cragg, R. D. Gillard, B. T. Heaton and M. F. Pilbrow, *J. Chem. Soc.* (*A*)., 1969, 1227.

4. (a) R. H. Grubbs and T. K. Brunck, *J. Am. Chem. Soc.*, 1972, **94**, 2538. (b) R. J. Haines and G. J. Leigh, *Chem. Soc. Rev.*, 1974, **4**, 155.

5. (a) T. J. Katz and N. Acton, *Tetrahedron Lett.,* 1967, 2601. (b) K. C. Bishop, *Chem. Rev.,* 1976, **76**, 461.

6. A. R. Fraser, P. H. Bird, S. A. Bezman, J. R. Shapley, R. White and J. A. Osborn, *J. Am. Chem. Soc.,* 1973, **95**, 597.

7. M. A. Bennett, R. N. Johnson and I. B. Tomkins, *J. Am. Chem. Soc.,* 1974, **96**, 61.

8. K. J. Ivin, J. J. Rooney, C. D. Stewart, M. L. H. Green and R. Mahtab, *J. Chem. Soc. Chem. Commun*., 1978, 604.

9. I. Omae, *Chem. Rev*., 1979, **79**, 287.

10. A. C. Cope and R. W. Siekman, *J. Am. Chem. Soc.,* 1965, **87**, 3272.

11. A. C. Cope and E. C. Friedrich, *J. Am. Chem. Soc.,* 1968, **90**, 909.

12. J. P. Kleiman and M. Dubeck, *J. Am. Chem. Soc.,* 1963, **85**, 1544.

13. J. Chatt and J. M. Davidson, *J. Chem. Soc.,* 1965, 843.

14. G. W. Parshall, *Acc*. *Chem*. *Res*., 1970, **3**, 139.

15. J. Dehand and M. Pfeffer, *Coord*. *Chem*. *Rev*., 1976, **18**, 327.

16. M. I. Bruce, *Angew*. *Chem. Int. Ed. Engl.,* 1977, **16**, 73.

17. L. N. Lewis and J. F. Smith, *J. Am. Chem. Soc.,* 1986, **108**, 2728.

18. L. N. Lewis, *J. Am. Chem. Soc.,* 1986, **108**, 743.

19. J. Dupont, C. S. Consorti and J. Spencer, *Chem. Rev*., 2005, **105**, 2527.

20. M. Ghedini, I. Aiello, A. Crispini, A. Golemme, M. La Deda and D. Pucci, *Coord. Chem. Rev*., 2006, **250**, 1373.

21. W. Chen, F. Yao, L. Zhe and G. Quing-Xiang, *Chin. J. Chem.*, 2008, **26**, 358.

22. J. Dehand, M. Pfeffer and M. Zinsius, *Inorg. Chim. Acta,* 1975, **13**, 229.

23. A. C. Cope and E. C. Friedrich, *J. Am. Chem. Soc.,* 1968, **90**, 909.

24. C. Arlen, M. Pfeffer, O. Bars and D. Grandjean, *J. Chem Soc., Dalton Trans.,* 1983, 1535.

25. J. Dehand, J. Jordanov, M. Pfeffer and M. Zinsius, *C. R. Hebd. Seances Acad. Sci., Ser. C,* 1975, **281**, 651.

26. P. Braunstein, J. Dehand and M. Pfeffer, *Inorg. Nucl. Chem. Lett.*, 1974, **10**, 581.

27. J. Dupont, N. R. Basso, M. R. Meneghetti, R. A. Konrath, R. Burrow and M. Horner, *Organometallics,* 1997, **16**, 2386.

28. A. C. Cope and R. W. Siekman, *J. Am. Chem. Soc.,* 1965, **87**, 3272.

29. R. D. O'Sullivan and A. W. Parkins, *J. Chem. Soc., Chem. Commun.,* 1984, 1165.

30. J. Vicente, I. Saurallamas and P. G. Jones, *J. Chem. Soc., Dalton Trans.,* 1993, 3619.

31. R. Vanhelder and G. Verberg, *Recl. Trav. Chim. Pays-Bas,* 1965, **84**, 1263.

32. I. R. Girling and D. A. Widdowson, *Tetrahedron Lett.,* 1982, **23**, 1957.

33. A. Kasahara, *Bull. Chem. Soc. Jpn.,* 1968, **41**, 1272.

34. E. C. Constable, A. M. W. C. Thompson, T. A. Leese, D. G. F. Reese and D. A. Tocher, *Inorg. Chim. Acta,* 1991, **182**, 93.

35. H. Alper, *J. Organomet. Chem.,* 1973, **61**, C62.

36. N. D. Cameron and M. Kilner, *J. Chem. Soc., Chem. Commun.,* 1975, 687.

37. H. Horino and N. Inoue, *J. Org. Chem.,* 1981, **46**, 4416.

38. V. S. Goncharov, V. S. Raida and E. E. Sirotina, *Izv. Sib. Otd. Akad. Nauk SSSR, Ser. Khim. Nauk,* 1986, **3**, 77.

39. J. Dehand, A. Mauro, H. Ossor, M. Pfeffer, R. H. D. Santos and J. R. Lechat, *J. Organomet. Chem.,* 1983, **250**, 537.

40. J. Dupont, N. Beydoun and M. Pfeffer, *J. Chem. Soc., Dalton Trans.,* 1989, 1715.

41. S. Trofimenko, *Inorg. Chem.,* 1973, **12**, 1215.

42. A. B. Goel and M. Pfeffer, *Inorg. Synth.,* 1989, **26**, 211.

43. Q. Yao, E. P. Kinney and C. Zheng, *Org. Lett.,* 2004, **6**, 2997.

44. M. Albrecht, *Chem. Rev*., 2010, **110**, 576.

45. J. March, *Advanced Organic Chemistry*, Wiley-Interscience: New York, 1992.

46. M. Albrecht, A. L. Spek and G. van Koten, *J. Am. Chem. Soc.,* 2001, **123**, 7233.

47. D. L. Davies, S. M. A. Donald and S. A. Macgregor, *J. Am. Chem. Soc.,* 2005, **127**, 13754.

48. D. Solé, L. Vallverdú, X. Solans, M. Font-Bardía and J. Bonjoch, *J. Am. Chem. Soc.,* 2003, **125**, 1587.

49. G. Rodriguez, M. Albrecht, J. Schoenmaker, A. Ford, M. Lutz, A. L. Spek and G. Van Koten, *J. Am. Chem. Soc.,* 2002, **123**, 5127.

50. E. Wehman, G. Vankoten, J. T. B. H. Jastrzebski, H. Ossor and M. Pfeffer, *J. Chem. Soc., Dalton Trans.,* 1988, 2975.

51. A. Berger, A. De Cian, J. P. Djukic, J. Fischer and M. Pfeffer, *Organometallics,* 2001, **20**, 3230.

52. A. Berger, J. P. Djukic, M. Pfeffer, A. De Cian, N. Kyritsakas-Gruber, J. Lacour and L. Vial, *Chem. Commun.,* 2003, 658.

53. A. Berger, J. P. Djukic and M. Pfeffer, *Organometallics,* 2003, **22**, 5243.

54. S. A. Kurzeev, A. S. Vilesov, T. V. Fedorova, E. V. Stepanova, O. V. Koroleva, C. Bukh, M. J. Bjerrum, I. V. Kurnikov and A. D. Ryabov, *Biochemistry,* 2009, **48**, 4519.

55. D. Lafrance, J. L. Davis, R. Dhawan and B. A. Arndtsen, *Organometallics,* 1989, **8**, 1431.

56. J. Albert, J. M. Cadena, J. Granell, X. Solans and M. Font-Bardia, *J. Organomet. Chem.,* 2004, **689**, 4889.

57. M. I. Bruce, B. L. Goodall and F. G. A. Stone, *J. Chem. Soc., Dalton Trans.,* 1978, 687.

58. M. Beller, H. Fischer, W. A. Herrmann, K. Öfele and C. Brossmer, *Angew. Chem. Int. Ed. Engl*., 1995, **34**, 1848.

59. R. B. Bedford, *Chem. Commun.*, 2003, 1787.

60. I. P. Beletskaya and A. V. Cheprakov, *J. Organomet. Chem.,* 2004, **689**, 4055.

61. T. Mizoroki, K. Mori and A. Ozaki, *Bull. Chem. Soc. Jpn.*, 1971, **44**, 581.

62. R. F. Heck and J. P. Nolley, *J. Org. Chem*., 1972, **37**, 2320.

63. W. A. Herrmann, K. Olefe, D. v. Preysing and S. K. Schneider, *J. Organomet. Chem*., 2003, **687**, 229.

64. L. F. Tietze and H. Schirok, *Angew. Chem. Int. Ed. Engl*., 1997, **36**, 1124.

65. M. Beller, A. Tafesh and W. A. Herrmann, German Patent DE 19503/119, 1996.

66. N. Miyaura, T. Yanagi and A. Suzuki, *Synth. Commun*., 1981, **11**, 513.

67. N. Miyaura, K. Yamada, H. Suginome and A. Suzuki, *J. Am. Chem. Soc.*, 1985, **107**, 972.

68. N. Miyaura, T. Ishiyama, M. Ishikawa and A. Suzuki, *Tetrahedron Lett*., 1986, **27**, 6369.

69. N. Miyaura, T. Ishiyama, H. Sasaki, M. Ishikawa, M. Sato and A. Suzuki, *J. Am. Chem. Soc*., 1989, **111**, 314.

70. N. Mungwe, The Synthesis of the Cyclometallated Palladium Complexes and their Applications in Olefin Oligomerisation and in Phenylacetylene Oligomerisation/ Polymerisation, *M.Sc. Thesis*, University of the Western Cape, 2007.

71. C. Wang, S. Friedrich, T. R. Younkin, R. T. Li, R. H. Grubbs, M. W. Day and D. A. Bansleben, *Organometallics*, 1998, **17**, 3149.

72. T. R. Younkin, E. F. Connor, J. L. Henderson, S. K. Friedrich, R. H. Grubbs and D. A. Bansleben, *Science*, 2000, **287**, 460.

73. L. Zhang, M. Brookhart, and P. S. White, *Organometallics*, 2006, **25**, 1868.

74. D. M. Philipp, R. P. Muller, W. A. Goddard, M. McAdon and M. Mullin, *J. Am. Chem. Soc*., 2002, **124**, 10198.

75. A. Michalak and T. Ziegler, *Top. Organomet. Chem*., 2005, **12**, 145.

76. A. Michalak and T. Ziegler, *J. Am. Chem. Soc.,* 2001, **123**, 12266.

77. L. K. Johnson, C. M. Killian and M. Brookhart, *J. Am. Chem. Soc*., 1995, **117**, 6414.

78. S. Mecking, L. K. Johnson, L. Wang and M. Brookhart, *J. Am. Chem. Soc*., 1998, **120**, 888.

79. M. Mitoraj and A. Michalak, *J. Mol. Model*., 2005, **11**, 341.

Chapter 2

The synthesis of neutral cyclopalladated and non-cyclopalladated complexes derived from Schiff base imine ligands

2.1 Introduction

Schiff bases, also named azomethines, as they contain an azomethine group (-HC=N-), refer to a class of compounds that are formed upon the chemical reaction of aldehydes or ketones with primary amines in a condensation process (**Scheme 2-1.**). They are named after Hugo Schiff, a German chemist, who discovered this class of compounds in 1864.[1] The presence of a lone pair of electrons in an sp^2 hybridised orbital of the nitrogen participates in binding with metal ions which is of significant chemical and biological importance.

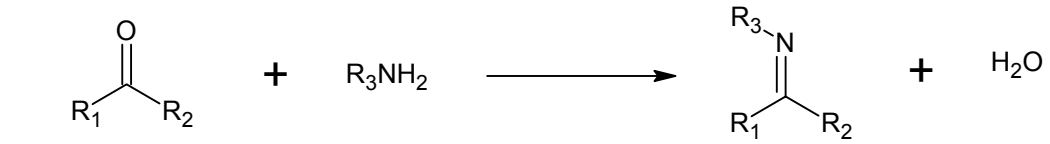

R_1 = aryl, alkyl or H

R_2 = aryl, alkyl or H

R_3 = aryl or alkyl

Scheme 2-1. General procedure of the Schiff base condensation that involves the reaction of an aldehyde or ketone functionality with a primary amine.

The use of Schiff bases in a variety of applications has been the subject of widespread research over the past 25 years. Their ease of synthesis allows for simple and cheap bulk production, which is a crucial factor when applications in industrial processes are required. Depending on their eventual intended application, these ligands can be designed to be either

mono- or multi-functional. The mono-, bi-, tri- and tetra-dentate chelating Schiff base ligands are designed according to their binding environments (**Figure 2-1.**).

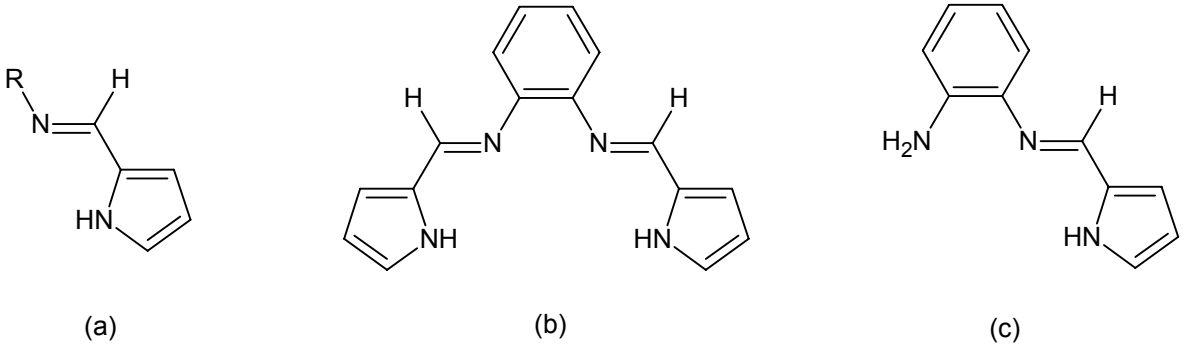

(a) (b) (c)

Figure 2-1. Schiff base ligands with (a) bi-, (b) tetra- and (c) tri-dentate binding environments.

This ability to be multidentate means that for most metals, where several binding sites are occupied, vacant sites for potential catalytic or enzymatic activity can be exposed. In addition, the properties of Schiff bases can be fine-tuned by the intentional positioning of substituents on the aromatic ring in order to modify the electronic or steric properties of the resulting complexes. The use of metal complexes of several chiral Schiff base ligands as catalysts shows stereoselectivity in organic transformations. This ability has made the synthesis of chiral complexes an important subject of research in coordination chemistry. Following the first reported isolation of the chiral binaphthyl Schiff base ligands by O'Connor *et al.*[2] (**Figure 2-2.** (c)), a wide variety of these ligands have been prepared. Che *et al.*[3] exploited the (*R*)-[Cr(III)(L^4)Cl]-MCM-41(m) analogue (**Scheme 2-2.**) for the epoxidation of alkenes in an example of a heterogenised metal catalyst derived from chiral binaphthyl Schiff base ligands.

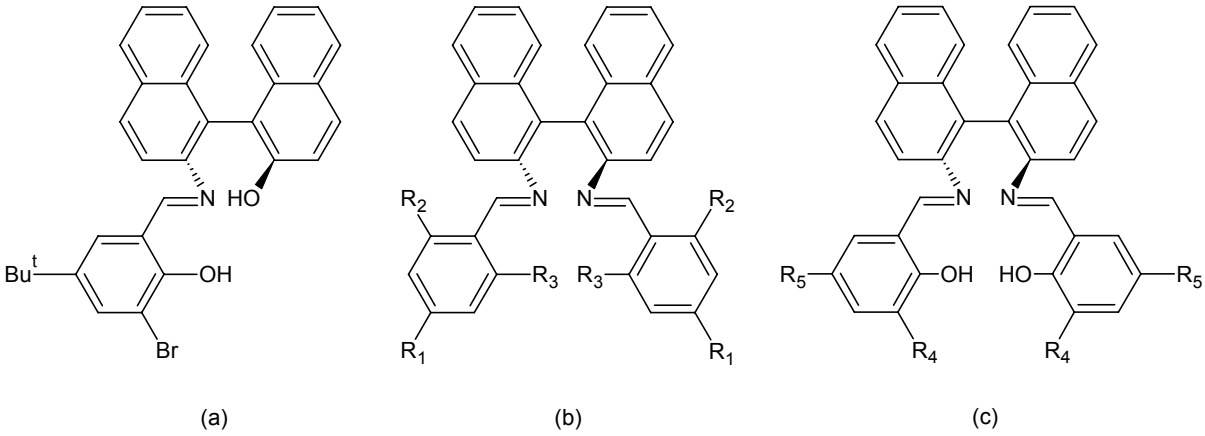

Figure 2-2. The chiral binaphthyl Schiff base ligands, designed for asymmetric catalysis, isolated by (a) Carreira *et al.*[4], (b) Suga *et al.*[5] and (c) O'Connor *et al.*[2]

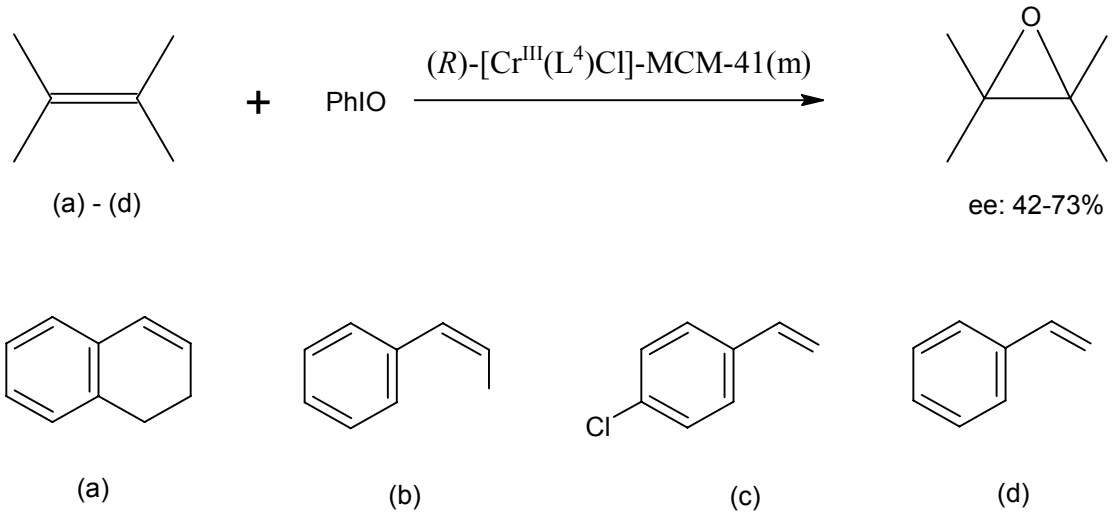

Scheme 2-2. The epoxidation of alkenes with chiral binaphthyl Schiff base ligands by Che *et al.*[3] L^4 = chiral binaphthyl Schiff base (**Figure 2-2.** (c)) with $R_4 = R_5 = Br$.

The versatility of the metal complexes of Schiff bases makes further investigation in this area highly desirable for biological, analytical and industrial applications.

Synthetic chemists have attempted to design biomimetic reactions that can imitate the efficiency and elegance of the biosynthetic machinery that occurs in natural reaction pathways. These biomimetic reactions are often a combination of several chemical transformations in a particular sequence that produce complicated structures from fairly simple starting materials. It was in 1981 when Matsumuto *et al.*[6] prepared Co(II), Mn(II) and Fe(II) transition metal complexes from the Schiff base ligand, *bis*(salicylaldehyde) ethylenediimine (salen) as catalysts for the synthesis of carpanone by the oxidation of *trans*-2-(1-propenyl)-4,5-methylenedioxyphenol with molecular oxygen (**Scheme 2-3.**).

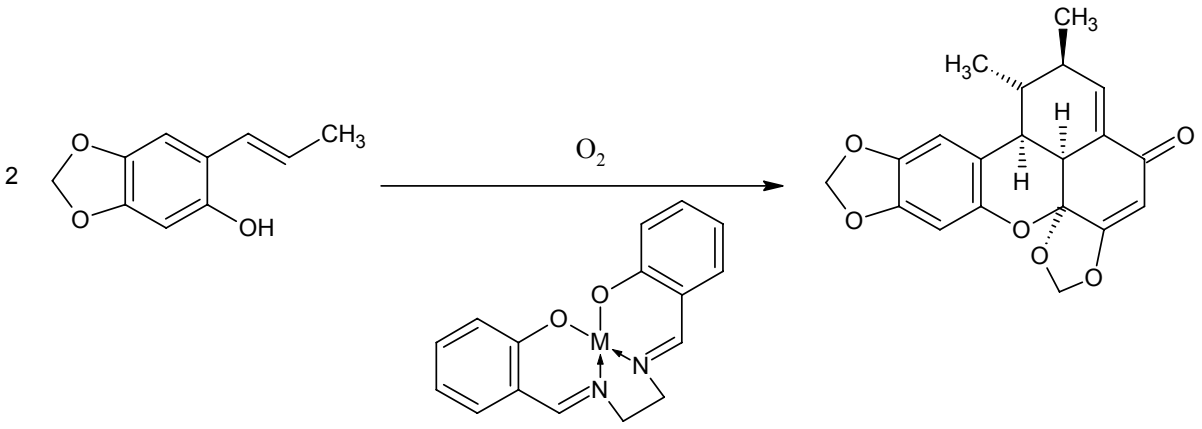

M = Co(II), Mn(II) or Fe(II); Yield = 94%, 80% and 78% respectively

Scheme 2-3. Matsumuto *et al.*[6] found a biological application for transition metal complexes of the tetra-dentate Schiff base ligand *bis*(salicylaldehyde) ethylenediimine.

Schiff base complexes of transition metals have proven to be highly efficient catalysts in both homogeneous and heterogeneous reactions. The activity of the complexes relies on the type of ligands, coordination sites and metals used. An excellent review by Gupta *et al.*[7] highlights the significant role of Schiff base complexes of transition metals as catalysts in various reactions to enhance their yields and product selectivities. The review also demonstrates the versatility and efficiency of the Schiff base complexes of transition metals

as catalysts for reactions of commercial importance and their suitability to catalyse various reactions under mild experimental conditions.

Vázquez-García *et al*.[8] demonstrated the versatile behaviour of the cyclopalladation of a Schiff base ligand, isolating products that are palladated at an aliphatic or sterically hindered aromatic carbon by varying the reaction conditions (**Scheme 2-4.**).

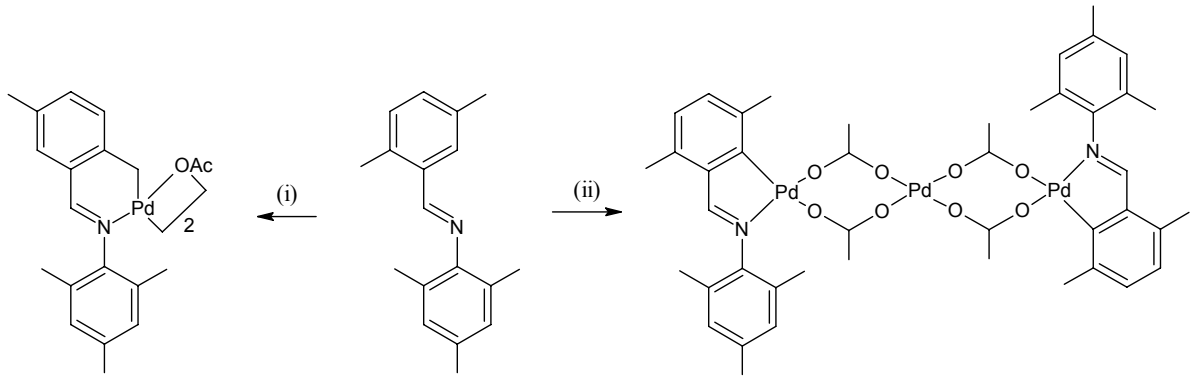

(i) $Pd(OAc)_2$, acetic acid, reflux

(ii) $Pd(OAc)_2$, toluene, room temperature

Scheme 2-4. Cyclopalladation via C-H bond activation of (i) an sp^3 hybridised carbon, yielding a μ-OAc binuclear complex and (ii) an sp^2 hybridised carbon, yielding a μ-OAc trinuclear complex.[8]

The synthetic methodology employed for the cyclopalladation of a range of prepared monofunctional Schiff base imine ligands and the characterisation thereof are described and discussed. The subsequent cleavage of the resulting μ-Cl binuclear cyclopalladated complexes with the appropriate phosphine molecules follows these.

2.2 Results and discussion

2.2.1 The preparation of monofunctional Schiff base imine ligands

Schiff base imine ligands **L1 – L5** were prepared by the Schiff base condensation of various mono-substituted aromatic aldehydes and the primary aromatic amine, 2,6-diisopropylaniline, in the presence of anhydrous magnesium sulphate (**Scheme 2-5.**). The latter serves to remove water that forms as a by-product during the reaction process yielding the imine products.

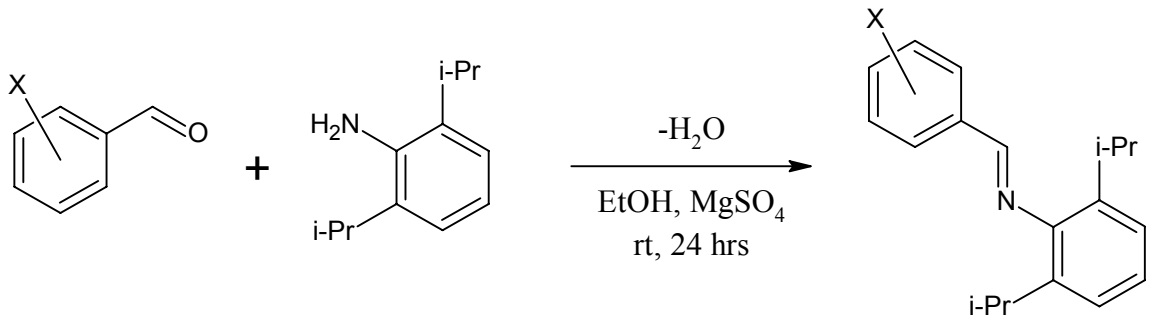

L1: X = *o*-Cl

L2: X = *o*-Br

L3: X = H

L4: X = *o*-Me

L5: X = *p*-Me

Scheme 2-5. Synthetic methodology employed for the preparation of the monofunctional Schiff base imine ligands.

All compounds were isolated in very good yields (69 – 96 %) as bright yellow crystals that are soluble in polar organic solvents at room temperature. The ligands are stable in solution and in the solid state. Ligands **L1**,[9] **L2**,[10] **L3**[10] and **L5**[11] have been reported previously whereas **L4** is novel.

The choice of 2,6-diisopropylaniline in the ligand design is that the bulkiness of the two isopropyl substituents is helpful in protecting the ensuing active species[12] to be synthesised, to promote longer life-times which leads to higher catalytic activity. Previous studies report that bulkier substituents might also enhance the solubility of the impending palladacycle complexes.[13,14] The intentional variation in the choice of aldehyde used is to probe the effect of the electronic properties and relative positioning of the substituent for the ensuing complexes as potential catalyst precursors.

The monofunctional ligands were characterised by a range of analytical techniques including FT-IR and NMR spectroscopy. The FT-IR spectra of the resulting products indicate the formation of the desired Schiff base ligands. The absence of characteristic $\nu_{C=O}$ absorption bands corresponding to the aldehyde starting materials and the appearance of the $\nu_{C=N}$ absorption bands corresponding to the imine products in the range 1625 – 1638 cm^{-1} provides evidence of the product formation (**Table 2-1.**).

Table 2-1. Analytical data of ligands **L1 – L5**.

Ligand	FT-IR ($\nu_{C=N}$, cm^{-1})[a]	ESI-MS (*m/z*)[b]	Melting point (°C)[c]
L1	1630	301[11]	48
L2	1625	345[11]	75
L3	1637	266[11]	65
L4	1633	280	61
L5	1638	280[11]	89

[a] Recorded as neat samples on a ZnSe crystal, employing an ATR accessory. [b] Reported ion corresponds to the proton adduct of the molecular ion, $[M + H]^+$. [c] Melting points recorded are uncorrected.

The unambiguous $\nu_{C=N}$ absorption bands due to the imine are important for the duration of the project. Its relative position in wavenumbers for the impending palladium metal complexes that are generated from these ligands reveals information regarding the nature of the complexes. Expected fluctuations in the double-bond character of the imine are monitored throughout the synthetic route employed, and is therefore regarded as the signature peak for all the FT-IR spectra in this project.

Electrospray ionisation mass spectrometry, recorded in the positive ion mode, provides further evidence of the product formation. The base peak which corresponds to the proton adduct of the molecular ion, $[M + H]^+$, is present in the spectra for all analogues. No sequential fragmentation takes place (**Table 2-1.** and **Figure 2-3.**).

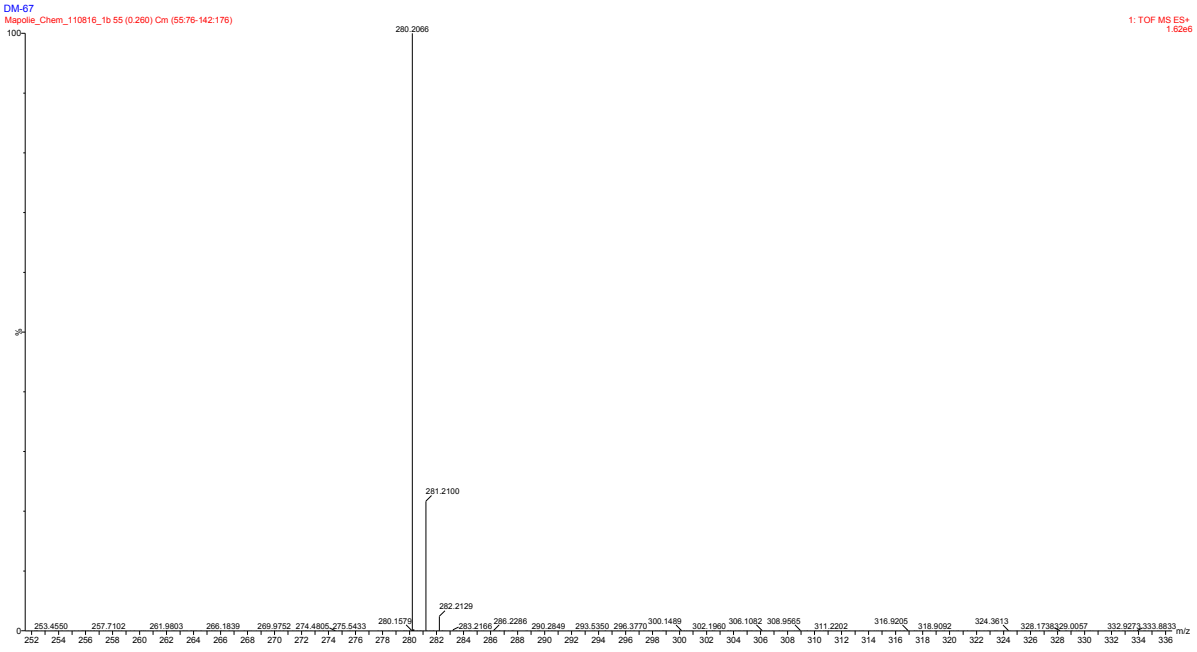

Figure 2-3. ESI-MS (+) spectrum in the region *m/z* 252 – 336 of ligand **L4**. A distinct peak at *m/z* 280.2 corresponds to the proton adduct of the molecular ion.

The presence of a singlet in the ^{1}H-NMR spectra in the downfield region of δ 8.22 – 8.67 ppm is due to the imine proton of the Schiff base products. It is clearly identifiable in all the spectra as it resonates furthest downfield of all the proton resonances. The nature of this resonance, i.e. the relative chemical shift, relative intensity and broadness as well as the splitting pattern, reveals crucial information about the molecule, especially for the impending palladium metal complexes that are generated from these ligands. Therefore, for the duration of this project, the imine proton resonance is regarded as the signature peak for all the obtained ^{1}H-NMR spectra since its nature generally validates the arrangement of the coordination sphere surrounding the metal centre.

Unsurprisingly, the imine proton resonances for ligands **L1** and **L2**, i.e. those with a halogen substituent at the *ortho* position, appear further downfield than the imine proton resonances for ligands **L3** – **L5**. This difference is due to the inductive effect of the halogen substituent.[15]

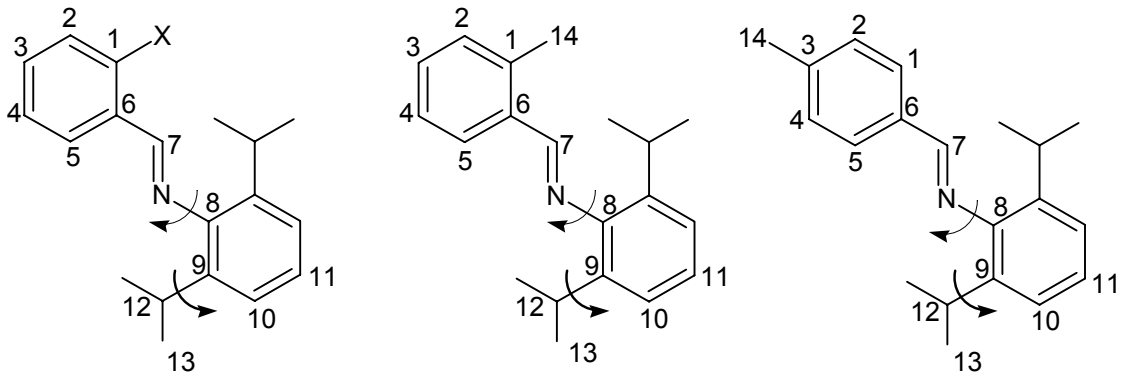

L1, **L2** and **L3** **L4** **L5**

X = Cl, Br and H respectively

Figure 2-4. Schematic representation of ligands **L1** – **L5** with the numbering for NMR spectral analysis.

^{1}H- and ^{13}C $\{^{1}$H$\}$- NMR spectral analysis reveals that in solution, at 298 K, for all the ligands, free rotation along the bond between the nitrogen and carbon (8) takes place which renders symmetry (mirror plane) to the entire diisopropyl phenyl moiety (**Figure 2-4.**). Free rotation along the bond between carbon (9) and carbon (12) also takes place.

The appearance of a septet in the region of δ 2.98 – 3.04 ppm in the ^{1}H-NMR spectra is due to the methine protons (H^{12}). A doublet in the region of δ 1.19 – 1.22 ppm is due to the isopropyl methyl protons (H^{13}). A singlet at δ 2.56 ppm in the spectrum for ligand **L4** and at δ 2.49 ppm in the spectrum for ligand **L5** is due to the protons of the methyl substituent (H^{14}) at the *ortho* and *para* position respectively. This indicates that the environment in which the protons of the *para*-substituted methyl substituent are positioned is relatively more shielded as compared to that of the *ortho*-substituted methyl substituent.

The imine carbon [carbon (7)] resonance in the ^{13}C $\{^{1}$H$\}$ NMR spectra appears furthest downfield of all the carbon resonances as a singlet in the downfield region of δ 159.2 – 162.2 ppm.

Identification of the resonances of all the protons in the ^{1}H-NMR spectra is possible for all five analogues. The clearly distinguishable resonances and coupling constants are assigned (**Table 2-2.** and **Figure 2-5.**).

Table 2-2. ^{1}H-NMR spectral data of Schiff base ligands **L1 – L5**.[a]

Ligand	HC=N	Aromatic region	Aliphatic region		
			$\underline{H}C(CH_3)_2$	$ArC\underline{H}_3$	$HC(C\underline{H}_3)_2$
L1	8.67 (s, 1H, H^7)	8.29 - 8.27 (m, 1H, H^2), 7.48 - 7.44 (m, 3H, $H^{3,4,5}$), 7.20 - 7.12 (m, 3H, $H^{10,11}$)	2.98 (sep, 2H, H^{12}, $^3J_{H\text{-}H}$ = 6.8Hz)		1.20 (d, 12H, H^{13}, $^3J_{H\text{-}H}$ = 6.8Hz)
L2	8.60 (s, 1H, H^7)	8.27 (dd, 1H, H^2, $^3J_{H\text{-}H}$ = 7.8Hz, $^4J_{H\text{-}H}$ = 1.9Hz), 7.66 (dd, 1H, H^5, $^3J_{H\text{-}H}$ = 8.1Hz, $^4J_{H\text{-}H}$ = 1.3Hz), 7.49 - 7.44 (m, 1H, H^3), 7.40 - 7.35 (m, 1H, H^4), 7.22 - 7.12 (m, 3H, $H^{10,11}$)	2.99 (sep, 2H, H^{12}, $^3J_{H\text{-}H}$ = 6.9Hz)		1.21 (d, 12H, H^{13}, $^3J_{H\text{-}H}$ = 6.9Hz)
L3	8.22 (s, 1H, H^7)	7.95 - 7.92 (m, 2H, $H^{1,5}$), 7.54 - 7.52 (m, 3H, $H^{2,3,4}$), 7.20 - 7.09 (m, 3H, $H^{10,11}$)	2.99 (sep, 2H, H^{12}, $^3J_{H\text{-}H}$ = 6.9Hz)		1.19 (d, 12H, H^{13}, $^3J_{H\text{-}H}$ = 6.9Hz)
L4	8.52 (s, 1H, H^7)	8.11 (dd, 1H, H^5, $^3J_{H\text{-}H}$ = 7.6Hz, $^4J_{H\text{-}H}$ = 1.4Hz), 7.44 - 7.34 (m, 2H, $H^{3,4}$), 7.29 - 7.27 (m, 1H, H^2), 7.20 - 7.11 (m, 3H, $H^{10,11}$)	3.02 (sep, 2H, H^{12}, $^3J_{H\text{-}H}$ = 7.0Hz)	2.56 (s, 3H, H^{14})	1.20 (d, 12H, H^{13}, $^3J_{H\text{-}H}$ = 7.0Hz)
L5	8.22 (s, 1H, H^7)	7.87 (d, 2H, $H^{1,5}$, $^3J_{H\text{-}H}$ = 8.0Hz), 7.37 (d, 2H, $H^{2,4}$, $^3J_{H\text{-}H}$ = 7.8Hz), 7.22 - 7.13 (m, 3H, $H^{10,11}$)	3.04 (sep, 2H, H^{12}, $^3J_{H\text{-}H}$ = 6.8Hz)	2.49 (s, 3H, H^{14})	1.22 (d, 12H, H^{13}, $^3J_{H\text{-}H}$ = 6.8Hz)

[a] Spectra recorded in $CDCl_3$ at 298 K. Chemical shifts reported in δ ppm values, referenced relative to the residual $CDCl_3$ peak. Superscripts denote protons as per numbering scheme (**Figure 2-4.**).

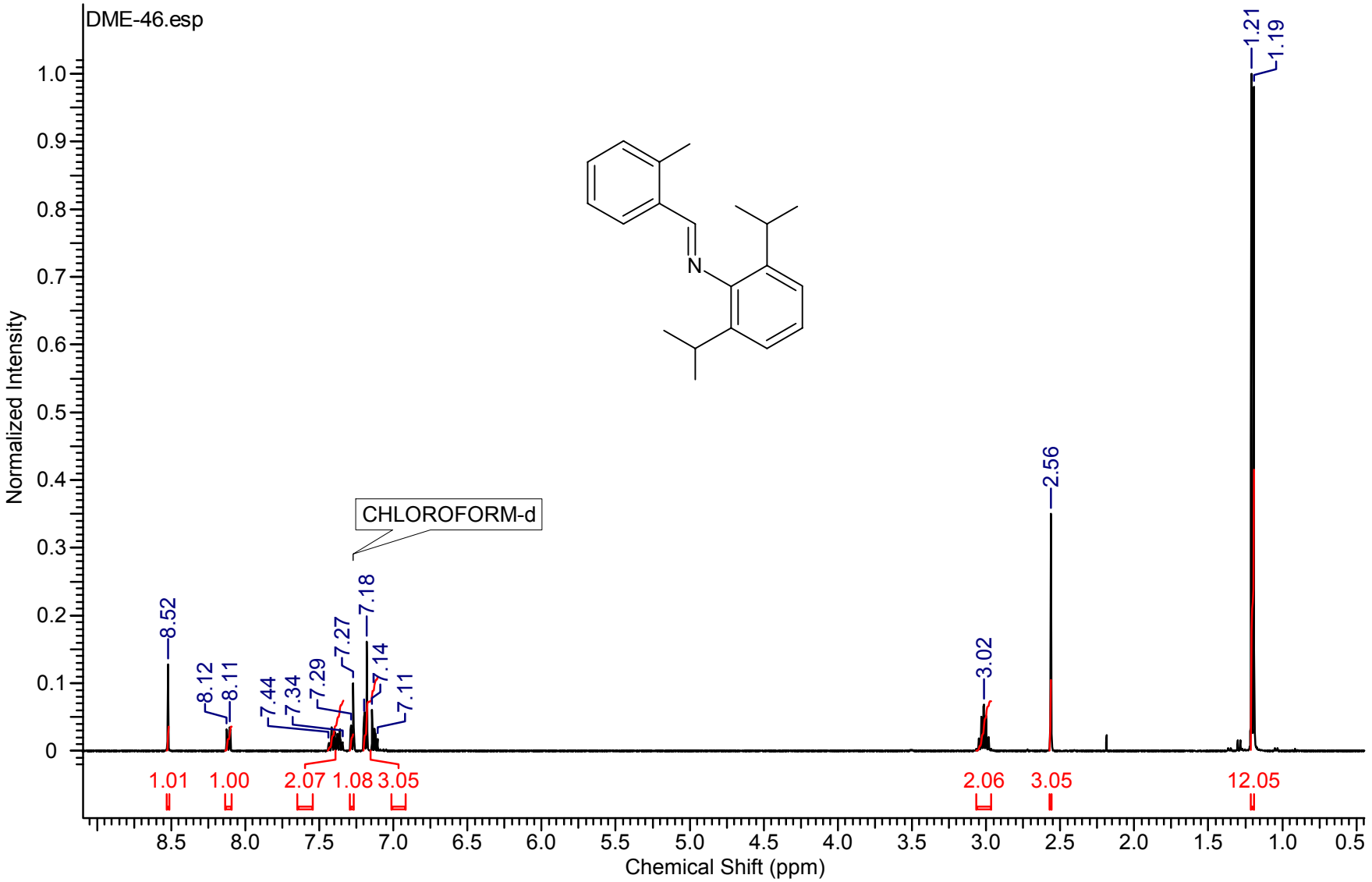

Figure 2-5. ^{1}H-NMR spectrum of ligand **L4**.

2.2.2 The preparation of μ-Cl binuclear cyclopalladated complexes

μ-Cl binuclear cyclopalladated complexes **C1 – C5** were prepared by the electrophilic C_{aryl}-H bond activation reaction of the various prepared Schiff base imine ligands and *bis*(acetonitrile) dichloropalladium(II) in the presence of sodium acetate (**Scheme 2-6.**). The latter serves to promote the removal of the *ortho* positioned proton of the Schiff base ligand during this cyclopalladation reaction.

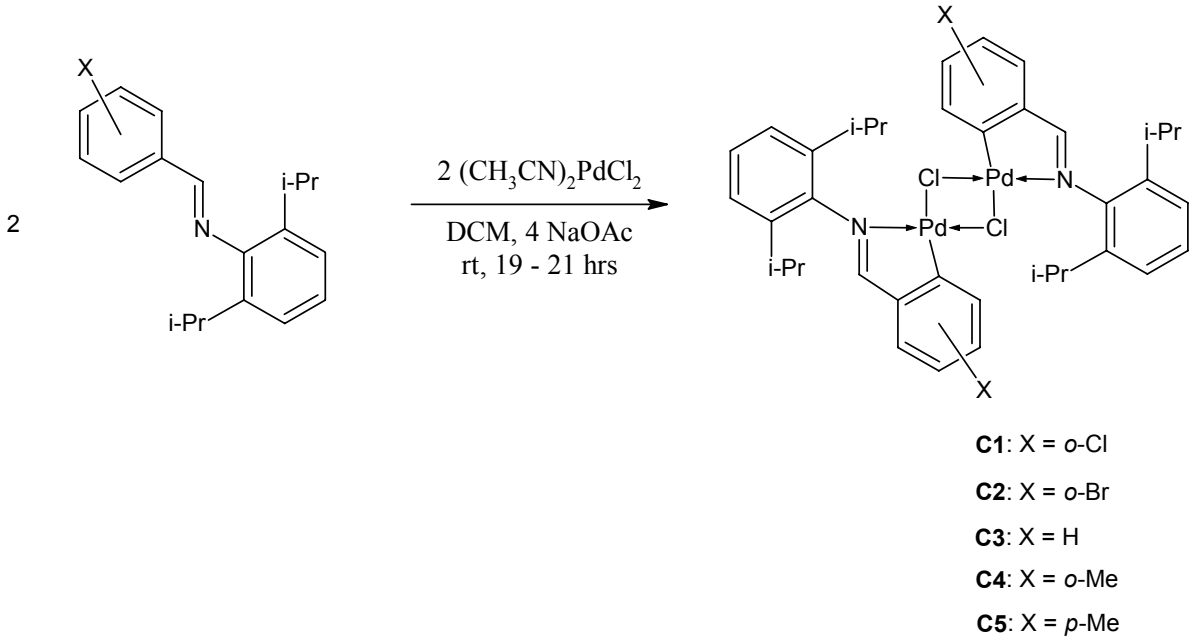

C1: X = *o*-Cl
C2: X = *o*-Br
C3: X = H
C4: X = *o*-Me
C5: X = *p*-Me

Scheme 2-6. Synthetic methodology employed for the preparation of the μ-Cl binuclear cyclopalladated complexes.

All compounds were isolated in good yields (74 – 87 %) as yellow solids that are soluble in chlorinated organic solvents at room temperature except for complexes **C1** and **C2** that are only partially soluble. The complexes are stable in the solid state and fairly stable in solution, since gradual decomposition into palladium black[9] takes place in solution over time. Complexes **C1,**[9] **C2,**[11] **C3**[9] and **C5**[11] have been reported previously whereas **C4** is novel.

A variety of analytical techniques were employed to characterise the μ-Cl binuclear cyclopalladated complexes similarly to that for the ligands **L1 – L5** (**2.2.1**). The FT-IR spectra of the resulting products indicate the formation of the desired cyclopalladated complexes. The absence of the $\nu_{C=N}$ absorption bands corresponding to the Schiff base ligand starting materials and the appearance of the $\nu_{C=N}$ absorption bands corresponding to the cyclopalladated products in the range 1585 – 1600 cm^{-1} provides evidence of the product formation (**Table 2-3.**).

Table 2-3. Analytical data of μ-Cl binuclear cyclopalladated complexes **C1 – C5**.

Comp.	FT-IR ($\nu_{C=N}$, cm^{-1})[a]	Decomposition temperature (°C)[b]
C1	1594	330 - 332
C2	1585	300 - 302
C3	1600	317 - 320
C4	1595	303 - 305
C5	1598	305 - 307

[a] Recorded as neat samples on a ZnSe crystal, employing an ATR accessory. [b] Melting points recorded are uncorrected. No melting prior to decomposition takes place.

The appearance of the $\nu_{C=N}$ absorption bands at lower wavenumbers in the FT-IR spectra, corresponding to the cyclopalladated products, together with the simultaneous disappearance of the $\nu_{C=N}$ absorption bands corresponding to the Schiff base ligand starting materials indicates that a decrease in imine double-bond character takes place upon cyclopalladation.[16] This is due to metalloaromaticity which is the manifestation of aromatic properties in the five-membered chelate metallacycles that form.[17]

The ^{1}H- and ^{13}C $\{^{1}$H$\}$-NMR spectra of the products confirm the formation of the five-membered chelate products. The expected appearance of a singlet due to the imine proton in the ^{1}H-NMR spectra in the region of δ 7.69 – 8.13 ppm, upfield as compared to the singlet due to the imine proton of the Schiff base ligands,[11] together with the simultaneous disappearance of the latter resonance, provides confirmation of successful cyclopalladation.

Similarly to the results for the Schiff base ligands, the imine proton resonances for complexes **C1** and **C2**, i.e. those with a halogen substituent at the *ortho* position, appear further downfield than the imine proton resonances for complexes **C3** – **C5**.

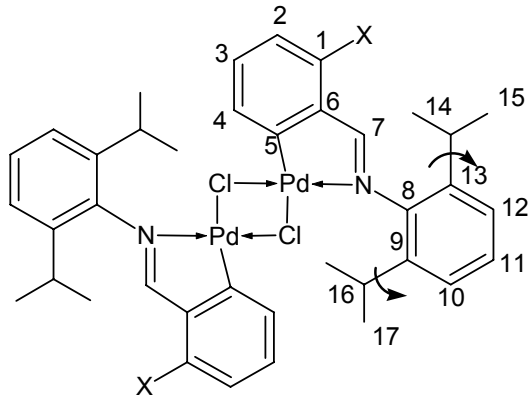

C1, **C2** and **C3**

X = Cl, Br and H respectively

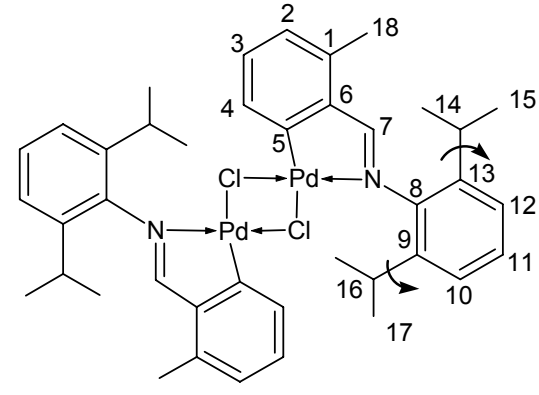

C4

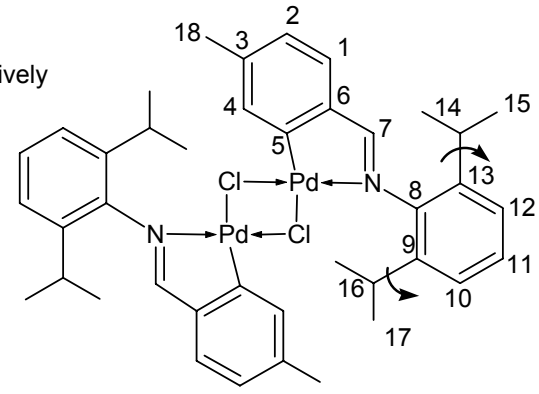

C5

Figure 2-6. Schematic representation of complexes **C1 – C5** with the numbering for NMR spectral analysis.

^{1}H- and ^{13}C $\{^{1}$H$\}$-NMR spectral analysis reveals that the rotation in solution, at 298 K, along the bond between the nitrogen and carbon (8) that is present in the ligands

becomes restricted upon complexation to the palladium precursor (**Figure 2-6.**). As a consequence, the symmetry of the diisopropyl phenyl moiety that is present for the ligands is absent for the μ-Cl binuclear complexes. Therefore certain atoms that are chemically equivalent for the ligands become inequivalent for the μ-Cl binuclear complexes. The free rotation along the bonds between carbon (9) and carbon (16) as well as between carbon (13) and carbon (14) is retained despite complexation.

A clear downfield shift for the resonance due to the two methine protons ($H^{14,16}$) takes place upon cyclopalladation. For the ligands these protons resonate as a septet, revealing their chemical equivalence, in the region of δ 2.98 – 3.04 ppm and for the μ-Cl binuclear complexes they resonate as two overlapping septets, i.e. multiplet, revealing their chemical inequivalence, in the region of δ 3.49 – 3.54 ppm. A downfield shift for the isopropyl methyl protons ($H^{15/17}$) also takes place. For the ligands these twelve protons resonate as a doublet, revealing their chemical equivalence, in the region of δ 1.19 – 1.22 ppm and for the μ-Cl binuclear complexes they resonate as two distinct doublets in the regions of δ 1.15 – 1.18 ppm and δ 1.39 – 1.39 ppm, revealing that H^{15} and H^{17} are chemically inequivalent. An upfield shift from δ 2.56 ppm to δ 2.40 ppm and from δ 2.49 ppm to δ 2.28 ppm takes place for the resonances due to the protons of the methyl substituents (H^{18}) for complexes **C4** and **C5** respectively. Similarly to the trend that is present for the ligands **L4** and **L5**, the environment in which the protons of the *para*-substituted methyl substituent are positioned is relatively more shielded as compared to that of the protons of the *ortho*-substituted methyl substituent.

The imine carbon [carbon (7)] resonance in the ^{13}C $\{^{1}H\}$-NMR spectra appears as a singlet in the downfield region of δ 174.15 – 176.21 ppm. The appearance of this resonance, downfield as compared to the singlet due to the imine carbon of the Schiff base ligands,[11] provides further confirmation of successful cyclopalladation.

Due to some expected overlapping of resonances in the aromatic region of the ^{1}H-NMR spectra, the multiplicities of certain resonances are not clear. All clearly distinguishable resonances and coupling constants are assigned (**Table 2-4.** and **Figure 2-7.**).

Table 2-4. ^{1}H-NMR spectral data of μ-Cl binuclear cyclopalladated complexes **C1 – C5**.[a]

Comp.	HC=N	Aromatic region	Aliphatic region		
			$\underline{H}C(CH_3)_2$	$ArC\underline{H}_3$	$HC(C\underline{H}_3)_2$
C1	8.13 (s, 2H, H^7)	7.36 - 7.31 (m, 2H, H^2), 7.22 - 7.19 (m, 4H), 7.08 - 6.97 (m, 6H)	3.49 (m, 4H, $H^{14,16}$)		1.39 (d, 12H, $H^{15/17}$, $^3J_{H\text{-}H}$ = 6.6Hz), 1.18 (d, 12H, $H^{15/17}$, $^3J_{H\text{-}H}$ = 6.6Hz)
C2	8.13 (s, 2H, H^7)	7.34 - 7.31 (m, 2H, H^2), 7.22 - 7.17 (m, 6H, $H^{10,11,12}$), 7.13 - 7.10 (m, 2H, H^3), 6.90 - 6.85 (m, 2H, H^4)	3.49 (m, 4H, $H^{14,16}$)		1.39 (d, 12H, $H^{15/17}$, $^3J_{H\text{-}H}$ = 6.6Hz), 1.18 (d, 12H, $H^{15/17}$, $^3J_{H\text{-}H}$ = 6.6Hz)
C3	7.75 (s, 2H, H^7)	7.35 - 7.28 (m, 4H, $H^{1,2}$), 7.21 - 7.19 (m, 6H, $H^{10,11,12}$), 7.09 - 7.05 (m, 4H, $H^{3,4}$)	3.53 (m, 4H, $H^{14,16}$)		1.39 (d, 12H, $H^{15/17}$, $^3J_{H\text{-}H}$ = 6.6Hz), 1.15 (d, 12H, $H^{15/17}$, $^3J_{H\text{-}H}$ = 6.6Hz)
C4	8.01 (s, 2H, H^7)	7.33 - 7.31 (m, 2H, H^2), 7.22 - 7.20 (m, 4H), 7.03 - 6.80 (m, 6H)	3.54 (m, 4H, $H^{14,16}$)	2.40 (s, 6H, H^{18})	1.39 (d, 12H, $H^{15/17}$, $^3J_{H\text{-}H}$ = 5.9Hz), 1.16 (d, 12H, $H^{15/17}$, $^3J_{H\text{-}H}$ = 6.4Hz)
C5	7.69 (s, 2H, H^7)	7.35 - 7.30 (m, 2H, H^1), 7.21 - 7.16 (m, 6H, $H^{10,11,12}$), 7.01 (s, 2H, H^4), 6.88 (d, 2H, H^2, $^3J_{H\text{-}H}$ = 7.5Hz)	3.53 (m, 4H, $H^{14,16}$)	2.28 (s, 6H, H^{18})	1.39 (d, 12H, $H^{15/17}$, $^3J_{H\text{-}H}$ = 6.6Hz), 1.15 (d, 12H, $H^{15/17}$, $^3J_{H\text{-}H}$ = 7.0Hz)

[a] Spectra recorded in $CDCl_3$ at 298 K. Chemical shifts reported in δ ppm values, referenced relative to the residual $CDCl_3$ peak. Superscripts denote protons as per numbering scheme (**Figure 2-6.**).

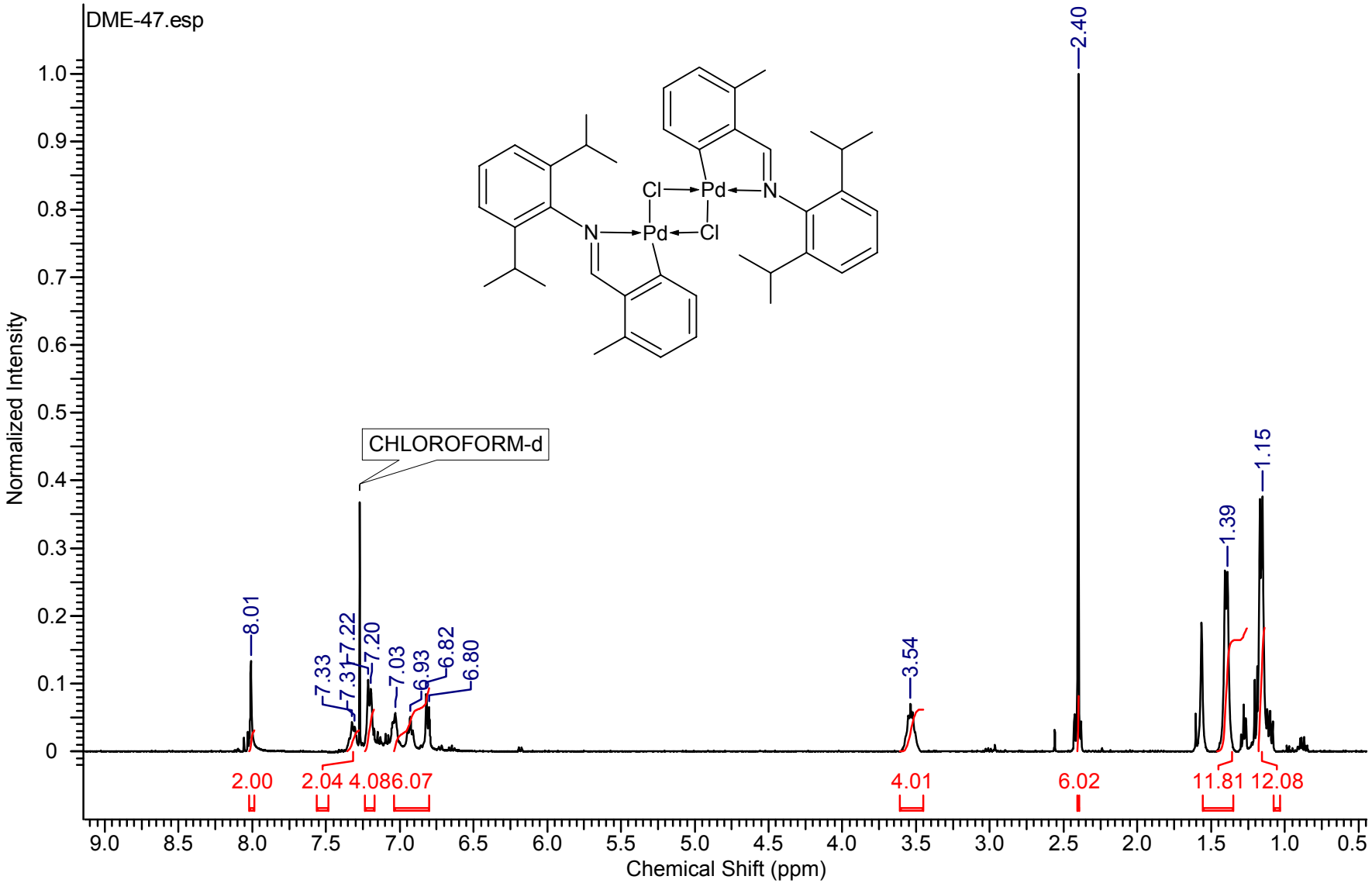

Figure 2-7. ^{1}H-NMR spectrum of complex **C4**.

2.2.3 The preparation of mononuclear, neutral cyclopalladated complexes

Mononuclear, neutral cyclopalladated complexes **C6 – C10** were prepared by the cleavage of the previously discussed μ-Cl binuclear cyclopalladated complexes with two mol equivalents of triphenylphosphine (**Scheme 2-7.**).

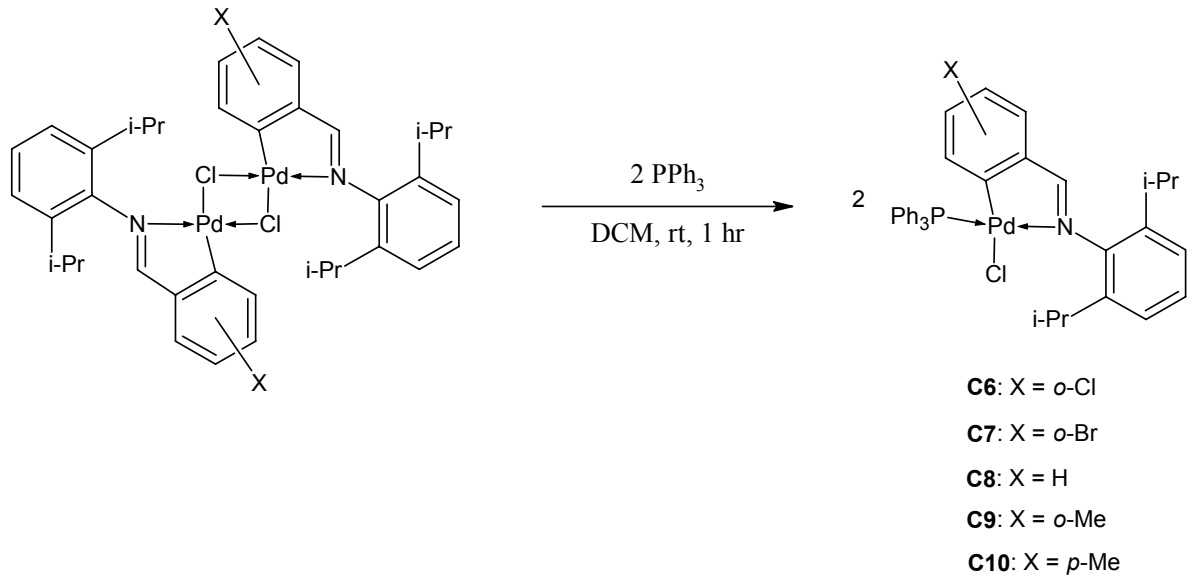

C6: X = *o*-Cl
C7: X = *o*-Br
C8: X = H
C9: X = *o*-Me
C10: X = *p*-Me

Scheme 2-7. Synthetic methodology employed for the preparation of the mononuclear, neutral cyclopalladated complexes.

All compounds were isolated in good yields (68 – 91 %) as very pale yellow solids that are soluble in polar organic solvents at room temperature. The complexes are stable in solution and in the solid state. Complexes **C6,**[11] **C7,**[11] **C8**[11] and **C10**[11] have been reported previously whereas **C9** is novel.

A variety of analytical techniques were employed to characterise the mononuclear, neutral cyclopalladated complexes similarly to that done for the ligands **L1 – L5** (**2.2.1**). The FT-IR spectra of the resulting products indicate the formation of the desired neutral complexes (for the sake of convenience, this range of complexes (**C6 – C10**) is referred to as

the neutral complexes). The absence of the $\nu_{C=N}$ absorption bands corresponding to the μ-Cl binuclear cyclopalladated complex starting materials and the appearance of the $\nu_{C=N}$ absorption bands corresponding to the neutral products in the range 1604 – 1608 cm^{-1} provides evidence of the product formation (**Table 2-5.**).

Table 2-5. Analytical data of neutral cyclopalladated complexes **C6 – C10**.

Comp.	FT-IR ($\nu_{C=N}$, cm^{-1})[a]	ESI-MS (*m/z*)[b]	Decomposition temperature (°C)[c]
C6	1608	667[11]	234 - 237
C7	1606	711[11]	239 - 242
C8	1604	633[11]	225 - 227
C9	1605	648	245 - 248
C10	1608	648[11]	212 - 214

[a] Recorded as neat samples on a ZnSe crystal, employing an ATR accessory. [b] Recorded in the positive ion mode. Reported ion corresponds to $[M - Cl]^+$. [c] Melting points recorded are uncorrected. No melting prior to decomposition takes place.

The difference between the appearance of the $\nu_{C=N}$ absorption bands corresponding to the μ-Cl binuclear cyclopalladated complexes and those of the neutral products is clear. The presence of the coordinating two-electron donor ligand, triphenylphosphine, in the neutral complexes, with its superior sigma-donor ability compared to the previously bound chloride, simply increases the electron density within the five-membered palladacycle ring. This boosts the affect of metalloaromaticity, with the consequence of an increase in double-bond character of the imine bond as compared to that of the μ-Cl binuclear cyclopalladated complex starting materials.

Electrospray ionisation mass spectrometry, recorded in the positive ion mode, provides further evidence of the product formation. The base peak which corresponds to the $[M - Cl]^+$ fragment is present in the spectra for all analogues (**Table 2-5.**). This is due to the abstraction of the Cl^- ligand from the neutral complexes during the ionisation process. No further fragmentation takes place. The appearance of a cluster of peaks is due to the numerous isotopes of palladium that are present in the complex (**Figure 2-8.**). Calculated isotopic distributions of the fragments are consistent with the sample spectra for all analogues (**Figure 2-8. a**).[18]

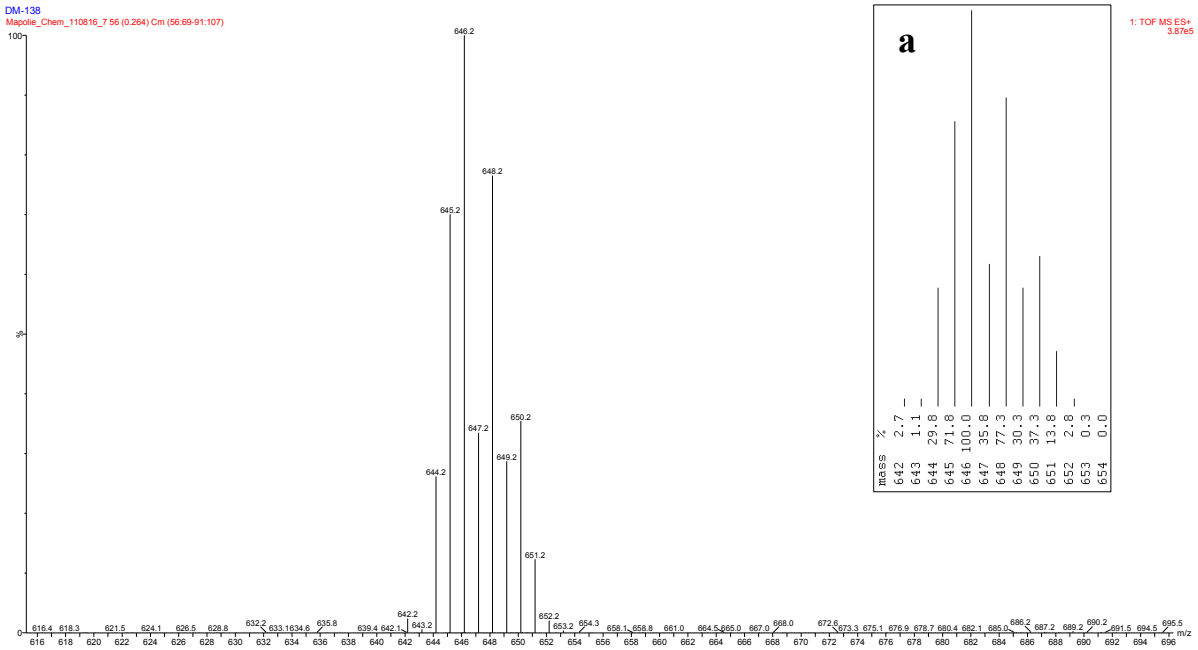

Figure 2-8. ESI-MS (+) spectrum in the region *m/z* 616 – 696 of complex **C9**. The cluster of peaks centred at *m/z* 648.2 corresponds to the $[M - Cl]^+$ fragment.

The ^{1}H-, ^{13}C $\{^1$H$\}$- and ^{31}P $\{^1$H$\}$-NMR spectra of the products confirm the formation of the neutral complexes. The appearance of a doublet in the region of δ 8.05 – 8.62 ppm for the imine proton in the ^{1}H-NMR spectra is due to the hetero-nuclear $^4J_{H\text{-}P}$ coupling to the NMR active ^{31}P atom of the coordinated triphenylphosphine ligand. This splitting pattern confirms

that the five-membered palladacycle is retained and that the phosphine is situated *trans* relative to the imine nitrogen. The coordinating two-electron donor contribution of the triphenylphosphine ligand increases the degree of electron delocalisation within the five-membered palladacycle which deshields the imine proton from the effect of the externally applied magnetic field. As a result the imine proton resonance appears further downfield as compared to the singlet due to the imine proton of the μ-Cl binuclear cyclopalladated complexes.

Similarly to the results for the Schiff base ligands and the μ-Cl binuclear cyclopalladated complexes, the imine proton resonances for complexes **C6** and **C7**, i.e. those with a halogen substituent at the *ortho* position, appear further downfield than the imine proton resonances for complexes **C8** – **C10**.

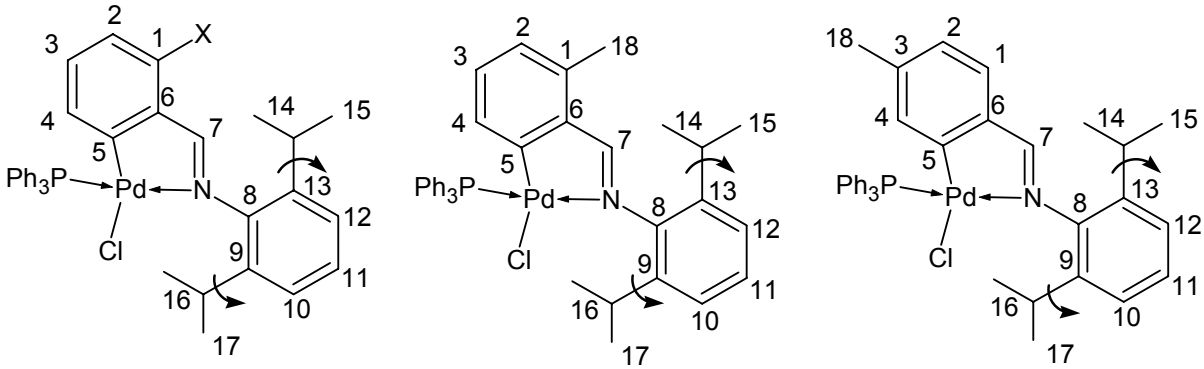

Figure 2-9. Schematic representation of complexes **C6 – C10** with the numbering for NMR spectral analysis.

^{1}H- and ^{13}C $\{^{1}$H$\}$-NMR spectral analysis reveals that rotation along the bond between the nitrogen and carbon (8) remains restricted in solution, at 298 K, after the cleavage reaction

with triphenylphosphine (**Figure 2-9.**). The free rotation along the bonds between carbon (9) and carbon (16) as well as between carbon (13) and carbon (14) is retained.

A slight upfield shift takes place for the multiplet due to the methine protons ($H^{14,16}$) from the region of δ 3.49 – 3.54 ppm for the μ-Cl binuclear cyclopalladated complexes (**C1 – C5**) to the region of δ 3.45 – 3.51 ppm for the neutral complexes. A clear change in chemical shifts for the isopropyl methyl protons ($H^{15/17}$) also takes place. For the μ-Cl binuclear cyclopalladated complexes, two distinct doublets that do not overlap resonate in the regions of δ 1.15 – 1.18 ppm and δ 1.39 – 1.39 ppm, revealing that H^{15} and H^{17} are chemically different. The two doublets due to H^{15} and H^{17} for the neutral complexes resonate in the regions of δ 1.20 – 1.25 ppm and δ 1.37 – 1.40 ppm. Their chemical inequivalence is less pronounced upon completion of the cleavage reaction. A downfield shift from δ 2.40 ppm to δ 2.49 ppm takes place for the singlet due to the protons of methyl substituent (H^{18}) for complex **C9**, while an upfield shift from δ 2.28 ppm to δ 1.79 ppm takes place for the singlet due to the protons of the methyl substituent (H^{18}) for complex **C10**. These trends in chemical shifts collectively reveal that the coordination of triphenylphosphine increases the degree of electron delocalisation within the five-membered palladacycle for all analogues.

The appearance of a clearly identifiable doublet in the ^{1}H-NMR spectrum due to the aromatic proton at carbon (4) for complex **C10** is due to $^{4}J_{H\text{-}P}$ coupling to the ^{31}P atom of the coordinated triphenylphosphine ligand. For complexes **C6 – C9** the aromatic proton at carbon (4) is involved in $^{3}J_{H\text{-}H}$ coupling to the aromatic proton at carbon (3) in addition to the $^{4}J_{H\text{-}P}$ coupling. As a result, their $^{4}J_{H\text{-}P}$ coupling constants are not clearly identifiable. Their splitting patterns are therefore assigned as multiplets.

The imine carbon [carbon (7)] resonance in the ^{13}C $\{^{1}$H$\}$-NMR spectra appears as a doublet in the downfield region of δ 174.80 – 177.70 ppm. This splitting pattern, due to the

hetero-nuclear $^{3}J_{C\text{-}P}$ coupling to the ^{31}P atom of the coordinated triphenylphosphine ligand, also provides confirmation that the five-membered palladacycle is retained. The appearance of this resonance slightly downfield as compared to that of the μ-Cl binuclear cyclopalladated complexes reveals once again that the coordination of triphenylphosphine increases the degree of electron delocalisation within the five-membered palladacycle.

A sharp, well-defined singlet due to the ^{31}P atom of the phosphine ligand appears in the region of δ 41.53 – 42.21 ppm in the ^{31}P $\{^{1}H\}$-NMR spectra for all analogues (**Table 2-6.** and **Figure 2-10.**). The ^{31}P atom in free triphenylphosphine resonates as a singlet at δ -4.84 ppm. This confirms that the ^{31}P atom of the triphenylphosphine ligand that is coordinated to the palladium metal centre is somewhat deshielded by the electron delocalisation ring current in the five-membered palladacycle.

Table 2-6. ^{31}P $\{^{1}H\}$-NMR spectral data of neutral complexes **C6 – C10**.

Comp.	δ (ppm)[a]
C6	41.76[11]
C7	41.53[11]
C8	42.21[11]
C9	42.07
C10	41.64[11]

[a] Spectra recorded in $CDCl_3$ at 298 K.

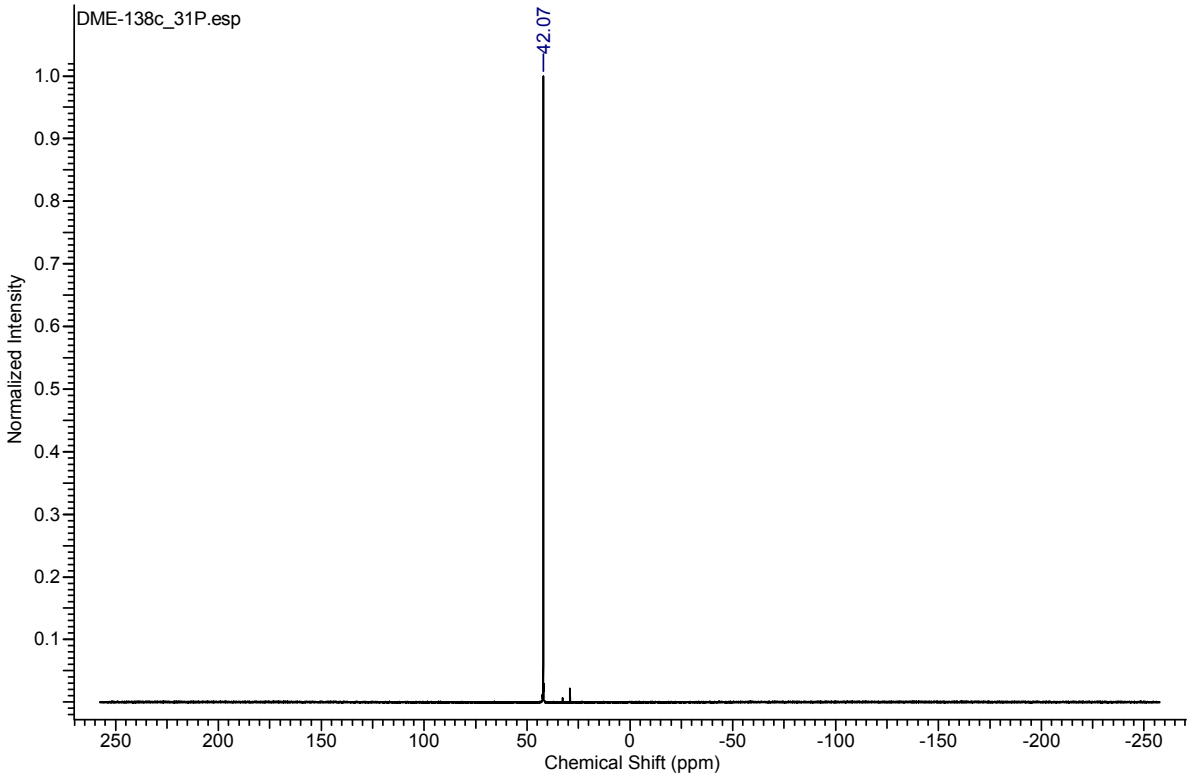

Figure 2-10. ^{31}P $\{^{1}H\}$-NMR spectrum of complex **C9**.

Due to some expected overlapping of resonances in the aromatic region of the ^{1}H-NMR spectra, the multiplicities of certain resonances are not identifiable. However, all clearly distinguishable resonances and coupling constants are assigned (**Table 2-7.** and **Figure 2-11.**).

Table 2-7. ^{1}H-NMR spectral data of neutral cyclopalladated complexes **C6 – C10**.[a]

Comp.	HC=N	Aromatic region	Aliphatic region		
			$\underline{H}C(CH_3)_2$	$ArC\underline{H}_3$	$HC(C\underline{H}_3)_2$
C6	8.62 (d, 1H, H^7, $^4J_{H\text{-}P}$ = 7.8Hz)	7.74 (d, 3H, $^3J_{H\text{-}H}$ = 7.8Hz), 7.72 (d, 3H, $^3J_{H\text{-}H}$ = 7.8Hz), 7.45 - 7.42 (m, 3H), 7.38 - 7.36 (m, 5H), 7.23 - 7.16 (m, 4H), 6.93 (d, 1H, H^2, $^3J_{H\text{-}H}$ = 7.9Hz), 6.61 (t, 1H, H^3, $^3J_{H\text{-}H}$ = 7.9Hz), 6.39 - 6.36 (m, 1H, H^4)	3.45 (m, 2H, $H^{14,16}$)		1.38 (d, 6H, $H^{15/17}$, $^3J_{H\text{-}H}$ = 6.8Hz), 1.24 (d, 6H, $H^{15/17}$, $^3J_{H\text{-}H}$ = 6.9Hz)
C7	8.62 (d, 1H, H^7, $^4J_{H\text{-}P}$ = 7.8Hz)	7.74 (d, 3H, $^3J_{H\text{-}H}$ = 7.9Hz), 7.72 (d, 3H, $^3J_{H\text{-}H}$ = 7.8Hz), 7.45 - 7.42 (m, 3H), 7.38 - 7.36 (m, 6H), 7.24 - 7.17 (m, 3H, $H^{10,11,12}$), 7.11 (d, 1H, H^2, $^3J_{H\text{-}H}$ = 7.9Hz), 6.51 (t, 1H, H^3, $^3J_{H\text{-}H}$ = 7.8Hz), 6.44 - 6.41 (m, 1H, H^4)	3.45 (m, 2H, $H^{14,16}$)		1.38 (d, 6H, $H^{15/17}$, $^3J_{H\text{-}H}$ = 6.8Hz), 1.25 (d, 6H, $H^{15/17}$, $^3J_{H\text{-}H}$ = 6.9Hz)
C8	8.14 (d, 1H, H^7, $^4J_{H\text{-}P}$ = 7.8Hz)	7.80 - 7.74 (m, 7H), 7.44 - 7.37 (m, 9H), 7.22 - 7.15 (m, 3H, $H^{10,11,12}$), 7.03 (t, 1H, H^2, $^3J_{H\text{-}H}$ = 7.2Hz), 6.71 (t, 1H, H^3, $^3J_{H\text{-}H}$ = 7.0Hz), 6.54 - 6.50 (m, 1H, H^4)	3.48 (m, 2H, $H^{14,16}$)		1.40 (d, 6H, $H^{15/17}$, $^3J_{H\text{-}H}$ = 6.8Hz), 1.23 (d, 6H, $H^{15/17}$, $^3J_{H\text{-}H}$ = 6.9Hz)
C9	8.47 (d, 1H, H^7, $^4J_{H\text{-}P}$ = 7.9Hz)	7.79 - 7.73 (m, 6H), 7.43 - 7.34 (m, 9H), 7.24 - 7.16 (m, 3H, $H^{10,11,12}$), 6.76 (d, 1H, H^2, $^3J_{H\text{-}H}$ = 7.5Hz), 6.60 (t, 1H, H^3, $^3J_{H\text{-}H}$ = 7.6Hz), 6.40 - 6.36 (m, 1H, H^4)	3.51 (m, 2H, $H^{14,16}$)	2.49 (s, 3H, H^{18})	1.40 (d, 6H, $H^{15/17}$, $^3J_{H\text{-}H}$ = 6.9Hz), 1.24 (d, 6H, $H^{15/17}$, $^3J_{H\text{-}H}$ = 6.9Hz)
C10	8.05 (d, 1H, H^7, $^4J_{H\text{-}P}$ = 8.0Hz)	7.79 - 7.74 (m, 6H), 7.45 - 7.35 (m, 9H), 7.30 (d, 1H, H^1, $^3J_{H\text{-}H}$ = 7.6Hz), 7.21 - 7.14 (m, 3H, $H^{10,11,12}$), 6.82 (d, 1H, H^2, $^3J_{H\text{-}H}$ = 7.4Hz), 6.18 (d, 1H, H^4, $^4J_{H\text{-}P}$ = 6.2Hz)	3.49 (m, 2H, $H^{14,16}$)	1.79 (s, 3H, H^{18})	1.37 (d, 6H, $H^{15/17}$, $^3J_{H\text{-}H}$ = 6.8Hz), 1.20 (d, 6H, $H^{15/17}$, $^3J_{H\text{-}H}$ = 6.8Hz)

[a] Spectra recorded in $CDCl_3$ at 298 K. Chemical shifts reported in δ ppm values, referenced relative to the residual $CDCl_3$ peak. Superscripts denote protons as per numbering scheme (**Figure 2-9.**).

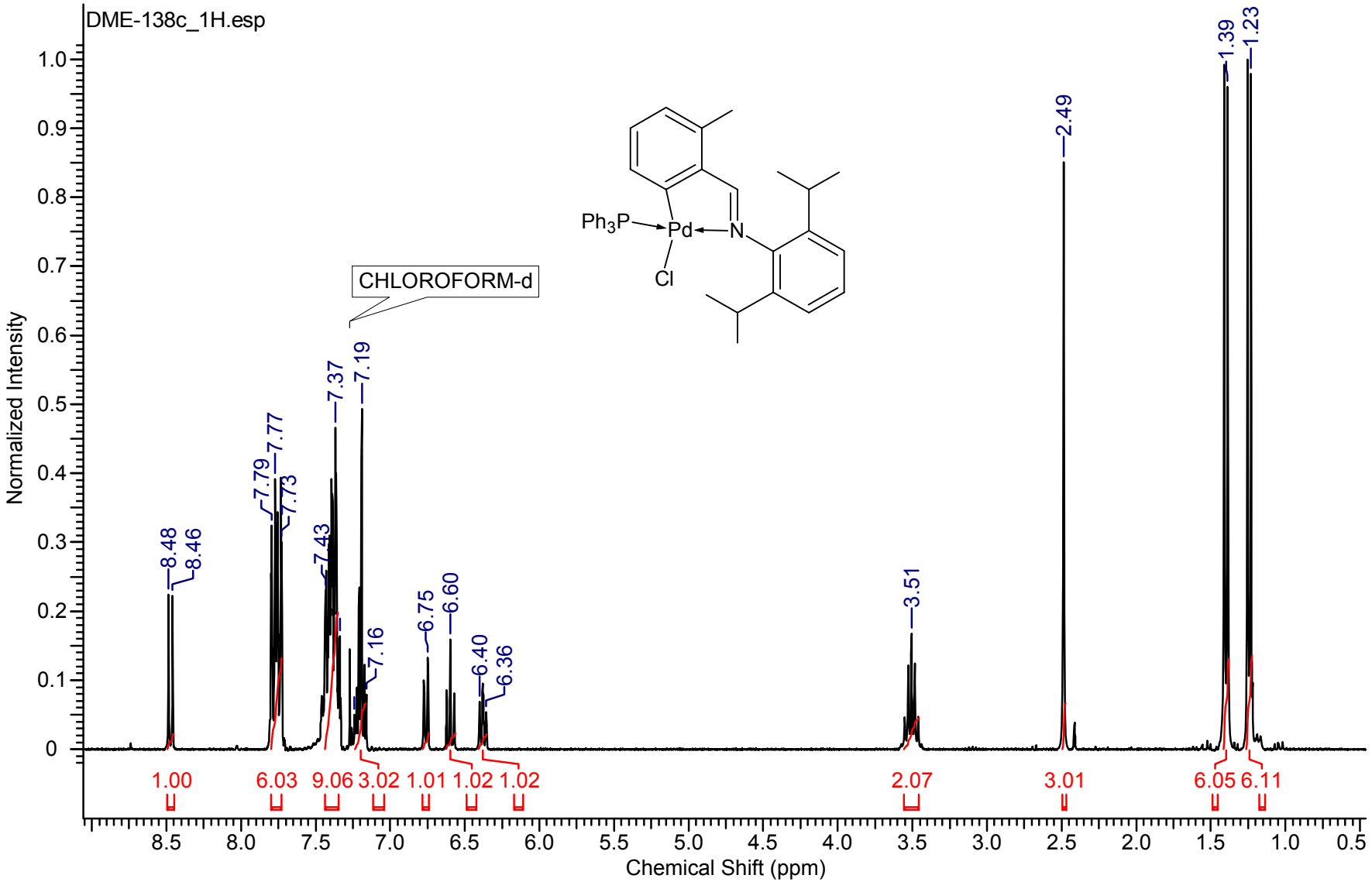

Figure 2-11. ^{1}H-NMR spectrum of complex **C9**.

Crystals suitable for single crystal diffraction analysis were obtained of complex **C9** (**Figure 2-12.**). Recrystallisation by means of slow evaporation from dichloromethane/*n*-pentane at low temperature (-4 °C) resulted in the formation of light yellow single crystals.

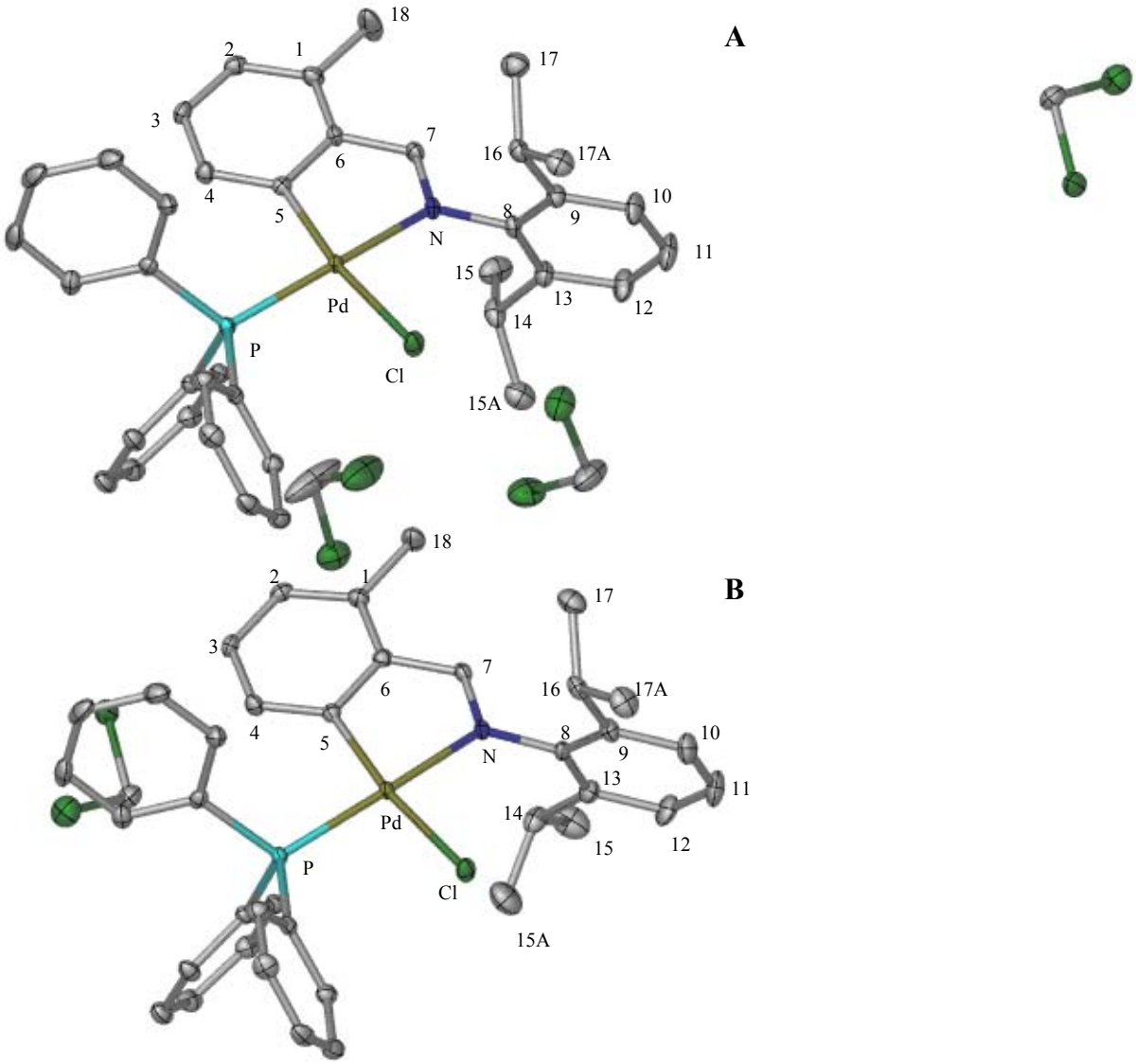

Figure 2-12. Molecular structures of complex **C9**, **A** and **B,** shown with 50 % probability ellipsoids and the numbering scheme (hydrogen atoms are omitted for clarity).

The asymmetric unit comprises two cyclopalladated complex molecules and four dichloromethane solvent molecules. The geometry of the palladium atom for both **A** and **B** is

distorted square planar in a similar manner to the previously reported complex **C10** analogue.[11] This study confirms that the chloride ligand that remains bound to the palladium after the cleavage reaction is *trans* to the Pd-C bond. Selected bond lengths, bond angles and torsion angles are listed in **Table 2-9.**.

A number of weak noncovalent intermolecular interactions are present in the packing arrangement of complex **C9** (**Figure 2-13.**). These include, amongst others, C-Cl···H and Pd-Cl···H interactions.

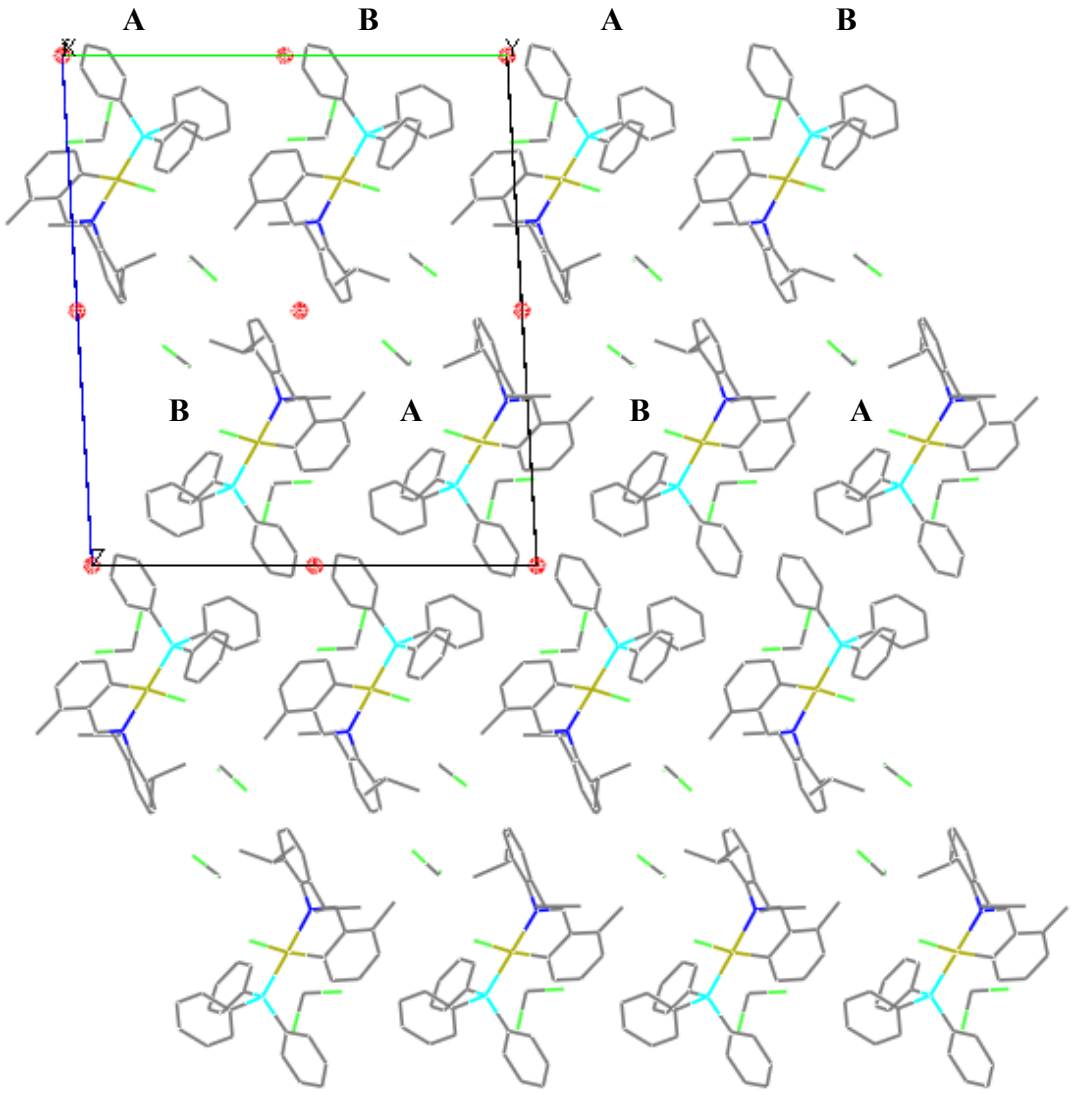

Figure 2-13. Packing diagram of the molecules of complex **C9** shown along the a-axis, which illustrates the alternating packing arrangement of structures **A** and **B**. Inversion centres are marked with ● (hydrogen atoms are omitted for clarity).

Table 2-8. Crystallographic data and structure refinement parameters of complex **C9**.

Empirical formula	$C_{80}H_{86}Cl_{10}N_2P_2Pd_2$
M_r (g/mol)	1704.75
Crystal system	triclinic
Space group	$P\bar{1}$ (No.2)
a (Å)	9.3799 (1)
b (Å)	19.048 (2)
c (Å)	21.878 (2)
α (deg)	86.326 (1)
β (deg)	85.818 (1)
γ (deg)	85.297 (1)
Volume (Å^3)	3878.8 (7)
Z	2
D_{calc} (g cm^{-3})	1.460
F000	1744
λ (MoK_α) (Å)	0.71073
Temperature (K)	103 (2)
2θ max (deg)	57.8
Lp and absorption corrections applied (μ)	0.894 mm^{-1}
Data/restraints/par.	18614/0/875
R_1 [$I > 2\sigma(I)$]	0.0294
wR_2 (all reflections)	0.0751
Goodness of fit on F^2	1.036
Max/min residual electron density (e Å^{-3})	0.725 / -0.788

Table 2-9. Selected bond lengths, bond angles and torsion angles of the crystallographically determined structures **A** and **B** of complex **C9** and complex **C10**[11].[a]

	C9 (A)	**C9 (B)**	**C10**[11]
		Bond lengths (Å)	
Pd-C(5)	2.026	2.025	2.011
Pd-N	2.104	2.109	2.102
Pd-Cl	2.358	2.365	2.365
Pd-P	2.267	2.265	2.252
C(7)-N	1.289	1.284	1.285
C(8)-N	1.444	1.447	-
C(1)-C(18)	1.511	1.512	-
		Bond angles (degrees)	
N-Pd-Cl	90.58	91.51	91.80
Cl-Pd-P	93.10	92.70	92.13
P-Pd-C(5)	95.10	94.98	96.40
C(5)-Pd-N	81.38	80.96	80.80
		Torsion angles (degrees)	
C(8)-C(13)-C(14)-C(15)	99.09	147.56	-
C(8)-C(9)-C(16)-C(17)	-90.16	-83.00	-

[a] Atom labelling as per numbering scheme (**Figure 2-12.** for complex **C9** and **Figure 2-9.** for complex **C10**).

The distorted square planar geometry of the palladium atom is noticeably demonstrated by the bond angles at the coordination sphere. An angle of between 80.80 – 81.38° for the chelating C-Pd-N clearly reveals the distortion.

Thermogravimetric analysis (TGA) of complex **C9** confirms the presence of the included dichloromethane solvent molecules in the packing arrangement. The inflection point at 230 °C is due to the loss of dichloromethane (**Figure 2-14.**). The presence of a thermal event at around 300 °C is ascribed to the release of the organic ligand together with uptake of O_2, leading to the partial conversion of Pd to PdO. The third and final step corresponds to the decomposition of the remainder of the material to ultimately form PdO.

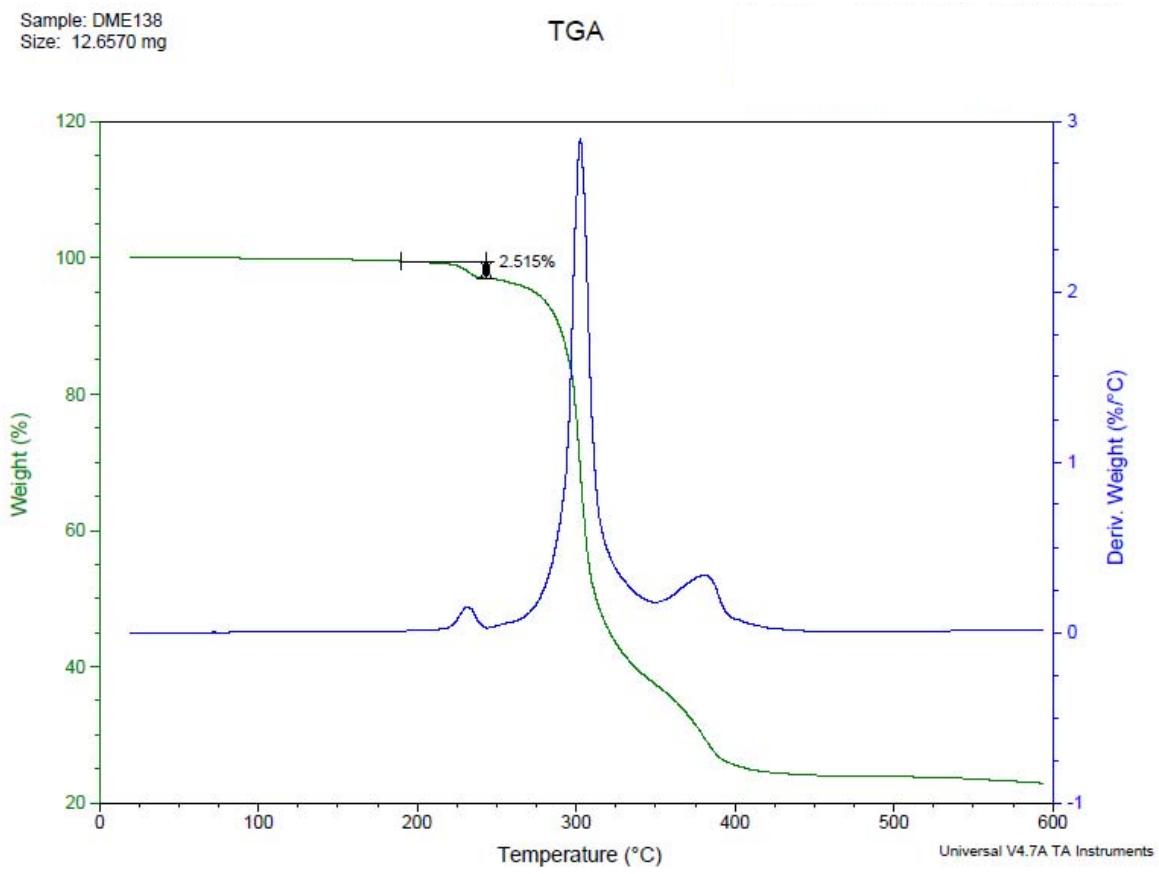

Figure 2-14. TGA curve of complex **C9** crystals.

2.2.4 The preparation of mononuclear, neutral, non-cyclopalladated complexes

Mononuclear, neutral, non-cyclopalladated complexes **C11 – C15** were prepared by the cleavage of the various prepared μ-Cl binuclear cyclopalladated complexes with excess trimethylphosphine (**Scheme 2-8.**).

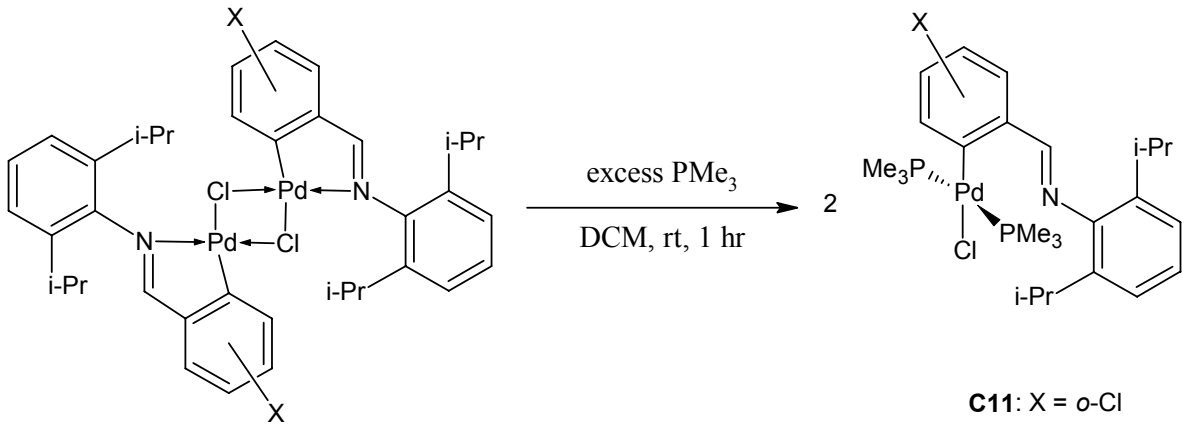

C11: X = *o*-Cl

C12: X = *o*-Br

C13: X = H

C14: X = *o*-Me

C15: X = *p*-Me

Scheme 2-8. Synthetic methodology employed for the preparation of the mononuclear, neutral, non-cyclopalladated complexes.

All compounds were isolated in fairly good yields (59 – 83 %) as light yellow solids that are soluble in polar organic solvents at room temperature. The complexes are stable in solution and in the solid state. Complexes **C11**,[9] **C12**[11] and **C15**[11] have been reported previously whereas **C13** and **C14** are novel.

The mononuclear, neutral, non-cyclopalladated complexes were characterised by a range of analytical techniques similarly to that for the ligands **L1 – L5** (**2.2.1**). The FT-IR spectra of the resulting products indicate the formation of the desired non-cyclopalladated complexes

(for the sake of convenience, this range of complexes (**C11 – C15**) is referred to as the non-cyclopalladated complexes). The absence of the $\nu_{C=N}$ absorption bands corresponding to the μ-Cl binuclear cyclopalladated complex starting materials and the appearance of the $\nu_{C=N}$ absorption bands corresponding to the non-cyclopalladated complex products in the range 1620 – 1627 cm^{-1} provides evidence of the product formation (**Table 2-10.**).

Table 2-10. Analytical data of neutral non-cyclopalladated complexes **C11 – C15**.

Comp.	FT-IR ($\nu_{C=N}$, cm^{-1})[a]	ESI-MS (*m/z*)	Melting point (°C)[e]
C11	1627	593[9, b]	152 - 155
C12	1620	602[11, c]	192 - 196
C13	1620	446[d]	185 - 187
C14	1627	460[d]	189 - 191
C15	1622	537[11, c]	168 - 171

[a] Recorded as neat samples on a ZnSe crystal, employing an ATR accessory. ESI-MS recorded in the positive ion mode. [b] Reported ion corresponds to the proton adduct of the molecular ion, $[M + H]^+$, [c] Reported ion corresponds to $[M - Cl]^+$, [d] Reported ion corresponds to $[M - Cl - (PMe_3)]^+$. [e] Melting points recorded are uncorrected.

The appearance of the $\nu_{C=N}$ absorption bands corresponding to the non-cyclopalladated complex products together with the simultaneous disappearance of the $\nu_{C=N}$ absorption bands corresponding to the μ-Cl binuclear cyclopalladated complex starting materials indicates that the coordinating bond of the imine nitrogen to the palladium metal centre breaks during the cleavage reaction. The range, in wavenumbers, of the $\nu_{C=N}$ bands, which reveals that the double-bond character of the imine increases upon completion of the cleavage reaction, is similar to the range of the $\nu_{C=N}$ bands for the free imines for ligands **L1 – L5**. This similarity

in double-bond character indicates that the compound is no longer subject to the effects of metalloaromaticity and is hence non-cyclopalladated. The coordination site vacated by the imine nitrogen is occupied by another trimethylphosphine molecule.

Electrospray ionisation mass spectrometry, recorded in the positive ion mode, provides further evidence of the product formation (**Table 2-10.**). For complex **C14**, the base peak corresponds to the $[M - Cl - (PMe_3)]^+$ fragment which appears as a cluster of peaks due to the many isotopes of palladium (**Figure 2-15. C**). Minor clusters corresponding to the parent ion **A,** $[M + H]^+$, and the sequential fragmentation ion **B**, $[M - Cl]^+$, appear at much lower intensity (**Scheme 2-9.** and **Figure 2-15.**). Calculated isotopic distributions of the fragments are in good agreement with the sample spectra (**Figure 2-16.** and **2-17.**).

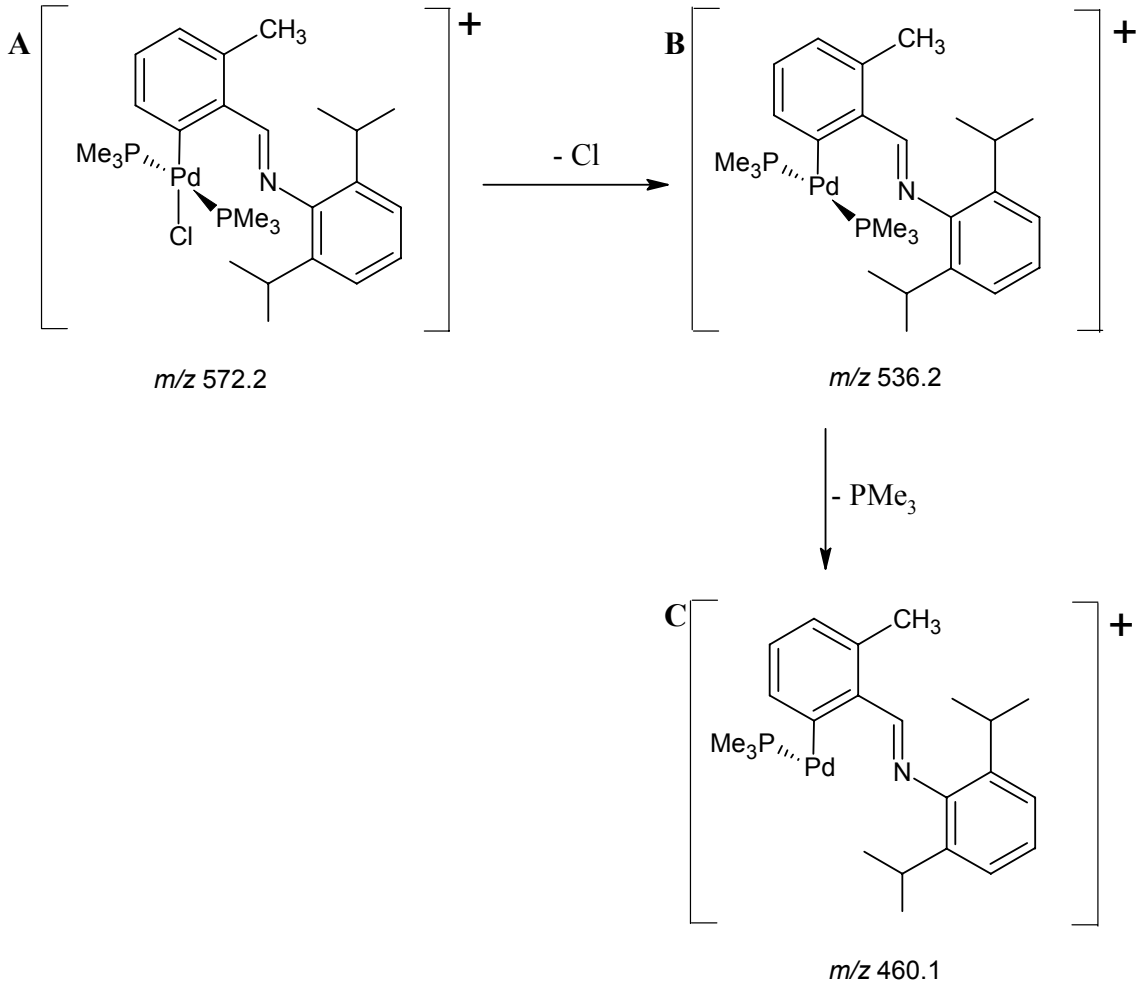

Scheme 2-9. Fragmentation sequence of complex **C14**.

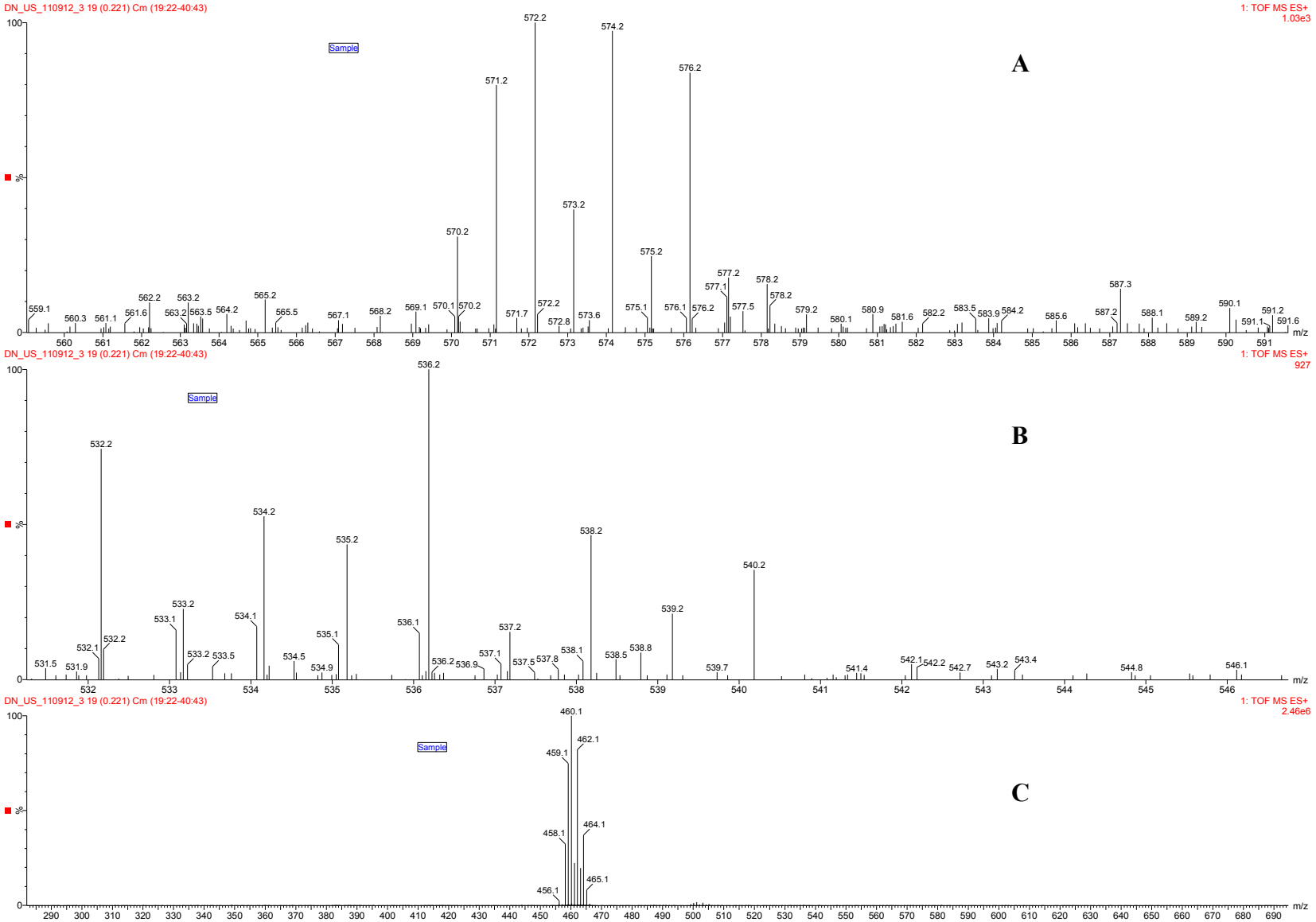

Figure 2-15. Selected regions of the ESI-MS (+) spectrum of complex **C14**. Clusters of peaks centred at *m/z* 572.2 (**A**), *m/z* 536.2 (**B**) and *m/z* 460.1 (**C**) correspond to the $[M + H]^+$, $[M - Cl]^+$ and $[M - Cl - (PMe_3)]^+$ fragments respectively.

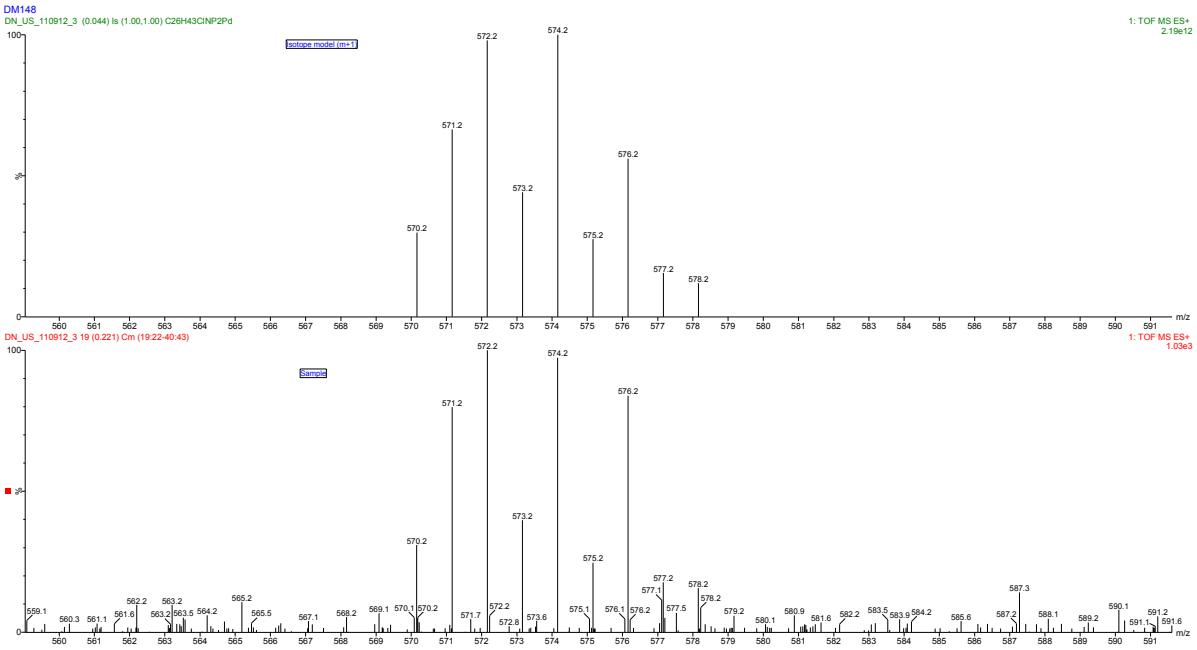

Figure 2-16. Simulated isotopic pattern (above) and the sample spectrum (below) of the parent ion, $[M + H]^+$, of complex **C14**.

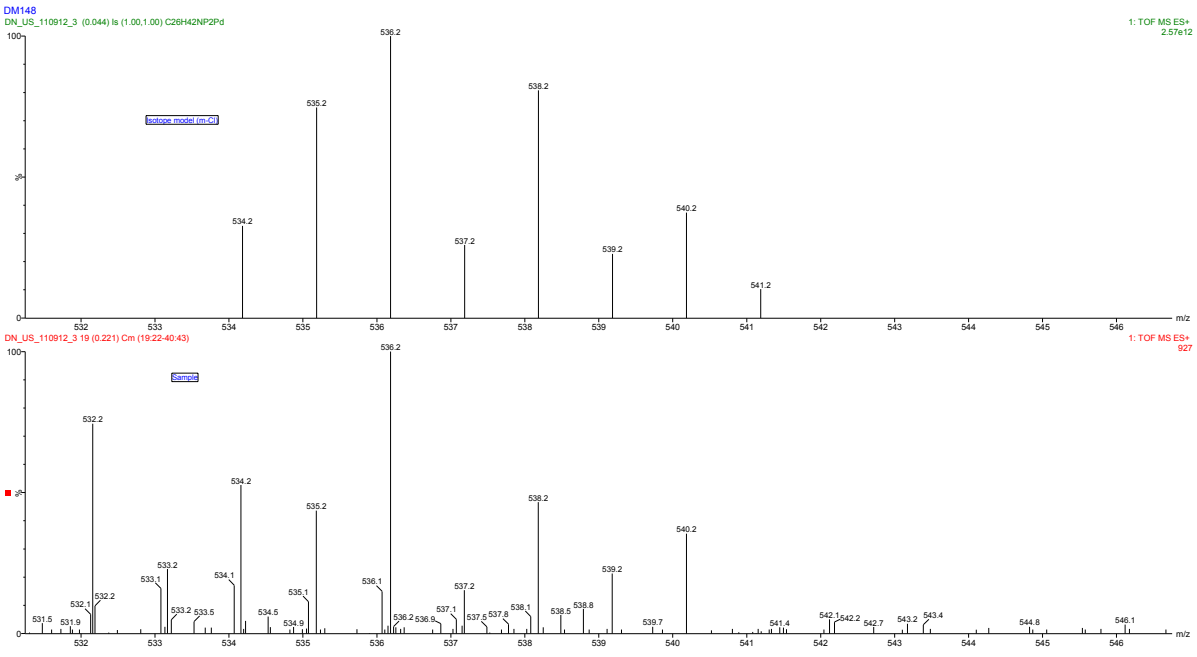

Figure 2-17. Simulated isotopic pattern (above) and the sample spectrum (below) of the $[M - Cl]^+$ fragment of complex **C14**.

The ^{1}H-, ^{13}C {^{1}H}- and ^{31}P {^{1}H}-NMR spectra of the products confirm the formation of the non-cyclopalladated complexes. The appearance of a singlet in the region of δ 8.72 – 8.98 ppm for the imine proton in the ^{1}H-NMR spectra, downfield as compared to the singlet due to the imine proton of the μ-Cl binuclear cyclopalladated complexes, together with the simultaneous disappearance of the latter resonance, is due to the breaking of the coordinating bond of the imine nitrogen to the palladium metal centre.

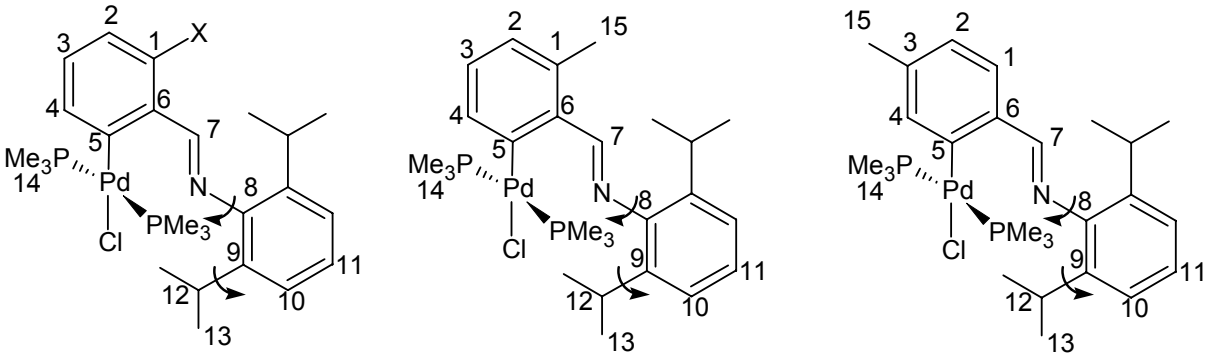

Figure 2-18. Schematic representation of complexes **C11 – C15** with the numbering for NMR spectral analysis.

^{1}H-, ^{13}C {^{1}H}- and ^{31}P {^{1}H}-NMR spectral analysis reveals that the behaviour of the non-cyclopalladated complexes differ from each other in solution at 298 K. For complexes **C11**, **C12** and **C14**, i.e. those that possess a substituent at the *ortho* position, free rotation along the bonds between the palladium and phosphine phosphorous takes place while no rotation takes place along these bonds for complexes **C13** and **C15** (see discussion below). For all complexes, free rotation along the bond between the nitrogen and carbon (8) is restored after the cleavage reaction with excess trimethylphosphine (**Figure 2-18.**). This renders symmetry

(mirror plane) to the entire diisopropyl phenyl moiety, similarly to that for ligands **L1 – L5**. The free rotation along the bond between carbon (9) and carbon (12) is retained.

The resonances due to the protons of complexes **C11**, **C12** and **C14** are relatively broad. This reveals that there is some degree of rotation present which induces fast exchange of the chemical environments of the protons. When the exchange is fast, then the relaxation is fast, resulting in broader peaks in the spectra. This phenomenon is called motional broadening. The free rotation along the bond between the palladium and phosphine phosphorous continuously changes the chemical environment of the protons for these complexes. The resonances generated in the spectra are therefore relatively broad (**Figure 2-24.**). The resonances due to the protons of complexes **C13** and **C15** are sharp and well-defined revealing that no rotation takes place along the bond between the palladium and phosphine phosphorous for these analogues (**Figure 2-23.**). An upfield shift takes place for the resonance due to the methine protons (H^{12}) from a multiplet in the region of δ 3.49 – 3.54 ppm for the μ-Cl binuclear cyclopalladated complexes (**C1 – C5**) to a septet in the region of δ 3.00 – 3.34 ppm for the non-cyclopalladated complexes. The appearance of one doublet in the region of δ 1.16 – 1.21 ppm is due to the twelve isopropyl methyl protons (H^{13}), which reveals their chemical equivalence. This confirms the restoration of the free rotation along the bond between the nitrogen and carbon (8) for all complexes.

The resonance due to the 18 protons of the two trimethylphosphine ligands for complexes **C11**, **C12** and **C14** (H^{14}) is broad. The splitting patterns due to expected hetero-nuclear coupling to the ^{31}P atoms are not clear. For complexes **C13** and **C15** the appearance of a triplet for these protons in the ^{1}H-NMR spectra is due to virtual coupling with the phosphorous nuclei.[19,20] The appearance of a triplet instead of a doublet of doublets for these protons is because the $^{2}J_{P\text{-}P}$ coupling is much larger than the $|^{2}J_{H\text{-}P} - {}^{4}J_{H\text{-}P}|$ coupling. This confirms that the two phosphine ligands are situated *trans* relative to one another. Despite the

fact that this triplet overlaps with the doublet of the isopropyl methyl protons (H^{13}), the coupling is clearly identifiable in the spectra. A variable temperature ^{1}H-NMR spectroscopy experiment was conducted for complex **C12** in order to confirm that the broad resonance at δ 1.16 ppm is due to the protons of the two trimethylphosphine ligands (**Figure 2-19.**).

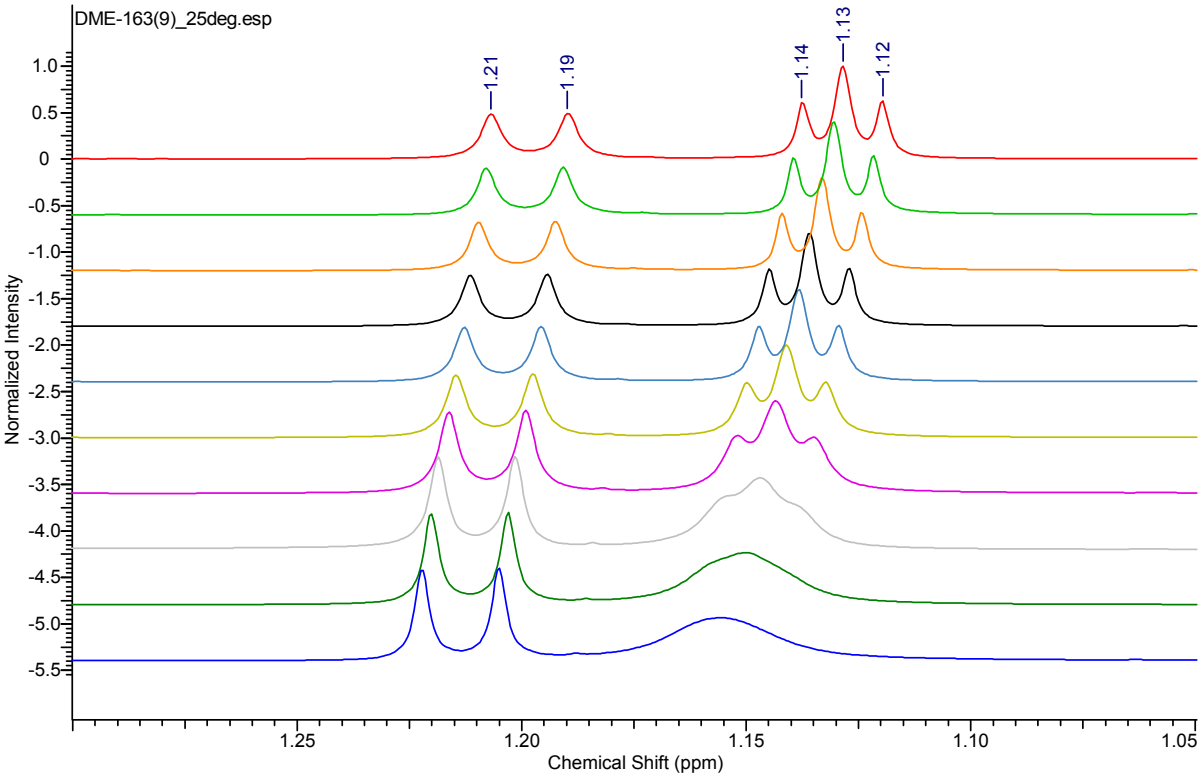

Figure 2-19. ^{1}H-NMR spectra of complex **C12** in the region of δ 1.30 – 1.05 ppm recorded from 25 °C (blue) to -20 °C (red) in increments of 5 °C.

The motional broadening that is present at 25 °C gradually decreases as the temperature decreases. The evolution of a triplet at δ 1.13 ppm at -20 °C from the broad resonance at δ 1.16 ppm at 25 °C confirms that the two trimethylphosphine ligands are situated *trans* relative to one another and that the rotation along the bonds between the palladium and phosphine phosphorous is completely restricted at -20 °C. The $^{2}J_{H\text{-}P}$ coupling constant of 3.51 Hz is similar to that which is present for complexes **C13** and **C15** at 25 °C (**Table 2-12.**).

Virtual coupling of the six carbons (C^{14}) is clearly evident in the ^{13}C {^{1}H}-NMR spectra for complexes **C11**, **C13** and **C14**. The appearance of a distinct triplet in the upfield region of δ 13.42 – 13.52 ppm provides further confirmation of the *trans* arrangement of the trimethylphosphine ligands (**Figure 2-20.**).

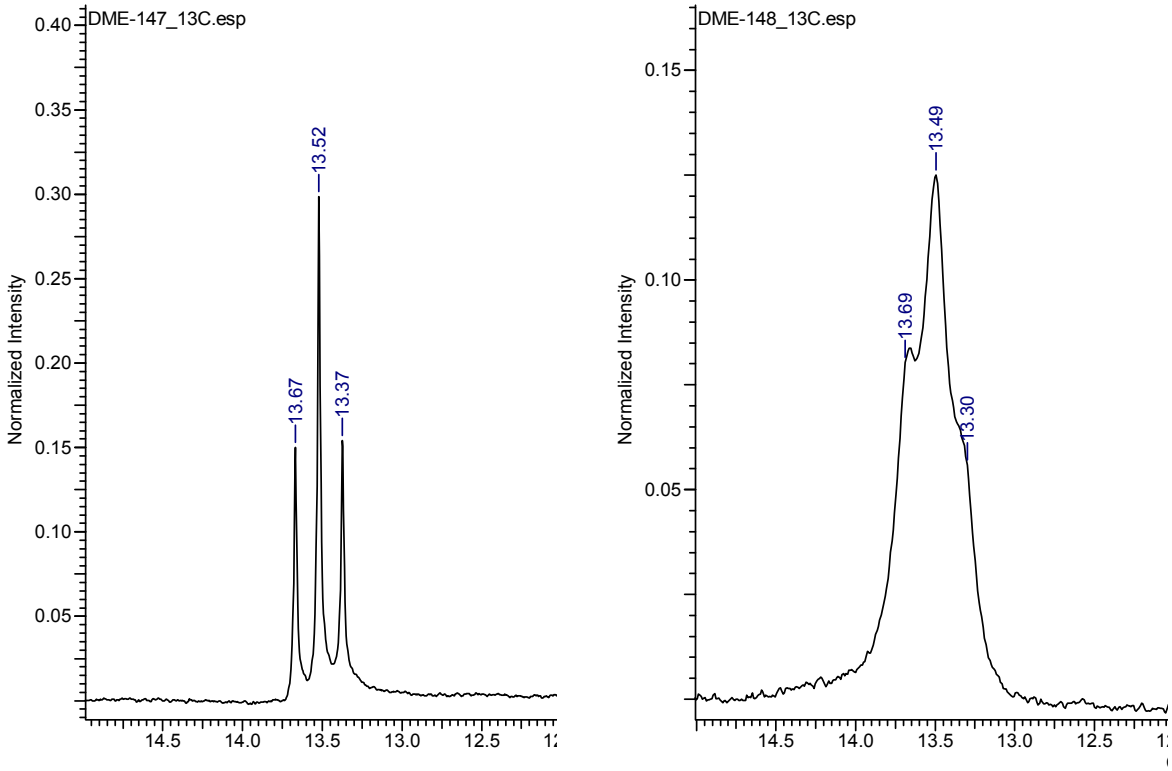

Figure 2-20. ^{13}C {^{1}H}-NMR spectra in the region of δ 15 – 12 ppm of complexes **C13** (left) and **C14** (right). The triplet is due to virtual coupling of the phosphine carbons to the phosphorous nuclei.

The imine carbon [carbon (7)] resonance in the ^{13}C {^{1}H}-NMR spectra appears as a singlet in the downfield region of δ 161.47 – 167.04 ppm. The appearance of this singlet upfield as compared to the singlet due to the imine carbon of the μ-Cl binuclear cyclopalladated complexes reveals once again that the imine carbon is no longer subject to

the effects of metalloaromaticity, hence less deshielded. The chemical shift region of the imine carbon resonances is similar to that of the imine carbon resonances for ligands **L1 – L5**.

A single peak due to the ^{31}P atoms of the two phosphine ligands appears in the region of δ -15.34 and -16.15 ppm in the ^{31}P $\{^{1}H\}$-NMR spectra for all analogues (**Table 2-11.**, **Figure 2-21.** and **Figure 2-22.**). The ^{31}P atom in free trimethylphosphine resonates as a single peak at δ -61.15 ppm. This confirms that the two ^{31}P atoms of the trimethylphosphine ligands are somewhat deshielded when coordinated to the palladium metal centre. Similarly to the resonances for the protons in the ^{1}H-NMR spectra, the peak due to the ^{31}P atoms for complexes **C11**, **C12** and **C14** is relatively broad as compared to that of complexes **C13** and **C15** which has a sharp, well-defined peak.

Table 2-11. ^{31}P $\{^{1}H\}$-NMR spectral data of non-cyclopalladated complexes **C11 – C15**.

Comp.	δ (ppm)[a]
C11	-16.11
C12	-16.15[11]
C13	-15.34
C14	-15.79
C15	-16.01[11]

[a] Spectra recorded in $CDCl_3$ at 298 K.

Due to some expected overlapping of resonances in the aromatic region of the ^{1}H-NMR spectra, the multiplicities of certain resonances are not clear. The clearly distinguishable resonances and coupling constants are assigned (**Table 2-12.**, **Figure 2-23.** and **Figure 2-24.**).

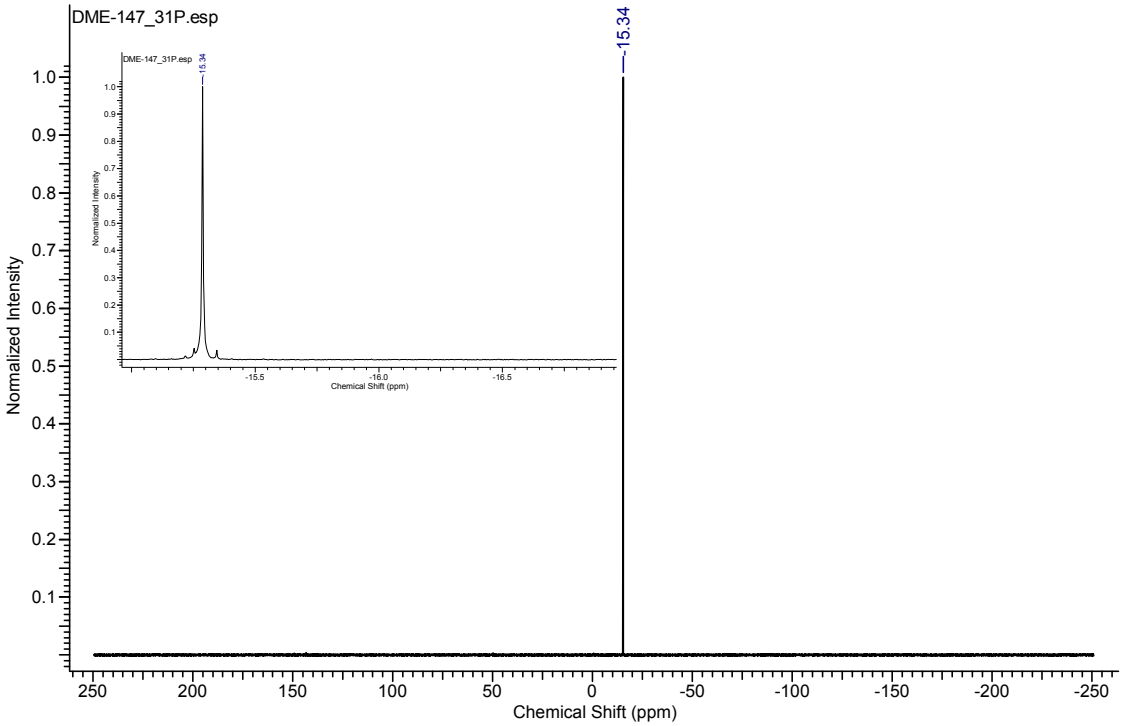

Figure 2-21. ^{31}P $\{^{1}H\}$-NMR spectrum of complex **C13** shown from δ 250 ppm to δ -250 ppm and from δ -15 ppm to δ -17 ppm.

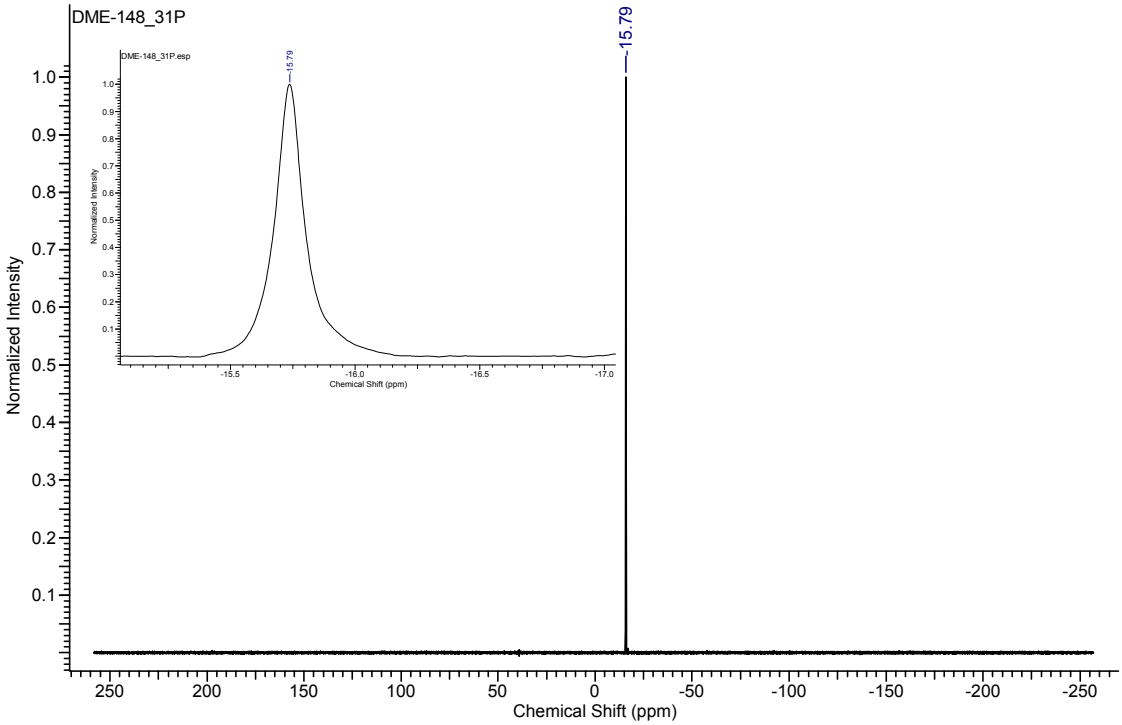

Figure 2-22. ^{31}P $\{^{1}H\}$-NMR spectrum of complex **C14** shown from δ 250 ppm to δ -250 ppm and from δ -15 ppm to δ -17 ppm.

Table 2-12. ^{1}H-NMR spectral data of neutral non-cyclopalladated complexes **C11 – C15**.[a]

Comp.	HC=N	Aromatic region	Aliphatic region			
			HC(CH$_3$)$_2$	ArCH$_3$	HC(CH$_3$)$_2$	P(CH$_3$)$_3$
C11	8.81 (s, 1H, H^{7})	7.55 (d, 1H, H^{2}, $^{3}J_{H-H}$ = 7.4Hz), 7.22 - 7.16 (m, 3H, H^{10,11}), 7.08 - 7.03 (m, 2H, H^{3,4})	3.34 (sep, 2H, H^{12}, $^{3}J_{H-H}$ = 6.8Hz)		1.21 (d, 12H, H^{13}, $^{3}J_{H-H}$ = 6.8Hz)	1.16 (br, 18H, H^{14})
C12	8.74 (s, 1H, H^{7})	7.60 (d, 1H, H^{2}, $^{3}J_{H-H}$ = 7.2Hz), 7.28 - 7.26 (m, 1H, H^{3}), 7.21 - 7.19 (m, 2H, H^{10}), 7.15 - 7.12 (m, 1H, H^{11}), 6.96 - 6.92 (m, 1H, H^{4})	3.34 (sep, 2H, H^{12}, $^{3}J_{H-H}$ = 6.8Hz)		1.21 (d, 12H, H^{13}, $^{3}J_{H-H}$ = 6.8Hz)	1.16 (br, 18H, H^{14})
C13	8.79 (s, 1H, H^{7})	8.12 (d, 1H, H^{1}, $^{3}J_{H-H}$ = 7.4Hz), 7.51 - 7.48 (m, 1H, H^{2}), 7.18 - 7.07 (m, 5H, H^{3,4,10,11})	3.01 (sep, 2H, H^{12}, $^{3}J_{H-H}$ = 6.8Hz)		1.18 (d, 12H, H^{13}, $^{3}J_{H-H}$ = 6.8Hz)	1.17 (t, 18H, H^{14}, $^{2}J_{H-P}$ = 3.5Hz)
C14	8.98 (s, 1H, H^{7})	7.41 (d, 1H, H^{2}, $^{3}J_{H-H}$ = 7.3Hz), 7.19 - 7.08 (m, 3H, H^{10,11}), 6.97 (t, 1H, H^{3}, $^{3}J_{H-H}$ = 7.3Hz), 6.88 - 6.85 (m, 1H, H^{4})	3.13 (sep, 2H, H^{12}, $^{3}J_{H-H}$ = 6.9Hz)	2.63 (s, 3H, H^{15})	1.19 (d, 12H, H^{13}, $^{3}J_{H-H}$ = 6.9Hz)	1.16 (br, 18H, H^{14})
C15	8.72 (s, 1H, H^{7})	7.99 (d, 1H, H^{1}, $^{3}J_{H-H}$ = 7.9Hz), 7.31 (s, 1H, H^{4}), 7.16 - 7.05 (m, 3H, H^{10,11}), 6.88 (d, 1H, H^{2}, $^{3}J_{H-H}$ = 7.9Hz)	3.00 (sep, 2H, H^{12}, $^{3}J_{H-H}$ = 6.9Hz)	2.31 (s, 3H, H^{15})	1.16 (d, 12H, H^{13}, $^{3}J_{H-H}$ = 6.9Hz)	1.16 (t, 18H, H^{14}, $^{2}J_{H-P}$ = 3.5Hz)

[a] Spectra recorded in $CDCl_3$ at 298 K. Chemical shifts reported in δ ppm values, referenced relative to the residual $CDCl_3$ peak. Superscripts denote protons as per numbering scheme (**Figure 2-18.**).

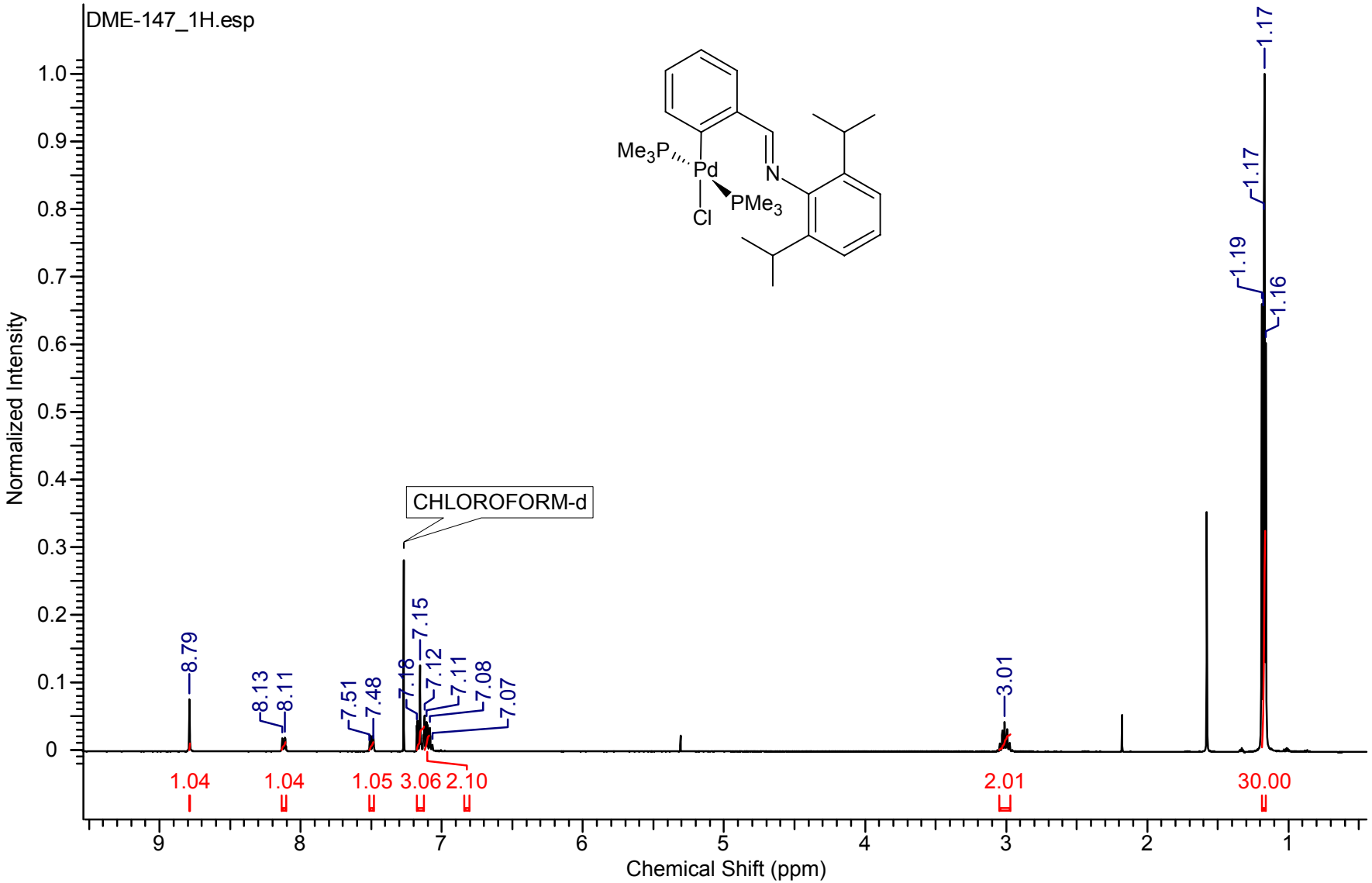

Figure 2-23. ^{1}H-NMR spectrum of complex **C13**.

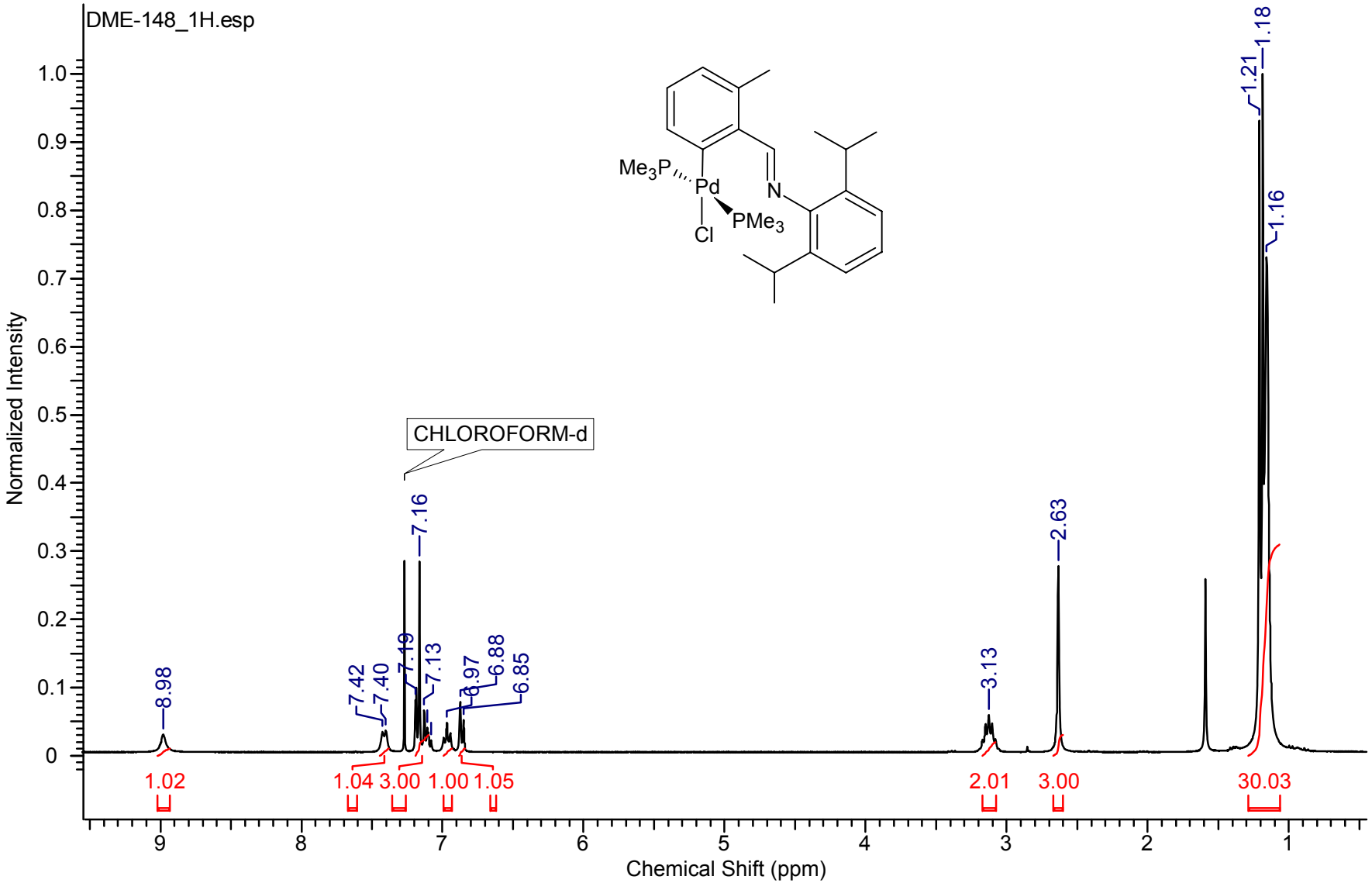

Figure 2-24. ^{1}H-NMR spectrum of complex **C14**.

Crystals suitable for single crystal diffraction analysis were obtained of complex **C14** (**Figure 2-25.**). Recrystallisation by means of slow evaporation from dichloromethane/*n*-pentane at low temperature (-4 °C) resulted in the formation of light yellow single crystals.

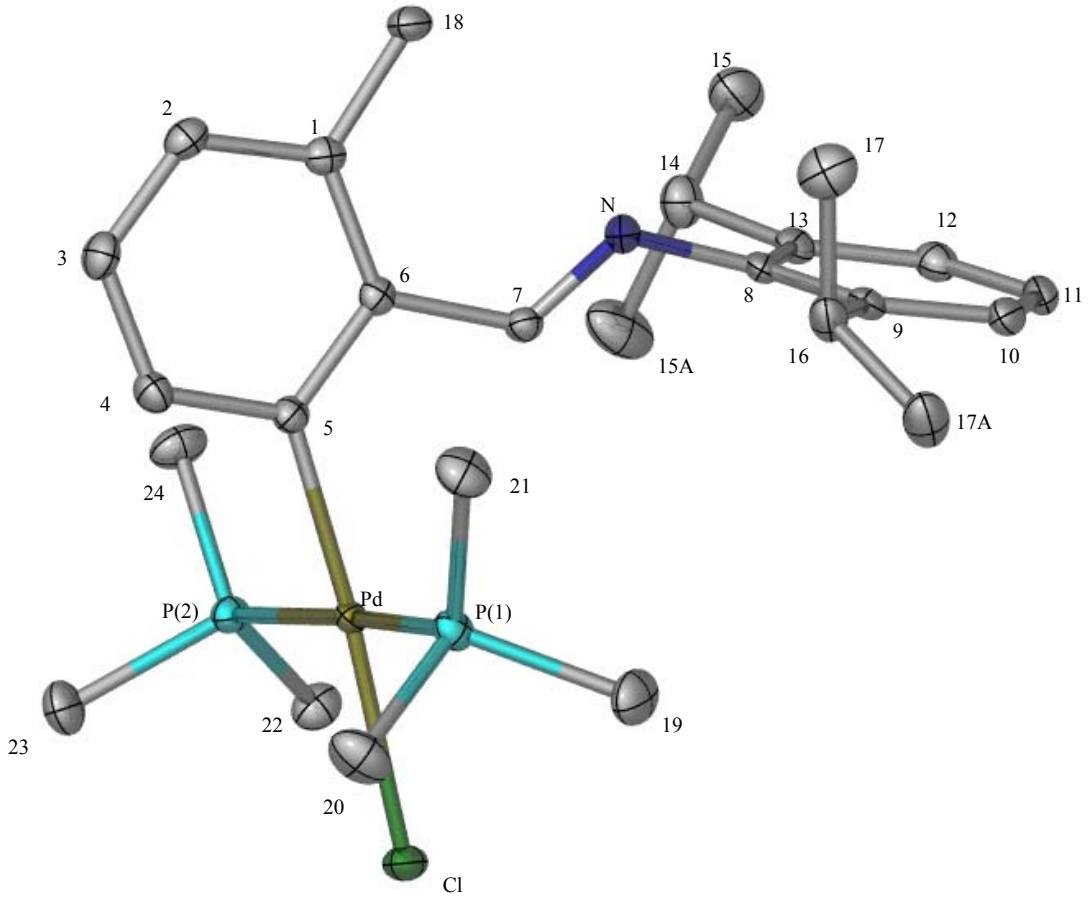

Figure 2-25. Molecular structure of complex **C14** shown with 50 % probability ellipsoids and the numbering scheme (hydrogen atoms are omitted for clarity).

The molecular structure provides unambiguous confirmation of the successful cleavage reaction. Apart from the expected square-planar coordination of the palladium atom, this study reveals that the two trimethylphosphine ligands are situated *trans* to one another, as the chloride is *trans* to the Pd-C bond. Selected bond lengths, bond angles and torsion angles are listed in **Table 2-14.**. The geometry of the palladium atom is only slightly distorted square planar since it is no longer subject to ring strain imposed on it when a member of a five-

membered palladacycle as was the case for complex **C9** (**Figure 2-12.**). This is similar to the previously reported complex **C11** analogue.[9]

A number of weak noncovalent intermolecular interactions are present in the packing arrangement of complex **C14** (**Figure 2-26.**). These include, amongst others, Pd-Cl···H and C-H···C interactions.

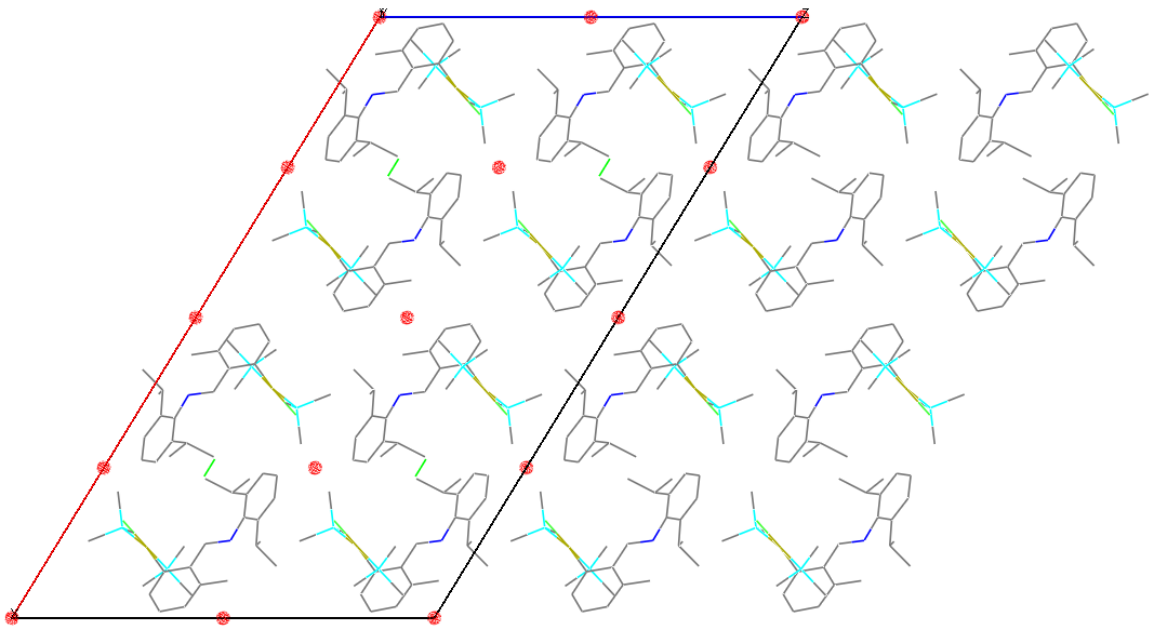

Figure 2-26. Packing diagram of complex **C14** shown along the b-axis. Inversion centres are marked with ● (hydrogen atoms are omitted for clarity).

Table 2-13. Crystallographic data and structure refinement parameters of complex **C14**.

Empirical formula	$C_{26}H_{42}ClNP_2Pd$
M_r (g/mol)	572.40
Crystal system	monoclinic
Space group	*C*2/*c* (No.15)
a (Å)	34.9409 (11)
b (Å)	9.1608 (3)
c (Å)	20.9458 (6)
α (deg)	90
β (deg)	121.46
γ (deg)	90
Volume (Å^3)	5719.2 (3)
Z	8
D_{calc} (g cm^{-3})	1.330
F000	2384
λ (MoK_α) (Å)	0.71073
Temperature (K)	100 (2)
2θ max (deg)	55.8
Lp and absorption corrections applied (μ)	0.868 mm^{-1}
Data/restraints/par.	6230/0/291
R_1 [$I > 2\sigma(I)$]	0.0232
wR_2 (all reflections)	0.0595
Goodness of fit on F^2	1.043
Max/min residual electron density (e Å^{-3})	0.650 / -0.508

Table 2-14. Selected bond lengths, bond angles and torsion angles of the crystallographically determined structures of complex **C14** and **C11**[9]. [a]

	C14	**C11**[9]
	Bond lengths (Å)	
Pd-C(5)	2.014	2.005
Pd-P(1)	2.300	2.300
Pd-P(2)	2.306	2.307
Pd-Cl	2.388	2.383
C(7)-N	1.265	1.265
C(8)-N	1.425	1.421
C(1)-C(18)	1.511	-
	Bond angles (degrees)	
P(1)-Pd-C(5)	91.69	90.71
C(5)-Pd-P(2)	89.01	88.11
P(2)-Pd-Cl	90.69	93.79
Cl-Pd-P(1)	88.21	87.28
	Torsion angles (degrees)	
C(8)-C(13)-C(14)-C(15)	141.33	110.60
C(8)-C(9)-C(16)-C(17)	-82.95	-114.71
C(21)-P(1)-P(2)-C(24)	11.35	43.04

[a] Atom labelling as per numbering scheme (**Figure 2-25.** for complex **C14** and **Figure 2-18.** for complex **C11**).

Despite the fact that for both complexes **C14** and **C11** the imine nitrogen is not coordinated to the palladium metal centre, it is important to note that the orientation of their

imine double-bond is different and should also be taken into consideration when comparing their parameters, including the imine bond length (**Figure 2-27.**).

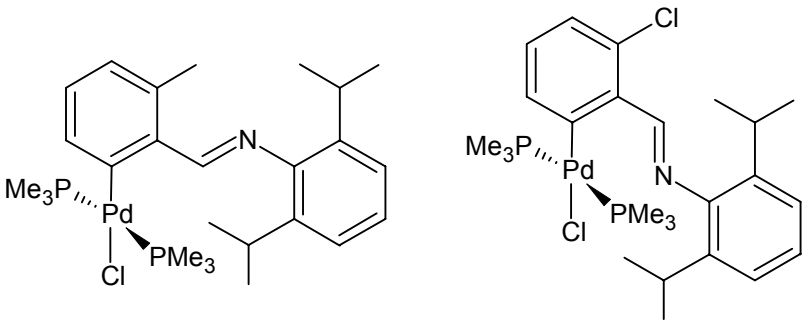

Figure 2-27. The orientation of the imine bond of complex **C14** (left) is different to that of complex **C11** (right) when packed in a crystal.

DFT calculations of complexes **C14** and **C11** confirm that the orientations of the imine double-bond as seen in **Figure 2-27.** are the most stable conformations (**4.2.2.2**).

There is a clear difference in the bond lengths of the imine double-bond when comparing the neutral complexes to the non-cyclopalladated complexes. For complexes **C9** and **C10**, the imine bond length is fairly extended, between 1.284 – 1.289 Å, and for complexes **C14** and **C11** the imine bond length is much shorter, at 1.265 Å, for both. This confirms that the double-bond character of the imine is greater for the non-cyclopalladated complexes as compared to that of the neutral cyclopalladated complexes for which there is some degree of back donation from the palladium metal centre to the imine. These results are in agreement with the conclusions derived from the previously discussed FT-IR spectral analyses.

There are no significant differences with respect to the Pd-C and Pd-Cl bond lengths when comparing complexes **C9** and **C10** to complexes **C14** and **C11**. These bond lengths are influenced by the nature and position of the substituents on the aromatic ring as well as the

nature and number of coordinating phosphine ligands, which are dissimilar. These bond lengths are therefore incomparable.

2.3 Conclusions

The Schiff base condensation, C_{aryl}-H bond activation and the subsequent cleavage reactions are suitable synthetic methodologies for the preparation of Schiff base imine ligands **L1 – L5**, μ-Cl binuclear cyclopalladated complexes **C1 – C5**, mononuclear, neutral, cyclopalladated complexes **C6 – C10** and mononuclear, neutral, non-cyclopalladated complexes **C11 – C15** respectively. The various analytical techniques that were employed to characterise the compounds were successful and complement each other well.

Single crystal X-ray diffraction analysis reveals that the geometry of the palladium atom is distorted square planar when a member of a cyclopalladated system and only slightly distorted square planar when a member of a non-cyclopalladated system.

2.4 Experimental section

2.4.1 General considerations

All reactions were carried out using standard Schlenk techniques under an inert atmosphere of dry nitrogen, unless specified otherwise. All solvents were dried using the appropriate drying agents and distilled before using.

Elemental analyses were carried out on a Thermo Elemental Analyser CHNS-O instrument at the University of Cape Town, Department of Chemistry and on a Vario-Elementar Microcube ELIII at Rhodes University, Department of Chemistry. ^{1}H- (299.74 and

399.94 MHz), ^{13}C {^{1}H}- (75.38 and 100.58 MHz) and ^{31}P {^{1}H}- (121.34 and 161.90 MHz) NMR spectra were recorded at 298 K on Varian VNMRS 300 MHz and Varian Unity Inova 400 MHz spectrometers. The chemical shift values are referenced to external tetramethylsilane. Chemical shifts (δ) and coupling constants (*J*) are expressed in ppm and in Hertz (Hz) respectively and the multiplicity as s = singlet, d = doublet, dd = doublet of doublets, t = triplet, sep = septet and m = multiplet; data in parentheses are given in the following order: multiplicity, number of atoms, labelling of the atom(s) (',' denotes 'and'; '/' denotes 'or') and coupling constants in Hz. ESI-MS analyses, in the positive ion mode, were performed on a Waters Synapt G2 instrument by direct injection of the sample. FT-IR analyses were performed on a Thermo Nicolet AVATAR 330, SMART PERFORMER, spectrometer and recorded as neat samples (ATR). Melting point determinations were performed on a Stuart Scientific, SMP3, melting point apparatus and are reported as uncorrected. Single crystal X-ray diffraction data collections were carried out on a Bruker Apex2 diffractometer with a CCD area detector[21] using graphite monochromated Mo-Kα radiation (λ = 0.71073 Å). The instrument is equipped with an Oxford Cryostream cooling system and the datasets for complexes **C9** and **C14** were collected at temperatures of 103 K and 100 K respectively. Data reduction was carried out by means of a standard procedure using the Bruker software package SAINT.[22] Absorption corrections and other systematic errors were accounted for where necessary using SADABS.[23] The structures were solved by Direct Methods or Patterson Interpretation using SHELXS-97 and refined using SHELXL-97.[24] X-Seed[25] was used as a graphical interface for the SHELX program suite to facilitate in exploring and analysing the structures. The POV-Ray[26] application using X-Seed was used to produce high quality molecular graphics. Due to their low scattering power it is difficult to locate hydrogen atoms using X-ray diffraction data. Hydrogen atoms were placed in calculated positions using riding models and isotropic thermal parameters were assigned.

All the employed aromatic aldehydes, diisopropyl aniline (both Sigma-Aldrich), anhydrous magnesium sulphate and anhydrous sodium acetate (both Merck), and triphenylphosphine and trimethylphosphine (1M in THF solution), (both Fluka, Sigma-Aldrich) were used as received. *bis*(acetonitrile) dichloropalladium(II) was prepared by reflux of $PdCl_2$ in excess acetonitrile for three hours, followed by filtration and drying.[27]

2.4.2 Synthetic methodology employed for the preparation of the monofunctional Schiff base imine ligands L1 – L5

General procedure for the synthesis of the monofunctional Schiff base imine ligands

The mono-substituted aromatic aldehyde (5.296 mmol) was added to a stirring solution of 2,6-diisopropylaniline (1 ml, 5.296 mmol) in ethanol (10 ml). The resulting yellow solution was stirred for 24 hrs at room temperature. The solvent was then removed and the remaining oily residue was redissolved in dichloromethane (20 ml) and then washed with H_2O (5 x 20 ml portions). The organic layer was dried over anhydrous magnesium sulphate, filtered and the solvent removed. Recrystallisation from cold methanol resulted in the isolation of bright yellow crystals.

(2-chlorophenyl-2,6-diisopropylphenyl) imine (**L1**)

Yield: 69 %.

Anal. Calcd for $C_{19}H_{22}ClN$:[11] C, 76.11; H, 7.40; N, 4.76. Found: C, 76.05; H, 7.35; N, 4.63.

^{13}C {^{1}H}-NMR (100 MHz, numbering as per **Figure 2-4.**):[11] δ 159.2 (C^{7}), 149.1 (C_{Ar}), 137.6 (C_{Ar}), 135.9 (C_{Ar}), 133.2 (C_{Ar}), 132.2 (C_{Ar}), 129.9 (C_{Ar}), 128.4 (C_{Ar}), 127.2 (C_{Ar}), 124.4 (C_{Ar}), 123.1 (C_{Ar}), 27.9 (C^{12}), 23.5 (C^{13}).

(2-bromophenyl-2,6-diisopropylphenyl) imine (L2)

Yield: 83 %.

Anal. Calcd for $C_{19}H_{22}BrN$:[11] C, 66.28; H, 6.44; N, 4.07. Found: C, 66.23; H, 6.41; N, 4.02.

^{13}C {^{1}H}-NMR (100 MHz, numbering as per **Figure 2-4.**):[11] δ 161.4 (C^{7}), 148.9 (C_{Ar}), 137.6 (C_{Ar}), 134.6 (C_{Ar}), 133.2 (C_{Ar}), 132.4 (C_{Ar}), 128.8 (C_{Ar}), 127.8 (C_{Ar}), 125.7 (C_{Ar}), 124.4 (C_{Ar}), 123.1 (C_{Ar}), 27.9 (C^{12}), 23.5 (C^{13}).

(phenyl-2,6-diisopropylphenyl) imine (L3)

Yield: 81 %.

Anal. Calcd for $C_{19}H_{23}N$:[11] C, 85.99; H, 8.74; N, 5.28. Found: C, 85.92; H, 8.70; N, 5.20.

^{13}C {^{1}H}-NMR (100 MHz, numbering as per **Figure 2-4.**):[11] δ 160.2 (C^{7}), 147.5 (C_{Ar}), 138.3 (C_{Ar}), 133.8 (C_{Ar}), 131.1 (C_{Ar}), 129.2 (C_{Ar}), 128.9 (C_{Ar}), 126.7 (C_{Ar}), 124.7 (C_{Ar}), 27.96 (C^{12}), 23.45 (C^{13}).

(2-methylphenyl-2,6-diisopropylphenyl) imine (L4)

Yield: 96 %.

Anal. Calcd for $C_{20}H_{25}N$: C, 85.97; H, 9.02; N, 5.01. Found: C, 85.91; H, 9.96; N, 5.02.

^{13}C {^{1}H}-NMR (75 MHz, numbering as per **Figure 2-4.**): δ 160.99 (C^{7}), 149.73 (C_{Ar}), 138.34 (C_{Ar}), 137.60 (C_{Ar}), 134.02 (C_{Ar}), 131.03 (C_{Ar}), 130.97 (C_{Ar}), 127.77 (C_{Ar}), 126.40 (C_{Ar}), 124.05 (C_{Ar}), 123.00 (C_{Ar}), 27.88 (C^{12}), 23.53 (C^{13}), 19.41 (C^{14}).

(4-methylphenyl-2,6-diisopropylphenyl) imine (L5)

Yield: 82 %.

Anal. Calcd for $C_{20}H_{25}N$:[11] C, 85.97; H, 9.02; N, 5.01. Found: C, 85.90; H, 9.01; N, 4.96.

^{13}C {^{1}H}-NMR (100 MHz, numbering as per **Figure 2-4.**):[11] δ 162.2 (C^{7}), 148.7 (C_{Ar}), 142.3 (C_{Ar}), 137.9 (C_{Ar}), 133.0 (C_{Ar}), 129.6 (C_{Ar}), 128.8 (C_{Ar}), 124.3 (C_{Ar}), 123.3 (C_{Ar}), 27.9 (C^{12}), 23.5 (C^{13}), 21.6 (C^{14}).

2.4.3 Synthetic methodology employed for the preparation of the *μ*-Cl binuclear cyclopalladated complexes C1 – C5

General procedure for the synthesis of the *μ*-Cl binuclear cyclopalladated complexes

The Schiff base imine ligand (0.3855 mmol) was added to a stirring solution of *bis*(acetonitrile) dichloropalladium(II) (100 mg, 0.3855 mmol) and sodium acetate (63.24 mg, 0.7709 mmol) in dichloromethane (10 ml). The resulting dark red solution was stirred for 19 - 21 hrs at room temperature. The resulting light yellow solution was then filtered through celite and the solvent was then removed from the filtrate. The product was isolated, by triturating with *n*-hexane, as a light yellow solid.

[PdCl(2-ClC$_6$H$_3$)CH=N-{2,6-(*i*-Pr)$_2$-C$_6$H$_3$}]$_2$ (C1)

Yield: 74 %.

^{13}C {^{1}H}-NMR (75 MHz, numbering as per **Figure 2-6.**):[11] δ 174.75 (C^7), 156.38 (C$_{Ar}$), 142.88 (C$_{Ar}$), 141.40 (C$_{Ar}$), 133.82 (C$_{Ar}$), 132.25 (C$_{Ar}$), 130.52 (C$_{Ar}$), 128.04 (C$_{Ar}$), 127.97 (C$_{Ar}$), 124.89 (C$_{Ar}$), 123.35 (C$_{Ar}$), 28.28 (C^{14,16}), 24.48 and 22.94 (C^{15,17}).

[PdCl(2-BrC$_6$H$_3$)CH=N-{2,6-(*i*-Pr)$_2$-C$_6$H$_3$}]$_2$ (C2)

Yield: 76 %.

^{13}C {^{1}H}-NMR (75 MHz, numbering as per **Figure 2-6.**):[11] δ 174.15 (C^7), 156.89 (C$_{Ar}$), 142.56 (C$_{Ar}$), 141.35 (C$_{Ar}$), 133.85 (C$_{Ar}$), 132.45 (C$_{Ar}$), 130.62 (C$_{Ar}$), 128.35 (C$_{Ar}$), 127.95 (C$_{Ar}$), 124.73 (C$_{Ar}$), 123.30 (C$_{Ar}$), 28.25 (C^{14,16}), 24.49 and 22.90 (C^{15,17}).

[PdCl(C$_6$H$_4$)CH=N-{2,6-(*i*-Pr)$_2$-C$_6$H$_3$}]$_2$ (C3)

Yield: 87 %.

^{13}C {^{1}H}-NMR (75 MHz, numbering as per **Figure 2-6.**):[11] δ 176.21 (C^7), 155.43 (C$_{Ar}$), 145.67 (C$_{Ar}$), 141.48 (C$_{Ar}$), 133.90 (C$_{Ar}$), 132.56 (C$_{Ar}$), 130.86 (C$_{Ar}$), 128.29 (C$_{Ar}$), 127.74 (C$_{Ar}$), 124.68 (C$_{Ar}$), 123.23 (C$_{Ar}$), 28.19 (C^{14,16}), 24.45 and 22.99 (C^{15,17}).

[PdCl(2-CH$_3$C$_6$H$_3$)CH=N-{2,6-(*i*-Pr)$_2$-C$_6$H$_3$}]$_2$ (C4)

Yield: 86 %.

^{13}C $\{^{1}H\}$-NMR (100 MHz, numbering as per **Figure 2-6.**): δ 174.17 (C^{7}), 158.84 (C_{Ar}), 143.95 (C_{Ar}), 141.59 (C_{Ar}), 138.37 (C_{Ar}), 131.80 (C_{Ar}), 131.53 (C_{Ar}), 127.76 (C_{Ar}), 121.71 (C_{Ar}), 126.50 (C_{Ar}), 123.26 (C_{Ar}), 123.00 (C_{Ar}), 28.13 ($C^{14,16}$), 24.56 and 22.97 ($C^{15,17}$) 19.85 (C^{18}).

[PdCl(4-$CH_3C_6H_3$)CH=N-{2,6-(*i*-Pr)$_2$-C_6H_3}]$_2$ (C5)

Yield: 74 %.

^{13}C $\{^{1}H\}$-NMR (100 MHz, numbering as per **Figure 2-6.**):[11] δ 176.18 (C^{7}), 155.43 (C_{Ar}), 145.67 (C_{Ar}), 141.47 (C_{Ar}), 133.91 (C_{Ar}), 132.69 (C_{Ar}), 130.87 (C_{Ar}), 128.31 (C_{Ar}), 127.88 (C_{Ar}), 124.68 (C_{Ar}), 123.24 (C_{Ar}), 28.20 ($C^{14,16}$), 23.01 and 22.91 ($C^{15,17}$) , 22.46 (C^{18}).

2.4.4 Synthetic methodology employed for the preparation of the neutral cyclopalladated complexes C6 – C10

General procedure for the synthesis of the neutral cyclopalladated complexes

The μ-Cl binuclear cyclopalladated complex (0.1135 mmol) was added to a stirring solution of triphenylphosphine (59.52 mg, 0.2269 mmol) in dichloromethane (10 ml). The resulting yellow solution was stirred for 1 hr at room temperature. The solvent was then removed and the product was isolated, by triturating with diethyl ether, as a very light yellow solid. Recrystallisation of complex **C9** was achieved by means of slow evaporation from dichloromethane/*n*-pentane at low temperature (-4 °C).

$PdClPPh_3(2\text{-}ClC_6H_3)CH{=}N\text{-}\{2,6\text{-}(i\text{-}Pr)_2\text{-}C_6H_3\}$ (C6)

Yield: 79 %.

Anal. Calcd for $C_{37}H_{36}Cl_2NPPd$:[11] C, 63.22; H, 5.16; N, 1.99. Found: C, 63.18; H, 5.11; N, 1.92.

^{13}C $\{^1H\}$-NMR (75 MHz, numbering as per **Figure 2-9.**):[11] δ 175.58 (C^7), 160.21 (C_{Ar}), 145.81 (C_{Ar}), 141.05 (C_{Ar}), 140.38 (C_{Ar}), 138.14 (C_{Ar}), 135.04 (C_{Ar}), 134.96 (C_{Ar}), 130.76 (C_{Ar}), 130.71 (C_{Ar}), 128.22 (C_{Ar}), 128.03 (C_{Ar}), 127.19 (C_{Ar}), 124.12 (C_{Ar}), 122.86 (C_{Ar}), 28.64 ($C^{14,16}$), 24.56 and 22.97 ($C^{15,17}$).

$PdClPPh_3(2\text{-}BrC_6H_3)CH{=}N\text{-}\{2,6\text{-}(i\text{-}Pr)_2\text{-}C_6H_3\}$ (C7)

Yield: 68 %.

Anal. Calcd for $C_{37}H_{36}BrClNPPd$:[11] C, 59.46; H, 4.85; N, 1.87. Found: C, 59.40; H, 4.82; N, 1.80.

^{13}C $\{^1H\}$-NMR (75 MHz, numbering as per **Figure 2-9.**):[11] δ 177.70 (C^7), 160.69 (C_{Ar}), 145.92 (C_{Ar}), 141.23 (C_{Ar}), 140.74 (C_{Ar}), 137.27 (C_{Ar}), 135.04 (C_{Ar}), 134.96 (C_{Ar}), 130.84 (C_{Ar}), 130.49 (C_{Ar}), 128.29 (C_{Ar}), 128.01 (C_{Ar}), 127.13 (C_{Ar}), 124.38 (C_{Ar}), 122.13 (C_{Ar}), 28.65 ($C^{14,16}$), 24.58 and 22.96 ($C^{15,17}$).

$PdClPPh_3(C_6H_4)CH{=}N\text{-}\{2,6\text{-}(i\text{-}Pr)_2\text{-}C_6H_3\}$ (C8)

Yield: 91%.

Anal. Calcd for $C_{37}H_{37}ClNPPd$:[11] C, 66.47; H, 5.58; N, 2.10. Found: C, 66.42; H, 5.54; N, 2.04.

^{13}C {^{1}H}-NMR (75 MHz, numbering as per **Figure 2-9.**):[11] δ 177.03 (C^{7}), 159.54 (C_{Ar}), 145.15 (C_{Ar}), 141.48 (C_{Ar}), 140.80 (C_{Ar}), 138.20 (C_{Ar}), 135.41 (C_{Ar}), 135.04 (C_{Ar}), 131.68 (C_{Ar}), 130.83 (C_{Ar}), 130.56 (C_{Ar}), 128.84 (C_{Ar}), 127.92 (C_{Ar}), 126.88 (C_{Ar}), 124.09 (C_{Ar}), 122.77 (C_{Ar}), 28.64 ($C^{14,16}$), 24.51 and 23.02 ($C^{15,17}$).

$PdClPPh_3(2\text{-}CH_3C_6H_3)CH{=}N\text{-}\{2,6\text{-}(i\text{-}Pr)_2\text{-}C_6H_3\}$ (C9)

Yield: 84 %.

Anal. Calcd for $C_{38}H_{39}ClNPPd$: C, 66.87; H, 5.76; N, 2.05. Found: C, 66.93; H, 6.60; N, 2.04.

^{13}C {^{1}H}-NMR (75 MHz, numbering as per **Figure 2-9.**): δ 174.83 (d, C^{7}, $^{3}J_{C\text{-}P}$ = 4.5 Hz), 161.02 (C_{Ar}), 145.83 (C_{Ar}), 145.59 (C_{Ar}), 140.90 (C_{Ar}), 138.68 (C_{Ar}), 136.21 (C_{Ar}), 135.34 (C_{Ar}), 135.18 (C_{Ar}), 131.53 (C_{Ar}), 130.87 (C_{Ar}), 130.49 (C_{Ar}), 128.06 (C_{Ar}), 127.92 (C_{Ar}), 126.87 (C_{Ar}), 126.23 (C_{Ar}), 122.79 (C_{Ar}), 28.50 ($C^{14,16}$), 24.62 and 22.99 ($C^{15,17}$), 20.49 (C^{18}).

$PdClPPh_3(4\text{-}CH_3C_6H_3)CH{=}N\text{-}\{2,6\text{-}(i\text{-}Pr)_2\text{-}C_6H_3\}$ (C10)

Yield: 89 %.

Anal. Calcd for $C_{38}H_{39}ClNPPd$:[11] C, 66.87; H, 5.76; N, 2.05. Found: C, 66.85; H, 5.72; N, 2.00.

^{13}C {^{1}H}-NMR (75 MHz, numbering as per **Figure 2-9.**):[11] δ 176.44 (C^{7}), 159.27 (C_{Ar}), 145.15 (C_{Ar}), 141.61 (C_{Ar}), 140.94 (C_{Ar}), 138.81 (C_{Ar}), 135.28 (C_{Ar}), 135.03 (C_{Ar}), 131.57

(C_{Ar}), 130.50 (C_{Ar}), 128.71 (C_{Ar}), 128.06 (C_{Ar}), 126.78 (C_{Ar}), 124.78 (C_{Ar}), 122.73 (C_{Ar}), 28.55 ($C^{14,16}$), 24.52 and 22.98 ($C^{15,17}$), 21.94 (C^{18}).

2.4.5 Synthetic methodology employed for the preparation of the neutral non-cyclopalladated complexes C11 – C15

General procedure for the synthesis of the neutral non-cyclopalladated complexes

The μ-Cl binuclear cyclopalladated complex (0.125 mmol) was added to a stirring solution of trimethylphosphine (1M in THF solution) (0.5 ml, 0.5 mmol) in dichloromethane (5 ml). The resulting yellow solution was stirred for 1 hr at room temperature. The solvent was then removed and the product was isolated, by triturating with diethyl ether, as a very light yellow solid. Recrystallisation of complex **C14** was achieved by means of slow evaporation from dichloromethane/*n*-pentane at low temperature (-4 °C).

$PdCl(PMe_3)_2(2\text{-}ClC_6H_3)CH{=}N\text{-}\{2,6\text{-}(i\text{-}Pr)_2\text{-}C_6H_3\}$ (C11)

Yield: 82 %.

^{13}C $\{^1H\}$-NMR (75 MHz, numbering as per **Figure 2-18.**): δ 164.02 (C^7), 160.20 (C_{Ar}), 148.88 (C_{Ar}), 138.25 (C_{Ar}), 136.82 (C_{Ar}), 136.06 (C_{Ar}), 134.97 (C_{Ar}), 129.32 (C_{Ar}), 124.55 (C_{Ar}), 124.26 (C_{Ar}), 123.28 (C_{Ar}), 27.71 (C^{12}), 24.67 (C^{13}) and 13.42 (t, C^{14}, $^1J_{C\text{-}P}$ = 14.0 Hz).

PdCl(PMe$_3$)$_2$ (2-BrC$_6$H$_3$)CH=N-{2,6-(*i*-Pr)$_2$-C$_6$H$_3$} (C12)

Yield: 76 %.

Anal. Calcd for $C_{25}H_{39}BrClNP_2Pd$:[11] C, 47.11; H, 6.17; N, 2.20. Found: C, 47.02; H, 5.99; N, 2.05.

^{13}C {^{1}H}-NMR (100 MHz, numbering as per **Figure 2-18.**):[11] δ 161.47 (C^7), 148.87 (C_{Ar}), 140.71 (C_{Ar}), 135.57 (C_{Ar}), 133.19 (C_{Ar}), 132.43 (C_{Ar}), 128.80 (C_{Ar}), 127.78 (C_{Ar}), 125.74 (C_{Ar}), 124.37 (C_{Ar}), 123.05 (C_{Ar}), 27.92 (C^{12}), 24.76 (C^{13}) and 13.46 (C^{14}).

PdCl(PMe$_3$)$_2$ (C$_6$H$_4$)CH=N-{2,6-(*i*-Pr)$_2$-C$_6$H$_3$} (C13)

Yield: 83 %.

^{13}C {^{1}H}-NMR (100 MHz, numbering as per **Figure 2-18.**): δ 165.83 (C^7), 160.61 (C_{Ar}), 149.21 (C_{Ar}), 140.26 (C_{Ar}), 136.93 (C_{Ar}), 135.29 (C_{Ar}), 129.79 (C_{Ar}), 127.58 (C_{Ar}), 123.81 (C_{Ar}), 123.46 (C_{Ar}), 122.94 (C_{Ar}), 27.87 (C^{12}), 23.39 (C^{13}) and 13.52 (t, C^{14}, $^1J_{C\text{-}P}$ = 14.7 Hz).

PdCl(PMe$_3$)$_2$ (2-CH$_3$C$_6$H$_3$)CH=N-{2,6-(*i*-Pr)$_2$-C$_6$H$_3$} (C14)

Yield: 67 %.

^{13}C {^{1}H}-NMR (75 MHz, numbering as per **Figure 2-18.**): δ 167.04 (C^7), 161.27 (C_{Ar}), 140.29 (C_{Ar}), 136.89 (C_{Ar}), 133.10 (C_{Ar}), 128.19 (C_{Ar}), 126.70 (C_{Ar}), 123.69 (C_{Ar}), 122.96 (C_{Ar}), 27.84 (C^{12}), 23.75 (C^{13}), 22.82 (C^{15}) and 13.49 (t, C^{14}, $^1J_{C\text{-}P}$ = 14.6 Hz).

$PdCl(PMe_3)_2$ (4-$CH_3C_6H_3$)CH=N-{2,6-(*i*-$Pr)_2$-C_6H_3} (C15)

Yield: 59 %.

Anal. Calcd for $C_{26}H_{42}ClNP_2Pd$:[11] C, 54.55; H, 7.40; N, 2.45. Found: C, 54.33; H, 7.29; N, 2.29.

^{13}C {^1H}-NMR (100 MHz, numbering as per **Figure 2-18.**):[11] δ 162.32 (C^7), 148.64 (C_{Ar}), 142.46 (C_{Ar}), 138.10 (C_{Ar}), 133.14 (C_{Ar}), 129.62 (C_{Ar}), 128.73 (C_{Ar}), 124.28 (C_{Ar}), 123.42 (C_{Ar}), 27.83 (C^{12}), 23.59 (C^{13}), 21.64 (C^{15}) and 13.42 (C^{14}).

References

1. H. Schiff, *Ann. Suppl.*, 1864, **3**, 343.
2. M. J. O'Connor, R. E. Ernst and R. H. Holm, *J. Am. Chem. Soc*., 1968, **90**, 4561.
3. C. M. Che and J. S. Huang, *Coord. Chem. Rev*., 2003, **242**, 97.
4. E. M. Carreira, R. A. Singer and W. Lee, *J. Am. Chem. Soc*., 1994, **116**, 8837.
5. H. Suga, T. Fudo and T. Ibata, *Synlett*., 1998, **8**, 933.
6. M. Matsumuto and K. Kuroda, *Tetrahedron Lett*., 1981, **22**, 4437.
7. K. C. Gupta and A. K. Sutar, *Coord. Chem. Rev*., 2008, **252**, 1420.
8. D. Vázquez-García, A. Fernández, M. López-Torres, A. Rodríguez, N. Gómez-Blanco, C. Viader, J. M. Vila and J. J. Fernández, *Organometallics*, 2010, **29**, 3303.

9. N. Mungwe, The Synthesis of the Cyclometallated Palladium Complexes and their Applications in Olefin Oligomerisation and in Phenylacetylene Oligomerisation/ Polymerisation, *M.Sc. Thesis*, University of the Western Cape, 2007.

10. C. L. Chen, Y. H. Liu, S. M. Peng and S. T. Liu, *J. Organomet. Chem.*, 2004, **689**, 1806.

11. A. J. Swarts, Mononuclear and Multinuclear Palladacycles as Catalyst Precursors, *M.Sc. Thesis*, Stellenbosch University, 2011.

12. G. J. P. Britovsek, S. Mastroianni, G. A. Solan, S. P. D. Baugh, C. Redshaw, V. C. Gibson, A. J. P. White, D. J. Williams and M. R. J. Elsegood, *Chem. Eur. J.*, 2000, **6**, 2221.

13. G. J. P. Britovsek, V. C. Gibson and D. F. Wass, *Angew. Chem. Int. Ed.*, 1999, **38**, 428.

14. S. D. Ittel, L. K. Johnson and M. Brookhart, *Chem. Rev.*, 2000, **100**, 1169.

15. J. Albert, J. Granell and J. Sales, *J. Organomet. Chem.*, 1984, **273**, 393.

16. H. Onoue and L. Moritani, *J. Organomet. Chem.*, 1972, **43**, 431.

17. H. Masui, *Coord. Chem. Rev.*, 2001, **219-221**, 957.

18. http://winter.group.shef.ac.uk/chemputer/isotopes.html

19. A. Pidcock, *Chem. Commun. (London)*, 1968, 92.

20. R. K. Harris, *Canad. J. Chem.*, 1964, **42**, 2275.

21. APEX2, *Data Collection Software, Version 2010.11-3, Bruker AXS*, 2010.

22. SAINT, *Data Reduction Software, Version 6.45, Bruker AXS*, 2003.

23. (a) R. H. Blessing, *Acta Crystallogr., Sect. A: Found. Crystallogr.*, 1995, **51**, 33;
(b) SADABS, *Version 2.05, Bruker AXS*, 2002.

24. G. M. Sheldrick, *Acta Crystallogr., Sect. A: Found. Crystallogr.*, 2008, **64**, 112.

25. L. J. Barbour, *J. Supramol. Chem.*, 2001, **1**, 189.

26. POV-Ray™, *Version 3.6, Williamstown, Australia, Persistence of Vision Raytracer Pty. Ltd. 2004*.

27. F. R. Hartley, S. G. Murray and C. A. McAuliffe, *Inorg. Chem.*, 1979, **18**, 1394.

Chapter 3

The synthesis of cationic cyclopalladated complexes derived from neutral cyclopalladated and non-cyclopalladated complexes

3.1 Results and discussion

3.1.1 The preparation of cationic cyclopalladated complexes of acetonitrile

Cationic cyclopalladated complexes **C16 – C20** were prepared by the abstraction of the chloride ligand of the previously discussed neutral cyclopalladated complexes (**Chapter 2, 2.2.3**) in the presence of acetonitrile using sodium tetrakis [3,5-*bis*(trifluoromethyl)phenyl] borate (**Scheme 3-1.**). The latter serves to firstly abstract the chloride ligand, forming sodium chloride as a by-product, and in so doing, create a vacant coordination site on the palladium metal centre. The vacant site is subsequently occupied by the weakly coordinating acetonitrile.

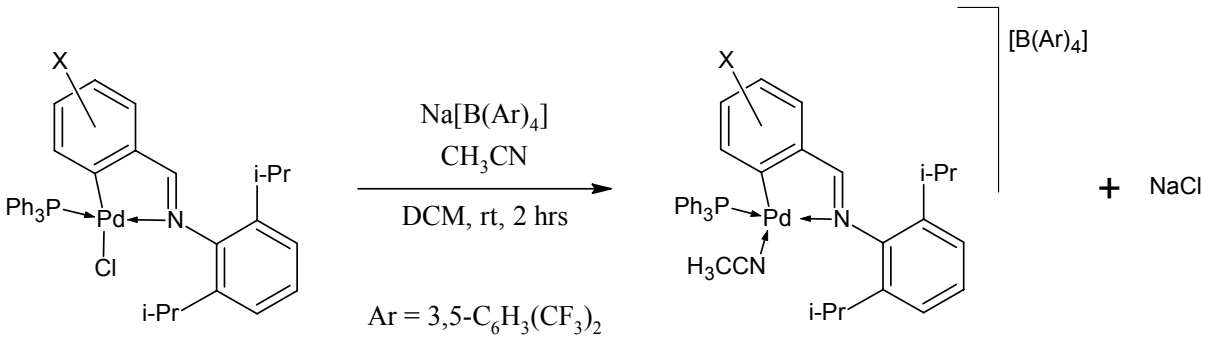

C16: X = *o*-Cl
C17: X = *o*-Br
C18: X = H
C19: X = *o*-Me
C20: X = *p*-Me

Scheme 3-1. Synthetic methodology employed for the preparation of the cationic cyclopalladated complexes of acetonitrile.

Secondly, the liberated tetrakis [3,5-*bis*(trifluoromethyl)phenyl] borate anion acts as the counterion to the formed cationic complex.

All compounds were isolated in good yields (62 – 93 %) as off-white solids that are soluble in polar organic solvents at room temperature. The complexes are stable in solution and in the solid state. Complexes **C16**,[1] **C17**[1] and **C18**[1] have been reported previously whereas **C19** and **C20** are novel.

A variety of analytical techniques, including FT-IR and NMR spectroscopy, were employed for the characterisation of the cationic complexes of acetonitrile. The FT-IR spectra of the resulting products indicate the formation of the desired cationic complexes (for the sake of convenience, this range of complexes (**C16 – C20**) is referred to as the cationic complexes of acetonitrile). The absence of the $\nu_{C=N}$ absorption bands corresponding to the neutral complex starting materials and the appearance of the $\nu_{C=N}$ absorption bands corresponding to the cationic products in the range 1604 – 1616 cm^{-1} provides evidence of the product formation (**Table 3-1.**).

The difference between the appearance of the $\nu_{C=N}$ absorption bands corresponding to the neutral complexes and those of the cationic products is discernable but not particularly significant. The double-bond character of the imine bond in the cationic complexes of acetonitrile is similar to that of the neutral complexes.

The appearance of characteristic, very strong ν_{C-F} absorption bands of CF_3 at ~ 1354, 1275 and 1116 cm^{-1} are present for all analogues in the FT-IR spectra. These are due to the various stretching modes of the trifluoromethyl substituents in the $[B(Ar)_4]^-$ counterion. A strong ν_{C-B} stretch absorption band appears at ~ 838 cm^{-1} for all analogues.

Table 3-1. Analytical data of cationic cyclopalladated complexes **C16 – C20**.

Comp.	FT-IR ($\nu_{C=N}$, cm^{-1})[a]	ESI-MS M^+ (*m/z*)	ESI-MS M^- (*m/z*)[d]	Melting point (°C)[e]
C16	1612	709[1, b]	863[1]	160 - 162
C17	1612	712[c]	863	165 - 167
C18	1616	673[1, b]	863[1]	168 - 170
C19	1604	648[c]	863	165 - 167
C20	1613	648[c]	863	167 - 169

[a] Recorded as neat samples on a ZnSe crystal, employing an ATR accessory. [b] Reported ion corresponds to the proton adduct of the molecular ion, $[M + H]^+$, [c] Reported ion corresponds to $[M - (CH_3CN)]^+$, [d] Reported ion corresponds to the molar mass of the anion, $[B(Ar)_4]^-$. [e] Melting points recorded are uncorrected.

Electrospray ionisation mass spectrometry, recorded in both the positive and negative ion mode, provides further evidence of the product formation. For complexes **C17**, **C19** and **C20**, the base peak in the spectra in the positive ion mode corresponds to the $[M - (CH_3CN)]^+$ fragment (**Table 3-1.**). No further fragmentation takes place. The appearance of multiple peaks is due to the many isotopes of palladium that are present in the complex (**Figure 3-1.**). Calculated isotopic distributions of the fragments are in good agreement with the sample spectra for all analogues (**Figure 3-1. a** and **3-2. a**).[2] The major fragment in the negative ion mode, for all analogues, corresponds to the molar mass of the $[B(Ar)_4]^-$ counterion. Fewer isotopes in the counterion as compared to the cationic complex results in the appearance of fewer peaks for the base peak in the spectra (**Figure 3-2.**).

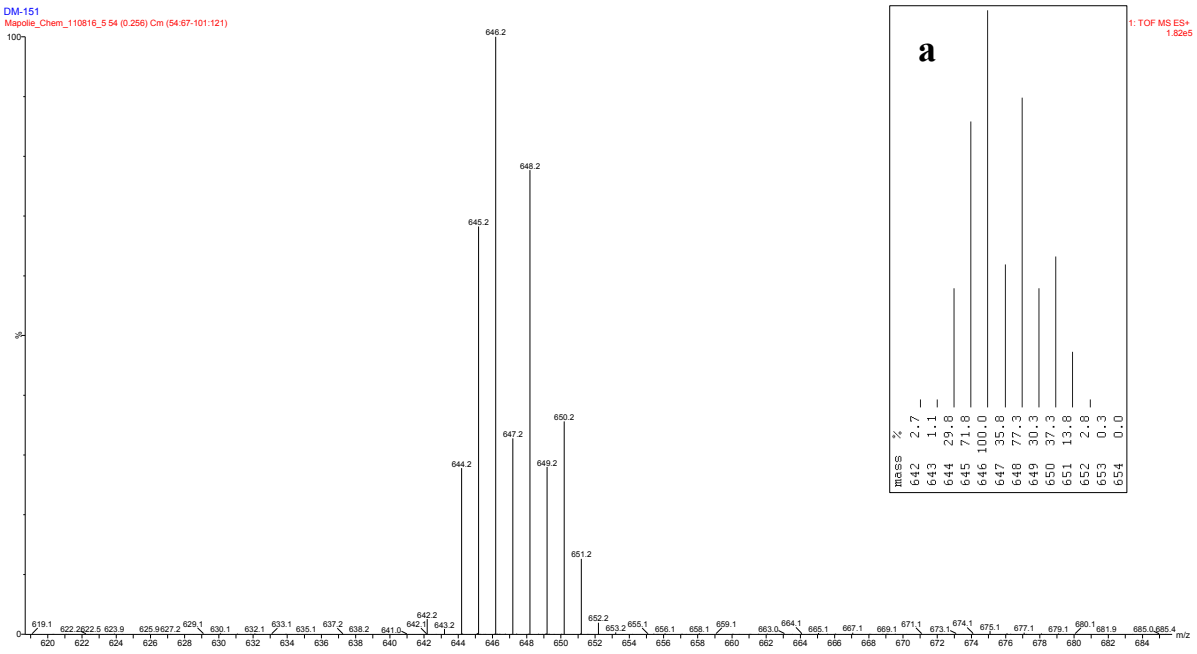

Figure 3-1. ESI-MS (+) spectrum in the region *m/z* 619 – 685 of complex **C19**. The cluster of peaks centred at *m/z* 648.2 corresponds to the $[M - (CH_3CN)]^+$ fragment.

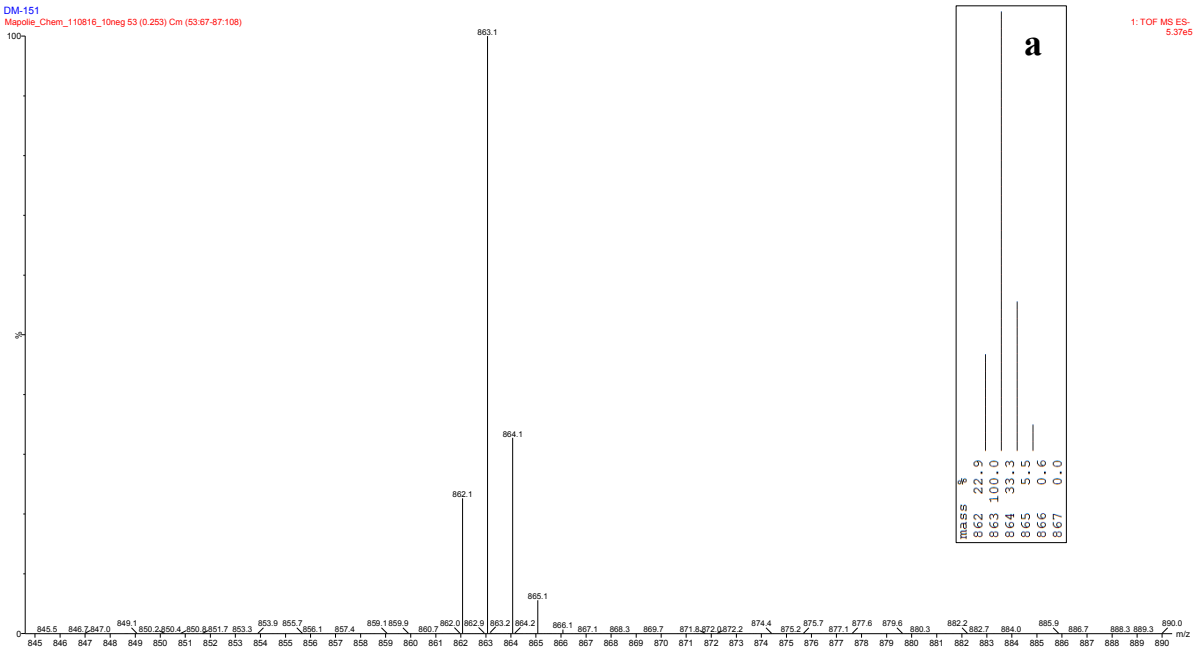

Figure 3-2. ESI-MS (-) spectrum in the region *m/z* 845 – 890 of complex **C19**. A distinct peak at *m/z* 863.1 corresponds to the molar mass of the $[B(Ar)_4]^-$ counterion.

The ^{1}H-, ^{13}C $\{^{1}$H$\}$- and ^{31}P $\{^{1}$H$\}$-NMR spectra of the products confirm the formation of the cationic complexes. The proton resonance of the imine functionality in the ^{1}H-NMR spectra appears as a doublet in the region of δ 8.05 – 8.61 ppm which is due to the hetero-nuclear $^{4}J_{H\text{-}P}$ coupling to the NMR active ^{31}P atom of the coordinated triphenylphosphine ligand. The appearance of this resonance slightly upfield as compared to that of the neutral complexes reveals that the presence of acetonitrile in the place of chloride slightly decreases the degree of electron delocalisation in the palladacycle. As a result the imine proton is slightly less deshielded as compared to that of the neutral complexes.

Similarly to the results for the neutral complexes, the imine proton resonances for complexes **C16** and **C17**, i.e. those with a halogen substituent at the *ortho* position, appear further downfield than the imine proton resonances for complexes **C18 – C20**.

^{1}H- and ^{13}C $\{^{1}$H$\}$-NMR spectral analysis reveals that there is no rotation along the bond between the imine nitrogen and carbon (8) in solution, at 298 K, after the substitution reaction with acetonitrile (**Figure 3-3.**). The free rotation along the bonds between carbon (9) and carbon (16) as well as between carbon (13) and carbon (14) is retained. Free rotation along the single bond between carbon (19) and carbon (20) also takes place. ^{13}C $\{^{1}$H$\}$-NMR spectra clearly reveals the presence of free rotation along the single bonds between boron and carbon (21) as well as between carbon (23) and carbon (25) in the $[B(Ar)_4]^-$ counterion.

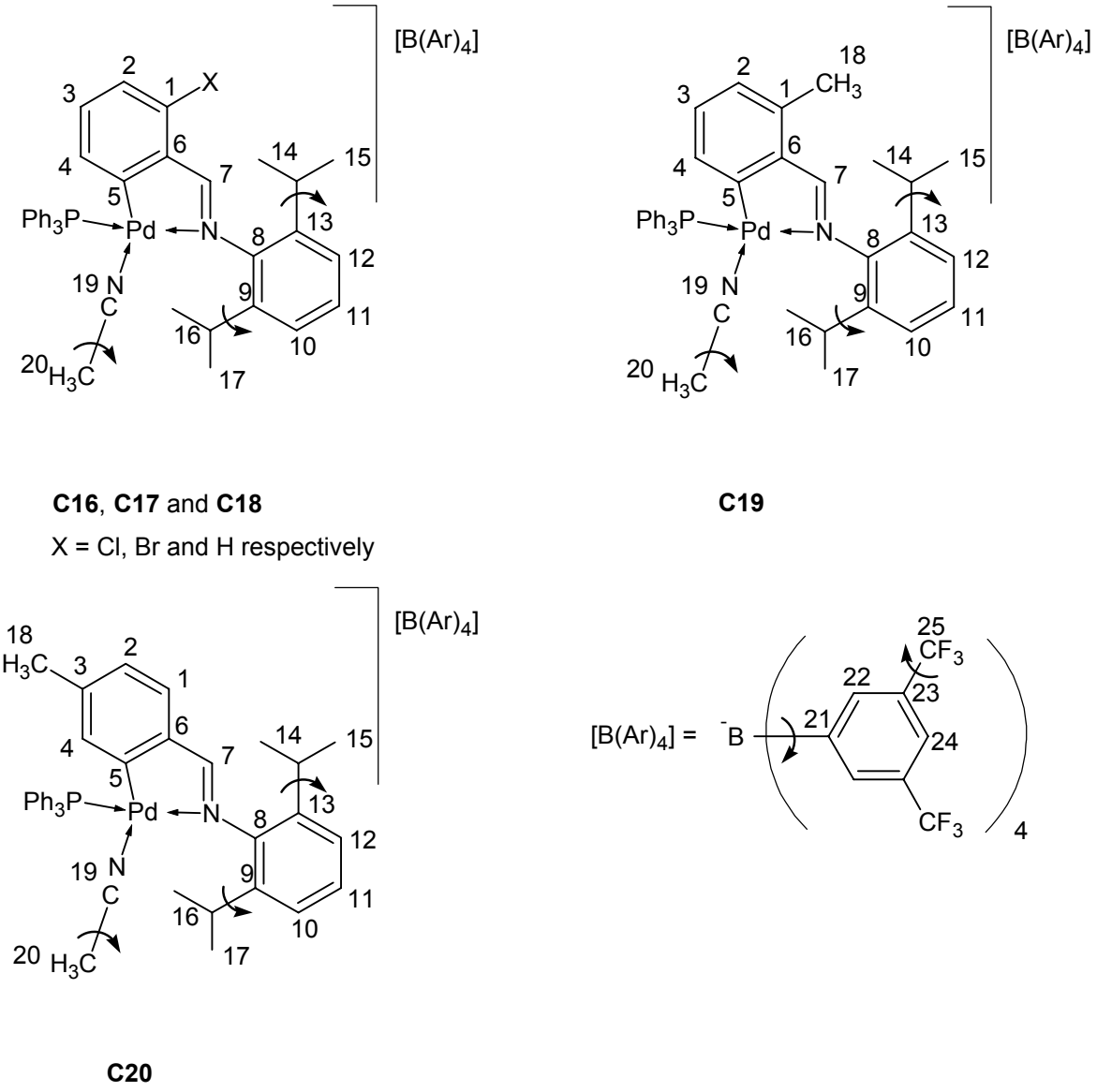

Figure 3-3. Schematic representation of complexes **C16 – C20**, including the $[B(Ar)_4]^-$ counterion, with the numbering for NMR spectral analysis.

A clear upfield shift takes place for the multiplet due to the methine protons ($H^{14,16}$) from the region of δ 3.45 – 3.51 ppm for the neutral complexes (**C6 – C10**) to the region of δ 3.34 – 3.36 ppm for the cationic complexes of acetonitrile. A clear change in chemical shifts for the resonances due to the isopropyl methyl protons ($H^{15/17}$) also takes place. For the neutral complexes, two distinct doublets that do not overlap resonate in the regions of

δ 1.20 – 1.25 ppm and δ 1.37 – 1.40 ppm, revealing that H^{15} and H^{17} are chemically inequivalent. In contrast, the two doublets due to H^{15} and H^{17} for the cationic complexes of acetonitrile overlap in the regions of δ 1.25 – 1.30 ppm and δ 1.28 – 1.31 ppm, revealing that their chemical inequivalence is somewhat reduced upon completion of the substitution reaction. The ability of the chloride ligand, as opposed to the acetonitrile ligand, to be involved in weak noncovalent Pd-Cl···H intramolecular interactions with the protons of one of the isopropyl substituents (H^{14} and H^{15} or H^{16} and H^{17}) causes the chemical environments of the two isopropyl substituents to be fairly inequivalent to one another for the neutral complexes. No significant shifts take place for the resonances of H^{18} for both complexes **C19** and **C20**.

A very important resonance in the ^{1}H-NMR spectra is the singlet that appears furthest upfield of all the resonances in the region of δ 1.04 – 1.07 ppm. This resonance is due to the protons of the acetonitrile ligand, H^{20}, and is clearly identifiable upon the completion of the substitution reaction for all analogues.

The imine carbon [carbon (7)] resonance in the ^{13}C $\{^{1}H\}$-NMR spectra appears as a doublet in the downfield region of δ 176.02 – 178.92 ppm. This splitting pattern is due to the hetero-nuclear $^{3}J_{C\text{-}P}$ coupling to the ^{31}P atom of the coordinated triphenylphosphine ligand.

The $[B(Ar)_4]^-$ counterion consists of two NMR active atoms, i.e. ^{11}B, with a spin quantum number of 3/2 at an 80.42% abundance and ^{19}F with a spin quantum number of ½ at a 100% abundance. Therefore, predictable splitting patterns are expected in the ^{13}C $\{^{1}H\}$-NMR spectra which are clearly identifiable. Carbon (21) resonates as a quartet (1:1:1:1) in the downfield region of ~ δ 161.7 ppm due to $^{1}J_{C\text{-}B}$ coupling to the ^{11}B atom. Carbon (25) resonates as a quartet (1:3:3:1) in the region of ~ δ 124.5 ppm due to $^{1}J_{C\text{-}F}$ coupling to the three ^{19}F atoms. Carbon (23) resonates as a quartet of quartets in the region of ~ δ 128.9 ppm

due to $^{2}J_{C\text{-}F}$ coupling to the ^{19}F atoms and $^{3}J_{C\text{-}B}$ coupling to the ^{11}B atom. Carbon (24) resonates as a septet (1:6:15:20:15:6:1) in the region of ~ δ 117.4 ppm due to $^{3}J_{C\text{-}F}$ coupling to the ^{19}F atoms of both the trifluoromethyl substituents.

A sharp, well-defined singlet due to the ^{31}P atom of the phosphine ligand appears in the region of δ 40.95 – 41.66 ppm in the ^{31}P $\{^{1}H\}$-NMR spectra for all analogues (**Table 3-2.** and **Figure 3-4.**). Again, the appearance of this peak slightly upfield as compared to that of the neutral complexes reveals that the presence of acetonitrile in the place of chloride slightly decreases the degree of electron delocalisation in the palladacycle. As a result the ^{31}P atom is slightly less deshielded as compared to in the neutral complexes.

Table 3-2. ^{31}P $\{^{1}H\}$-NMR spectral data of cationic complexes **C16 – C20**.

Comp.	δ (ppm)[a]
C16	41.15
C17	40.95
C18	41.66
C19	41.61
C20	41.23

[a] Spectra recorded in $CDCl_3$ at 298 K.

Due to some expected overlapping of resonances in the aromatic region of the ^{1}H-NMR spectra, the multiplicities of certain resonances are not identifiable. However, all clearly distinguishable resonances and coupling constants are assigned (**Table 3-3.** and **Figure 3-5.**).

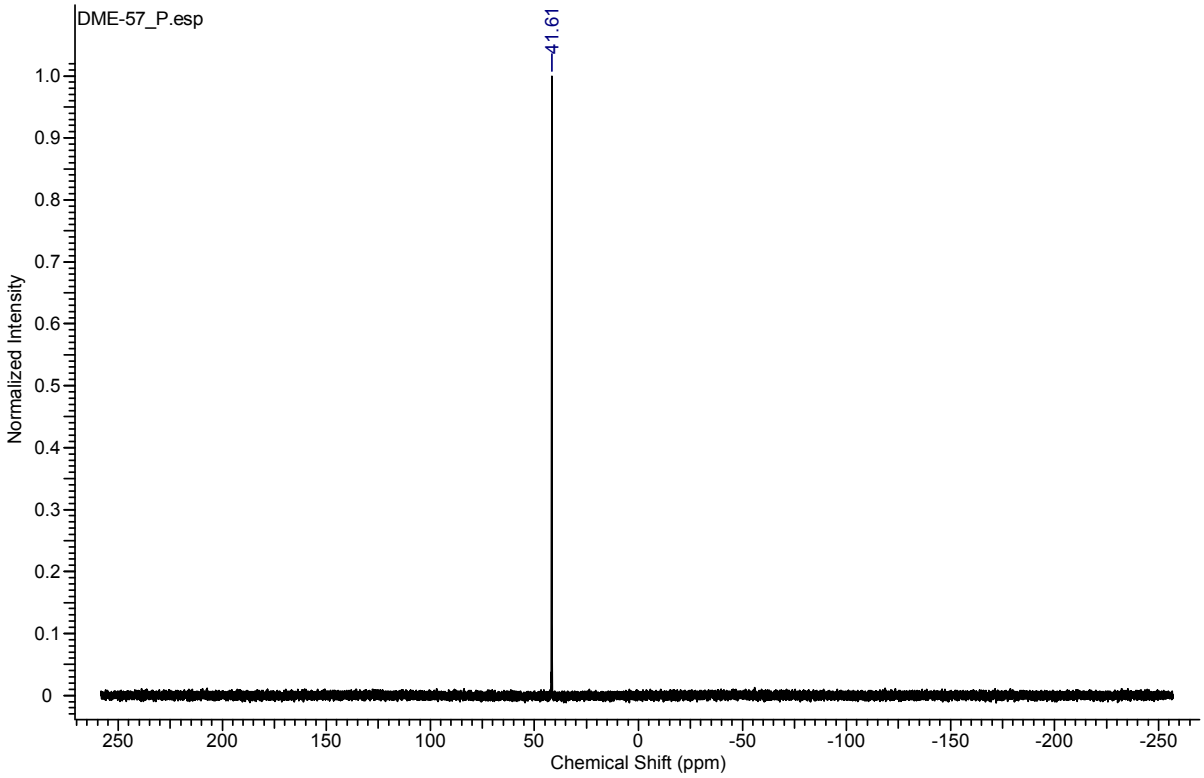

Figure 3-4. ^{31}P $\{^{1}H\}$-NMR spectrum of complex **C19**.

Table 3-3. ^{1}H-NMR spectral data of cationic cyclopalladated complexes **C16 – C20**.[a]

Comp.	HC=N	Aromatic region	Aliphatic region			
			$\underline{H}C(CH_3)_2$	$ArC\underline{H}_3$	$HC(C\underline{H}_3)_2$	$N\equiv C\text{-}C\underline{H}_3$
C16	8.59 (d, 1H, H^7, $^4J_{H\text{-}P}$ = 7.6Hz)	7.70 - 7.63 (m, 14H), 7.53 - 7.51 (m, 7H), 7.47 - 7.43 (m, 6H), 7.30 - 7.21 (m, 3H, $H^{10,11,12}$), 7.07 (d, 1H, H^2, $^3J_{H\text{-}H}$ = 8.2Hz), 6.70 (t, 1H, H^3, $^3J_{H\text{-}H}$ = 8.0Hz), 6.37 - 6.33 (m, 1H, H^4)	3.34 (m, 2H, $H^{14,16}$)		1.30 (d, 6H, $H^{15/17}$, $^3J_{H\text{-}H}$ = 6.6Hz), 1.28 (d, 6H, $H^{15/17}$, $^3J_{H\text{-}H}$ = 6.8Hz)	1.05 (s, 3H, H^{20})
C17	8.61 (d, 1H, H^7, $^4J_{H\text{-}P}$ = 7.6Hz)	7.74 - 7.70 (m, 10H), 7.68 - 7.63 (m, 5H), 7.53 - 7.42 (m, 12H), 7.31 - 7.23 (m, 4H, $H^{2,10,11,12}$), 6.61 (t, 1H, H^3, $^3J_{H\text{-}H}$ = 7.9Hz), 6.44 - 6.39 (m, 1H, H^4)	3.36 (m, 2H, $H^{14,16}$)		1.31 (d, 6H, $H^{15/17}$, $^3J_{H\text{-}H}$ = 6.9Hz), 1.30 (d, 6H, $H^{15/17}$, $^3J_{H\text{-}H}$ = 6.8Hz)	1.07 (s, 3H, H^{20})
C18	8.12 (d, 1H, H^7, $^4J_{H\text{-}P}$ = 7.6Hz)	7.71 - 7.64 (m, 15H), 7.51 - 7.42 (m, 13H), 7.28 - 7.19 (m, 3H, $H^{10,11,12}$), 7.15 - 7.10 (m, 1H, H^2), 6.81 - 6.75 (m, 1H, H^3), 6.50 - 6.42 (m, 1H, H^4)	3.35 (m, 2H, $H^{14,16}$)		1.29 (d, 6H, $H^{15/17}$, $^3J_{H\text{-}H}$ = 6.8Hz), 1.26 (d, 6H, $H^{15/17}$, $^3J_{H\text{-}H}$ = 6.8Hz)	1.06 (s, 3H, H^{20})
C19	8.41 (d, 1H, H^7, $^4J_{H\text{-}P}$ = 7.6Hz)	7.70 - 7.63 (m, 14H), 7.51 - 7.41 (m, 13H), 7.25 - 7.19 (m, 3H, $H^{10,11,12}$), 6.86 (d, 1H, H^2, $^3J_{H\text{-}H}$ = 7.6Hz), 6.65 (t, 1H, H^3, $^3J_{H\text{-}H}$ = 7.6Hz), 6.33 - 6.28 (m, 1H, H^4)	3.36 (m, 2H, $H^{14,16}$)	2.51 (s, 3H, H^{18})	1.29 (d, 6H, $H^{15/17}$, $^3J_{H\text{-}H}$ = 6.9Hz), 1.26 (d, 6H, $H^{15/17}$, $^3J_{H\text{-}H}$ = 6.9Hz)	1.04 (s, 3H, H^{20})
C20	8.05 (d, 1H, H^7, $^4J_{H\text{-}P}$ = 7.8Hz)	7.70 - 7.64 (m, 15H), 7.51 - 7.43 (m, 12H), 7.37 (d, 1H, H^1, $^3J_{H\text{-}H}$ = 7.6Hz), 7.27 - 7.18 (m, 3H, $H^{10,11,12}$), 6.92 (d, 1H, H^2, $^3J_{H\text{-}H}$ = 7.5Hz), 6.22 (d, 1H, H^4, $^4J_{H\text{-}P}$ = 6.5Hz)	3.34 (m, 2H, $H^{14,16}$)	1.79 (s, 3H, H^{18})	1.28 (d, 6H, $H^{15/17}$, $^3J_{H\text{-}H}$ = 6.9Hz), 1.25 (d, 6H, $H^{15/17}$, $^3J_{H\text{-}H}$ = 6.8Hz)	1.07 (s, 3H, H^{20})

[a] Spectra recorded in $CDCl_3$ at 298 K. Chemical shifts reported in δ ppm values, referenced relative to the residual $CDCl_3$ peak. Superscripts denote protons as per numbering scheme (**Figure 3-3.**).

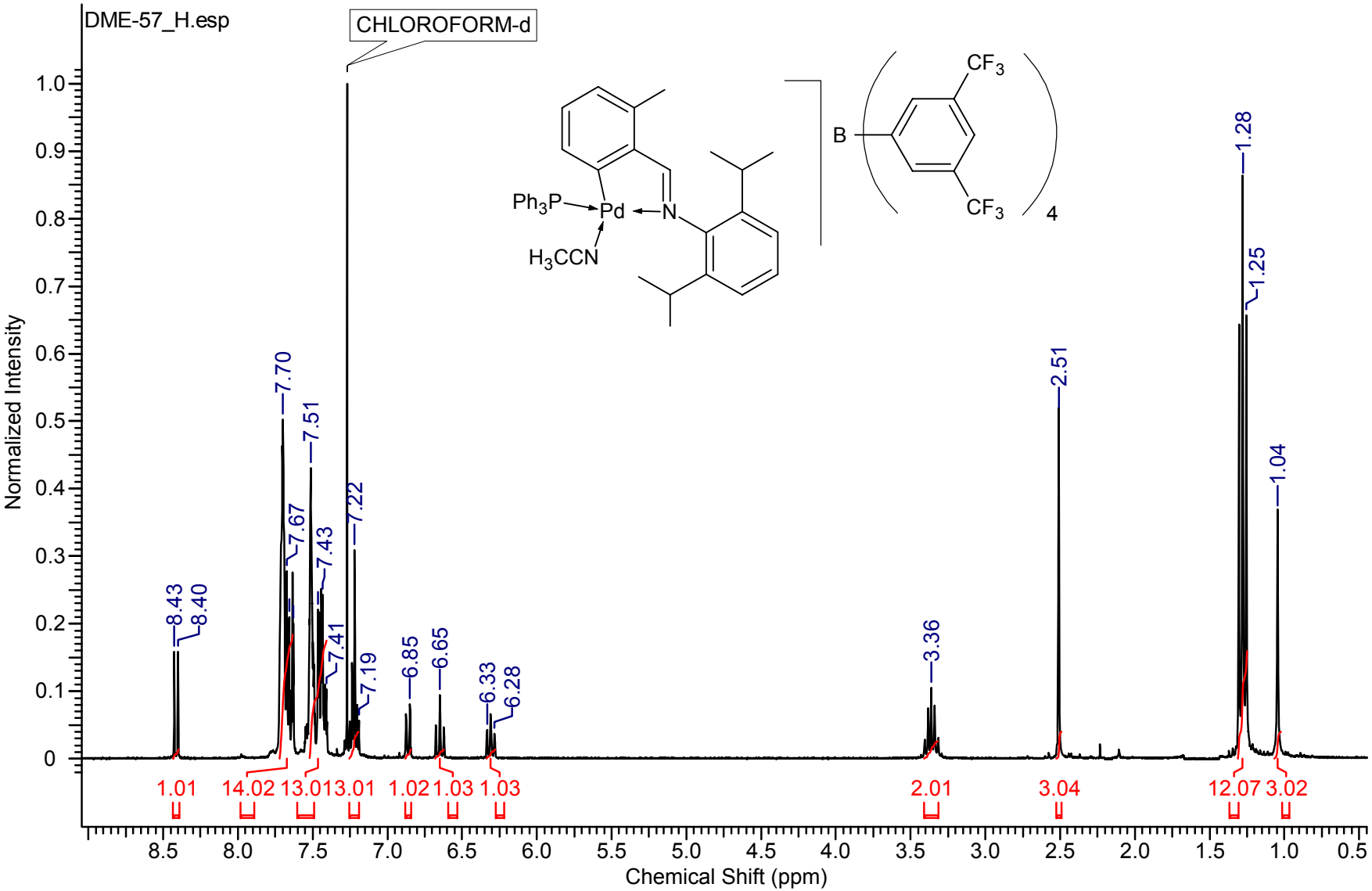

Figure 3-5. ^{1}H-NMR spectrum of complex **C19**.

Crystals suitable for single crystal diffraction analysis were obtained of complex **C19** (**Figure 3-6.**). Recrystallisation by means of slow evaporation from dichloromethane/*n*-pentane at room temperature resulted in the formation of colourless single crystals.

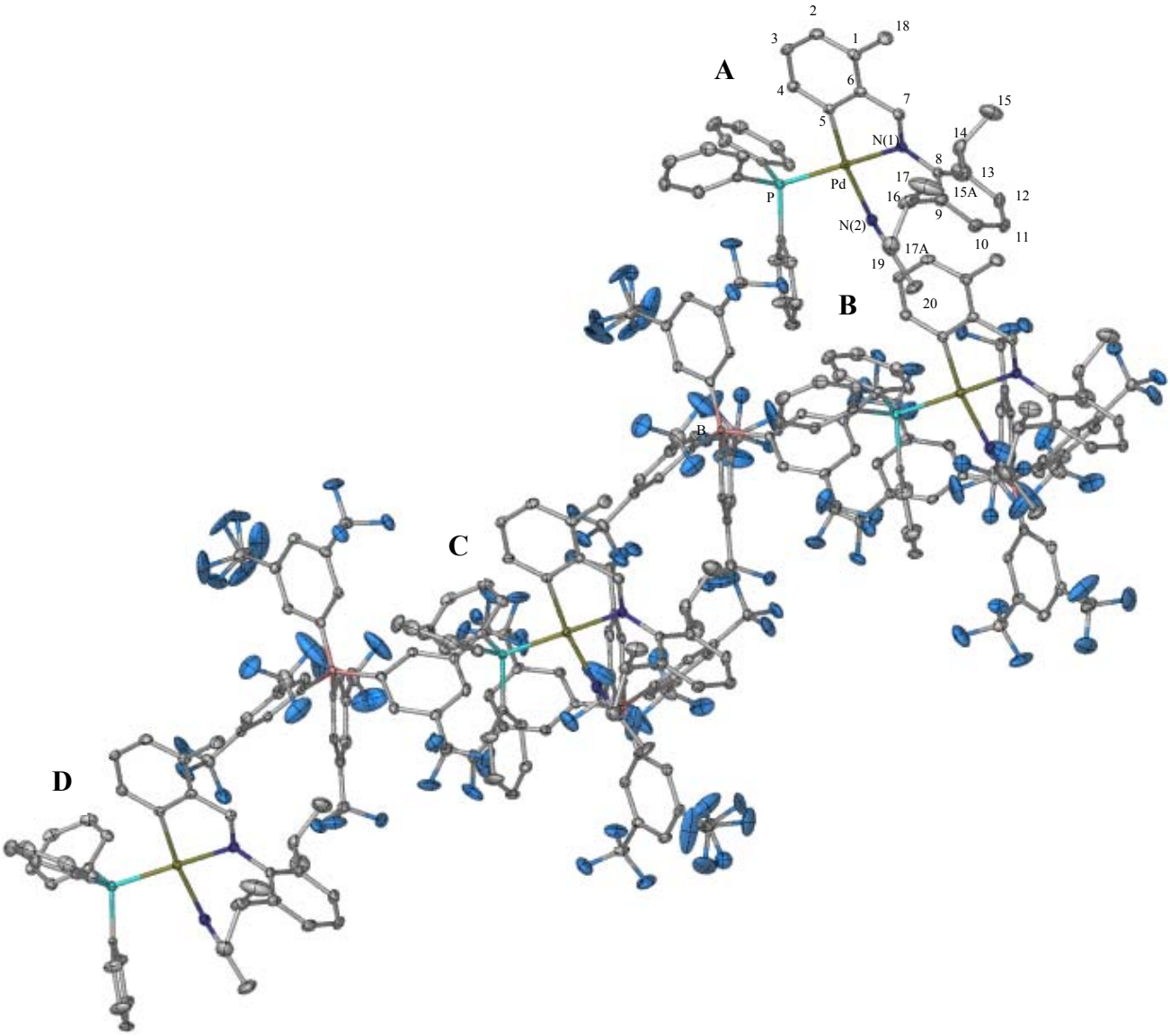

Figure 3-6. Molecular structures of complex **C19**, **A**, **B**, **C** and **D**, shown with 50 % probability ellipsoids and the numbering scheme (hydrogen atoms are omitted for clarity).

The molecular structure provides unambiguous confirmation of the successful substitution reaction. The asymmetric unit comprises four cationic complex molecules and

four $[B(Ar)_4]^-$ counterion molecules. The coordination of the palladium atom is distorted square-planar, in a similar manner to that of complex **C9** (**Chapter 2**), and the acetonitrile donor ligand is situated *trans* to the Pd-C bond. Selected bond lengths, bond angles and torsion angles are listed in **Table 3-4.**.

Table 3-4. Selected bond lengths, bond angles and torsion angles of the crystallographically determined structures **A, B, C** and **D** of complex **C19**.[a]

	A	**B**	**C**	**D**
		Bond lengths (Å)		
Pd-C(5)	2.000	2.009	1.996	1.988
Pd-N(1)	2.081	2.077	2.092	2.063
Pd-N(2)	2.091	2.087	2.095	2.098
Pd-P	2.274	2.272	2.270	2.273
C(7)-N(1)	1.285	1.287	1.287	1.290
C(8)-N(1)	1.438	1.443	1.440	1.444
C(1)-C(18)	1.515	1.515	1.506	1.509
		Bond angles (degrees)		
N(1)-Pd-N(2)	89.47	88.94	89.14	89.85
N(2)-Pd-P	93.64	94.22	93.93	93.46
P-Pd-C(5)	94.99	95.18	95.79	95.66
C(5)-Pd-N(1)	81.36	81.36	81.28	81.13
		Torsion angles (degrees)		
C(8)-C(13)-C(14)-C(15)	-110.96	-109.08	-112.53	-111.11
C(8)-C(9)-C(16)-C(17)	103.90	101.91	109.43	108.41

[a] Atom labelling as per numbering scheme **Figure 3-6.**.

Table 3-5. Crystallographic data and structure refinement parameters of complex **C19**.

Empirical formula	$C_{288}H_{216}B_4F_{96}N_8P_4Pd_4$
M_r (g/mol)	6205.4
Crystal system	triclinic
Space group	$P\bar{1}$ (No. 2)
a (Å)	20.644 (3)
b (Å)	25.504 (3)
c (Å)	28.575 (4)
α (deg)	85.391 (2)
β (deg)	79.812 (2)
γ (deg)	67.164 (1)
Volume (Å^3)	13646 (3)
Z	8
D_{calc} (g cm^{-3})	1.510
F000	6256
λ (MoK$_\alpha$) (Å)	0.71073
Temperature (K)	101 (2)
2θ max (deg)	57.8
Lp and absorption corrections applied (μ)	0.405 mm^{-1}
Data/restraints/par.	65520/3/3761
R_1 [$I > 2\sigma(I)$]	0.0464
wR_2 (all reflections)	0.1028
Goodness of fit on F^2	1.020
Max/min residual electron density (e Å^{-3})	0.835 / -0.846

3.1.2 The preparation of cationic cyclopalladated complexes of pyridine

Cationic cyclopalladated complexes **C21 – C25** were prepared by the abstraction of the chloride ligand of the previously discussed neutral cyclopalladated complexes (**Chapter 2, 2.2.3**) in the presence of pyridine using sodium tetrakis [3,5-*bis*(trifluoromethyl)phenyl] borate (**Scheme 3-2.**). The role of the latter is the same as in the reaction pertaining to the formation of the cationic complexes of acetonitrile. The vacant site is subsequently occupied by the weakly coordinating pyridine.

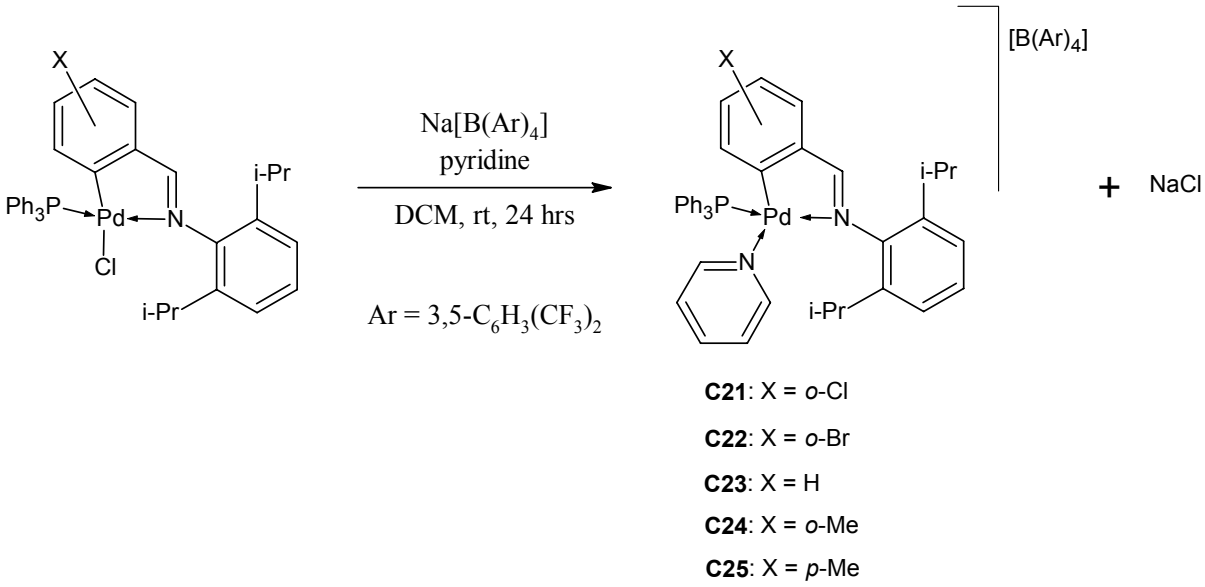

C21: X = *o*-Cl
C22: X = *o*-Br
C23: X = H
C24: X = *o*-Me
C25: X = *p*-Me

Scheme 3-2. Synthetic methodology employed for the preparation of the cationic cyclopalladated complexes of pyridine.

All compounds were isolated in good yields (70 – 89 %) as off-white solids that are soluble in polar organic solvents at room temperature. The complexes are stable in solution and in the solid state. All analogues are novel.

The cationic cyclopalladated complexes of pyridine were characterised by a range of analytical techniques similarly to that for the cationic complexes of acetonitrile (**3.1.1**). The

FT-IR spectra of the resulting products indicate the formation of the desired cationic complexes (for the sake of convenience, this range of complexes (**C21 – C25**) is referred to as the cationic complexes of pyridine). The absence of the $\nu_{C=N}$ absorption bands corresponding to the neutral complex starting materials and the appearance of the $\nu_{C=N}$ absorption bands corresponding to the cationic products in the range 1607 – 1614 cm^{-1} provides evidence of the product formation (**Table 3-6.**).

Table 3-6. Analytical data of cationic cyclopalladated complexes **C21 – C25**.

Comp.	FT-IR ($\nu_{C=N}$, cm^{-1})[a]	ESI-MS M^+ (*m/z*)[b]	ESI-MS M^- (*m/z*)[c]	Melting point (°C)[d]
C21	1614	668	863	151 - 153
C22	1613	712	863	158 - 160
C23	1612	634	863	157 - 159
C24	1607	648	863	148 - 150
C25	1611	648	863	157 - 159

[a] Recorded as neat samples on a ZnSe crystal, employing an ATR accessory. [b] Reported ion corresponds to $[M - py]^+$, [c] Reported ion corresponds to the molar mass of the anion, $[B(Ar)_4]^-$. [d] Melting points recorded are uncorrected.

The difference between the appearance of the $\nu_{C=N}$ absorption bands corresponding to the neutral complexes and those of the cationic products is discernable but not particularly significant. The double-bond character of the imine bond in the cationic complexes of pyridine is similar to that of the neutral complexes and to that of the cationic complexes of acetonitrile (**C16 – C20**).

Similarly to the results for the cationic complexes of acetonitrile, the appearance of characteristic, very strong $\nu_{C\text{-}F}$ absorption bands of CF_3 at ~ 1354, 1275 and 1116 cm^{-1} are present for all analogues in the FT-IR spectra. Again, a strong $\nu_{C\text{-}B}$ stretch absorption band appears at ~ 839 cm^{-1} for all analogues.

Electrospray ionisation mass spectrometry, recorded in both the positive and negative ion mode, provides further evidence of the product formation. Similarly to the results for the cationic complexes of acetonitrile, the base peak in the spectra in the positive ion mode is due to the loss of the weakly coordinating ligand (**Table 3-6.**). The $[M - py]^+$ fragment is present in the spectra for all analogues, with no further fragmentation taking place (**Figure 3-7.**). The major fragment in the negative ion mode, for all analogues, corresponds to the molar mass of the $[B(Ar)_4]^-$ counterion (**Figure 3-8.**). The isotopic distributions in the spectra are once again consistent with the simulated spectra.

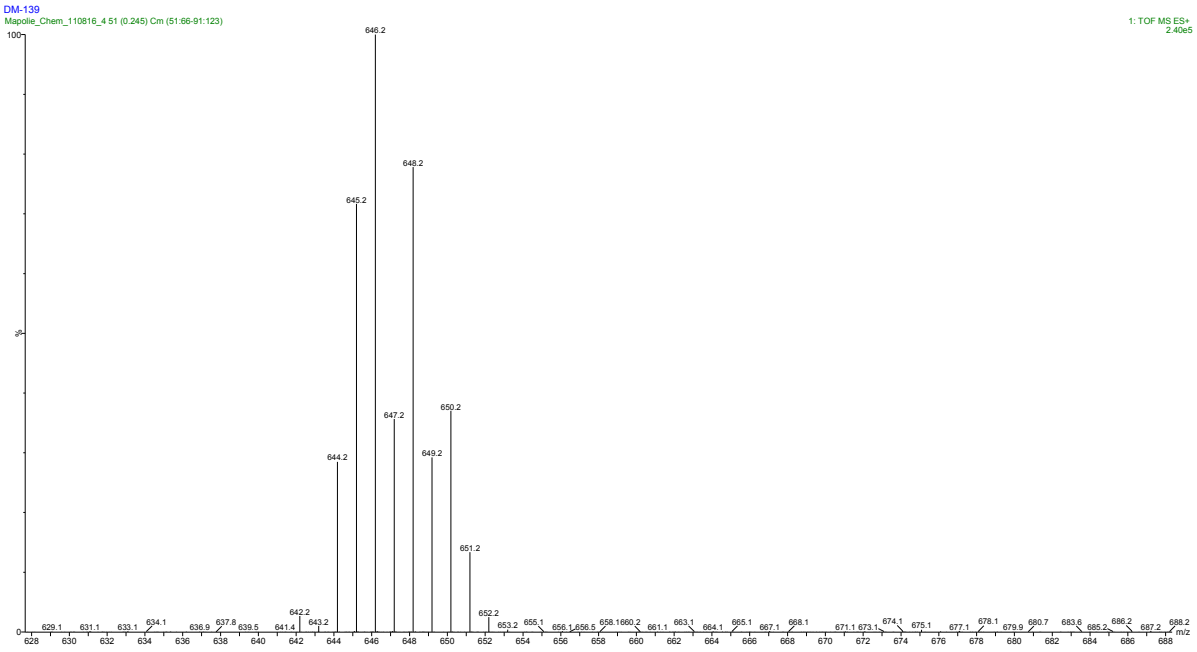

Figure 3-7. ESI-MS (+) spectrum in the region *m/z* 628 – 688 of complex **C24**. The cluster of peaks centred at *m/z* 648.2 corresponds to the $[M - py]^+$ fragment.

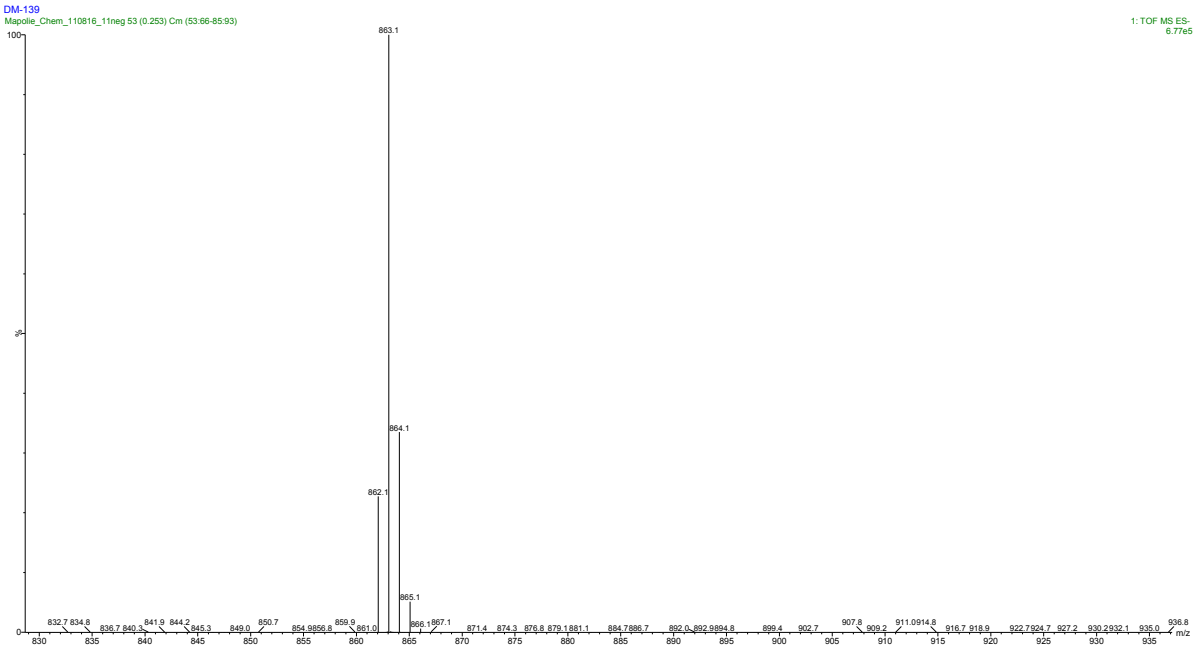

Figure 3-8. ESI-MS (-) spectrum in the region *m/z* 830 – 936 of complex **C24**. A distinct peak at *m/z* 863.1 corresponds to the molar mass of the $[B(Ar)_4]^-$ counterion.

The ^{1}H-, ^{13}C $\{^1$H$\}$- and ^{31}P $\{^1$H$\}$-NMR spectra of the products confirm the formation of the cationic complexes. The proton resonance of the imine functionality in the ^{1}H-NMR spectra appears as a doublet in the region of δ 8.10 – 8.68 ppm which is due to the hetero-nuclear $^4J_{H\text{-}P}$ coupling to the ^{31}P atom of the coordinated triphenylphosphine ligand. The appearance of this resonance slightly downfield as compared to that of the neutral complexes, and to that of the cationic complexes of acetonitrile, reveals that the presence of pyridine in the place of chloride slightly increases the degree of electron delocalisation in the palladacycle. As a result the imine proton is slightly more deshielded as compared to that of the neutral complexes and to that of the cationic complexes of acetonitrile. The degree of electron delocalisation in the palladacycle is directly affected by the relative basicity of the donor ligand. The higher the s-character of a particular orbital, the more strongly electrons

are held and shared with greater difficulty. Therefore, the basicity diminishes with change of hybridisation of nitrogen in the order $sp^3 > sp^2 > sp$ (**Figure 3-9.**).

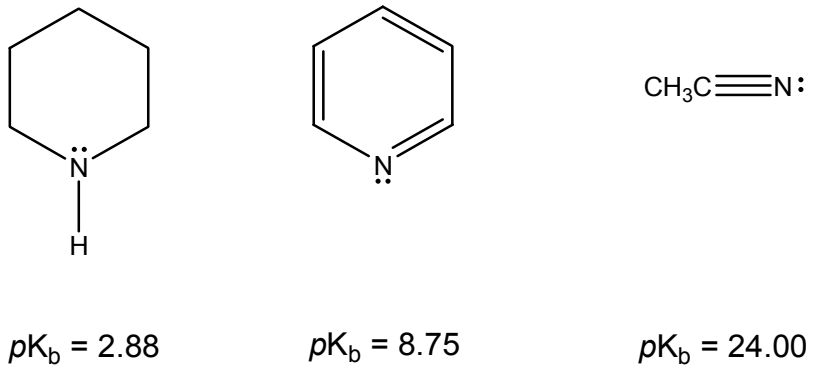

pK_b = 2.88 pK_b = 8.75 pK_b = 24.00

Figure 3-9. The pK_b values of piperidine (left), pyridine (middle) and acetonitrile (right).

The higher basicity of pyridine then, as compared to acetonitrile, causes the imine proton resonance to appear further downfield.

Similarly to the results for the neutral complexes, the imine proton resonances for complexes **C21** and **C22**, i.e. those with a halogen substituent at the *ortho* position, appear further downfield than the imine proton resonances for complexes **C23 – C25**.

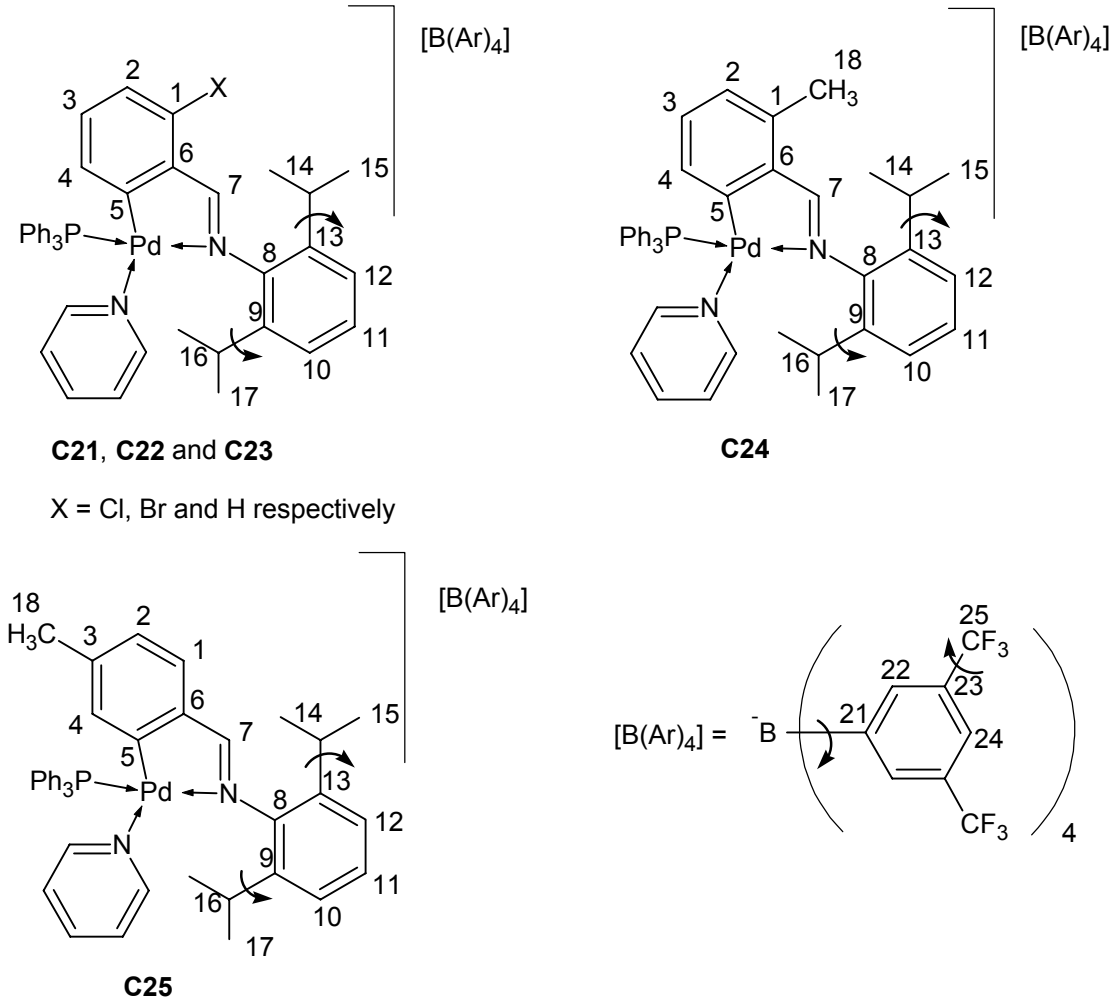

Figure 3-10. Schematic representation of complexes **C21 – C25**, including the $[B(Ar)_4]^-$ counterion, with the numbering for NMR spectral analysis.

^{1}H- and ^{13}C $\{^1$H$\}$-NMR spectral analysis reveals that there is no free rotation along the bond between the imine nitrogen and carbon (8) in solution, at 298 K, upon completion of the substitution reaction with pyridine (**Figure 3-10.**). The free rotation along the bonds between carbon (9) and carbon (16) as well as between carbon (13) and carbon (14) is retained. Similarly to the results for the cationic complexes of acetonitrile, the ^{13}C $\{^1$H$\}$-NMR spectra clearly reveals the presence of free rotation along the single bonds between boron and carbon (21) as well as between carbon (23) and carbon (25) in the $[B(Ar)_4]^-$ counterion.

A clear upfield shift takes place for the multiplet resonance due to the methine protons ($H^{14,16}$) from the region of δ 3.45 – 3.51 ppm for the neutral complexes (**C6 – C10**) to the region of δ 3.20 – 3.23 ppm for the cationic complexes of pyridine. This resonance is upfield as compared to that of the cationic complexes of acetonitrile (**C16 – C20**). A clear change in chemical shifts for the resonances due to the isopropyl methyl protons ($H^{15/17}$) also takes place. For the neutral complexes, two distinct doublets that do not overlap resonate in the regions of δ 1.20 – 1.25 ppm and δ 1.37 – 1.40 ppm, revealing that H^{15} and H^{17} are chemically inequivalent. In contrast, the two doublets due to H^{15} and H^{17} for the cationic complexes of pyridine appear much closer to one another in the regions of δ 1.13 – 1.18 ppm and δ 1.19 – 1.21 ppm, revealing that their chemical inequivalence is somewhat reduced upon completion of the substitution reaction. These resonances are upfield as compared to that of the cationic complexes of acetonitrile. No significant shifts take place for the resonances of H^{18} for both complexes **C24** and **C25**.

The imine carbon [carbon (7)] resonance in the ^{13}C $\{^{1}H\}$-NMR spectra appears as a doublet in the downfield region of δ 177.33 – 180.22 ppm. This splitting pattern is due to the hetero-nuclear $^{3}J_{C\text{-}P}$ coupling to the ^{31}P atom of the coordinated triphenylphosphine ligand. The appearance of this resonance is slightly downfield as compared to that of the cationic complexes of acetonitrile. This reveals once again that the presence of pyridine slightly increases the degree of electron delocalisation in the palladacycle, in contrast to acetonitrile which slightly decreases the degree of electron delocalisation, upon completion of the substitution reaction.

The chemical shifts and splitting patterns for carbons (21 – 25) of the $[B(Ar)_4]^-$ counterion in the ^{13}C $\{^{1}H\}$-NMR spectra are similar to those for the carbons of the $[B(Ar)_4]^-$ counterion for the cationic complexes of acetonitrile (**Figure 3-12.**).

A sharp, well-defined singlet due to the ^{31}P atom of the phosphine ligand appears in the region of δ 42.56 – 43.50 ppm in the ^{31}P $\{^{1}H\}$-NMR spectra for all analogues (**Table 3-7.** and **Figure 3-11.**). Again, the appearance of this peak slightly downfield as compared to that of the neutral complexes, and to that of the cationic complexes of acetonitrile, reveals that the presence of pyridine in the place of chloride slightly increases the degree of electron delocalisation in the palladacycle. As a result the ^{31}P atom is slightly more deshielded as compared to that of the neutral complexes and to that of the cationic complexes of acetonitrile.

Table 3-7. ^{31}P $\{^{1}H\}$-NMR spectral data of cationic complexes **C21 – C25**.

Comp.	δ (ppm)[a]
C21	42.74
C22	42.56
C23	43.50
C24	43.27
C25	42.98

[a] Spectra recorded in $CDCl_3$ at 298 K.

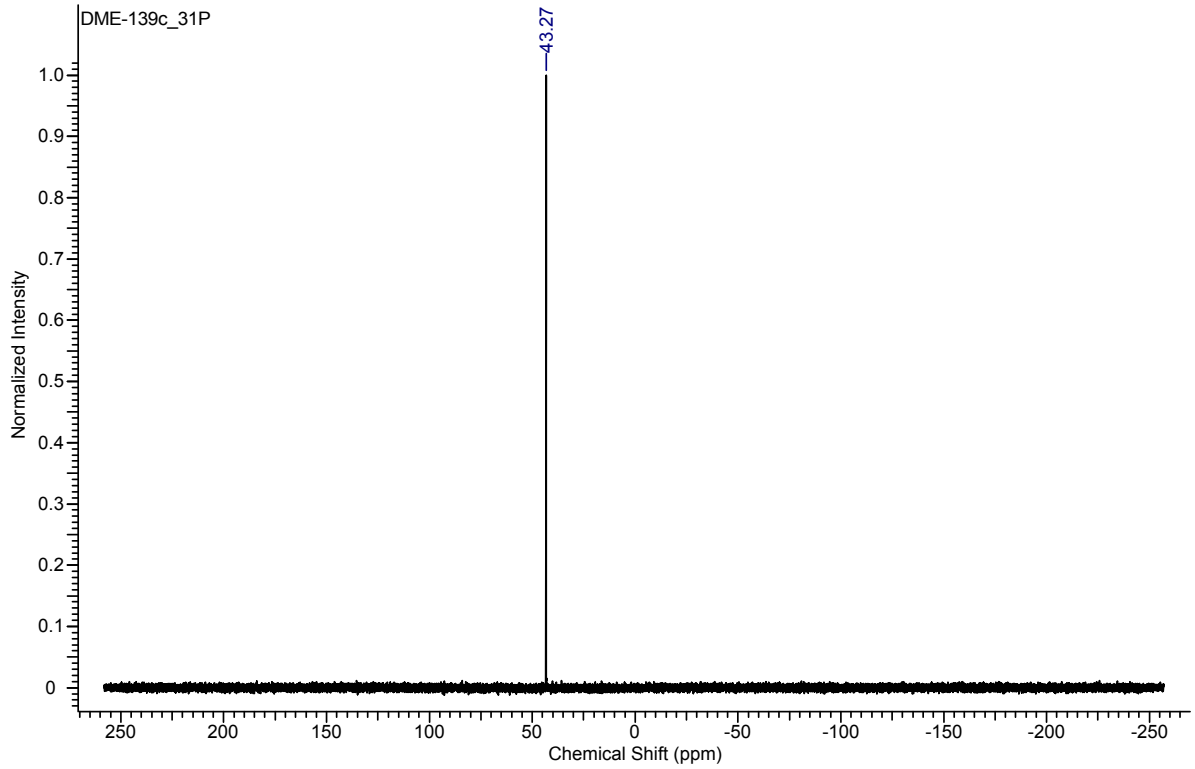

Figure 3-11. ^{31}P $\{^{1}H\}$-NMR spectrum of complex **C24**.

Due to some expected overlapping of resonances in the aromatic region of the ^{1}H-NMR spectra, the multiplicities of certain resonances are not assigned to specific protons. The resonances for the aromatic protons of the cationic cyclopalladated complexes of pyridine are particularly difficult to distinguish from each other due to intense overlap of resonances of more than 37 protons in a small region of the spectrum. However, all clearly distinguishable resonances and coupling constants are assigned for all analogues (**Table 3-8.**).

Table 3-8. ^{1}H-NMR spectral data of cationic cyclopalladated complexes **C21 – C25**.[a]

Comp.	HC=N	Aromatic region	Aliphatic region		
			$\underline{H}C(CH_3)_2$	$ArC\underline{H}_3$	$HC(C\underline{H}_3)_2$
C21	8.67 (d, 1H, H^7, $^4J_{H\text{-}P}$ = 7.6Hz)	7.72 (br, 12H), 7.67 - 7.64 (m, 3H), 7.52 (br, 10H), 7.46 - 7.40 (m, 3H), 7.34 - 7.30 (m, 5H), 7.08 - 7.06 (m, 1H), 6.91 - 6.89 (m, 2H), 6.72 (t, 1H, H^3, $^3J_{H\text{-}H}$ = 7.9Hz), 6.47 - 6.43 (m, 1H, H^4)	3.20 (m, 2H, $H^{14,16}$)		1.21 (d, 6H, $H^{15/17}$, $^3J_{H\text{-}H}$ = 6.8Hz), 1.18 (d, 6H, $H^{15/17}$, $^3J_{H\text{-}H}$ = 6.8Hz)
C22	8.68 (d, 1H, H^7, $^4J_{H\text{-}P}$ = 7.5Hz)	7.71 (br, 12H), 7.67 - 7.64 (m, 3H), 7.51 (br, 10H), 7.46 - 7.40 (m, 3H), 7.34 - 7.29 (m, 5H), 7.05 - 7.02 (m, 1H), 6.91 - 6.89 (m, 2H), 6.61 (t, 1H, H^3, $^3J_{H\text{-}H}$ = 7.8Hz), 6.52 - 6.47 (m, 1H, H^4)	3.21 (m, 2H, $H^{14,16}$)		1.22 (d, 6H, $H^{15/17}$, $^3J_{H\text{-}H}$ = 6.8Hz), 1.18 (d, 6H, $H^{15/17}$, $^3J_{H\text{-}H}$ = 6.8Hz)
C23	8.17 (d, 1H, H^7, $^4J_{H\text{-}P}$ = 7.5Hz)	7.72 (br, 12H), 7.68 - 7.66 (m, 3H), 7.52 (br, 10H), 7.46 - 7.40 (m, 3H), 7.35 - 7.29 (m, 5H), 7.16 - 7.11 (m, 1H), 7.04 - 6.99 (m, 1H), 6.90 - 6.87 (m, 2H), 6.82 - 6.77 (m, 1H), 6.60 - 6.55 (m, 1H, H^4)	3.21 (m, 2H, $H^{14,16}$)		1.20 (d, 6H, $H^{15/17}$, $^3J_{H\text{-}H}$ = 6.8Hz), 1.14 (d, 6H, $H^{15/17}$, $^3J_{H\text{-}H}$ = 6.8Hz)
C24	8.48 (d, 1H, H^7, $^4J_{H\text{-}P}$ = 7.6Hz)	7.71 (br, 12H), 7.68 - 7.65 (m, 3H), 7.52 (br, 10H), 7.45 - 7.40 (m, 3H), 7.33 - 7.30 (m, 5H), 7.05 - 6.99 (m, 1H), 6.91 - 6.86 (m, 3H), 6.44 - 6.39 (m, 1H, H^4)	3.23 (m, 2H, $H^{14,16}$)	2.51 (s, 3H, H^{18})	1.20 (d, 6H, $H^{15/17}$, $^3J_{H\text{-}H}$ = 6.8Hz), 1.15 (d, 6H, $H^{15/17}$, $^3J_{H\text{-}H}$ = 6.8Hz)
C25	8.10 (d, 1H, H^7, $^4J_{H\text{-}P}$ = 7.6Hz)	7.72 (br, 12H), 7.69 - 7.65 (m, 3H), 7.52 (br, 10H), 7.47 - 7.39 (m, 3H), 7.34 - 7.28 (m, 5H), 7.03 - 6.98 (m, 1H), 6.94 - 6.92 (m, 1H), 6.89 - 6.87 (m, 2H), 6.33 (d, 1H, H^4, $^4J_{H\text{-}P}$ = 6.2Hz)	3.20 (m, 2H, $H^{14,16}$)	1.79 (s, 3H, H^{18})	1.19 (d, 6H, $H^{15/17}$, $^3J_{H\text{-}H}$ = 6.8Hz), 1.13 (d, 6H, $H^{15/17}$, $^3J_{H\text{-}H}$ = 6.8Hz)

[a] Spectra recorded in $CDCl_3$ at 298 K. Chemical shifts reported in δ ppm values, referenced relative to the residual $CDCl_3$ peak. Superscripts denote protons as per numbering scheme (**Figure 3-10.**).

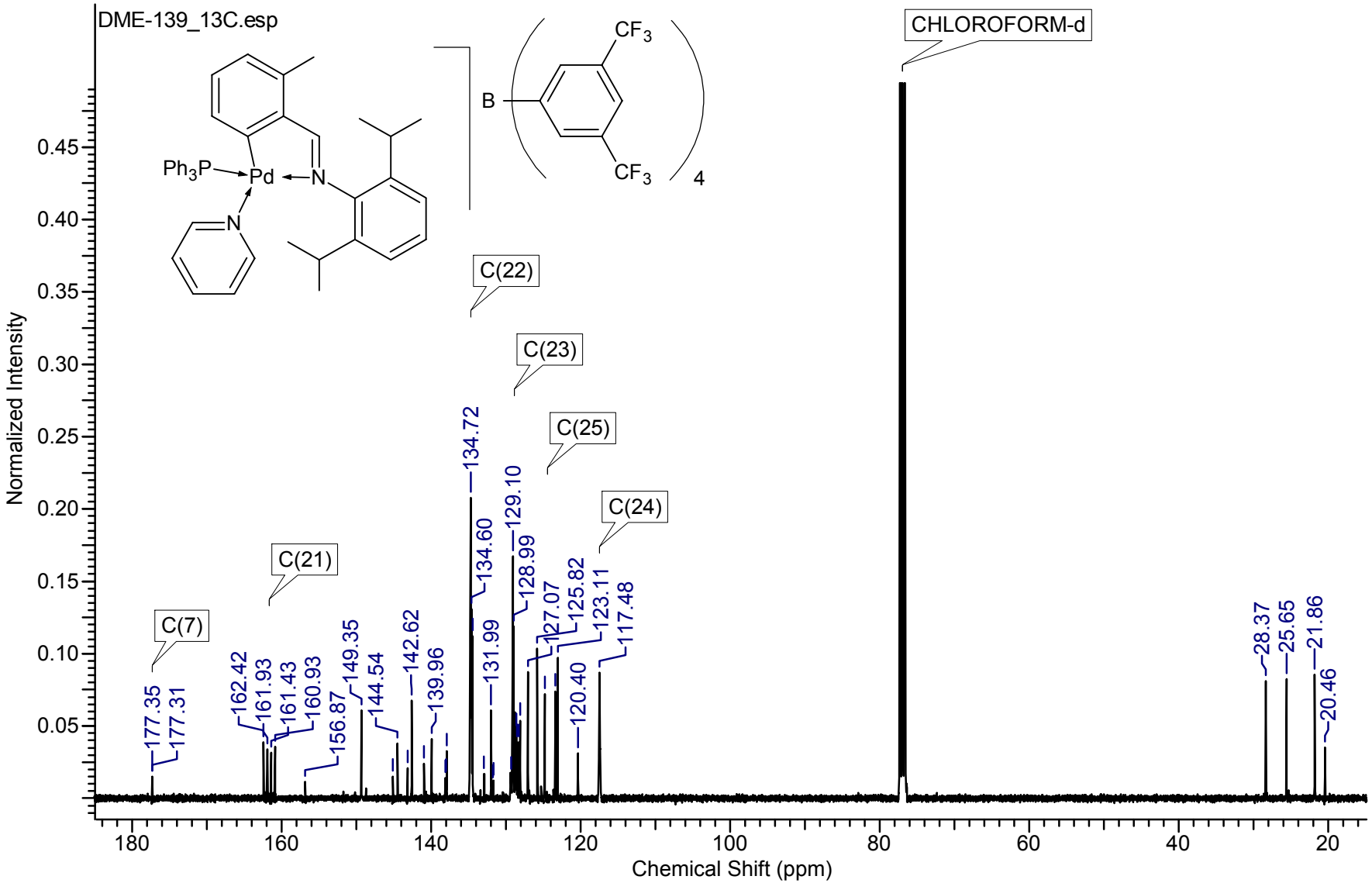

Figure 3-12. ^{13}C $\{^{1}H\}$-NMR spectrum of complex **C24**.

Crystals suitable for single crystal diffraction analysis were obtained of complex **C24** (**Figure 3-13.**). Recrystallisation by means of slow evaporation from dichloromethane/*n*-pentane at low temperature (-4 °C) resulted in the formation of colourless single crystals.

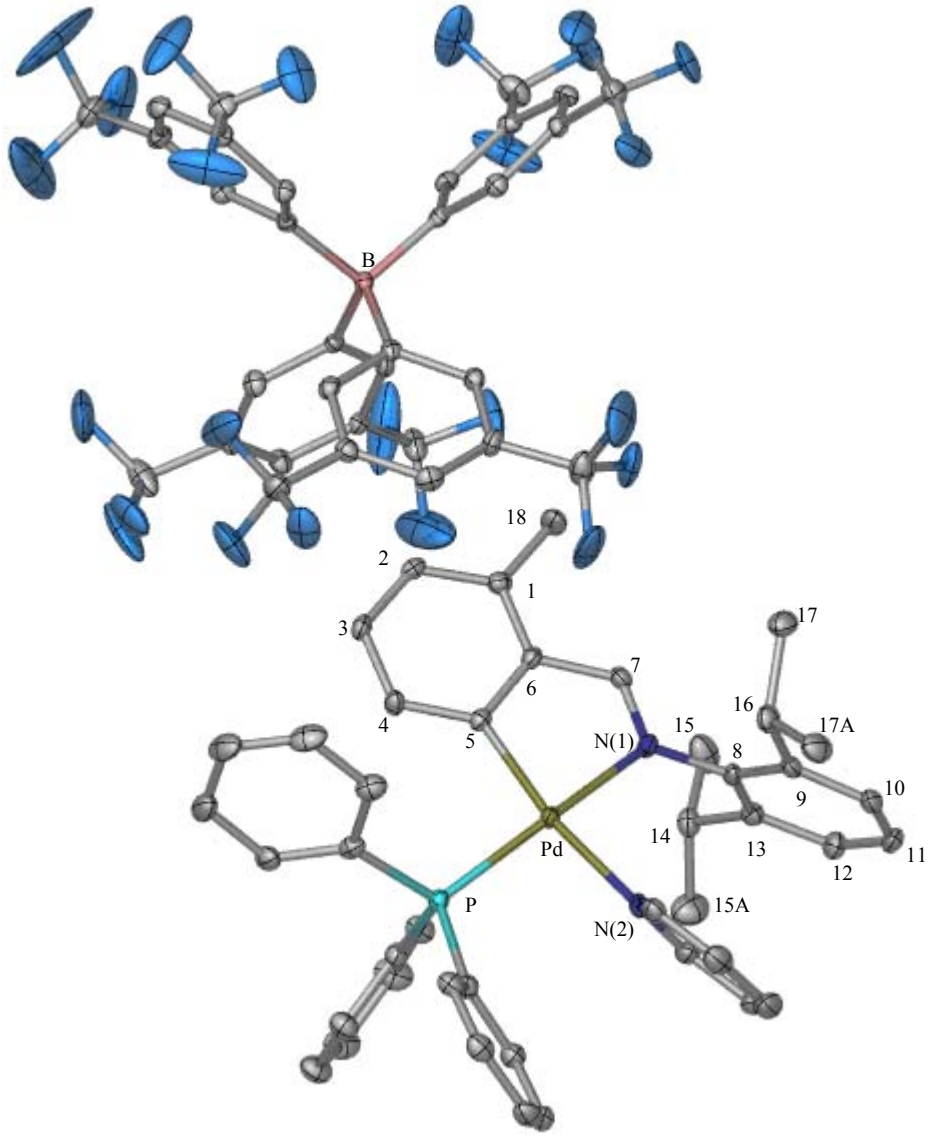

Figure 3-13. Molecular structure of complex **C24** shown with 50 % probability ellipsoids and the numbering scheme (hydrogen atoms are omitted for clarity).

The molecular structure provides unambiguous confirmation of the successful substitution reaction. The coordination of the palladium atom is distorted square-planar, in a

similar manner to that of complex **C19** and the pyridine donor ligand is situated *trans* to the Pd-C bond. Selected bond lengths, bond angles and torsion angles are listed in **Table 3-10.**.

A number of weak noncovalent intermolecular interactions are present in the packing arrangement of complex **C24** (**Figure 3-14.**). The fluorines of the trifluoromethyl substituents of the $[B(Ar)_4]^-$ counterion in particular contribute greatly towards the stability of the packing system. These include, amongst others, C-F···H, C-F···F and C-F···π interactions.

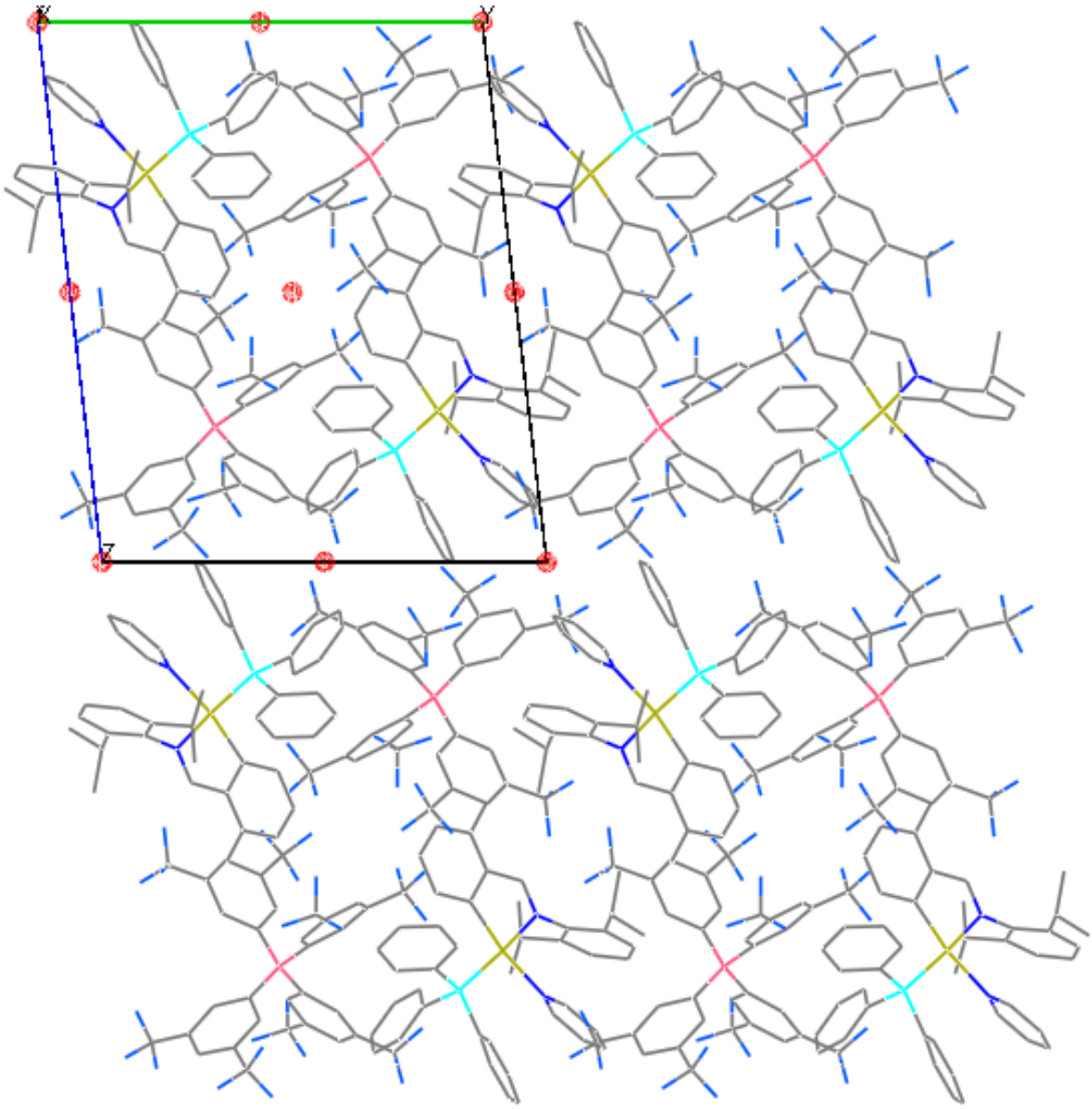

Figure 3-14. Packing diagram of complex **C24** shown along the a-axis. Inversion centres are marked with ● (hydrogen atoms are omitted for clarity).

Table 3-9. Crystallographic data and structure refinement parameters of complex **C24**.

Empirical formula	$C_{75}H_{53}BF_{24}N_2PPd$
M_r (g/mol)	1586.37
Crystal system	triclinic
Space group	$P\bar{1}$ (No.2)
a (Å)	12.3224 (19)
b (Å)	15.599 (2)
c (Å)	18.563 (3)
α (deg)	82.869 (2)
β (deg)	88.146 (2)
γ (deg)	82.276 (2)
Volume (Å^3)	3507.9 (9)
Z	2
D_{calc} (g cm^{-3})	1.502
F000	1598
λ (MoK_α) (Å)	0.71073
Temperature (K)	103 (2)
2θ max (deg)	57.8
Lp and absorption corrections applied (μ)	0.396 mm^{-1}
Data/restraints/par.	16756/0/941
R_1 [$I > 2\sigma(I)$]	0.0543
wR_2 (all reflections)	0.1462
Goodness of fit on F^2	0.981
Max/min residual electron density (e Å^{-3})	1.753 / -0.870

Table 3-10. Selected bond lengths, bond angles and torsion angles of the crystallographically determined structure of complex **C24**.[a]

Bond lengths (Å)	
Pd-C(5)	2.024
Pd-N(1)	2.103
Pd-N(2)	2.126
Pd-P	2.275
C(7)-N(1)	1.281
C(8)-N(1)	1.433
C(1)-C(18)	1.507
Bond angles (degrees)	
N(1)-Pd-N(2)	91.02
N(2)-Pd-P	92.09
P-Pd-C(5)	96.64
C(5)-Pd-N(1)	80.80
Torsion angles (degrees)	
C(8)-C(13)-C(14)-C(15)	99.28
C(8)-C(9)-C(16)-C(17)	-83.67

[a] Atom labelling as per numbering scheme (**Figure 3-13.**).

The bond distances and bond angles at the coordination sphere surrounding the metal centre are similar to those of complex **C19**. While the Pd-P bond distances are alike, the Pd-N(1), Pd-N(2) and Pd-C(5) distances are longer. Similarly to complex **C19**, the P-Pd-C(5) bond angle is the greatest while the chelating C(5)-Pd-N(1) angle is the smallest.

3.1.3 The preparation of cationic cyclopalladated complexes bearing two trimethylphosphine ligands

Cationic cyclopalladated complexes **C26 – C30** were prepared by the abstraction of the chloride ligand of the previously discussed neutral non-cyclopalladated complexes (**Chapter 2, 2.2.4**) using sodium tetrakis [3,5-*bis*(trifluoromethyl)phenyl] borate (**Scheme 3-3.**). The latter serves to abstract the chloride ligand, forming sodium chloride as a by-product, and in so doing, create a vacant coordination site on the palladium metal centre. The vacant site is subsequently occupied by the imine nitrogen.

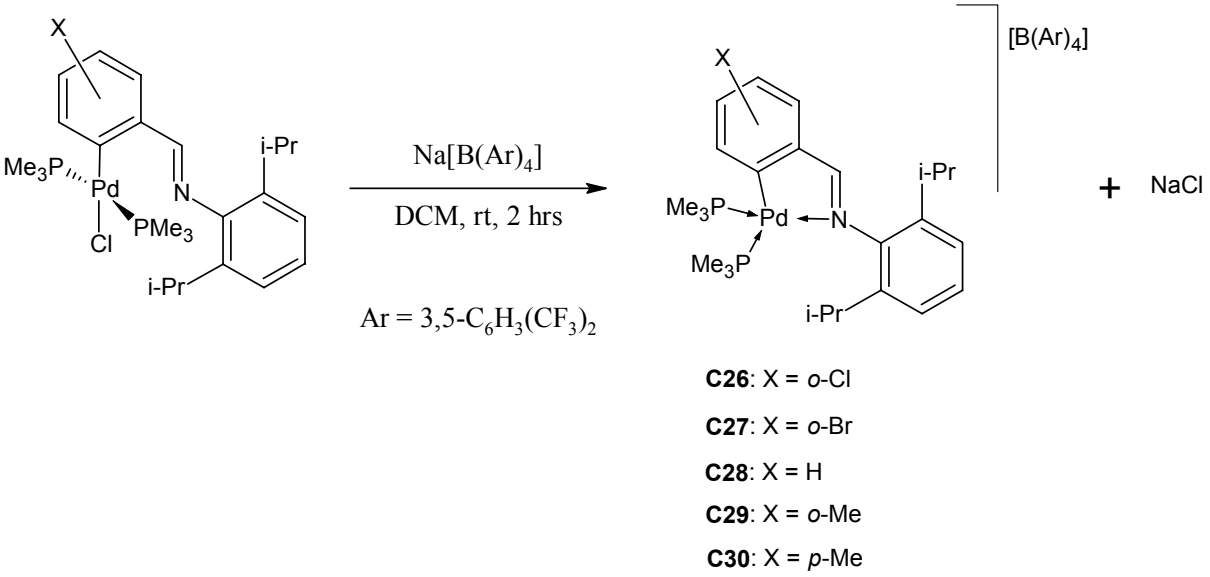

Scheme 3-3. Synthetic methodology employed for the preparation of the cationic cyclopalladated complexes bearing two trimethylphosphine ligands.

All compounds were isolated in good yields (67 – 88 %) as off-white solids that are soluble in polar organic solvents at room temperature. The complexes are stable in solution and in the solid state. All analogues are novel.

A variety of analytical techniques were employed to characterise the cationic complexes bearing two trimethylphosphine ligands similarly to that for the cationic complexes of acetonitrile (**3.1.1**). The FT-IR spectra of the resulting products indicate the formation of the desired cationic complexes (or the sake of convenience, this range of complexes (**C26 – C30**) is referred to as the cationic complexes bearing two trimethylphosphine ligands). The absence of the $\nu_{C=N}$ absorption bands corresponding to the non-cyclopalladated complex starting materials and the appearance of the $\nu_{C=N}$ absorption bands corresponding to the cationic products in the range 1605 – 1611 cm^{-1} provides evidence of the product formation (**Table 3-11.**).

Table 3-11. Analytical data of cationic cyclopalladated complexes **C26 – C30**.

Comp.	FT-IR ($\nu_{C=N}$, cm^{-1})[a]	ESI-MS M^+ (*m/z*)[b]	Melting point (°C)[c]
C26	1609	482	132 - 135
C27	1610	526	122 - 125
C28	1611	448	135 - 135
C29	1610	462	141 - 143
C30	1605	462	129 - 131

[a] Recorded as neat samples on a ZnSe crystal, employing an ATR accessory. [b] Reported ion corresponds to $[M - (PMe_3)]^+$, [c] Melting points recorded are uncorrected.

The appearance of the $\nu_{C=N}$ absorption bands corresponding to the cationic complex products together with the simultaneous disappearance of the $\nu_{C=N}$ absorption bands corresponding to the non-cyclopalladated complex starting materials indicate that the imine

nitrogen coordinates to the palladium metal centre during the reaction. The range, in wavenumbers, of the $\nu_{C=N}$ bands, which reveals that the double-bond character of the imine decreases upon completion of the abstraction of the chloride ligand, is similar to the range of the $\nu_{C=N}$ bands for the cationic complexes of acetonitrile (**C16 – C20**). This similarity in double-bond character indicates that the compound has once again become subject to the effects of metalloaromaticity. The coordination site vacated by the chloride ligand is occupied by the imine nitrogen.

Similarly to the results for the cationic complexes of acetonitrile and pyridine, the appearance of characteristic, very strong ν_{C-F} absorption bands of CF_3 at ~ 1354, 1275 and 1116 cm^{-1} are present for all analogues in the FT-IR spectra. Again, a strong ν_{C-B} stretch absorption band appears at ~ 839 cm^{-1} for all analogues.

Electrospray ionisation mass spectrometry, recorded in the positive ion mode, provides further evidence of the product formation. The base peak in the spectra, for all complexes, is due to the loss of one trimethylphosphine ligand, $[M - (PMe_3)]^+$ (**Table 3-11.**). For complexes **C26** and **C27**, minor clusters corresponding to the parent ion $[M + H]^+$ are also present, but at much lower intensity (**Figure 3-15.**). No subsequent fragmentation takes place. Calculated isotopic distributions of the fragments are consistent with the sample spectra for all analogues (**Figure 3-15. a** and **3-16. a**).[2]

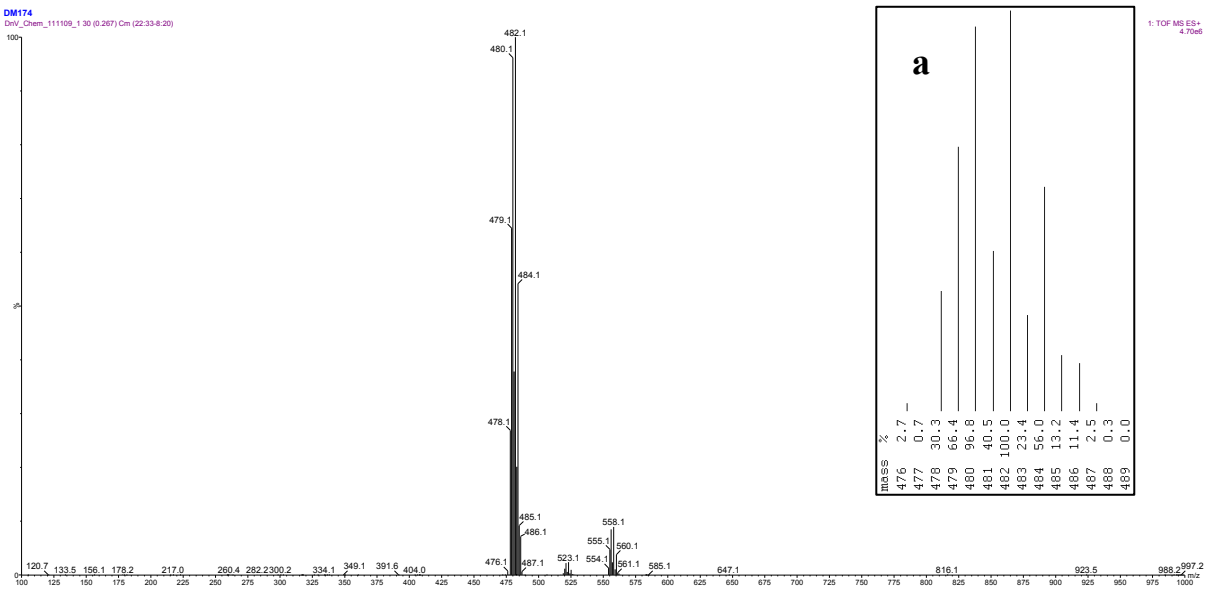

Figure 3-15. ESI-MS (+) spectrum in the region *m/z* 100 – 1000 of complex **C26**. The clusters of peaks centred at *m/z* 558.1 and 482.1 corresponds to the $[M + H]^+$ and $[M - (PMe_3)]^+$ fragments respectively.

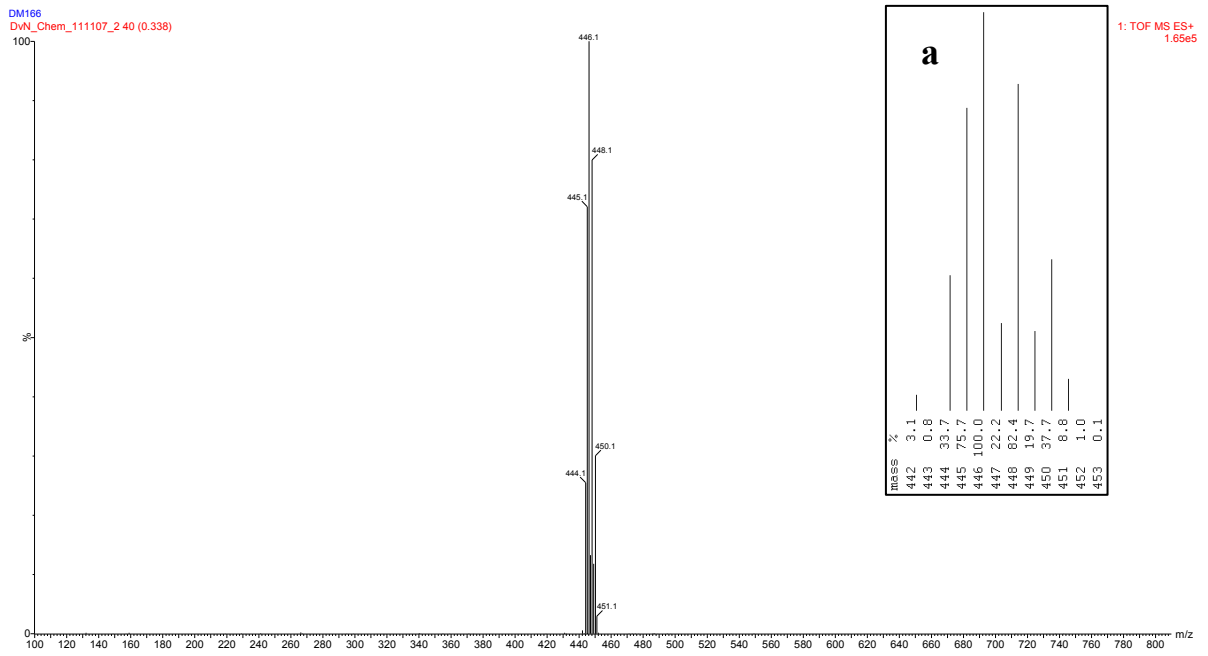

Figure 3-16. ESI-MS (+) spectrum in the region *m/z* 100 – 800 of complex **C28**. A cluster of peaks centred at *m/z* 448.1 corresponds to the $[M - (PMe_3)]^+$ fragment.

The ^{1}H-, ^{13}C {^{1}H}- and ^{31}P {^{1}H}-NMR spectra of the products confirm the formation of the cationic complexes. The appearance of a doublet of doublets in the region of δ 8.12 – 8.67 ppm for the imine proton in the ^{1}H-NMR spectra is due to hetero-nuclear $^{4}J_{H\text{-}P}$ coupling to the NMR active ^{31}P atoms of both the coordinated trimethylphosphine ligands. This splitting pattern confirms that the five-membered palladacycle is regenerated. The appearance of this resonance slightly upfield as compared to that of the non-cyclopalladated complexes confirms the presence of the previously discussed metalloaromaticity. As a result the imine proton is slightly less deshielded as compared to that of the non-cyclopalladated complexes.

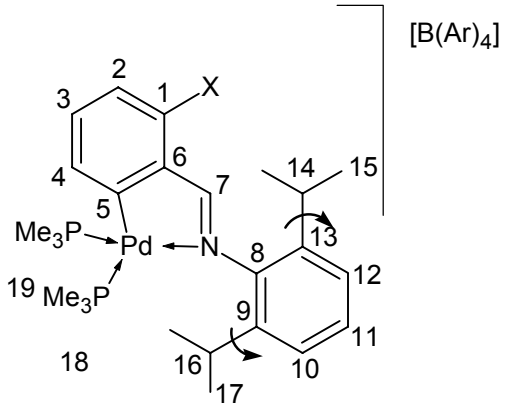

C26, **C27** and **C28**

X = Cl, Br and H respectively

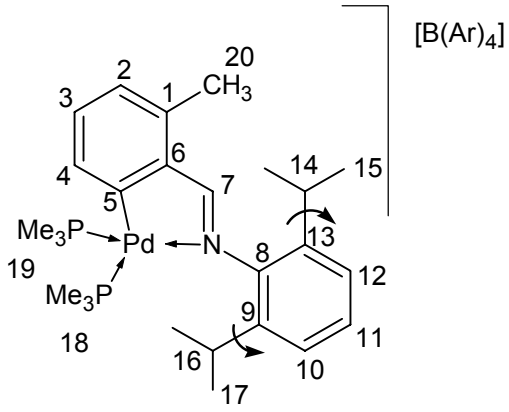

C29

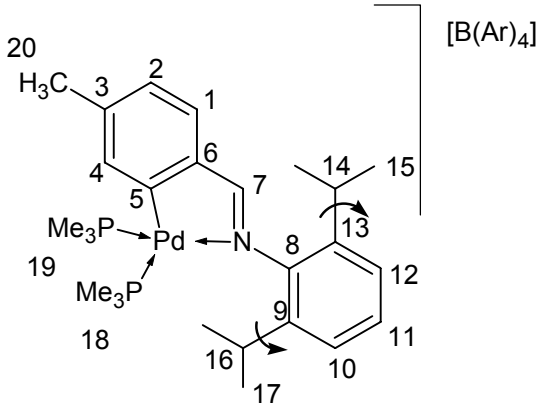

C30

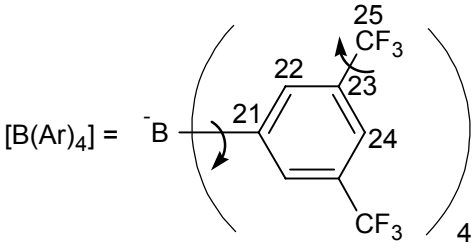

Figure 3-17. Schematic representation of complexes **C26 – C30**, including the $[B(Ar)_4]^-$ counterion, with the numbering for NMR spectral analysis.

Similarly to the results for complexes **C16 – C20** and **C21 – C25**, the imine proton resonances for complexes **C26** and **C27**, i.e. those with a halogen substituent at the *ortho* position, appear further downfield than the imine proton resonances for complexes **C28 – C30**.

^{1}H- and ^{13}C $\{^{1}$H$\}$-NMR spectral analysis reveals that there is no rotation along the bond between the nitrogen and carbon (8) in solution, at 298 K, upon completion of the abstraction of the chloride ligand (**Figure 3-17.**). The free rotation along the bonds between carbon (9) and carbon (16) as well as between carbon (13) and carbon (14) is retained. Similarly to the results for the cationic complexes of acetonitrile, the ^{13}C $\{^{1}$H$\}$-NMR spectra clearly reveals the presence of free rotation along the single bonds between boron and carbon (21) as well as between carbon (23) and carbon (25) in the $[B(Ar)_4]^-$ counterion.

The methine protons ($H^{14,16}$) resonate as a multiplet in the region of δ 3.28 – 3.33 ppm. For the non-cyclopalladated complexes they resonate as a septet in the region of δ 3.00 – 3.34 ppm. A clear change in chemical shifts for the resonances due to the isopropyl methyl protons ($H^{15/17}$) also takes place. For the non-cyclopalladated complexes, the appearance of one doublet in the region of δ 1.16 – 1.21 ppm reveals that H^{15} and H^{17} (H^{13}) are chemically equivalent. In contrast, the two doublets due to H^{15} and H^{17} for the cationic complexes **C26 – C30** appear in the regions of δ 1.14 – 1.18 ppm and δ 1.32 – 1.34 ppm, revealing that the rotation along the bond between the nitrogen and carbon (8) is restricted upon completion of the reaction. No significant shifts take place for the resonances of H^{20} for both complexes **C29** and **C30**.

The appearance of doublets at δ 0.98 ppm for H^{18} and in the region of δ 1.63 – 1.66 ppm for H^{19} is due to $^{2}J_{H\text{-}P}$ heteronuclear coupling of the protons of the two trimethylphosphine ligands to the phosphorous nuclei. The doublet at δ 0.98 ppm is due to the protons of H^{18}

since they are situated *trans* to the relatively electron-poor Pd-C bond, causing them to be shielded. The doublet in the region of δ 1.63 – 1.66 ppm is due to the protons of H^{19} since they are situated *trans* to the electron-richer Pd-N bond, causing them to be more deshielded. The $^{2}J_{H\text{-}P}$ coupling constant for H^{18} is in the region of 8.4 – 8.7 Hz and for H^{19} it is in the region of 10.5 – 10.6 Hz, which confirms the previously discussed assignment.

The imine carbon [carbon (7)] resonance in the ^{13}C $\{^{1}H\}$-NMR spectra appears as a doublet of doublets in the downfield region of δ 180.51 – 183.32 ppm. This splitting pattern is due to the hetero-nuclear $^{3}J_{C\text{-}P}$ coupling to the ^{31}P atoms of both the coordinated trimethylphosphine ligands. The appearance of this resonance is downfield as compared to that of the non-cyclopalladated complexes, which provides further confirmation of the presence of metalloaromaticity.

The chemical shifts and splitting patterns for carbons (21 – 25) of the $[B(Ar)_4]^-$ counterion in the ^{13}C $\{^{1}H\}$-NMR spectra are similar to those for the carbons of the $[B(Ar)_4]^-$ counterion for the cationic complexes of pyridine.

Two doublets, due to the two ^{31}P atoms, appear in the regions of δ -3.86 and δ -4.67 ppm and δ -25.24 and δ -26.42 ppm in the ^{31}P $\{^{1}H\}$-NMR spectra for all analogues (**Table 3-12.** and **Figure 3-18.**). The appearance of two doublets is due to $^{2}J_{P\text{-}P}$ coupling of the phosphorous nuclei to one another.

Identification of the resonances of all the protons in the ^{1}H-NMR spectra is possible for all five analogues. The clearly distinguishable resonances and coupling constants are assigned (**Table 3-13.** and **Figure 3-19.**).

Table 3-12. ^{31}P $\{^{1}H\}$-NMR spectral data of cationic complexes **C26 – C30**.

Comp.	δ (ppm)[a]
C26	-3.94 (d, P^{19}, $^{2}J_{P\text{-}P}$ = 47.7 Hz) and -25.27 (d, P^{18}, $^{2}J_{P\text{-}P}$ = 47.7 Hz)
C27	-4.20 (d, P^{19}, $^{2}J_{P\text{-}P}$ = 47.7 Hz) and -25.24 (d, P^{18}, $^{2}J_{P\text{-}P}$ = 47.7 Hz)
C28	-3.86 (d, P^{19}, $^{2}J_{P\text{-}P}$ = 46.7 Hz) and -26.09 (d, P^{18}, $^{2}J_{P\text{-}P}$ = 46.7 Hz)
C29	-4.67 (d, P^{19}, $^{2}J_{P\text{-}P}$ = 47.7 Hz) and -26.42 (d, P^{18}, $^{2}J_{P\text{-}P}$ = 47.7 Hz)
C30	-4.17 (d, P^{19}, $^{2}J_{P\text{-}P}$ = 46.7 Hz) and -26.13 (d, P^{18}, $^{2}J_{P\text{-}P}$ = 46.7 Hz)

[a] Spectra recorded in $CDCl_3$ at 298 K.

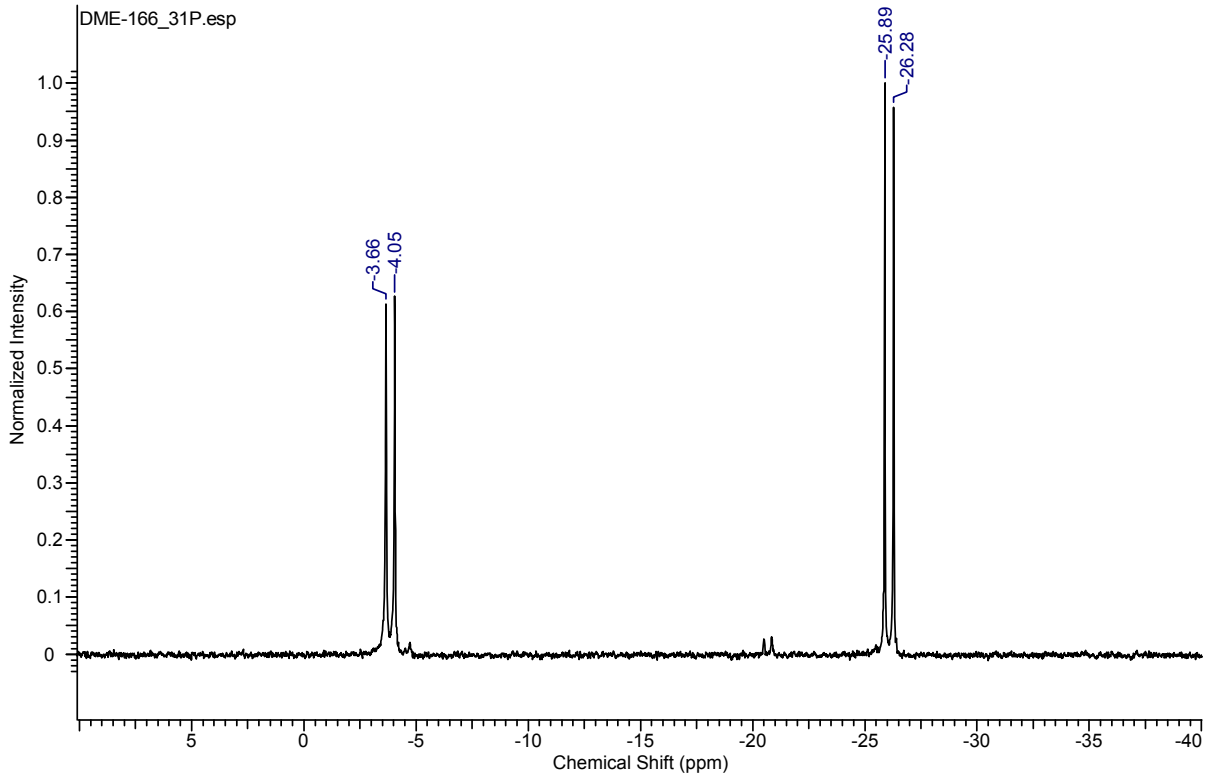

Figure 3-18. ^{31}P $\{^{1}H\}$-NMR spectrum of complex **C28**.

Table 3-13. ^{1}H-NMR spectral data of cationic cyclopalladated complexes **C26 – C30**.[a]

Comp.	HC=N	Aromatic region	Aliphatic region			
			$\underline{H}C(CH_3)_2$	$ArC\underline{H}_3$	$P(C\underline{H}_3)_3$	$HC(C\underline{H}_3)_2$
C26	8.67 (dd, 1H, H^7, $^4J_{H-P}$ = 7.0Hz, $^4J_{H-P}$ = 1.0Hz)	7.71 (br, 8H, H^{22}), 7.53 (br, 4H, H^{24}), 7.39 - 7.31 (m, 2H), 7.29 - 7.24 (m, 2H), 7.22 - 7.11 (m, 2H)	3.30 (m, 2H, $H^{14,16}$)		1.63 (d, 9H, H^{19}, $^2J_{H-P}$ = 10.6Hz), 0.98 (d, 9H, H^{18}, $^2J_{H-P}$ = 8.7Hz)	1.34 (d, 6H, $H^{15/17}$, $^3J_{H-H}$ = 6.9Hz), 1.18 (d, 6H, $H^{15/17}$, $^3J_{H-H}$ = 6.8Hz)
C27	8.67 (dd, 1H, H^7, $^4J_{H-P}$ = 7.0Hz, $^4J_{H-P}$ = 1.2Hz)	7.71 (br, 8H, H^{22}), 7.54 (br, 4H, H^{24}), 7.42 - 7.34 (m, 2H), 7.29 - 7.26 (m, 2H), 7.22 - 7.18 (m, 2H)	3.31 (m, 2H, $H^{14,16}$)		1.63 (d, 9H, H^{19}, $^2J_{H-P}$ = 10.6Hz), 0.98 (d, 9H, H^{18}, $^2J_{H-P}$ = 8.7Hz)	1.34 (d, 6H, $H^{15/17}$, $^3J_{H-H}$ = 6.8Hz), 1.18 (d, 6H, $H^{15/17}$, $^3J_{H-H}$ = 6.8Hz)
C28	8.17 (dd, 1H, H^7, $^4J_{H-P}$ = 7.0Hz, $^4J_{H-P}$ = 1.2Hz)	7.71 (br, 8H, H^{22}), 7.53 (br, 4H, H^{24}), 7.56 - 7.54 (m, 1H, H^1), 7.39 - 7.37 (m, 1H), 7.34 - 7.30 (m, 3H), 7.27 - 7.25 (m, 2H)	3.28 (m, 2H, $H^{14,16}$)		1.65 (d, 9H, H^{19}, $^2J_{H-P}$ = 10.5Hz), 0.98 (d, 9H, H^{18}, $^2J_{H-P}$ = 8.4Hz)	1.32 (d, 6H, $H^{15/17}$, $^3J_{H-H}$ = 6.8Hz), 1.15 (d, 6H, $H^{15/17}$, $^3J_{H-H}$ = 6.8Hz)
C29	8.48 (dd, 1H, H^7, $^4J_{H-P}$ = 7.0Hz, $^4J_{H-P}$ = 1.2Hz)	7.71 (br, 8H, H^{22}), 7.54 (br, 4H, H^{24}), 7.39 - 7.31 (m, 2H), 7.29 - 7.24 (m, 2H), 7.22 - 7.11 (m, 2H)	3.33 (m, 2H, $H^{14,16}$)	2.50 (s, 3H, H^{20})	1.64 (d, 9H, H^{19}, $^2J_{H-P}$ = 10.6Hz), 0.98 (d, 9H, H^{18}, $^2J_{H-P}$ = 8.4Hz)	1.33 (d, 6H, $H^{15/17}$, $^3J_{H-H}$ = 6.8Hz), 1.16 (d, 6H, $H^{15/17}$, $^3J_{H-H}$ = 6.8Hz)
C30	8.12 (dd, 1H, H^7, $^4J_{H-P}$ = 7.0Hz, $^4J_{H-P}$ = 1.2Hz)	7.71 (br, 8H, H^{22}), 7.54 (br, 4H, H^{24}), 7.45 - 7.43 (m, 1H), 7.35 - 7.31 (m, 1H), 7.26 - 7.24 (m, 2H), 7.14 - 7.10 (m, 2H)	3.29 (m, 2H, $H^{14,16}$)	2.41 (s, 3H, H^{20})	1.66 (d, 9H, H^{19}, $^2J_{H-P}$ = 10.5Hz), 0.98 (d, 9H, H^{18}, $^2J_{H-P}$ = 8.4Hz)	1.32 (d, 6H, $H^{15/17}$, $^3J_{H-H}$ = 6.8Hz), 1.14 (d, 6H, $H^{15/17}$, $^3J_{H-H}$ = 6.8Hz)

[a] Spectra recorded in $CDCl_3$ at 298 K. Chemical shifts reported in δ ppm values, referenced relative to the residual $CDCl_3$ peak. Superscripts denote protons as per numbering scheme (**Figure 3-17.**).

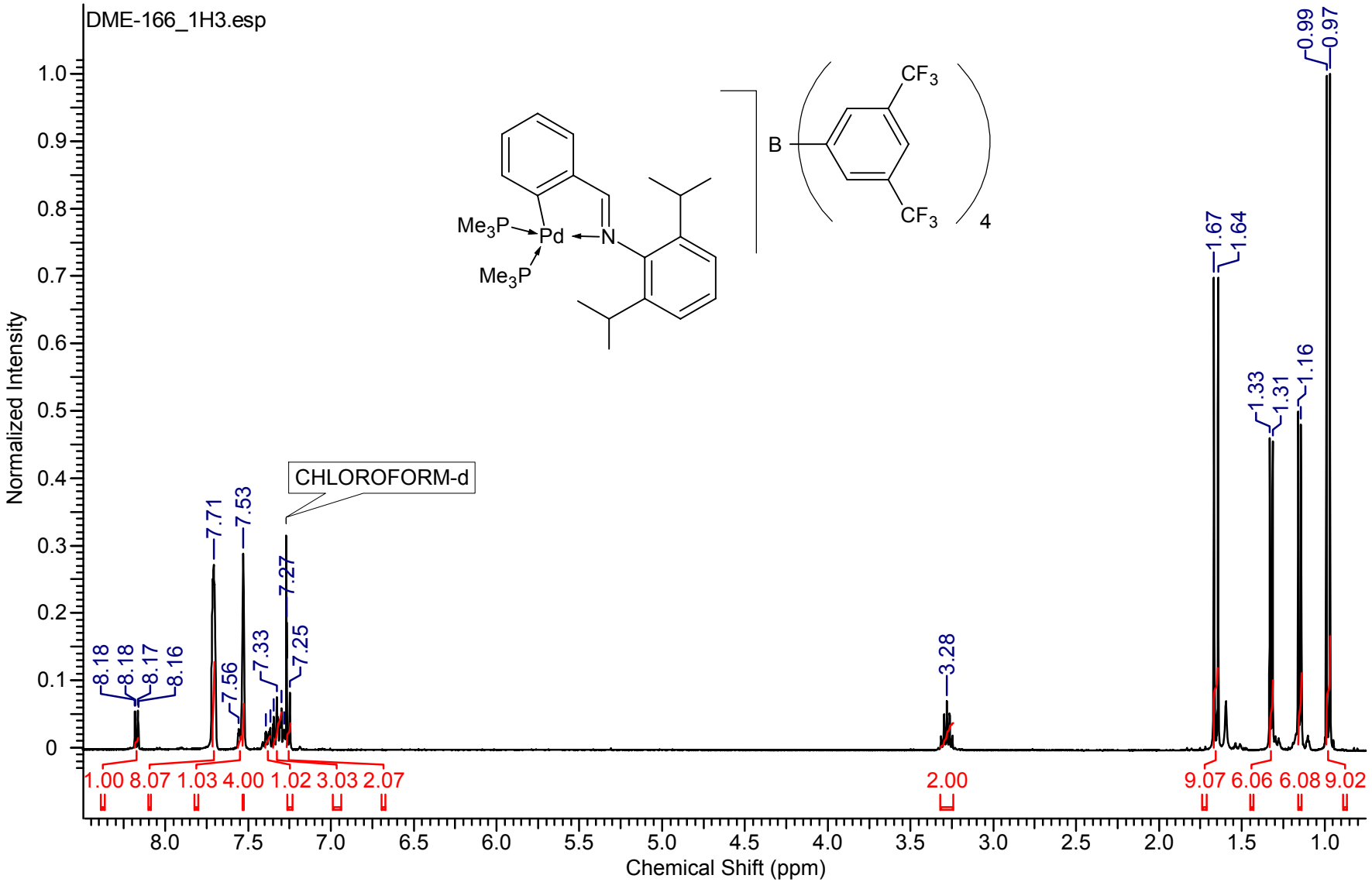

Figure 3-19. ^{1}H NMR spectrum of complex **C28**.

Crystals of complex **C29** were obtained for single crystal diffraction analysis. Slow evaporation from dichloromethane/*n*-pentane at low temperature (-4 °C) resulted in the formation of light yellow single crystals (**Figure 3-20.**).

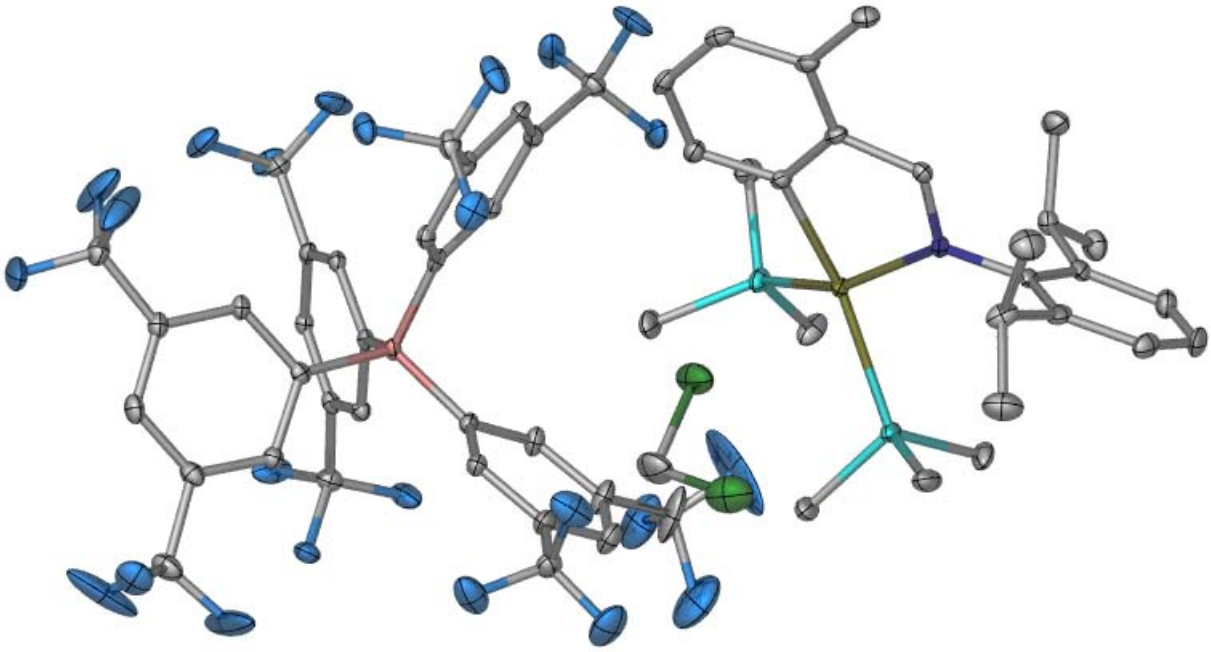

Figure 3-20. Molecular structure of complex **C29** shown with 30 % probability ellipsoids (hydrogen atoms are omitted for clarity).

The asymmetric unit comprises the cationic complex molecule with the $[B(Ar)_4]^-$ counterion and a dichloromethane solvent molecule. Despite the fact that the crystallographic data and structure refinement parameters are not suitable for publication, the solved structure confirms the distorted square-planar geometry of the palladium atom and that the coordination site vacated by the chloride during the abstraction process is displaced by the imine nitrogen. The distorted square-planar geometry of the palladium atom confirms that the formation of the sodium chloride precipitate is the driving force of the substitution reaction.

The reaction as seen in **Scheme 3-3.** was repeated for the *o*-Cl analogue in the presence of excess trimethylphosphine (**Scheme 3-4.**) The vacant coordination site on the palladium metal centre that is created upon abstraction of the chloride ligand is subsequently occupied by the trimethylphosphine.

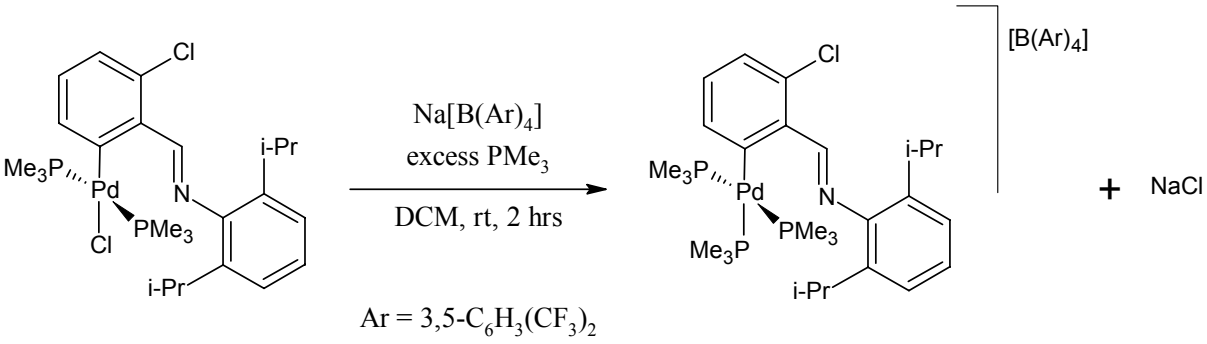

Scheme 3-4. Synthetic methodology employed for the preparation of the cationic non-cyclopalladated complex **C31** bearing three trimethylphosphine ligands.

The novel compound, complex **C31**, was isolated in 82 % yield as an off-white solid that is soluble in polar organic solvents at room temperature. It is stable in solution and in the solid state.

The appearance of the $\nu_{C=N}$ absorption band at 1611 cm^{-1} in the FT-IR spectrum does not provide sufficient evidence of the product formation (**Figure 3-21.**). The $\nu_{C=N}$ absorption band is very close to that obtained in the FT-IR spectrum for complex **C26**, which appears at 1609 cm^{-1}.

The appearance of characteristic, very strong ν_{C-F} absorption bands of CF_3 at 1355, 1276 and 1120 cm^{-1} and a strong ν_{C-B} stretch absorption band at 887 cm^{-1} is present in the FT-IR spectrum. These bands confirm the formation of the cationic complex but not whether or not the vacated coordination site is occupied by the imine nitrogen or the trimethylphosphine.

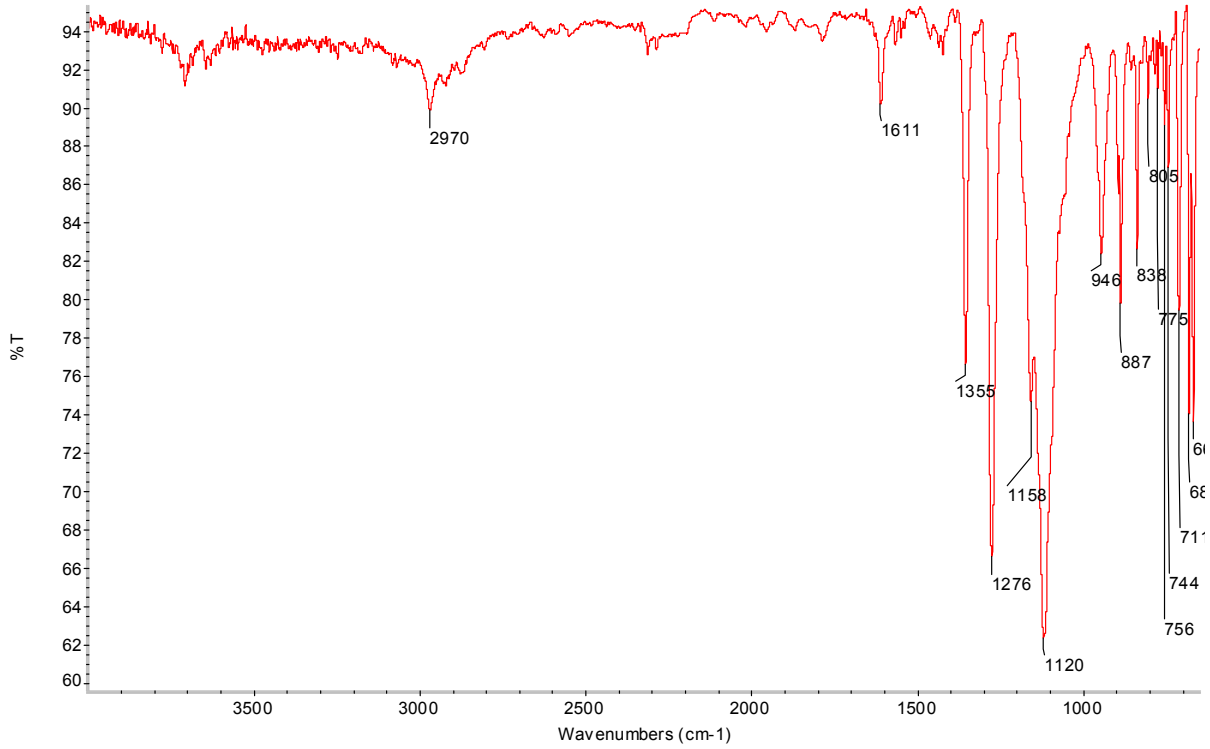

Figure 3-21. FT-IR spectrum of complex **C31**.

Electrospray ionisation mass spectrometry, recorded in the positive ion mode, gives a spectrum similar to that for complex **C26**. The base peak in the spectrum appears at *m/z* 482.1, which corresponds to the $[M - (2\ PMe_3)]^+$ fragment, and a minor cluster of peaks appears at *m/z* 558.1, which corresponds to the $[M - (PMe_3)]^+$ fragment (**Figure 3-22.**).

The ^{1}H-, ^{13}C $\{^1H\}$- and ^{31}P $\{^1H\}$-NMR spectra of the product confirm the formation of the non-cyclopalladated cationic complex. The proton resonance of the imine functionality in the ^{1}H-NMR spectra appears as a singlet at δ 8.87 ppm, slightly downfield as compared to the corresponding singlet for complex **C11**, which confirms that the vacant site vacated by the chloride ligand is occupied by trimethylphosphine and not the imine nitrogen (**Figure 3-24.**).

The imine carbon resonance in the ^{13}C $\{^1H\}$-NMR spectrum appears as a singlet at δ 176.05 ppm. This resonance is downfield as compared to that of the neutral non-

cyclopalladated complex starting material **C11** and upfield as compared to the doublet of doublets for complex **C26**, which provides further confirmation that the vacated site is occupied by trimethylphosphine.

The chemical shifts and splitting patterns for carbons (21 – 25) of the $[B(Ar)_4]^-$ counterion in the ^{13}C $\{^1H\}$-NMR spectrum is similar to those for the carbons of the $[B(Ar)_4]^-$ counterion for the cationic complexes bearing two trimethylphosphine ligands.

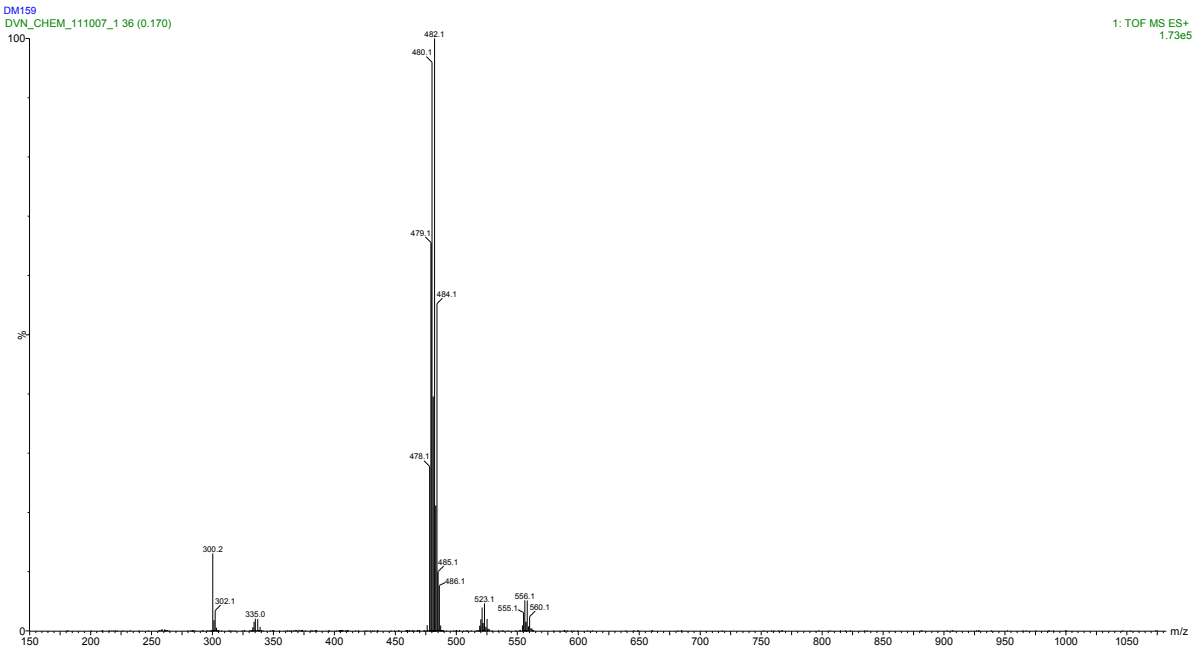

Figure 3-22. ESI-MS (+) spectrum in the region *m/z* 150 – 1050 of complex **C31**. The clusters of peaks centred at *m/z* 558.1 and 482.1 corresponds to the [M - (PMe_3)] and $[M - (2\ PMe_3)]^+$ fragments respectively.

The appearance of a doublet at δ -22.30 ppm ($^2J_{P\text{-}P}$ = 41.5 Hz) is due to the ^{31}P atoms of the two chemically equivalent trimethylphosphine ligands that are situated *cis* to the Pd-C bond (**Figure 3-23.**). The triplet that appears at δ -25.62 ppm ($^2J_{P\text{-}P}$ = 41.5 Hz) is due to the ^{31}P atom of the phosphine ligand that is situated *trans* to the Pd-C bond.

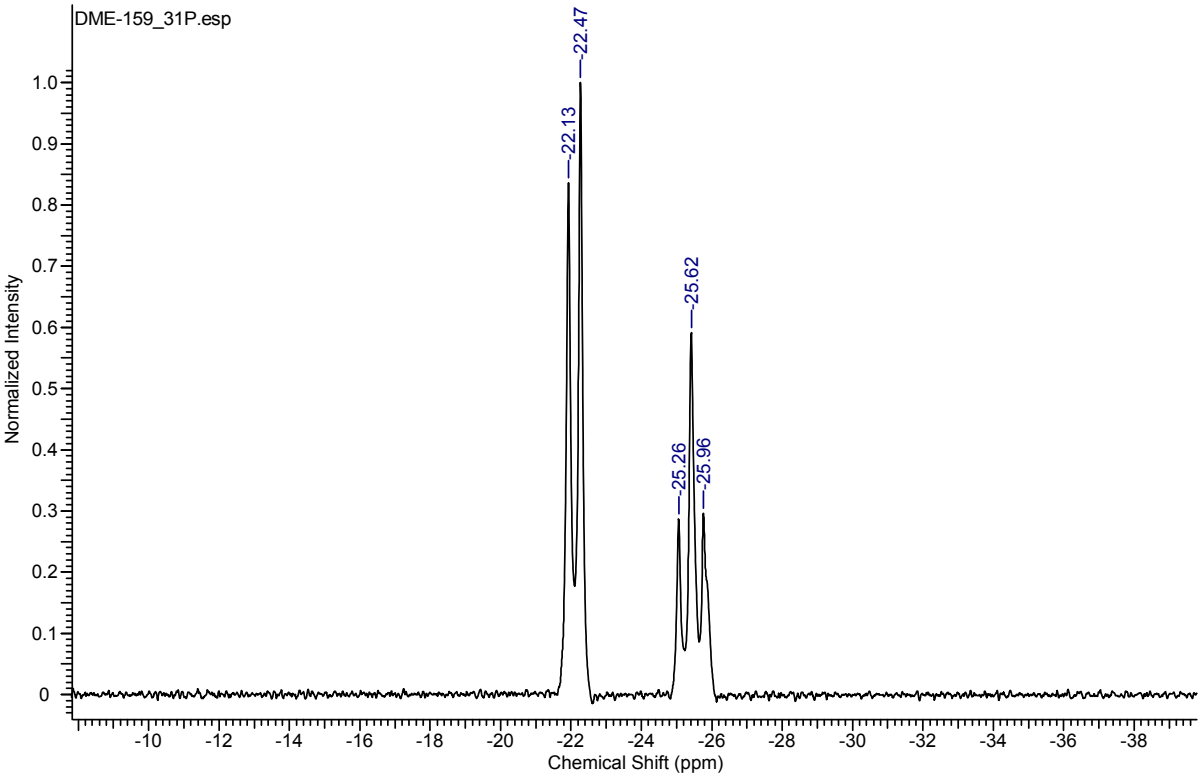

Figure 3-23. ^{31}P $\{^{1}H\}$-NMR spectrum of complex **C31**.

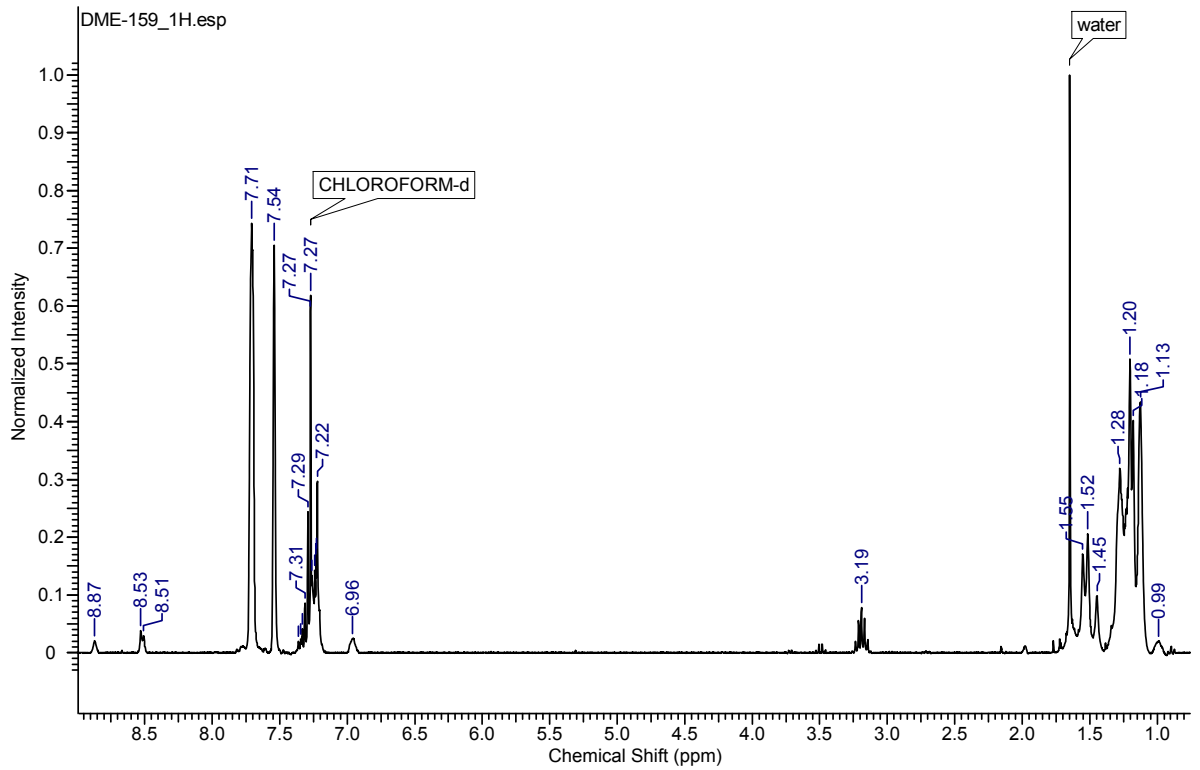

Figure 3-24. ^{1}H NMR spectrum of complex **C31**.

Crystals suitable for single crystal diffraction analysis were obtained of complex **C31** (**Figure 3-25.**). Recrystallisation by means of slow evaporation from dichloromethane/*n*-pentane at room temperature resulted in the formation of colourless single crystals.

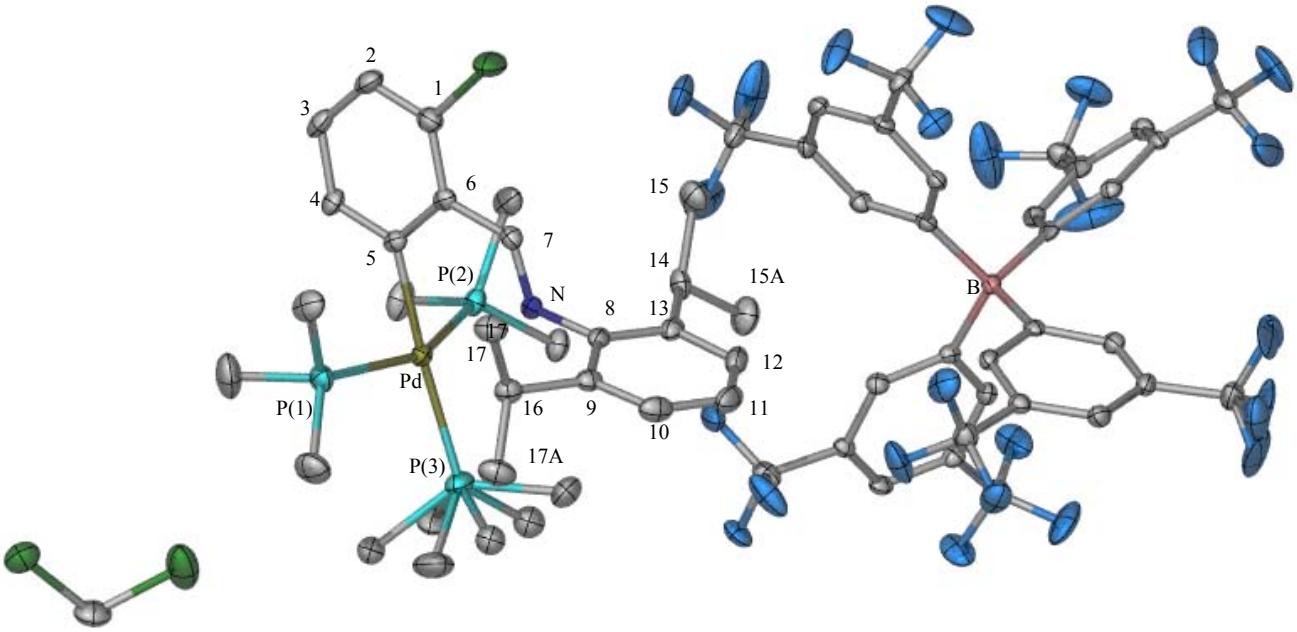

Figure 3-25. Molecular structure of complex **C31** shown with 50 % probability ellipsoids and the numbering scheme (hydrogen atoms are omitted for clarity).

The molecular structure confirms that the coordination site that was created upon abstraction of the chloride ligand is occupied by trimethylphosphine. The asymmetric unit comprises the non-cyclopalladated, cationic complex molecule with the $[B(Ar)_4]^-$ counterion and a dichloromethane solvent molecule. The coordination of the palladium atom is distorted square-planar, which is dissimilar to that of the starting material, complex **C11** (**Chapter 2**). The disorder of the methyl groups of P(3) indicates that rotation along the bond between the palladium and the phosphorous [P(3)] takes place. The large ellipsoids at the two modelled positions confirm the rotation (**Figure 3-25.**). Selected bond lengths, bond angles and torsion angles are listed in **Table 3-15.**.

Table 3-14. Crystallographic data and structure refinement parameters of complex **C31**.

Empirical formula	$C_{60.38}H_{60.76}BCl_{1.75}F_{24}NP_3Pd$
M_r (g/mol)	1528.72
Crystal system	monoclinic
Space group	$P2_1/c$ (No.14)
a (Å)	12.7825 (13)
b (Å)	27.726 (3)
c (Å)	18.8014 (19)
α (deg)	90
β (deg)	90.755 (2)
γ (deg)	90
Volume (Å^3)	6662.8 (12)
Z	4
D_{calc} (g cm^{-3})	1.524
F000	3087
λ (MoK$_\alpha$) (Å)	0.71073
Temperature (K)	107 (2)
2θ max (deg)	57.8
Lp and absorption corrections applied (μ)	0.527 mm^{-1}
Data/restraints/par.	16134/0/906
R_1 [$I > 2\sigma(I)$]	0.0469
wR_2 (all reflections)	0.0961
Goodness of fit on F^2	1.053
Max/min residual electron density (e Å^{-3})	0.536 / -0.677

Table 3-15. Selected bond lengths, bond angles and torsion angles of the crystallographically determined structure of complex **C31**.[a]

Bond lengths (Å)	
Pd-C(5)	2.043
Pd-P(1)	2.338
Pd-P(2)	2.350
Pd-P(3)	2.344
C(7)-N	1.277
C(8)-N	1.433
Bond angles (degrees)	
P(1)-Pd-C(5)	82.96
C(5)-Pd-P(2)	82.28
P(2)-Pd-P(3)	95.00
P(3)-Pd-P(1)	100.43
Torsion angles (degrees)	
C(8)-C(13)-C(14)-C(15)	-94.02
C(8)-C(9)-C(16)-C(17)	89.11

[a] Atom labelling as per numbering scheme (**Figure 3-25.**).

The bond distances and bond angles at the coordination sphere surrounding the metal centre are rather dissimilar to those of the starting material, complex **C11**. The Pd-C(5), Pd-P(1) and Pd-P(2) bond distances are longer following the substitution of the chloride ligand for trimethylphosphine. More significantly, the geometry of the palladium atom becomes distorted square-planar upon completion of the substitution reaction. The P(2)-Pd-Cl and Cl-

Pd-P(1) bond angles of 93.79° and 87.28° respectively pertaining to complex **C11** develop into P(2)-Pd-P(3) and P(3)-Pd-P(1) bond angles of 95.00° and 100.43° respectively for complex **C31**. This is due to the greater size (sterics) of the trimethylphosphine ligand as compared to the previously bound chloride ligand. The imine bond [C(7)-N] length for complex **C31** is longer than that of complex **C11**, revealing that the double-bond character decreases upon completion of the substitution reaction. This result is in agreement with the conclusions derived from the previously discussed FT-IR spectral analyses.

3.2 Conclusions

The chloride abstraction reaction of the neutral cyclopalladated complexes **C6 – C10** and the non-cyclopalladated complexes **C11 – C15** using sodium tetrakis [3,5-*bis*(trifluoromethyl)phenyl] borate is a suitable synthetic methodology for the preparation of cyclopalladated cationic complexes **C16 – C25**, **C26 – C30** and the non-cyclopalladated cationic complex **C31**. The various analytical techniques that were employed to characterise the compounds were successful and complement each other well.

The higher basicity of pyridine as compared to acetonitrile results in a greater degree of electron delocalisation in the palladacycle. The formation of the non-cyclopalladated cationic complex **C31** reveals that trimethylphosphine is more basic than the imine nitrogen.

3.3 Experimental section

3.3.1 General considerations

All reactions were carried out using standard Schlenk techniques under an inert atmosphere of dry nitrogen, unless specified otherwise. All solvents were dried using the appropriate drying agents and distilled before using.

Elemental analyses were carried out on a Thermo Elemental Analyser CHNS-O instrument at the University of Cape Town, Department of Chemistry and on a Vario-Elementar Microcube ELIII at Rhodes University, Department of Chemistry. ^{1}H- (299.74 and 399.94 MHz), ^{13}C $\{^{1}$H$\}$- (75.38 and 100.58 MHz) and ^{31}P $\{^{1}$H$\}$- (121.34 and 161.90 MHz) NMR spectra were recorded at 298 K on Varian VNMRS 300 MHz and Varian Unity Inova 400 MHz spectrometers. The chemical shift values are referenced to external tetramethylsilane. Chemical shifts (δ) and coupling constants (*J*) are expressed in ppm and in Hertz (Hz) respectively and the multiplicity as s = singlet, d = doublet, dd = doublet of doublets, t = triplet, q = quartet, qq = quartet of quartets, sep = septet and m = multiplet; data in parentheses are given in the following order: multiplicity, number of atoms, labelling of the atom(s) (',' denotes 'and'; '/' denotes 'or') and coupling constants in Hz. ESI-MS analyses, in the positive and negative ion mode, were performed on a Waters Synapt G2 instrument by direct injection of the sample. FT-IR analyses were performed on a Thermo Nicolet AVATAR 330, SMART PERFORMER, spectrometer and recorded as neat samples (ATR). Melting point determinations were performed on a Stuart Scientific, SMP3, melting point apparatus and are reported as uncorrected. Single crystal X-ray diffraction data collections were carried out on a Bruker Apex2 diffractometer with a CCD area detector[3] using graphite monochromated Mo-Kα radiation (λ = 0.71073 Å). The instrument is equipped with an Oxford Cryostream cooling system and the dataset for complexes **C19**, **C24**, **C29** and

C31 were collected at temperatures of 101 K, 103 K, 107 K and 107 K respectively. Data reduction was carried out by means of a standard procedure using the Bruker software package SAINT.[4] Absorption corrections and other systematic errors were accounted for where necessary using SADABS.[5] The structures were solved by Direct Methods or Patterson Interpretation using SHELXS-97 and refined using SHELXL-97.[6] X-Seed[7] was used as a graphical interface for the SHELX program suite to facilitate in exploring and analysing the structures. The POV-Ray[8] application using X-Seed was used to produce high quality molecular graphics. Due to their low scattering power it is difficult to locate hydrogen atoms using X-ray diffraction data. Hydrogen atoms were placed in calculated positions using riding models and isotropic thermal parameters were assigned.

The employed acetonitrile (Sigma-Aldrich), pyridine (Fluka, Sigma-Aldrich), trimethylphosphine (1M in THF solution) (Fluka, Sigma-Aldrich) and sodium tetrakis [3,5-*bis*(trifluoromethyl)phenyl] borate (Boulder Scientific Company and Alfa Aesar), were used as received.

3.3.2 Synthetic methodology employed for the preparation of the cationic cyclopalladated complexes of acetonitrile C16 – C20

General procedure for the synthesis of the cationic complexes of acetonitrile

The neutral cyclopalladated complex (0.0564 mmol), dissolved in dichloromethane (4 ml), was added to a stirring solution of $Na[B(Ar)_4]$ (60 mg, 0.0564 mmol), dissolved in acetonitrile (3 ml). The resulting light yellow solution was stirred for 2 hrs at room temperature. The sodium chloride precipitate was filtered from the resulting reaction mixture

and the solvent was removed from the filtrate. The product was isolated, by triturating with *n*-pentane, as an off-white powder. Recrystallisation of complex **C19** was achieved by means of slow evaporation from dichloromethane/*n*-pentane at room temperature.

[Pd(CH$_3$CN)PPh$_3$(2-ClC$_6$H$_3$)CH=N-{2,6-(*i*-Pr)$_2$-C$_6$H$_3$}]$^+$[B(Ar)$_4$]$^-$ (C16)

Yield: 78 %.

Anal. Calcd for $C_{71}H_{51}BClF_{24}N_2PPd \cdot 1.5\ CH_2Cl_2$: C, 50.19; H, 3.03; N, 1.65. Found: C, 50.52; H, 2.57; N, 0.51.

^{13}C {^{1}H}-NMR (100 MHz, numbering as per **Figure 3-3.**): δ 176.61 (d, C^7, $^3J_{C\text{-}P}$ = 4.6 Hz), 161.65 (q, C^{21}, $^1J_{C\text{-}B}$ = 49.9 Hz), 155.26 (C$_{Ar}$), 144.76 (C$_{Ar}$), 144.75 (C$_{Ar}$), 143.96 (C$_{Ar}$), 140.32 (C$_{Ar}$), 140.31 (C$_{Ar}$), 137.32 (C$_{Ar}$), 137.20 (C$_{Ar}$), 134.74 (br, C^{22}), 134.67 (C$_{Ar}$), 134.55 (C$_{Ar}$), 133.78 (C$_{Ar}$), 133.72 (C$_{Ar}$), 132.39 (C$_{Ar}$), 132.37 (C$_{Ar}$), 129.24 (C$_{Ar}$), 129.13 (C$_{Ar}$), 128.86 (qq, C^{23}, $^2J_{C\text{-}F}$ = 31.6 Hz, $^3J_{C\text{-}B}$ = 3.0 Hz), 128.52 (C$_{Ar}$), 128.41 (C$_{Ar}$), 127.89 (C$_{Ar}$), 127.35 (C$_{Ar}$), 124.51 (q, C^{25}, $^1J_{C\text{-}F}$ = 272.5 Hz), 123.76 (C$_{Ar}$), 117.44 (sep, C^{24}, $^3J_{C\text{-}F}$ = 3.8 Hz), 28.67 (C^{14,16}), 24.20 and 22.61 (C^{15,17}), 0.12 (C^{19}).

[Pd(CH$_3$CN)PPh$_3$(2-BrC$_6$H$_3$)CH=N-{2,6-(*i*-Pr)$_2$-C$_6$H$_3$}]$^+$[B(Ar)$_4$]$^-$ (C17)

Yield: 91 %.

Anal. Calcd for $C_{71}H_{51}BBrF_{24}N_2PPd \cdot 0.5\ CH_2Cl_2$: C, 51.41; H, 3.10; N, 1.69. Found: C, 51.27; H, 2.80; N, 0.50.

^{13}C {^{1}H}-NMR (75 MHz, numbering as per **Figure 3-3.**): δ 178.92 (d, C^7, $^3J_{C\text{-}P}$ = 4.5 Hz), 161.67 (q, C^{21}, $^1J_{C\text{-}B}$ = 49.8 Hz), 155.34 (C$_{Ar}$), 146.06 (C$_{Ar}$), 146.05 (C$_{Ar}$), 143.94 (C$_{Ar}$),

140.33 (C_{Ar}), 137.99 (C_{Ar}), 137.83 (C_{Ar}), 134.77 (br, C^{22}), 134.69 (C_{Ar}), 134.53 (C_{Ar}), 133.88 (C_{Ar}), 133.79 (C_{Ar}), 132.39 (C_{Ar}), 132.36 (C_{Ar}), 130.62 (C_{Ar}), 129.26 (C_{Ar}), 129.11 (C_{Ar}), 128.88 (qq, C^{23}, $^{2}J_{C\text{-}F}$ = 31.6 Hz, $^{3}J_{C\text{-}B}$ = 3.0 Hz), 128.52 (C_{Ar}), 128.49 (C_{Ar}), 127.79 (C_{Ar}), 124.53 (q, C^{25}, $^{1}J_{C\text{-}F}$ = 272.8 Hz), 123.77 (C_{Ar}), 123.54 (C_{Ar}), 119.40 (C_{Ar}), 117.45 (sep, C^{24}, $^{3}J_{C\text{-}F}$ = 3.8 Hz), 28.69 ($C^{14,16}$), 24.21 and 22.57 ($C^{15,17}$), 0.08 (C^{19}).

[Pd(CH$_3$CN)PPh$_3$(C$_6$H$_4$)CH=N-{2,6-(*i*-Pr)$_2$-C$_6$H$_3$}]$^+$[B(Ar)$_4$]$^-$ (C18)

Yield: 88 %.

Anal. Calcd for $C_{71}H_{52}BF_{24}N_2PPd{\cdot}0.5\ CH_2Cl_2$: C, 53.98; H, 3.32; N, 1.77. Found: C, 53.55; H, 2.92; N, 1.06.

^{13}C {^{1}H}-NMR (75 MHz, numbering as per **Figure 3-3.**): δ 178.18 (d, C^7, $^{3}J_{C\text{-}P}$ = 4.5 Hz), 161.67 (q, C^{21}, $^{1}J_{C\text{-}B}$ = 49.8 Hz), 153.99 (C_{Ar}), 147.67 (C_{Ar}), 143.76 (C_{Ar}), 140.40 (C_{Ar}), 138.98 (C_{Ar}), 138.83 (C_{Ar}), 134.75 (br, C^{22}), 134.59 (C_{Ar}), 132.54 (C_{Ar}), 132.45 (C_{Ar}), 132.24 (C_{Ar}), 132.21 (C_{Ar}), 130.73 (C_{Ar}), 129.18 (C_{Ar}), 129.03 (C_{Ar}), 128.88 (qq, C^{23}, $^{2}J_{C\text{-}F}$ = 31.5 Hz, $^{3}J_{C\text{-}B}$ = 3.0 Hz), 128.87 (C_{Ar}), 128.28 (C_{Ar}), 128.18 (C_{Ar}), 126.44 (C_{Ar}), 124.43 (q, C^{25}, $^{1}J_{C\text{-}F}$ = 272.8 Hz), 123.67 (C_{Ar}), 119.20 (C_{Ar}), 117.43 (sep, C^{24}, $^{3}J_{C\text{-}F}$ = 3.8 Hz), 28.59 ($C^{14,16}$), 24.10 and 22.63 ($C^{15,17}$), 0.13 (C^{19}).

[Pd(CH$_3$CN)PPh$_3$(2-CH$_3$C$_6$H$_3$)CH=N-{2,6-(*i*-Pr)$_2$-C$_6$H$_3$}]$^+$[B(Ar)$_4$]$^-$ (C19)

Yield: 93 %.

Anal. Calcd for $C_{72}H_{54}BF_{24}N_2PPd{\cdot}1\ CH_2Cl_2$: C, 52.85; H, 3.33; N, 1.71. Found: C, 53.34; H, 3.58; N, 1.11.

^{13}C {^{1}H}-NMR (75 MHz, numbering as per **Figure 3-3.**): δ 176.02 (d, C^{7}, $^{3}J_{C-P}$ = 4.5 Hz), 161.66 (q, C^{21}, $^{1}J_{C-B}$ = 49.8 Hz), 155.33 (C_{Ar}), 145.69 (C_{Ar}), 144.23 (C_{Ar}), 141.20 (C_{Ar}), 140.50 (C_{Ar}), 137.12 (C_{Ar}), 136.96 (C_{Ar}), 134.77 (br, C^{22}), 134.61 (C_{Ar}), 133.11 (C_{Ar}), 133.02 (C_{Ar}), 132.16 (C_{Ar}), 132.13 (C_{Ar}), 129.14 (C_{Ar}), 128.99 (C_{Ar}), 128.87 (qq, C^{23}, $^{2}J_{C-F}$ = 31.6 Hz, $^{3}J_{C-B}$ = 3.0 Hz), 128.54 (C_{Ar}), 128.33 (C_{Ar}), 128.28 (C_{Ar}), 124.43 (q, C^{25}, $^{1}J_{C-F}$ = 272.8 Hz), 123.70 (C_{Ar}), 119.13 (C_{Ar}), 117.42 (sep, C^{24}, $^{3}J_{C-F}$ = 3.8 Hz), 28.56 ($C^{14,16}$), 24.23 and 22.63 ($C^{15,17}$), 20.54 (C^{20}), 0.14 (C^{19}).

[Pd(CH$_3$CN)PPh$_3$(4-CH$_3$C$_6$H$_3$)CH=N-{2,6-(*i*-Pr)$_2$-C$_6$H$_3$}]$^+$[B(Ar)$_4$]$^-$ (C20)

Yield: 62 %.

Anal. Calcd for $C_{72}H_{54}BF_{24}N_2PPd$: C, 55.74; H, 3.51; N, 1.81. Found: C, 55.69; H, 3.41; N, 0.88.

^{13}C {^{1}H}-NMR (75 MHz, numbering as per **Figure 3-3.**): δ 177.54 (d, C^{7}, $^{3}J_{C-P}$ = 4.5 Hz), 161.67 (q, C^{21}, $^{1}J_{C-B}$ = 49.8 Hz), 153.83 (C_{Ar}), 144.82 (C_{Ar}), 143.86 (C_{Ar}), 143.80 (C_{Ar}), 140.56 (C_{Ar}), 139.97 (C_{Ar}), 139.82 (C_{Ar}), 134.75 (br, C^{22}), 134.58 (C_{Ar}), 132.17 (C_{Ar}), 132.14 (C_{Ar}), 130.50 (C_{Ar}), 129.13 (C_{Ar}), 128.98 (C_{Ar}), 128.85 (qq, C^{23}, $^{2}J_{C-F}$ = 31.6 Hz, $^{3}J_{C-B}$ = 3.0 Hz), 128.81 (C_{Ar}), 128.17 (C_{Ar}), 128.12 (C_{Ar}), 126.93 (C_{Ar}), 124.43 (q, C^{25}, $^{1}J_{C-F}$ = 272.8 Hz), 123.64 (C_{Ar}), 119.22 (C_{Ar}), 117.43 (sep, C^{24}, $^{3}J_{C-F}$ = 3.8 Hz), 28.56 ($C^{14,16}$), 24.12 and 22.63 ($C^{15,17}$), 21.79 (C^{20}), 0.18 (C^{19}).

3.3.3 Synthetic methodology employed for the preparation of the cationic cyclopalladated complexes of pyridine C21 – C25

General procedure for the synthesis of the cationic complexes of pyridine

Pyridine (3 ml) was added to a stirring solution of neutral cyclopalladated complex (0.0564 mmol) and Na[B(Ar)$_4$] (60 mg, 0.0564 mmol) in dichloromethane (4 ml). The resulting light yellow solution was stirred for 24 hrs at room temperature. The sodium chloride precipitate was filtered from the resulting reaction mixture and the solvent was removed from the filtrate. The product was isolated, by triturating with *n*-pentane, as an off-white powder. Recrystallisation of complex **C24** was achieved by means of slow evaporation from dichloromethane/*n*-pentane at low temperature (-4 °C).

[Pd(C$_5$H$_5$N)PPh$_3$(2-ClC$_6$H$_3$)CH=N-{2,6-(*i*-Pr)$_2$-C$_6$H$_3$}]$^+$[B(Ar)$_4$]$^-$ (C21)

Yield: 71 %.

Anal. Calcd for $C_{74}H_{53}BClF_{24}N_2PPd \cdot 0.5\ CH_2Cl_2$: C, 53.79; H, 3.23; N, 1.70. Found: C, 53.97; H, 3.43; N, 1.90.

^{13}C {^{1}H}-NMR (75 MHz, numbering as per **Figure 3-10.**): δ 177.86 (d, C^7, $^3J_{C\text{-}P}$ = 3.8 Hz), 161.68 (q, C^{21}, $^1J_{C\text{-}B}$ = 49.8 Hz), 157.27 (C$_{Ar}$), 157.24 (C$_{Ar}$), 151.60 (C$_{Ar}$), 149.30 (C$_{Ar}$), 148.69 (C$_{Ar}$), 146.19 (C$_{Ar}$), 144.12 (C$_{Ar}$), 142.88 (C$_{Ar}$), 140.57 (C$_{Ar}$), 140.51 (C$_{Ar}$), 140.11 (C$_{Ar}$), 139.78 (C$_{Ar}$), 138.31 (C$_{Ar}$), 138.19 (C$_{Ar}$), 134.76 (br, C^{22}), 134.55 (C$_{Ar}$), 134.39 (C$_{Ar}$), 133.67 (C$_{Ar}$), 133.59 (C$_{Ar}$), 133.29 (C$_{Ar}$), 132.24 (C$_{Ar}$), 132.21 (C$_{Ar}$), 131.85 (C$_{Ar}$), 131.72 (C$_{Ar}$), 129.25 (C$_{Ar}$), 129.10 (C$_{Ar}$), 128.89 (qq, C^{23}, $^2J_{C\text{-}F}$ = 31.6 Hz, $^3J_{C\text{-}B}$ = 2.8 Hz), 128.39 (C$_{Ar}$), 128.22 (C$_{Ar}$), 127.52 (C$_{Ar}$), 127.37 (C$_{Ar}$), 127.19 (C$_{Ar}$), 127.06 (C$_{Ar}$), 125.42 (C$_{Ar}$), 124.99 (C$_{Ar}$), 124.51 (q, C^{25}, $^1J_{C\text{-}F}$ = 272.5 Hz), 123.76 (C$_{Ar}$), 123.44 (C$_{Ar}$), 117.45 (sep, C^{24}, $^3J_{C\text{-}F}$ = 3.8 Hz), 28.52 (C^{14,16}), 25.61 and 21.86 (C^{15,17}).

[Pd(C_5H_5N)PPh_3(2-BrC_6H_3)CH=N-{2,6-(*i*-Pr)$_2$-C_6H_3}]$^+$[B(Ar)$_4$]$^-$ (C22)

Yield: 89 %.

Anal. Calcd for $C_{74}H_{53}BBrF_{24}N_2PPd$·1 CH_2Cl_2: C, 51.10; H, 3.07; N, 1.61. Found: C, 51.11; H, 3.09; N, 1.87.

^{13}C {^1H}-NMR (100 MHz, numbering as per **Figure 3-10.**): δ 180.22 (d, C^7, $^3J_{C\text{-}P}$ = 4.2 Hz), 161.68 (q, C^{21}, $^1J_{C\text{-}B}$ = 49.9 Hz), 157.35 (C_{Ar}), 157.34 (C_{Ar}), 149.29 (C_{Ar}), 145.40 (C_{Ar}), 145.39 (C_{Ar}), 144.47 (C_{Ar}), 142.83 (C_{Ar}), 142.67 (C_{Ar}), 139.76 (C_{Ar}), 139.75 (C_{Ar}), 138.92 (C_{Ar}), 138.81 (C_{Ar}), 138.20 (C_{Ar}), 134.72 (br, C^{22}), 134.52 (C_{Ar}), 134.40 (C_{Ar}), 133.74 (C_{Ar}), 133.69 (C_{Ar}), 132.24 (C_{Ar}), 132.22 (C_{Ar}), 131.81 (C_{Ar}), 131.70 (C_{Ar}), 130.36 (C_{Ar}), 129.30 (C_{Ar}), 129.24 (C_{Ar}), 129.13 (C_{Ar}), 128.94 (qq, C^{23}, $^2J_{C\text{-}F}$ = 31.6 Hz, $^3J_{C\text{-}B}$ = 3.0 Hz), 128.41 (C_{Ar}), 128.11 (C_{Ar}), 127.59 (C_{Ar}), 127.04 (C_{Ar}), 125.00 (C_{Ar}), 124.47 (q, C^{25}, $^1J_{C\text{-}F}$ = 272.5 Hz), 123.75 (C_{Ar}), 123.44 (C_{Ar}), 117.47 (sep, C^{24}, $^3J_{C\text{-}F}$ = 3.8 Hz), 28.53 ($C^{14,16}$), 25.60 and 21.86 ($C^{15,17}$).

[Pd(C_5H_5N)PPh_3(C_6H_4)CH=N-{2,6-(*i*-Pr)$_2$-C_6H_3}]$^+$[B(Ar)$_4$]$^-$ (C23)

Yield: 85 %.

Anal. Calcd for $C_{74}H_{54}BF_{24}N_2PPd$·1 CH_2Cl_2: C, 53.53; H, 3.28; N, 1.69. Found: C, 53.44; H, 3.51; N, 1.69.

^{13}C {^1H}-NMR (75 MHz, numbering as per **Figure 3-10.**): δ 179.49 (d, C^7, $^3J_{C\text{-}P}$ = 3.8 Hz), 161.67 (q, C^{21}, $^1J_{C\text{-}B}$ = 49.8 Hz), 155.49 (C_{Ar}), 155.46 (C_{Ar}), 149.35 (C_{Ar}), 147.18 (C_{Ar}), 147.16 (C_{Ar}), 142.72 (C_{Ar}), 140.48 (C_{Ar}), 139.96 (C_{Ar}), 139.84 (C_{Ar}), 137.99 (C_{Ar}), 134.75 (br, C^{22}), 134.60 (C_{Ar}), 134.44 (C_{Ar}), 132.36 (C_{Ar}), 132.29 (C_{Ar}), 132.07 (C_{Ar}), 132.04 (C_{Ar}),

130.63 (C_{Ar}), 129.30 (C_{Ar}), 129.14 (C_{Ar}), 129.00 (C_{Ar}), 128.88 (qq, C^{23}, $^{2}J_{C\text{-}F}$ = 31.6 Hz, $^{3}J_{C\text{-}B}$ = 2.9 Hz), 128.59 (C_{Ar}), 128.14 (C_{Ar}), 127.90 (C_{Ar}), 127.47 (C_{Ar}), 126.21 (C_{Ar}), 124.87 (C_{Ar}), 124.50 (q, C^{25}, $^{1}J_{C\text{-}F}$ = 272.8 Hz), 123.36 (C_{Ar}), 117.45 (sep, C^{24}, $^{3}J_{C\text{-}F}$ = 3.8 Hz), 28.44 ($C^{14,16}$), 25.58 and 21.88 ($C^{15,17}$).

$[Pd(C_5H_5N)PPh_3(2\text{-}CH_3C_6H_3)CH{=}N\text{-}\{2,6\text{-}(i\text{-}Pr)_2\text{-}C_6H_3\}]^+[B(Ar)_4]^-$ (C24)

Yield: 89 %.

Anal. Calcd for $C_{75}H_{56}BF_{24}N_2PPd{\cdot}1.5\ CH_2Cl_2$: C, 52.47; H, 3.29; N, 1.63. Found: C, 52.11; H, 3.29; N, 1.83.

^{13}C {^{1}H}-NMR (100 MHz, numbering as per **Figure 3-10.**): δ 177.33 (d, C^{7}, $^{3}J_{C\text{-}P}$ = 3.8 Hz), 161.68 (q, C^{21}, $^{1}J_{C\text{-}B}$ = 49.9 Hz), 156.87 (C_{Ar}), 156.85 (C_{Ar}), 149.35 (C_{Ar}), 145.13 (C_{Ar}), 144.54 (C_{Ar}), 143.17 (C_{Ar}), 142.62 (C_{Ar}), 140.96 (C_{Ar}), 139.96 (C_{Ar}), 138.12 (C_{Ar}), 138.00 (C_{Ar}), 137.95 (C_{Ar}), 134.72 (br, C^{22}), 134.60 (C_{Ar}), 134.48 (C_{Ar}), 132.96 (C_{Ar}), 132.90 (C_{Ar}), 131.99 (C_{Ar}), 131.97 (C_{Ar}), 131.81 (C_{Ar}), 131.71 (C_{Ar}), 129.30 (C_{Ar}), 129.18 (C_{Ar}), 129.10 (C_{Ar}), 129.99 (C_{Ar}), 128.94 (qq, C^{23}, $^{2}J_{C\text{-}F}$ = 31.6 Hz, $^{3}J_{C\text{-}B}$ = 3.0 Hz), 128.64 (C_{Ar}), 128.28 (C_{Ar}), 128.13 (C_{Ar}), 127.07 (C_{Ar}), 124.84 (C_{Ar}), 124.47 (q, C^{25}, $^{1}J_{C\text{-}F}$ = 272.5 Hz), 123.38 (C_{Ar}), 117.48 (sep, C^{24}, $^{3}J_{C\text{-}F}$ = 3.8 Hz), 28.37 ($C^{14,16}$), 25.65 and 21.86 ($C^{15,17}$), 20.46 (C^{18}).

$[Pd(C_5H_5N)PPh_3(4\text{-}CH_3C_6H_3)CH{=}N\text{-}\{2,6\text{-}(i\text{-}Pr)_2\text{-}C_6H_3\}]^+[B(Ar)_4]^-$ (C25)

Yield: 70 %.

Anal. Calcd for $C_{75}H_{56}BF_{24}N_2PPd{\cdot}1\ CH_2Cl_2$: C, 53.80; H, 3.37; N, 1.67. Found: C, 54.33; H, 3.36; N, 1.92.

^{13}C {^{1}H}-NMR (75 MHz, numbering as per **Figure 3-10.**): δ 178.85 (d, C^{7}, $^{3}J_{C\text{-}P}$ = 3.8 Hz), 161.69 (q, C^{21}, $^{1}J_{C\text{-}B}$ = 49.8 Hz), 155.39 (C_{Ar}), 155.36 (C_{Ar}), 149.36 (C_{Ar}), 146.83 (C_{Ar}), 144.36 (C_{Ar}), 144.34 (C_{Ar}), 143.65 (C_{Ar}), 143.58 (C_{Ar}), 142.84 (C_{Ar}), 141.57 (C_{Ar}), 141.14 (C_{Ar}), 141.00 (C_{Ar}), 140.38 (C_{Ar}), 140.02 (C_{Ar}), 137.95 (C_{Ar}), 135.41 (C_{Ar}), 135.25 (C_{Ar}), 134.75 (br, C^{22}), 134.59 (C_{Ar}), 134.43 (C_{Ar}), 131.99 (C_{Ar}), 131.95 (C_{Ar}), 131.25 (C_{Ar}), 130.41 (C_{Ar}), 129.35 (C_{Ar}), 129.29 (C_{Ar}), 129.11 (C_{Ar}), 128.97 (C_{Ar}), 128.91 (qq, C^{23}, $^{2}J_{C\text{-}F}$ = 31.5 Hz, $^{3}J_{C\text{-}B}$ = 2.8 Hz), 128.81 (C_{Ar}), 128.53 (C_{Ar}), 128.51 (C_{Ar}), 128.37 (C_{Ar}), 128.02 (C_{Ar}), 127.85 (C_{Ar}), 127.24 (C_{Ar}), 126.75 (C_{Ar}), 124.85 (C_{Ar}), 124.50 (q, C^{25}, $^{1}J_{C\text{-}F}$ = 272.5 Hz), 123.32 (C_{Ar}), 122.99 (C_{Ar}), 117.45 (sep, C^{24}, $^{3}J_{C\text{-}F}$ = 3.8 Hz), 28.42 ($C^{14,16}$), 25.57 and 21.89 ($C^{15,17}$), 21.80 (C^{18}).

3.3.4 Synthetic methodology employed for the preparation of the cationic cyclopalladated complexes bearing two trimethylphosphine ligands C26 – C30

General procedure for the synthesis of the cationic cyclopalladated complexes bearing two trimethylphosphine ligands

The neutral non-cyclopalladated complex (0.0564 mmol), dissolved in dichloromethane (4 ml), was added to a stirring solution of $Na[B(Ar)_4]$ (60 mg, 0.0564 mmol), dissolved in dichloromethane (3 ml). The resulting light yellow solution was stirred for 2 hrs at room temperature. The sodium chloride precipitate was filtered from the resulting reaction mixture and the solvent was removed from the filtrate. The product was isolated, by triturating with *n*-pentane, as an off-white powder.

$[Pd(PMe_3)_2(2\text{-}ClC_6H_3)CH{=}N\text{-}\{2,6\text{-}(i\text{-}Pr)_2\text{-}C_6H_3\}]^+[B(Ar)_4]^-$ (C26)

Yield: 74 %.

^{13}C $\{^1H\}$-NMR (75 MHz, numbering as per **Figure 3-17.**): δ 181.11 (dd, C^7, $^3J_{C\text{-}P}$ = 5.1 Hz, $^3J_{C\text{-}P}$ = 3.8 Hz), 170.35 (C_{Ar}), 168.69 (C_{Ar}), 161.66 (q, C^{21}, $^1J_{C\text{-}B}$ = 49.6 Hz), 146.87 (C_{Ar}), 143.91 (C_{Ar}), 140.10 (C_{Ar}), 134.76 (br, C^{22}), 128.89 (qq, C^{23}, $^2J_{C\text{-}F}$ = 31.4 Hz, $^3J_{C\text{-}B}$ = 2.8 Hz), 128.88 (C_{Ar}), 127.73 (C_{Ar}), 124.52 (q, C^{25}, $^1J_{C\text{-}F}$ = 272.5 Hz), 124.45 (C_{Ar}), 117.47 (sep, C^{24}, $^3J_{C\text{-}F}$ = 3.8 Hz), 28.86 ($C^{14,16}$), 25.67 and 21.78 ($C^{15,17}$), 17.75 (dd, C^{19}, $^1J_{C\text{-}P}$ = 34.0 Hz, $^3J_{C\text{-}P}$ = 4.1 Hz), 14.79 (d, C^{18}, $^1J_{C\text{-}P}$ = 23.5 Hz).

$[Pd(PMe_3)_2(2\text{-}BrC_6H_3)CH{=}N\text{-}\{2,6\text{-}(i\text{-}Pr)_2\text{-}C_6H_3\}]^+[B(Ar)_4]^-$ (C27)

Yield: 85 %.

^{13}C $\{^1H\}$-NMR (75 MHz, numbering as per **Figure 3-17.**): δ 183.32 (dd, C^7, $^3J_{C\text{-}P}$ = 5.7 Hz, $^3J_{C\text{-}P}$ = 3.8 Hz), 170.45 (C_{Ar}), 168.79 (C_{Ar}), 161.65 (q, C^{21}, $^1J_{C\text{-}B}$ = 49.6 Hz), 146.78 (C_{Ar}), 145.25 (C_{Ar}), 140.08 (C_{Ar}), 134.75 (br, C^{22}), 131.01 (C_{Ar}), 128.89 (C_{Ar}), 128.88 (qq, C^{23}, $^2J_{C\text{-}F}$ = 31.4 Hz, $^3J_{C\text{-}B}$ = 2.8 Hz), 124.52 (q, C^{25}, $^1J_{C\text{-}F}$ = 272.5 Hz), 124.45 (C_{Ar}), 117.47 (sep, C^{24}, $^3J_{C\text{-}F}$ = 3.8 Hz), 28.86 ($C^{14,16}$), 25.70 and 21.76 ($C^{15,17}$), 17.70 (dd, C^{19}, $^1J_{C\text{-}P}$ = 34.0 Hz, $^3J_{C\text{-}P}$ = 4.1 Hz), 14.76 (d, C^{18}, $^1J_{C\text{-}P}$ = 23.5 Hz).

$[Pd(PMe_3)_2(C_6H_4)CH{=}N\text{-}\{2,6\text{-}(i\text{-}Pr)_2\text{-}C_6H_3\}]^+[B(Ar)_4]^-$ (C28)

Yield: 81 %.

^{13}C $\{^1H\}$-NMR (100 MHz, numbering as per **Figure 3-17.**): δ 182.54 (dd, C^7, $^3J_{C\text{-}P}$ = 5.9 Hz, $^3J_{C\text{-}P}$ = 3.8 Hz), 168.15 (C_{Ar}), 166.93 (C_{Ar}), 161.66 (q, C^{21}, $^1J_{C\text{-}B}$ = 49.7 Hz), 146.87 (C_{Ar}),

140.16 (C_{Ar}), 135.92 (C_{Ar}), 134.76 (br, C^{22}), 133.27 (C_{Ar}), 130.31 (C_{Ar}), 128.89 (qq, C^{23}, $^{2}J_{C\text{-}F}$ = 31.5 Hz, $^{3}J_{C\text{-}B}$ = 2.9 Hz), 128.65 (C_{Ar}), 126.92 (C_{Ar}), 124.52 (q, C^{25}, $^{1}J_{C\text{-}F}$ = 272.5 Hz), 124.39 (C_{Ar}), 117.46 (sep, C^{24}, $^{3}J_{C\text{-}F}$ = 3.8 Hz), 28.75 ($C^{14,16}$), 25.62 and 21.82 ($C^{15,17}$), 17.98 (dd, C^{19}, $^{1}J_{C\text{-}P}$ = 34.1 Hz, $^{3}J_{C\text{-}P}$ = 4.2 Hz), 14.97 (d, C^{18}, $^{1}J_{C\text{-}P}$ = 22.8 Hz).

$[Pd(PMe_3)_2(2\text{-}CH_3C_6H_3)CH{=}N\text{-}\{2,6\text{-}(i\text{-}Pr)_2\text{-}C_6H_3\}]^+[B(Ar)_4]^-$ (C29)

Yield: 88 %.

^{13}C {^{1}H}-NMR (75 MHz, numbering as per **Figure 3-17.**): δ 180.51 (dd, C^{7}, $^{3}J_{C\text{-}P}$ = 5.7 Hz, $^{3}J_{C\text{-}P}$ = 3.8 Hz), 169.97 (C_{Ar}), 168.36 (C_{Ar}), 161.66 (q, C^{21}, $^{1}J_{C\text{-}B}$ = 49.6 Hz), 147.18 (C_{Ar}), 144.94 (C_{Ar}), 140.78 (C_{Ar}), 140.72 (C_{Ar}), 140.21 (C_{Ar}), 134.76 (br, C^{22}), 128.89 (C_{Ar}), 128.88 (qq, C^{23}, $^{2}J_{C\text{-}F}$ = 31.5 Hz, $^{3}J_{C\text{-}B}$ = 2.9 Hz), 128.61 (C_{Ar}), 124.53 (q, C^{25}, $^{1}J_{C\text{-}F}$ = 272.5 Hz), 124.38 (C_{Ar}), 117.47 (sep, C^{24}, $^{3}J_{C\text{-}F}$ = 3.8 Hz), 28.69 ($C^{14,16}$), 25.73 and 21.74 ($C^{15,17}$), 20.44 (C^{20}), 17.86 (dd, C^{19}, $^{1}J_{C\text{-}P}$ = 33.4 Hz, $^{3}J_{C\text{-}P}$ = 4.1 Hz), 14.94 (d, C^{18}, $^{1}J_{C\text{-}P}$ = 22.9 Hz).

$[Pd(PMe_3)_2(4\text{-}CH_3C_6H_3)CH{=}N\text{-}\{2,6\text{-}(i\text{-}Pr)_2\text{-}C_6H_3\}]^+[B(Ar)_4]^-$ (C30)

Yield: 67 %.

^{13}C {^{1}H}-NMR (100 MHz, numbering as per **Figure 3-17.**): δ 181.98 (dd, C^{7}, $^{3}J_{C\text{-}P}$ = 5.5 Hz, $^{3}J_{C\text{-}P}$ = 3.8 Hz), 168.31 (C_{Ar}), 167.10 (C_{Ar}), 161.67 (q, C^{21}, $^{1}J_{C\text{-}B}$ = 49.7 Hz), 146.82 (C_{Ar}), 144.52 (C_{Ar}), 144.16 (C_{Ar}), 140.28 (C_{Ar}), 136.98 (C_{Ar}), 134.76 (br, C^{22}), 128.89 (qq, C^{23}, $^{2}J_{C\text{-}F}$ = 31.5 Hz, $^{3}J_{C\text{-}B}$ = 2.8 Hz), 128.52 (C_{Ar}), 127.52 (C_{Ar}), 124.52 (q, C^{25}, $^{1}J_{C\text{-}F}$ = 272.5 Hz), 124.33 (C_{Ar}), 117.46 (sep, C^{24}, $^{3}J_{C\text{-}F}$ = 3.8 Hz), 28.72 ($C^{14,16}$), 25.60 and 21.79 ($C^{15,17}$), 22.35 (C^{20}), 17.95 (dd, C^{19}, $^{1}J_{C\text{-}P}$ = 33.9 Hz, $^{3}J_{C\text{-}P}$ = 4.0 Hz), 14.97 (d, C^{18}, $^{1}J_{C\text{-}P}$ = 22.3 Hz).

3.3.5 Synthetic methodology employed for the preparation of the cationic non-cyclopalladated complex bearing three trimethylphosphine ligands C31

Procedure for the synthesis of the cationic non-cyclopalladated complex bearing three trimethylphosphine ligands

The neutral non-cyclopalladated complex **C11** (0.0564 mmol), dissolved in dichloromethane (4 ml), was added to a stirring solution of Na[B(Ar)$_4$] (60 mg, 0.0564 mmol) and trimethylphosphine (0.1 ml, 0.1 mmol) in dichloromethane (3 ml). The resulting light yellow solution was stirred for 2 hrs at room temperature. The sodium chloride precipitate was filtered from the resulting reaction mixture and the solvent was removed from the filtrate. The product was isolated, by triturating with *n*-pentane, as an off-white powder.

[Pd(PMe$_3$)$_3$(2-ClC$_6$H$_3$)CH=N-{2,6-(*i*-Pr)$_2$-C$_6$H$_3$}]$^+$[B(Ar)$_4$]$^-$ (C31)

Yield: 82 %.

^{13}C {^{1}H}-NMR (75 MHz, numbering as per **Figure 3-25.**): δ 176.05 (C^7), 166.65 (C$_{Ar}$), 161.66 (q, C^{21}, $^1J_{C\text{-}B}$ = 49.9 Hz), 140.61 (C$_{Ar}$), 137.28 (C$_{Ar}$), 134.75 (br, C^{22}), 128.99 (qq, C^{23}, $^2J_{C\text{-}F}$ = 31.5 Hz, $^3J_{C\text{-}B}$ = 2.8 Hz), 128.46 (C$_{Ar}$), 127.65 (C$_{Ar}$), 127.15 (C$_{Ar}$), 124.52 (q, C^{25}, $^1J_{C\text{-}F}$ = 272.6 Hz), 123.68 (C$_{Ar}$), 119.09 (C$_{Ar}$), 117.47 (sep, C^{24}, $^3J_{C\text{-}F}$ = 3.8 Hz), 28.43 (C^{14,16}), 24.37 and 22.53 (C^{15,17}), 16.16 (C$^{\{P(1)\}\text{ and }\{P(2)\}}$) and 15.58 (C$^{\{P(3)\}}$).

References

1. N. Mungwe, The Synthesis of the Cyclometallated Palladium Complexes and their Applications in Olefin Oligomerisation and in Phenylacetylene Oligomerisation/ Polymerisation, *M.Sc. Thesis*, University of the Western Cape, 2007.

2. http://winter.group.shef.ac.uk/chemputer/isotopes.html

3. APEX2, *Data Collection Software, Version 2010.11-3, Bruker AXS*, 2010.

4. SAINT, *Data Reduction Software, Version 6.45, Bruker AXS*, 2003.

5. (a) R. H. Blessing, *Acta Crystallogr., Sect. A: Found. Crystallogr.*, 1995, **51**, 33;
(b) SADABS, *Version 2.05, Bruker AXS*, 2002.

6. G. M. Sheldrick, *Acta Crystallogr., Sect. A: Found. Crystallogr.*, 2008, **64**, 112.

7. L. J. Barbour, *J. Supramol. Chem.*, 2001, **1**, 189.

8. POV-Ray^{TM}, *Version 3.6, Williamstown, Australia, Persistence of Vision Raytracer Pty. Ltd. 2004*.

Chapter 4

Density functional theory (DFT) studies relating to the reactivity and physical properties of the prepared cyclopalladated complexes

4.1 Introduction

The ability of density functional theory to routinely define the structures and energies of reactive intermediates and transition states in late transition metal systems is particularly important.[1] It provides information that is often very difficult or impossible to obtain from experimental work and therefore the use of computational studies being performed in parallel with experiment is increasing. A thorough understanding of the experimental work as described in **Chapter 2** and **Chapter 3** is achieved with computer modelling to provide further insight into the reactivity and physical properties of the prepared cyclopalladated and non-cyclopalladated palladium complexes.

4.2 Results and Discussion

4.2.1 Schiff base imine ligands and μ-Cl binuclear cyclopalladated complexes

A brief investigation into the properties of the Schiff base imine ligands **L1**, **L3** and **L4** and the μ-Cl binuclear cyclopalladated complexes **C1**, **C3** and **C4** was performed. The thermodynamically most stable conformation for a given molecule was identified and subsequent frequency calculations were performed in order to verify that the conformation is at an energy minimum, and to monitor the expected fluctuation in wavenumbers of the signature peak frequency, i.e. the $\nu_{C=N}$ stretch absorption band corresponding to the imine.

For ligand **L1**, four stable conformations were identified (**Figure 4-1.**).

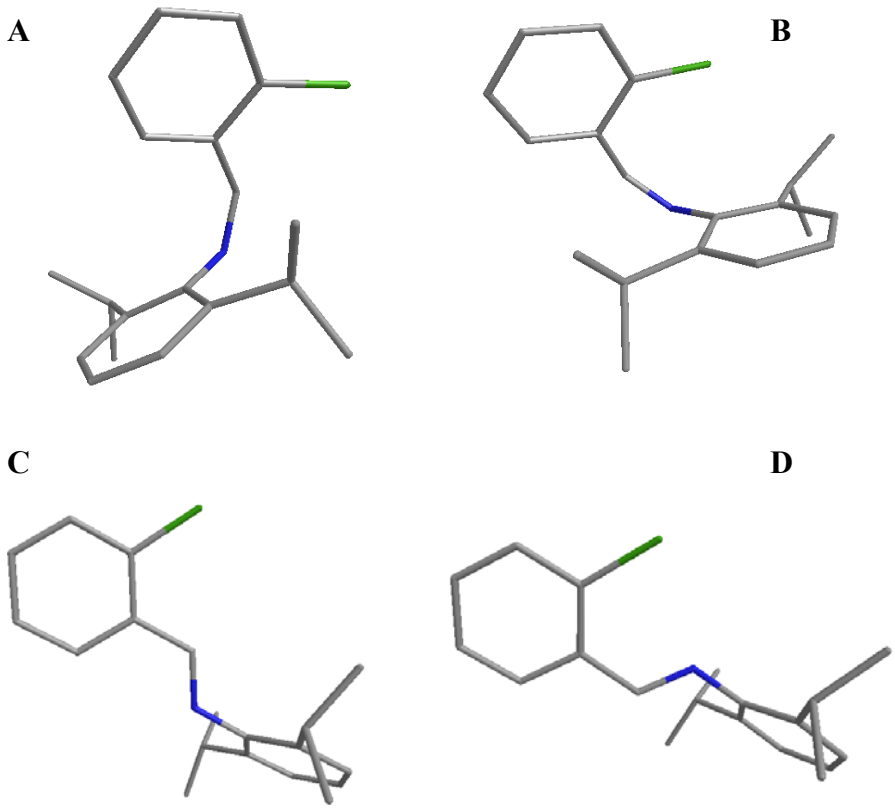

Figure 4-1. Conformation analysis of ligand **L1** with *Z* (**A** and **B**) and *E* (**C** and **D**) isomers with respect to the imine double bond.

The relative orientation of the two isopropyl substituents on the aromatic ring is an important contributing factor to the potential energy of the molecules. Their orientation as seen in **Figure 4-1.**, i.e. eclipsed, with both the methine protons aligned in parallel and pointed towards the nitrogen of the imine group, represents the most stable orientation for the diisopropyl phenyl moiety. Calculations that identify this orientation as the most stable are described in detail in **4.2.2**.

Conformation **C** is the most stable one for ligand **L1** and the calculated $\nu_{C=N}$ absorption band is at 1670 cm^{-1}. A similar procedure to the one that identifies the most stable

conformation of ligand **L1** was performed for ligands **L3** (only one *Z* and one *E* isomer) and **L4** and complexes **C1** (**Figure 4-2.**), **C3** and **C4** (**Scheme 4-1**.).

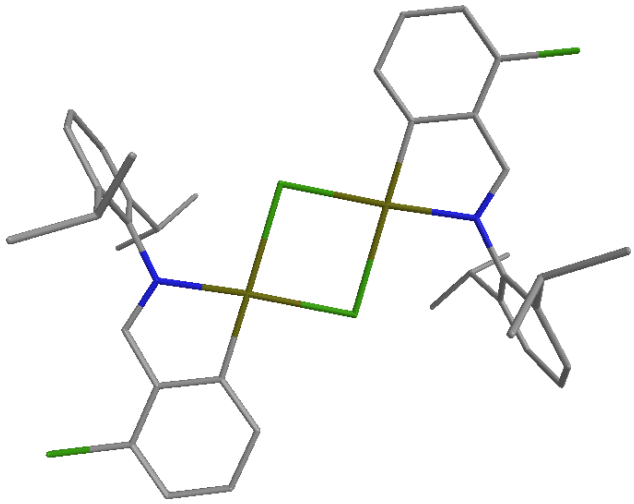

Figure 4-2. Optimised energy conformation of complex **C1**.

The C-H bond activation of the prepared ligands **L1 – L5** as described in Chapter 2 (**2.2.2**) yields five-membered chelate products. These reactions proceed via a C_{aryl}-H bond activation at the *ortho* position of the ligand. For ligand **L4** the possibility of C_{allyl}-H bond activation at the methyl substituent exists. Such an activation process would lead to the formation of a six-membered chelate product **C4i** (**Scheme 4-1.**).

Complex **C4** is 14 kJ/mol lower in energy than **C4i.** This difference is too small to draw any conclusions regarding its favoured formation. An investigation of the mechanistic insights into the C-H bond activation process would provide comprehensive answers as to why activation of the C_{aryl}-H bond is favourable. This is interesting though unnecessary for the purpose of this project. Boutadla *et al.*[1] discuss the activation in late transition metal systems with lone pair assistance via heteroatom co-ligands or carboxylates in studies that

might be useful for future investigations into the mechanisms of the cyclopalladation reactions that were done in this project.

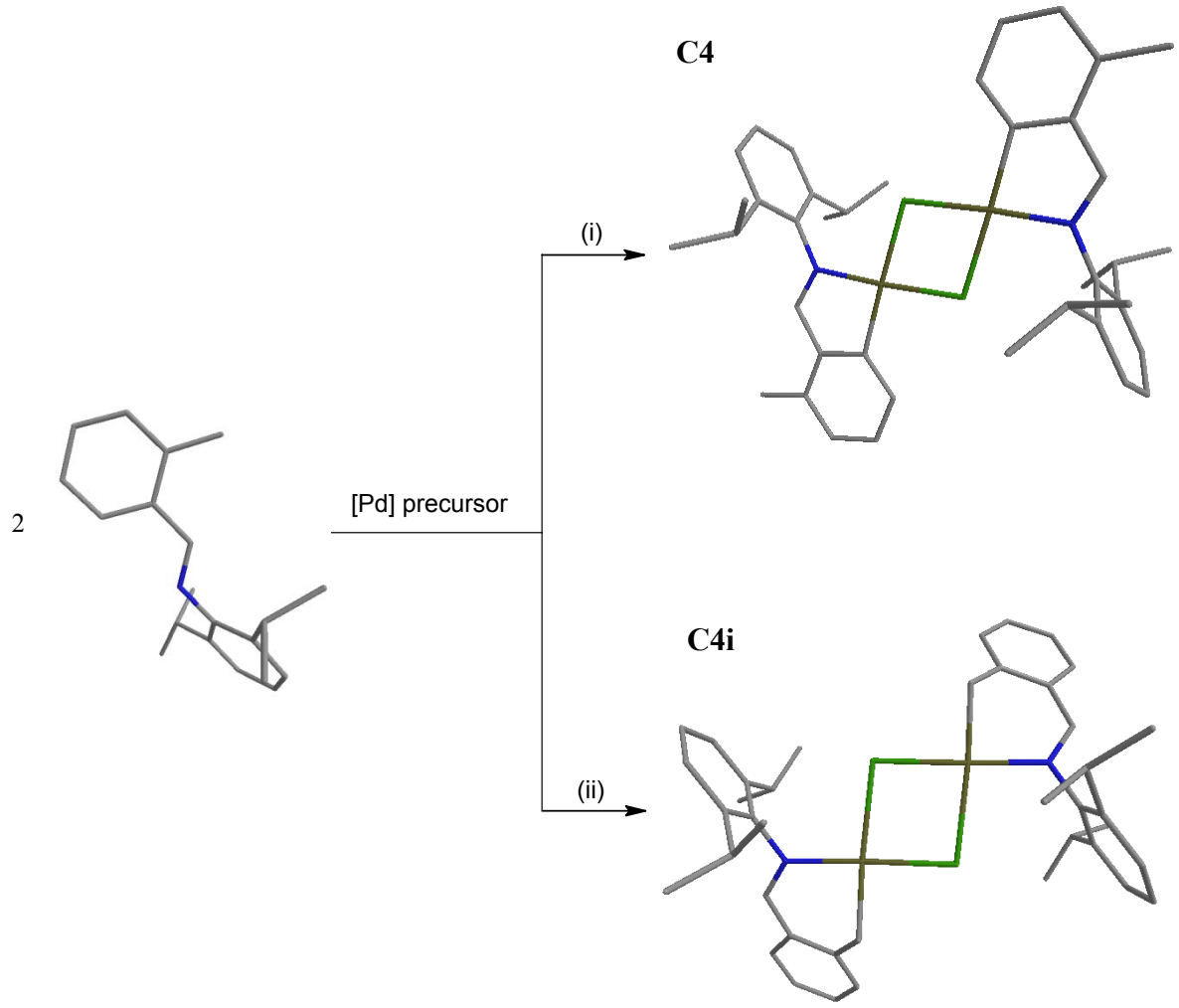

Scheme 4-1. Cyclopalladation of ligand **L4** via C-H bond activation of (i) an sp^2 hybridised carbon, yielding complex **C4** and (ii) an sp^3 hybridised carbon, yielding complex **C4i**.

The FT-IR spectra of the Schiff base imine ligands and μ-Cl binuclear cyclopalladated complexes as described in Chapter 2 (**2.2.2**) reveals that a decrease in imine double-bond character takes place upon cyclopalladation of the Schiff base ligands. The same trend is seen computationally (**Table 4-1.**).

Table 4-1. The $\nu_{C=N}$ absorption band frequencies of ligands **L1**, **L3** and **L4** and complexes **C1**, **C3** and **C4** in cm^{-1}.

	Computational		Experimental	
X[a]	**Schiff base ligands**	**μ-Cl binuclear complexes**	**Schiff base ligands**	**μ-Cl binuclear complexes**
Cl	1670	1632	1630	1594
H	1680	1635	1637	1600
CH_3	1673	1629	1633	1595

[a] X = substituent at the *ortho* position.

Although the frequencies generated from DFT calculations show higher wavenumbers, the same trend is seen, as a decrease in the imine double-bond character takes place upon cyclopalladation. Taking a scale factor into account and the fact that the calculations are based on isolated molecules in the gas phase as opposed to non-isolated molecules in the solid phase for the experimentally obtained frequencies, an agreement between the computationally and experimentally obtained results regarding the double-bond character of the imine is seen.

4.2.2 Neutral cyclopalladated and non-cyclopalladated complexes

The cleavage reactions of the μ-Cl binuclear cyclopalladated complexes as described in Chapter 2 (**2.2.3** and **2.2.4**) yield neutral products that remain cyclopalladated or that become non-cyclopalladated, i.e. when the coordinating bond from the nitrogen of the imine group breaks and is displaced by another phosphine molecule, depending on the character and mol

ratio of the phosphine employed. Computer modelling is used to confirm the product formation results of the neutral complexes that are synthesised. Included are some predictive calculations of cleavage products that may form when employing analogous phosphines.

First the optimised energy conformations of the triphenylphosphine coordinated cyclopalladated complexes **C6**, **C8** and **C9** and the trimethylphosphine coordinated non-cyclopalladated complexes **C11**, **C13** and **C14** were calculated in order to compare to the experimentally obtained product formation results.

4.2.2.1 Neutral cyclopalladated complexes

The cleavage of the μ-Cl binuclear cyclopalladated complexes **C1** with triphenylphosphine could form neutral complexes that bear a coordinating phosphine ligand that is situated in either a *cis* or *trans* fashion relative to the Pd-C bond (**Scheme 4-2.**).

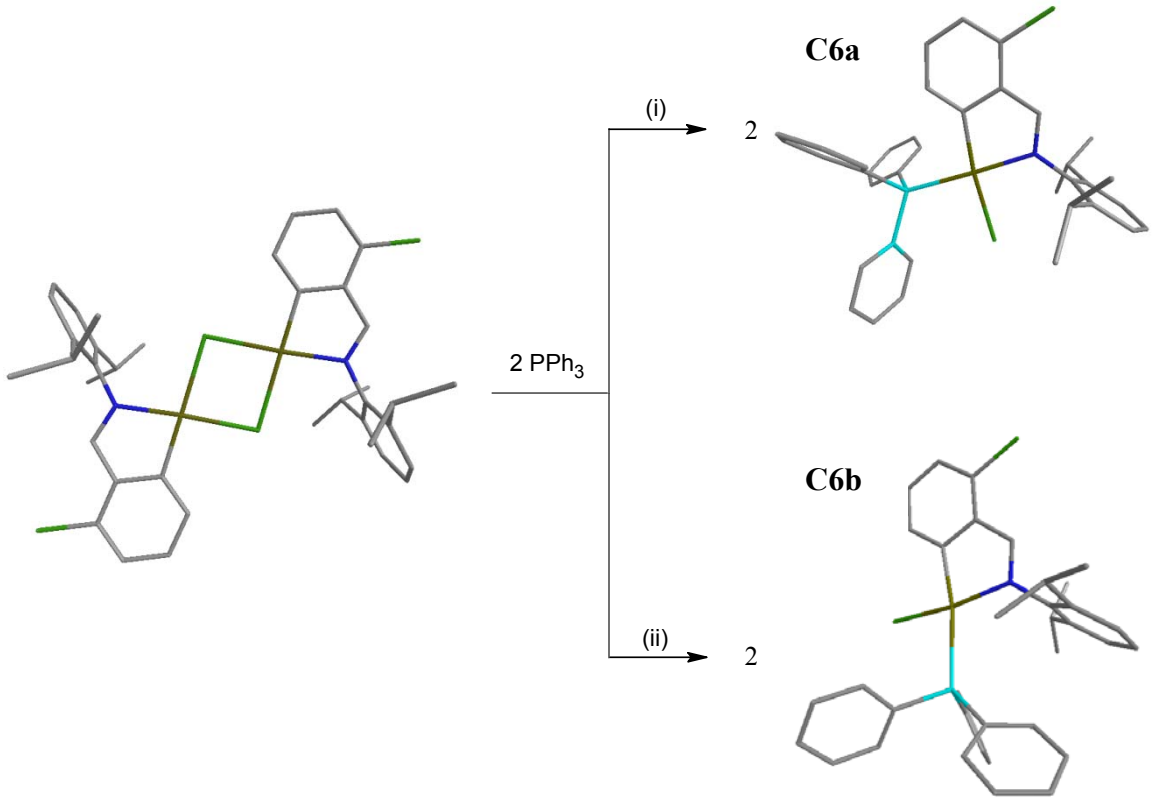

Scheme 4-2. Cleavage of complex **C1** with triphenylphosphine.

The thermodynamically more stable product has the coordinated triphenylphosphine ligand situated in a *cis* fashion relative to the Pd-C bond, which is in agreement with the conclusions derived from the previously discussed NMR spectral analyses (**2.2.3**). The *cis* conformation, **C6a**, is 24 kJ/mol lower in energy than the *trans* conformation, **C6b**. Similar results were obtained for the cleaved complexes **C8** and **C9**.

A comparison between the calculated and crystallographically determined structures for complex **C9** (**Figure 2-12.**) reveals that the only significant discrepancies between the two are the torsion angles of the isopropyl substituents. The distortion of this substituent when packed in a crystal is due to interactions with the solvent molecules and/or with neighbouring complexes in its immediate environment which are absent for the modelled complex. A good agreement between the calculated and crystallographically determined structures for complex **C10**[2] is also seen (**Figure 4-3.** and **Table 4-2.**).

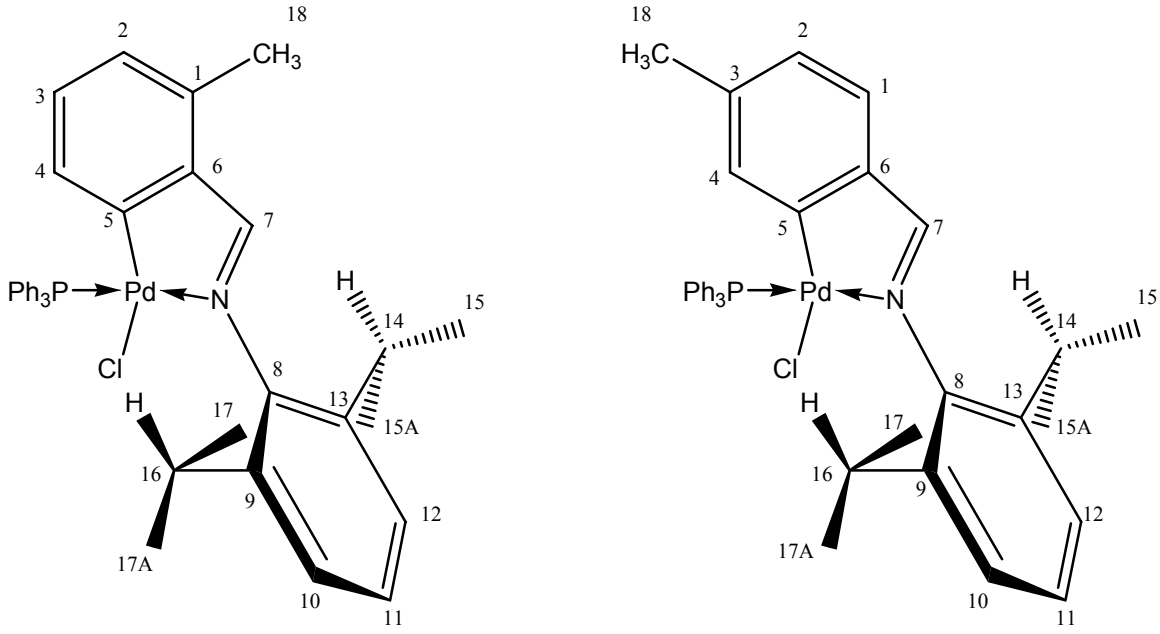

Figure 4-3. Skeletal structures of complexes **C9** (left) and **C10** (right) shown with the numbering scheme.

Table 4-2. Selected bond lengths, bond angles and torsion angles of the DFT and crystallographically determined structures of complexes **C9** and **C10**.[a]

	Complex C9			**Complex C10**	
	Calculated	**X-Ray**[b]		**Calculated**	**X-Ray**[2]
		A	**B**		
Bond lengths (Å)					
Pd-C(5)	2.053	2.026	2.025	2.054	2.011
Pd-N	2.101	2.104	2.109	2.110	2.102
Pd-Cl	2.460	2.358	2.365	2.460	2.365
Pd-P	2.421	2.267	2.265	2.419	2.252
C(7)-N	1.309	1.289	1.284	1.309	1.285
C(8)-N	1.453	1.444	1.447	1.452	-
C(1)-C(18)	1.521	1.511	1.512	1.518	-
Bond angles (degrees)					
N-Pd-Cl	92.53	90.58	91.51	92.07	91.80
Cl-Pd-P	89.79	93.10	92.70	90.05	92.13
P-Pd-C(5)	96.94	95.10	94.98	96.93	96.40
C(5)-Pd-N	80.77	81.38	80.96	81.05	80.80
Torsion angles (degrees)					
C(8)-C(13)-C(14)-C(15)	114.04	99.09	147.56	117.73	-
C(8)-C(9)-C(16)-C(17)	-118.44	-90.16	-83.00	-115.19	-

[a] Atom labelling as per numbering scheme (**Figure 4-3.**). [b] **A** and **B** as per **Figure 2-12.**, **Chapter 2**.

The atoms in the DFT calculations are static whereas the atoms in a crystal are not, but oscillate about their mean positions. Therefore the bond lengths determined from the calculations are mostly longer than those for the crystallographically determined structures.

Optimised energy conformations for complex **C6**, and analogous **C6i** and **C6ii** cyclopalladated complexes were determined (**Figure 4-4.**).

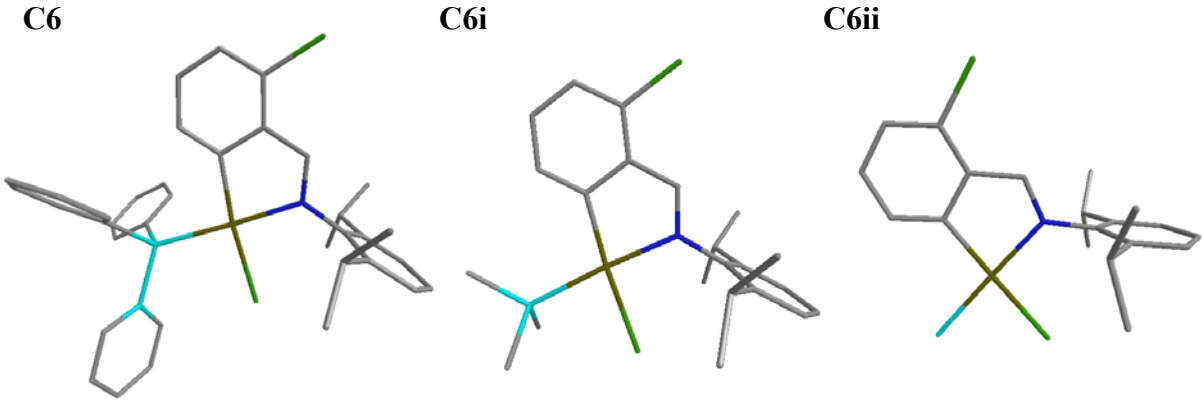

Figure 4-4. The most stable conformations of cyclopalladated complexes **C6**, **C6i** and **C6ii** bearing a coordinating triphenylphosphine, trimethylphosphine and phosphine ligand respectively.

For complexes such as the cyclopalladated species seen in **Figure 4-4.**, where several binding sites are occupied, vacant sites for potential catalytic activity can be exposed. In fact, complexes **C6**, **C7**, **C8** and **C10** have been successfully employed as catalyst precursors in the Heck coupling of iodobenzene and 1-octene, as well as in the isomerisation of 1-hexene.[2] However, the nature of the active catalyst is not known. This means that the stability of the coordinating phosphine ligand to the palladium metal centre is an important characteristic, since the active catalyst is possibly formed upon its dissociation. The substituents on the aromatic ring affect the electronic and steric properties of the complexes, which also contributes to the lability of the coordinated phosphine ligands. Therefore the bond dissociation energies of the various phosphines were calculated and compared (**Scheme 4-3.** and **Table 4-3.**). Optimised energy conformations for all reaction participants were used for

these calculations. A similar procedure was performed for cyclopalladated complexes **C8**, **C8i** and **C8ii** and complexes **C9**, **C9i** and **C9ii**.

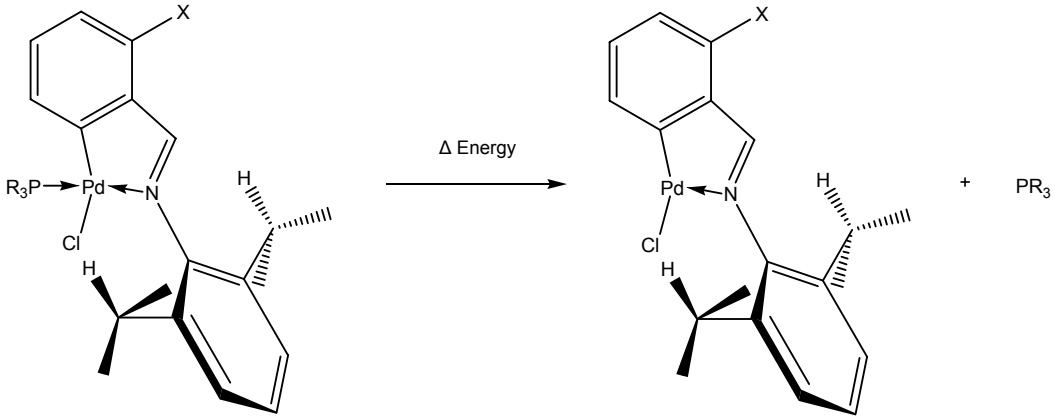

Scheme 4-3. Methodology employed to calculate the energy required to create a vacant coordination site by dissociation of a coordinated phosphine ligand (X = Cl, H or CH_3 and R = Ph, CH_3 or H).

Table 4-3. Energies required to remove a coordinated phosphine ligand from the neutral cyclopalladated complexes.[a]

R	X	Δ Energy (kJ/mol)
H	Cl	130
	H	126
	CH_3	124
CH_3	Cl	167
	H	163
	CH_3	160
Ph	Cl	139
	H	134
	CH_3	131

[a] Variables R and X as per **Scheme 4-3.**.

The trimethylphosphine ligand, due to the greater electron-releasing ability caused by the methyl groups as compared to the phenyl or hydrogen groups, requires more energy to dissociate from the palladium metal centre than either triphenylphosphine or phosphine, for all analogues. The influence of the substituent X on the aromatic ring is discernable but not significant. Electron-withdrawing chloride, which decreases the electron density on the palladium metal centre, results in a slightly stronger coordination of the phosphine ligand, while electron-releasing methyl, which increases the electron density on the palladium metal centre, results in a slightly weaker coordination of the phosphine ligand.

4.2.2.2 Neutral non-cyclopalladated complexes

The identification of the most stable conformations of the non-cyclopalladated complexes of trimethylphosphine required a thorough investigation of a number of parameters. The orientation of the imine double bond, the two trimethylphosphine ligands that can be situated in either a *cis* or *trans* fashion relative to one another, and the relative orientation of the two isopropyl substituents of the diisopropyl phenyl moiety collectively have an effect on the potential energy of the molecule. Initially, four stable conformations for complex **C11** were identified (**Figure 4-5.**). All four of the initial conformations, **A** – **D**, have the two isopropyl substituents eclipsed, with their methine protons aligned in parallel and pointed towards the imine nitrogen.

Calculations confirm that conformations **A** and **C** as seen in **Figure 4-5.** are lower in energy than **B** and **D** respectively. The next parameter investigated was the relative orientation of the two isopropyl substituents for conformations **A** and **C**. Rotations of the isopropyl substituents were performed in increments of 30°, followed directly by an energy optimisation at each increment, for twelve steps in an experiment that scans the potential

energy of the molecule as a function of the relative orientation of the two isopropyl substituents. The complete computational job comprises 169 potential energy data points.

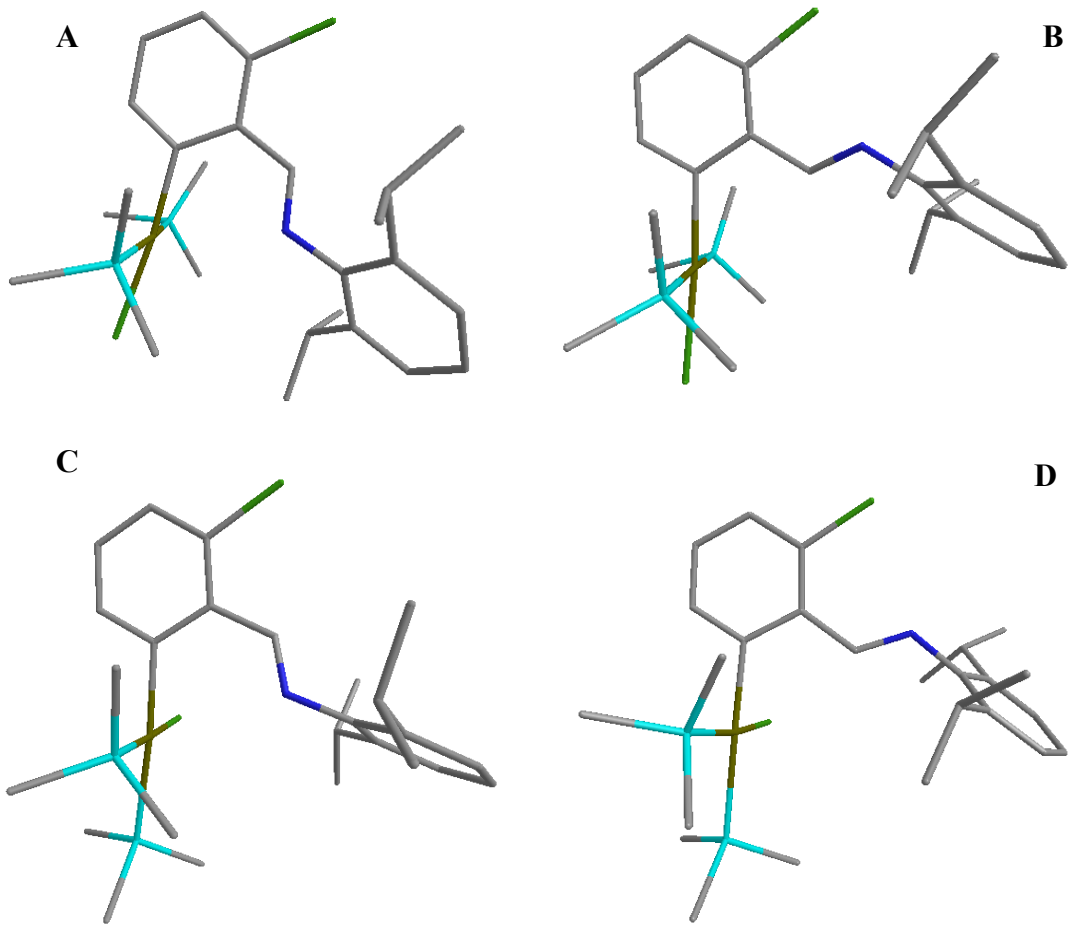

Figure 4-5. Conformation analysis of non-cyclopalladated complex **C11**.

Conformation **A** was first investigated (**Figure 4-6.**). The initial input coordinates has the eclipsed conformation with both the methine protons aligned in parallel and pointed towards the nitrogen of the imine group, i.e. with both torsion angles 1-2-3-4 and 1-5-6-7 ≈ 0°.

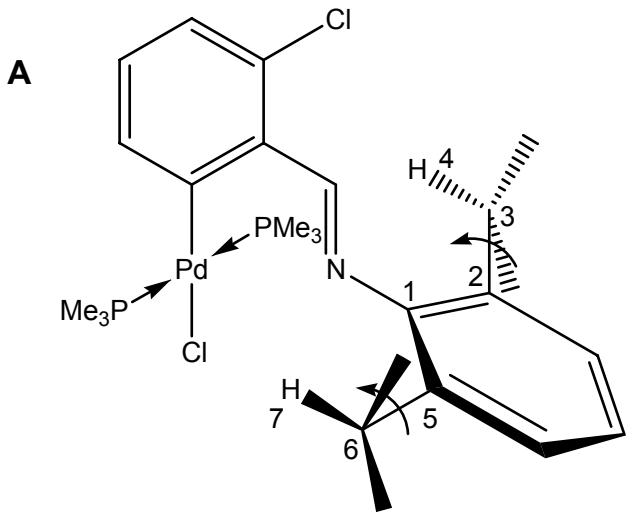

Figure 4-6. Conformation **A** of complex **C11**.

The most stable conformation is the initial input conformation with both torsion angles 1-2-3-4 and 1-5-6-7 ≈ 0°. This can be identified on the potential energy contour map and three dimensional potential energy surface representations (**Figure 4-8.** and **Figure 4-9.**). A similar procedure and result was obtained for the rotation of torsion angles 1□-2□-3□-4□ and

1□-5□-6□-7□ of conformation **C** (**Figure 4-7.**).

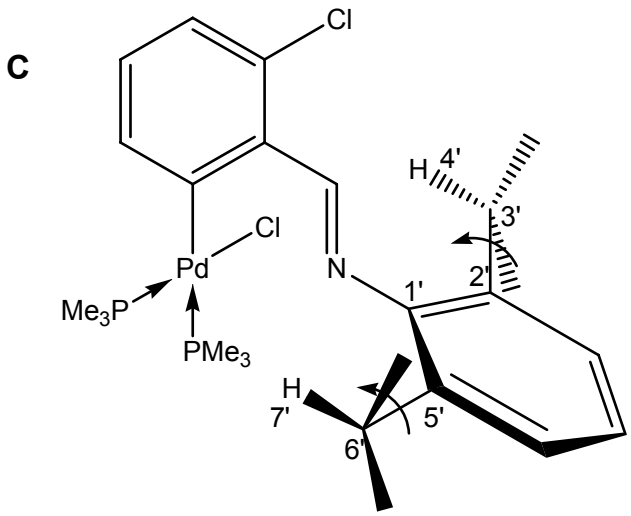

Figure 4-7. Conformation **C** of complex **C11**.

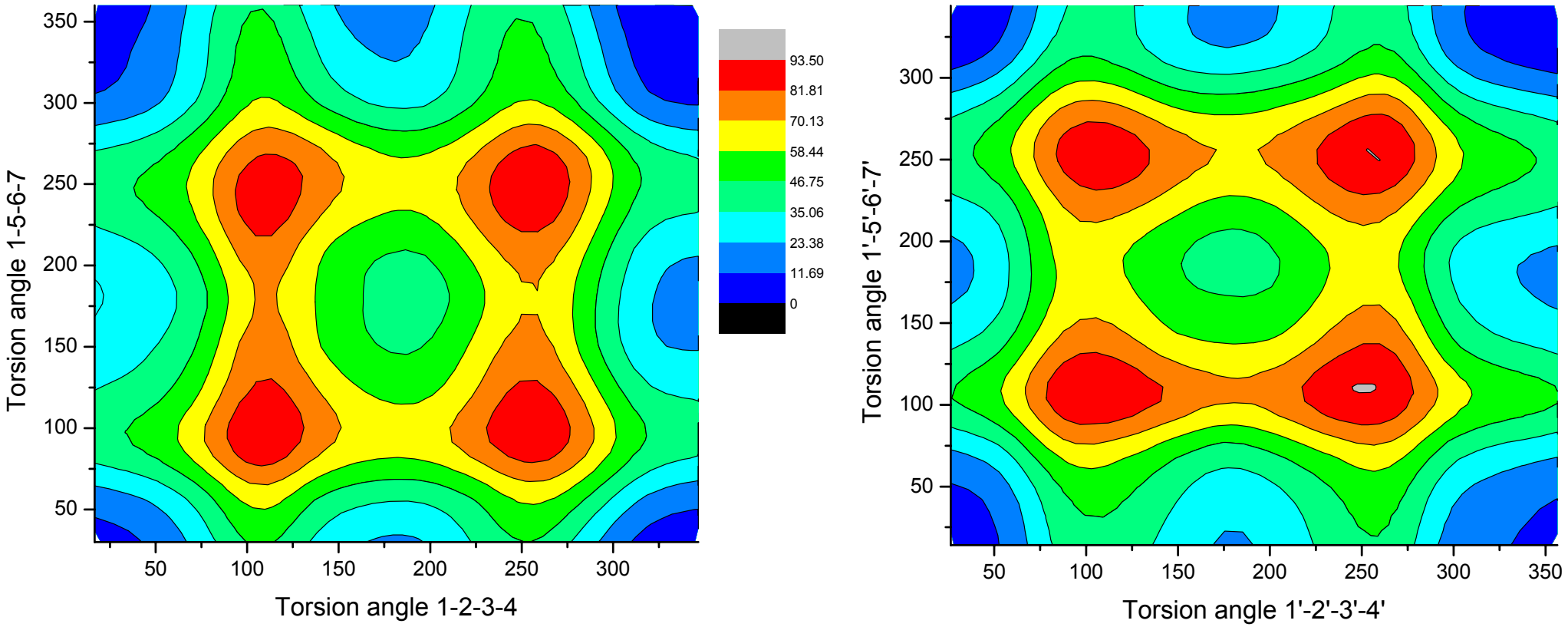

Figure 4-8. Contour maps of the relative potential energy surface of conformation **A** as a function of torsion angles 1-2-3-4 and 1-5-6-7 (left) and of conformation **C** as a function of torsion angles 1□-2□-3□-4□ and 1□-5□-6□-7□ (right) viewed from the top.

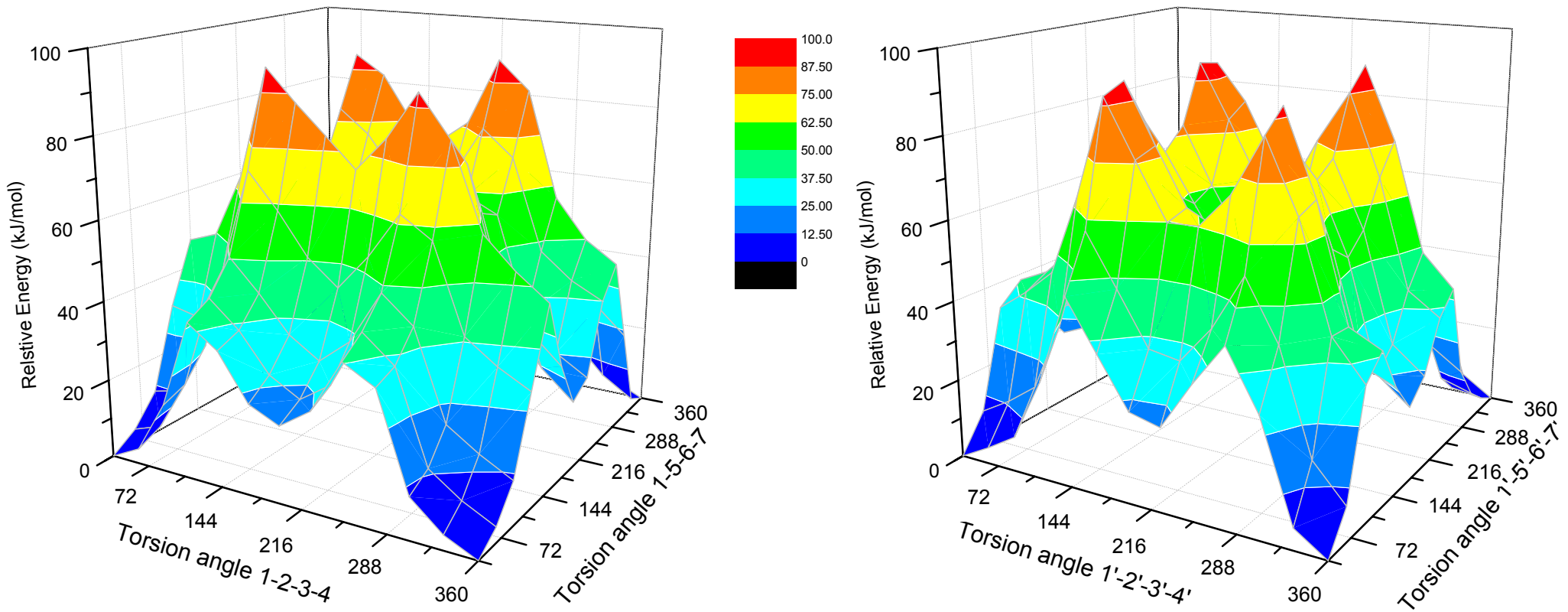

Figure 4-9. Three-dimensional relative potential energy surface of conformation **A** as a function of torsion angles 1-2-3-4 and 1-5-6-7 (left) and of conformation **C** as a function of torsion angles 1□-2□-3□-4□ and 1□-5□-6□-7□ (right) viewed from the side.

The most stable conformation of **A** is 38 kJ/mol lower in energy than the most stable conformation of **C**. The two trimethylphosphine ligands in complex **C11** favour a *trans* arrangement. This result is in agreement with the conclusions derived from the previously discussed ^{1}H- and ^{13}C {^{1}H}-NMR spectral analyses in Chapter 2 (**2.2.4**).

The last parameter investigated for the optimisation of complex **C11** is the relative orientation of the two trimethylphosphine ligands (**Figure 4-10.**).

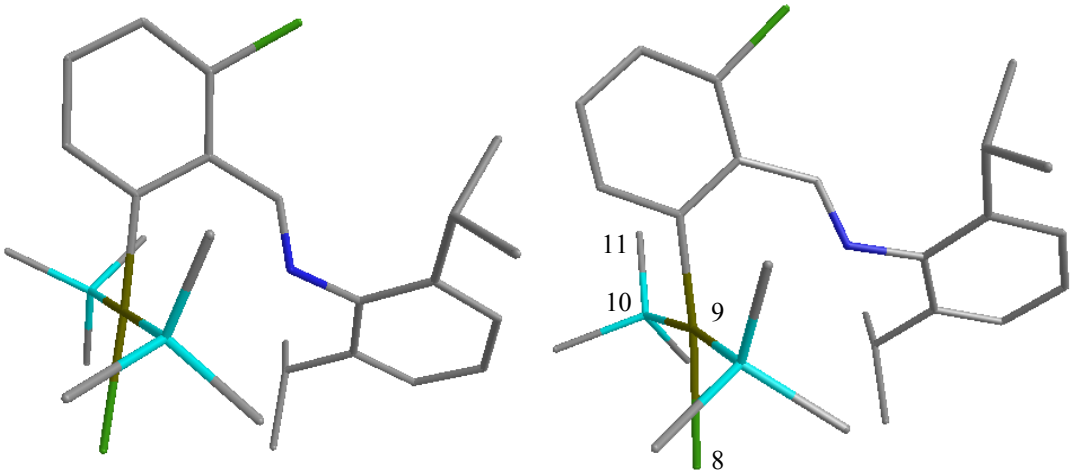

Figure 4-10. The two trimethylphosphine ligands of complex **C11** orientated in a staggered (left) and eclipsed (right) conformation.

A similar procedure to the experiment involving the rotations of the two isopropyl substituents was performed for the torsion angle 8-9-10-11 (**Figure 4-10.**, eclipsed conformation). Increments of 30°, followed directly by an energy optimisation at each increment, for one complete rotation of the trimethylphosphine ligand, was employed to scan the potential energy of the molecule as a function of the relative orientation of the two trimethylphosphine ligands (**Figure 4-11.**).

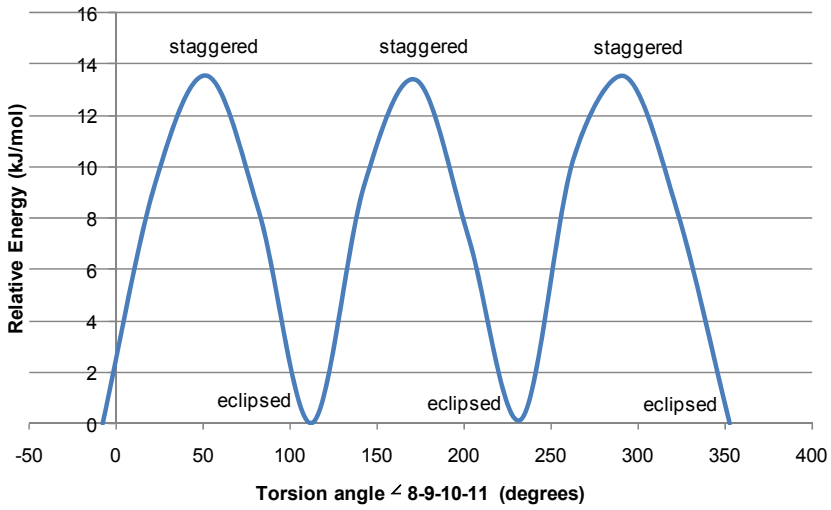

Figure 4-11. The relative changes in potential energy of complex **C11** as a function of the orientation of the two trimethylphosphine ligands.

Although the results for this set of calculations indicate that the eclipsed conformation is energetically favoured, single crystal diffraction analysis of complex **C11** indicates that these molecules arrange the trimethylphosphine ligands in a staggered conformation when packed in a crystal.[3] This single discrepancy between the computationally and experimentally obtained results is due to the fact that the calculations are based on isolated molecules in the gas phase as opposed to non-isolated molecules in the solid phase when packed in a crystal. All the other determined parameters, including the orientation of the imine double bond and the relative orientation of the two isopropyl substituents are similar for both the computational and experimental results.

A similar procedure to the one that identifies the most stable conformation of complex **C11** was performed for complexes **C13** and **C14**. The orientation of the imine bond was different for both as compared to **C11** (**Figure 4-12.**). This difference is in agreement with

the previously discussed crystallographically determined results for complexes **C11** and **C14** (**2.2.4**).

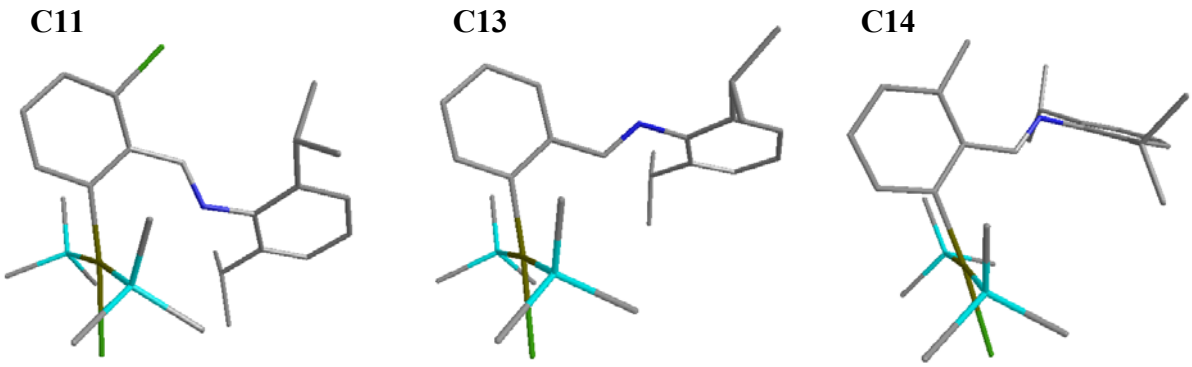

Figure 4-12. The most stable conformations of non-cyclopalladated complexes **C11**, **C13** and **C14**.

A good agreement between the calculated and crystallographically determined results for complexes **C11** and **C14** is seen (**Figure 4-13.** and **Table 4-4.**).

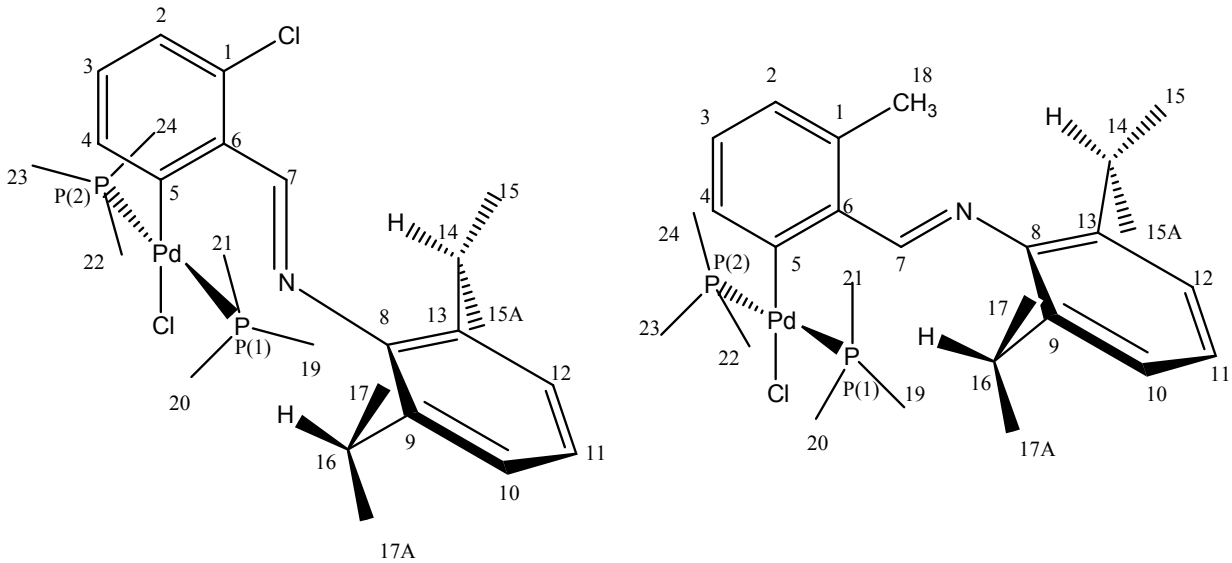

Figure 4-13. Skeletal structures of complexes **C11** (left) and **C14** (right) shown with the numbering scheme.

Table 4-4. Selected bond lengths, bond angles and torsion angles of the DFT and crystallographically determined structures of complexes **C14** and **C11**.[a]

	Complex C14		**Complex C11**	
	Calculated	**X-Ray**	**Calculated**	**X-Ray**[3]
		Bond lengths (Å)		
Pd-C(5)	2.041	2.014	2.029	2.005
Pd-P(1)	2.415	2.300	2.407	2.300
Pd-P(2)	2.409	2.306	2.423	2.307
Pd-Cl	2.498	2.388	2.496	2.383
C(7)-N	1.299	1.265	1.297	1.265
C(8)-N	1.429	1.425	1.436	1.421
C(1)-C(18)	1.518	1.511	-	-
		Bond angles (degrees)		
P(1)-Pd-C(5)	91.94	91.69	93.01	90.71
C(5)-Pd-P(2)	92.47	89.01	91.43	88.11
P(2)-Pd-Cl	87.37	90.69	87.48	93.79
Cl-Pd-P(1)	87.96	88.21	87.50	87.28
		Torsion angles (degrees)		
C(8)-C(13)-C(14)-C(15)	112.29	141.33	104.31	110.60
C(8)-C(9)-C(16)-C(17)	-113.74	-82.95	-118.23	-114.71
C(21)-P(1)-P(2)-C(24)	-7.90	11.35	8.34	43.04

[a] Atom labelling as per numbering scheme (**Figure 4-13.**).

A set of calculations to confirm the favoured formation of the non-cyclopalladated complexes of trimethylphosphine in the presence of excess trimethylphosphine during the cleavage reaction was done (**Scheme 4-4.**). Such a reaction involves the breaking of the coordinating bond from the nitrogen of the imine group to the palladium metal centre which is displaced by a trimethylphosphine molecule. Optimised energy conformations for all reaction participants were used for these calculations.

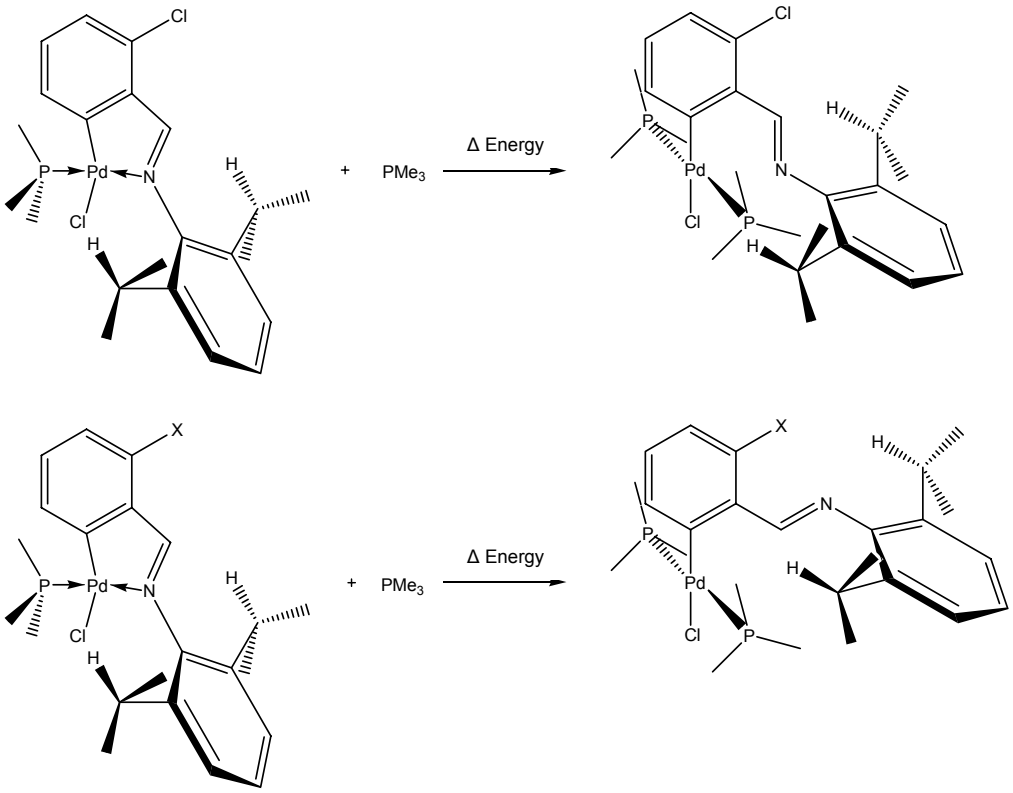

Scheme 4-4. Methodology employed to calculate the energy released during the formation of the non-cyclopalladated complexes of trimethylphosphine in the presence of excess trimethylphosphine (X = H or CH_3).

Formation of the non-cyclopalladated complexes of trimethylphosphine in the presence of excess trimethylphosphine is a favourable process (**Table 4-5.**). The results indicate that the nature of the substituent has no significant effect during the substitution.

Table 4-5. The change in energy during the formation of the non-cyclopalladated complexes of trimethylphosphine.[a]

X	Δ Energy (kJ/mol)
Cl	-17
H	-18
CH_3	-17

[a] X = substituent at the *ortho* position; as per **Scheme 4-4.**.

The calculated $\nu_{C=N}$ absorption band frequencies for the non-cyclopalladated complexes at higher wavenumbers confirms that the imine double-bond character is greater as compared to that of the cyclopalladated complexes (**Table 4-6.**).

Table 4-6. The $\nu_{C=N}$ absorption band frequencies of cyclopalladated complexes **C6**, **C8**, **C9** and non-cyclopalladated complexes **C11**, **C13** and **C14** in cm^{-1}.[a]

X	Computational		Experimental	
	Cyclopalladated	Non-cyclopalladated	Cyclopalladated	Non-cyclopalladated
Cl	1647	1663	1608	1627
H	1650	1665	1604	1620
CH_3	1644	1659	1605	1627

[a] X = substituent at the *ortho* position.

Although the frequencies generated from DFT calculations show higher wavenumbers, the same trend is seen. This result is in agreement with the conclusions derived from the previously discussed FT-IR spectral and single crystal diffraction analyses in **Chapter 2** (**2.2.4.**).

The synthetic procedure employed for the preparation of the neutral cyclopalladated complexes as described in **Chapter 2 (Scheme 2-7.)** involves the cleavage of one mol equivalent μ-Cl binuclear cyclopalladated complex and two mol equivalents triphenylphosphine. The products remain cyclopalladated, i.e. the coordinating bond from the nitrogen of the imine to the palladium metal centre is not broken in the process. When the reaction is repeated with excess triphenylphosphine, the same neutral cyclopalladated complexes are isolated, i.e. coordination of excess triphenylphosphine molecule does not take place, for all analogues. A set of calculations to confirm that the formation of cyclopalladated complexes is energetically favourable was done.

Since the optimised energy conformations for complexes **C6**, **C8** and **C9** have been confirmed, the identification of the optimised conformations for non-cyclopalladated complexes bearing two triphenylphosphine ligands was investigated. A similar procedure to the one that identified the most stable conformations of the non-cyclopalladated complexes bearing two trimethylphosphine ligands was employed.

For convenience, the non-cyclopalladated complexes of triphenylphosphine with substituents Cl, H and CH_3 in the *ortho* positions are named complexes **C26**, **C27** and **C28** respectively. For complex **C26**, four stable conformations were identified (**Figure 4-14.**).

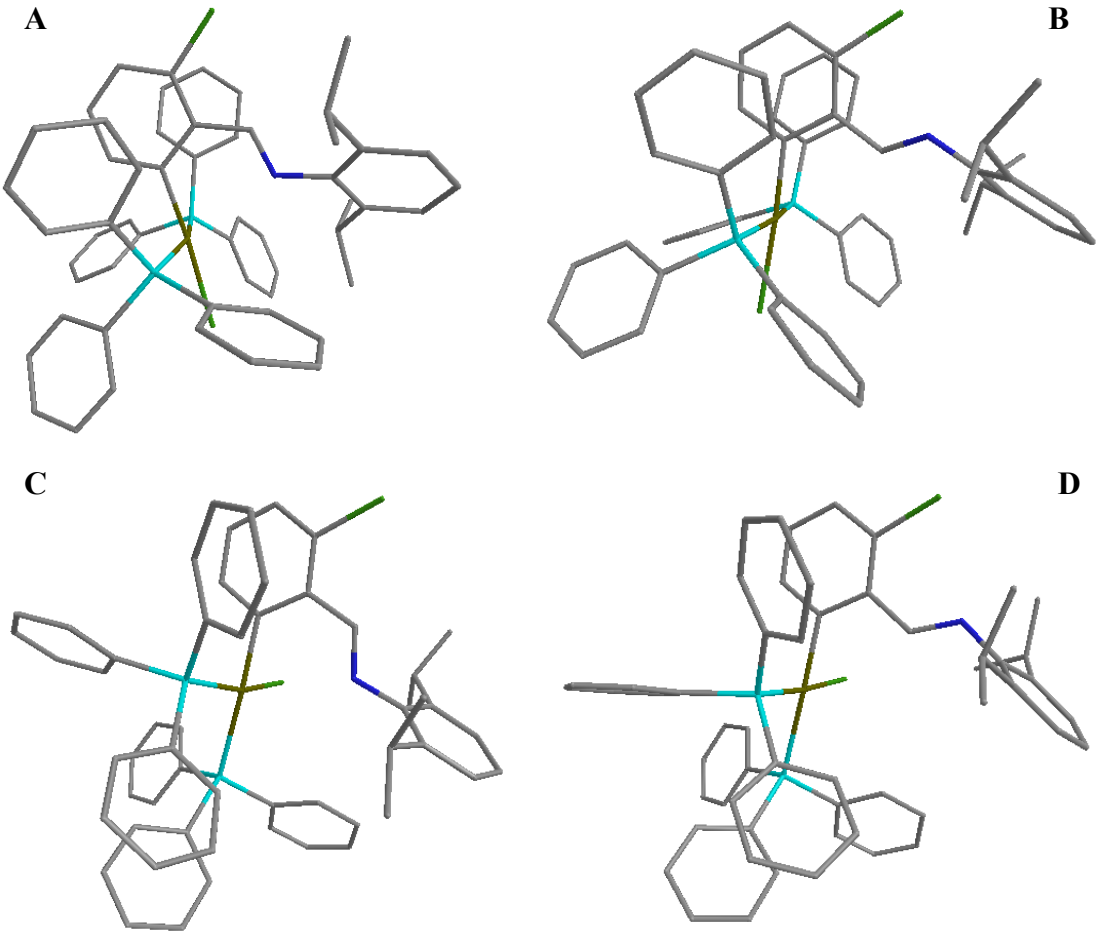

Figure 4-14. Conformation analysis of non-cyclopalladated complex **C26**.

Conformations **A – D** were identified and calculated based on the assumption that the two isopropyl substituents are eclipsed with the methine protons aligned in parallel and pointed towards the nitrogen of the imine group. Conformation **A** is the most stable one for complex **C26**. A similar procedure was performed for complexes **C27** and **C28**. Similarly to the results obtained for the non-cyclopalladated complexes of trimethylphosphine, the orientations of the imine bond for complexes **C27** and **C28** were both different to that of **C26** (**Scheme 4-5.**).

A set of calculations to confirm the non-formation of the non-cyclopalladated complexes of triphenylphosphine in the presence of excess triphenylphosphine during the cleavage reaction was done (**Scheme 4-5.**). Optimised energy conformations for all reaction participants were used for these calculations.

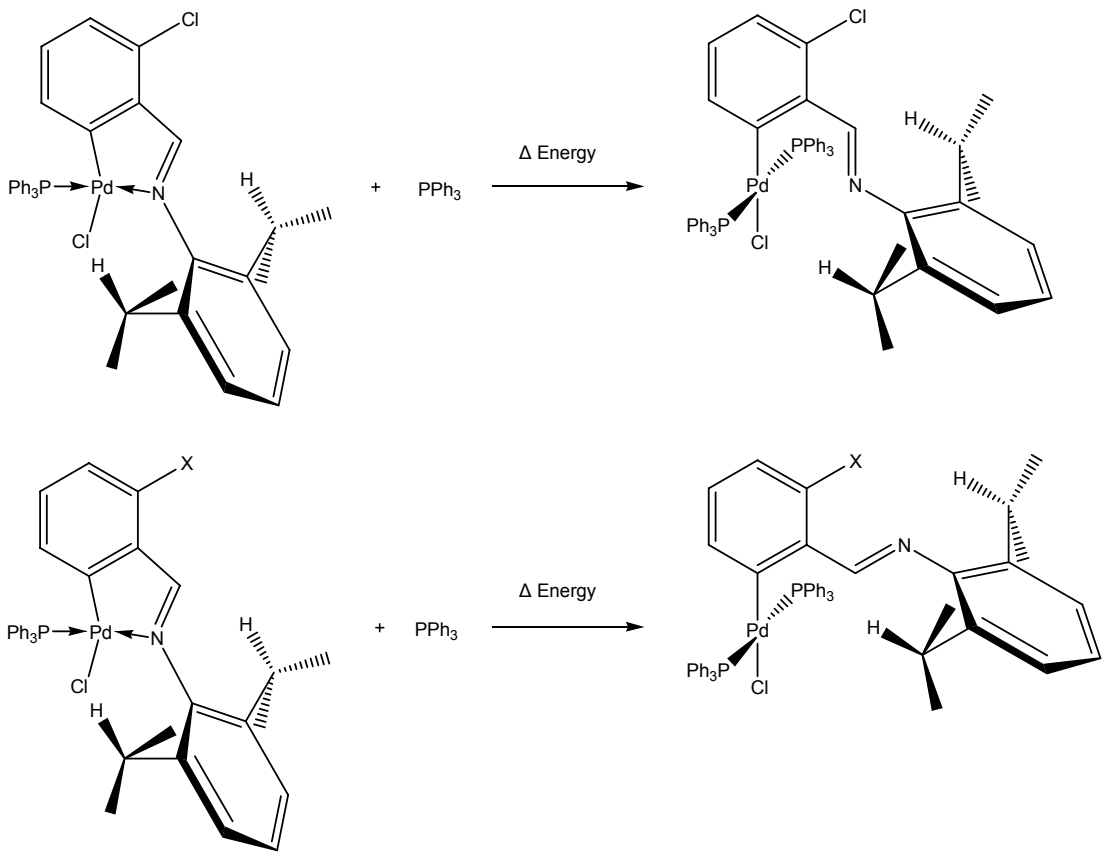

Scheme 4-5. Methodology employed to calculate the energy required during the formation of a non-cyclopalladated complex of triphenylphosphine in the presence of excess triphenylphosphine (X = H or CH_3).

The formation of the non-cyclopalladated complexes of triphenylphosphine in the presence of excess triphenylphosphine is an unfavourable process (**Table 4-7.**). These computational results explain why the products that were isolated experimentally are cyclopalladated despite the presence of available triphenylphosphine to potentially coordinate.

Table 4-7. The energy required during the formation of the non-cyclopalladated complexes of triphenylphosphine.[a]

X	Δ Energy (kJ/mol)
Cl	24
H	23
CH_3	14

[a] X = substituent at the *ortho* position; as per **Scheme 4-5.**.

The inability of triphenylphosphine to displace the coordinated imine in the presence of available triphenylphosphine to generate non-cyclopalladated complexes as opposed to trimethylphosphine could be due to either the fact that it is too big, i.e. sterically hindered, or that it is not basic enough relative to the imine nitrogen.

A computational experiment that incorporates a tertiary phosphine that has similar properties to both trimethylphosphine and triphenylphosphine was done in order to understand these results. The choice of tricyclohexylphosphine is ideal, since it is characterised by high basicity and a large ligand cone angle (**Table 4-8.**).

Table 4-8. pK_a (aq) and ligand cone angle values of tertiary phosphines.[4]

PR_3	pK_a	Cone angle (°)
PPh_3	2.73	145
PMe_3	8.65	115
$P(C_6H_{11})_3$	9.70	170

If the formation of non-cyclopalladated complexes with tricyclohexylphosphine is favourable in the presence of excess tricyclohexylphosphine, then the inability of triphenylphosphine to coordinate at two coordination sites is due to the fact that it is not basic enough. If the formation of non-cyclopalladated complexes with tricyclohexylphosphine is unfavourable in the presence of excess tricyclohexylphosphine, then the inability of triphenylphosphine to coordinate at two coordination sites is due to the fact that it is too big (sterically hindered).

A similar procedure to one that confirmed the favoured formation of the non-cyclopalladated complexes of trimethylphosphine in the presence of excess trimethylphosphine during the cleavage reaction was done for tricyclohexylphosphine (**Figure 4-15.** and **Scheme 4-6.**). Optimised energy conformations for all reaction participants were used for these calculations.

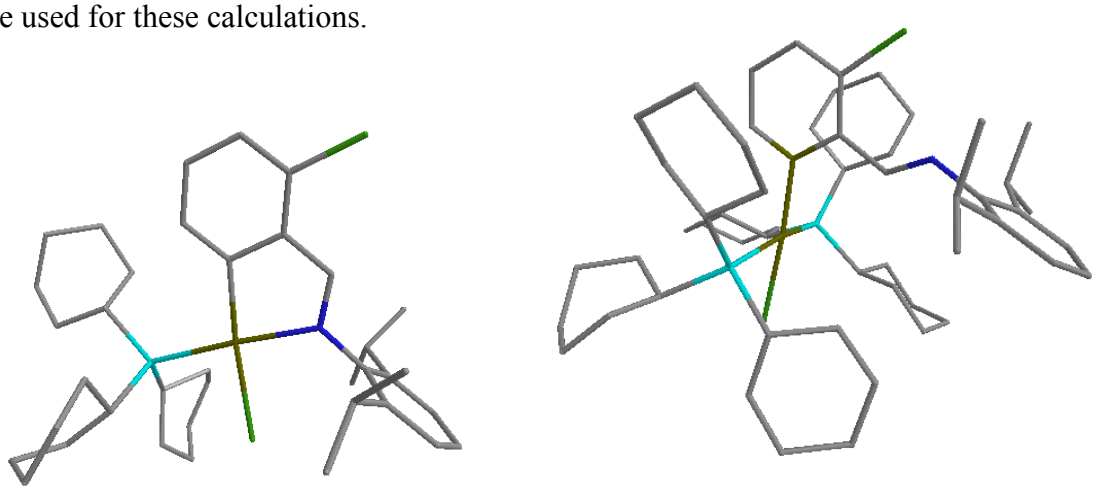

Figure 4-15. Optimised energy conformations of the cyclopalladated (left) and non-cyclopalladated (right) complexes of tricyclohexylphosphine (*ortho*-Cl analogue).

The thermodynamically most stable conformation for the non-cyclopalladated complexes has the two PCy_3 ligands situated in a *trans* fashion relative to one another in an eclipsed

conformation. Due to the large ligand cone angle of tricyclohexylphosphine, the imine orientation as seen in **Figure 4-15.** (right) is the thermodynamically most stable for the non-cyclopalladated complexes for all analogues.

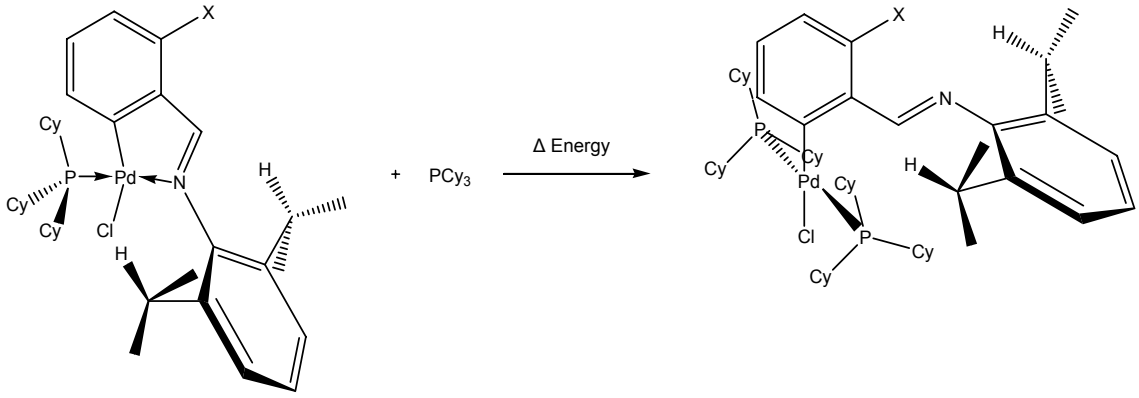

Scheme 4-6. Methodology employed to calculate the change in energy during the formation of a non-cyclopalladated complex of tricyclohexylphosphine in the presence of excess tricyclohexylphosphine (X = Cl, H or CH_3).

The formation of the non-cyclopalladated complexes of tricyclohexylphosphine in the presence of excess tricyclohexylphosphine during the cleavage reaction is favourable despite its large ligand cone angle (**Table 4-9.**). This result confirms that triphenylphosphine is not basic enough to displace the imine nitrogen and thus generate non-cyclopalladated complexes.

Table 4-9. The change in energy during the formation of the non-cyclopalladated complexes of tricyclohexylphosphine.[a]

X	Δ Energy (kJ/mol)
Cl	-75
H	-69
CH_3	-68

[a] X = substituent at the *ortho* position; as per **Scheme 4-6.**.

4.2.3 Cationic complexes of acetonitrile and pyridine

The successful application of cationic complexes **C16**, **C17** and **C18** as catalyst precursors for the polymerisation of phenylacetylene, without the use of a co-catalyst to produce *in-situ* active catalysts,[3] has led to the need for a thorough understanding of their reactivity and their physical properties. The potential of the previously discussed cationic complexes to be employed as catalyst precursors in various α-olefin oligomerisation and polymerisation reactions is investigated. This can be achieved by probing the bond dissociation energies (BDE's) of the labile ligands at the coordination sphere.

The proposed mechanism for α-olefin oligomerisation and polymerisation reactions involves the dissociation of a labile ligand from the metal centre in solution, creating a vacant coordination site to which the α-olefin first coordinates and then inserts into the M-C bond where polymerisation takes place until eventual chain termination, forming the desired polymer products. For cationic complexes **C16 – C20** and **C21 – C25** which possess two labile ligands as well as a coordinating imine, the active catalyst could be created by dissociation of either the tertiary phosphine, the donor ligand, acetonitrile or pyridine, or the imine. The bond dissociation energies of these coordinating groups are investigated.

A set of calculations were done in order to identify transition states for the dissociation of the three coordinating groups. The distance from a particular group to the palladium metal centre was increased in increments of 0.3 Å, followed directly by an energy optimisation at each increment, from the initial bond length of the optimised conformation of complex **C16ii** (**Figure 4-16.**). The potential energy of the system was thus monitored as a function of the distance.

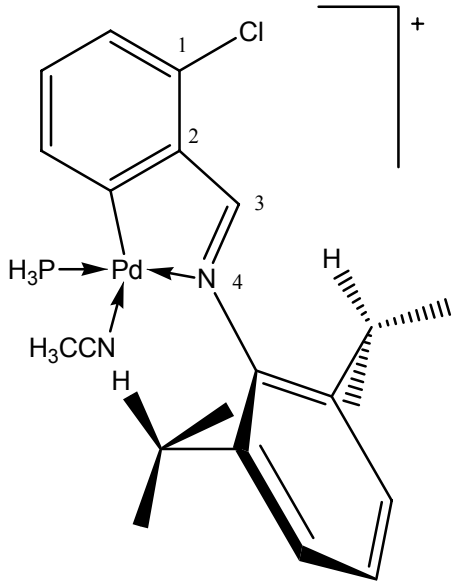

Figure 4-16. Cationic complex **C16ii** used to identify transition states for the dissociation of the coordinating groups.

The potential energy of the system continuously rises during the dissociation of phosphine from the palladium metal centre from an initial bond distance of 2.42 Å until a distance of 6.26 Å (**Figure 4-17.**). The sum of the van der Waals radii of palladium (1.63 Å) and phosphorous (1.80 Å) is 3.43 Å. No transition state can be identified for phosphine dissociation using this method.

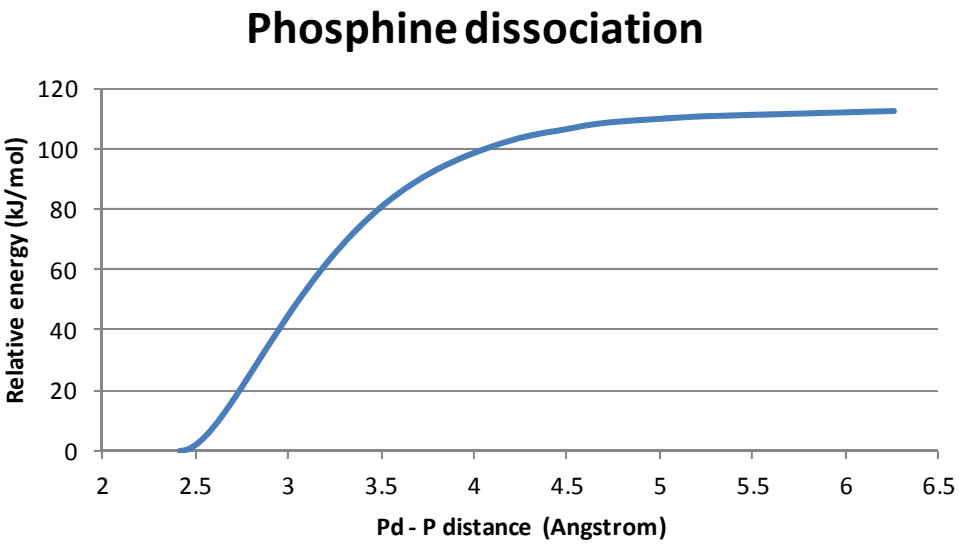

Figure 4-17. Change in energy when increasing the distance between palladium and the phosphine phosphorous.

An energy maximum is present during the dissociation of acetonitrile when the distance between the palladium and the acetonitrile nitrogen is 3.38 Å (**Figure 4-18.**). This data point cannot be described as a transition state since the potential energy of the system begins to increase again after the following energy minimum which means that the acetonitrile and the vacant site complex still "see" each other. If this were a transition state, the potential energy of the system would continuously decrease until an infinite distance between the palladium and nitrogen.

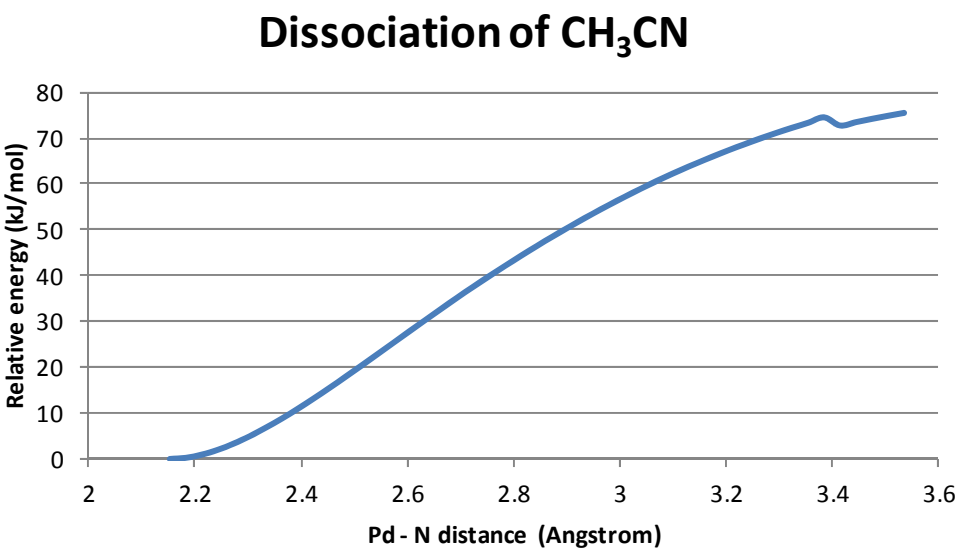

Figure 4-18. Change in energy when increasing the distance between palladium and the acetonitrile nitrogen.

A similar trend is seen when increasing the distance between palladium and the imine nitrogen. An energy maximum, which is 152 kJ/mol higher in energy than that of the optimised complex, is present at a distance of 3.22 Å (**Figure 4-19.**). The energy begins to increase again after the following energy minimum. This increase in energy could be due to strain imposed on the complex due to the instructions for the calculation or, similarly to that of the dissociation of acetonitrile, certain atoms still "see" each other. Either way, this method cannot identify the transition state for the dissociation of the imine nitrogen.

Instead of increasing the distance between the palladium and imine nitrogen, the torsion angle 1-2-3-4 (**Figure 4-16.**) was rotated in increments of 10°, followed directly by an energy optimisation at each increment, for 18 increments (**Figure 4-20.**). An energy maximum is present at 150°, but cannot be identified as a transition state since the imine hydrogen is in

very close proximity of the palladium at that data point which prevents the formation of a vacant coordination site which is the whole purpose of the computational experiment.

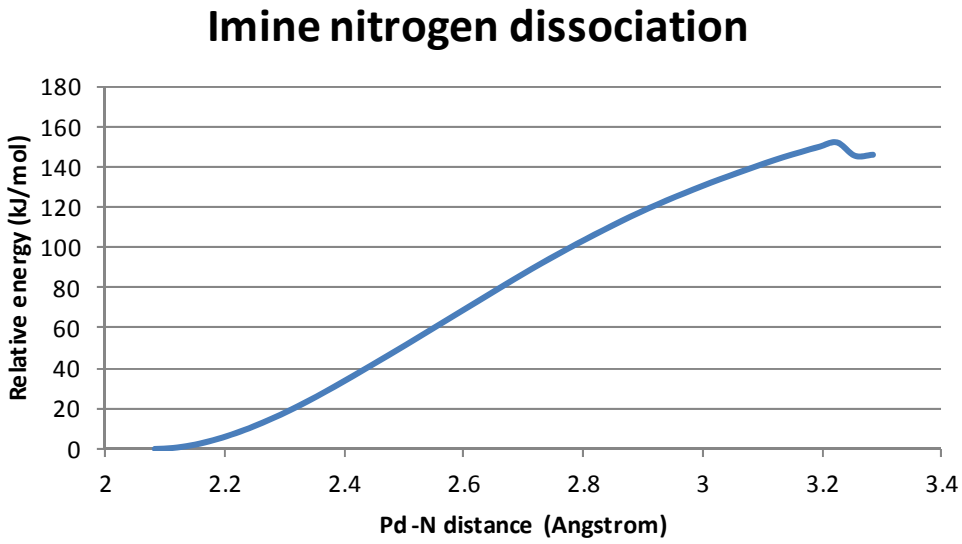

Figure 4-19. Change in energy when increasing the distance between palladium and the imine nitrogen.

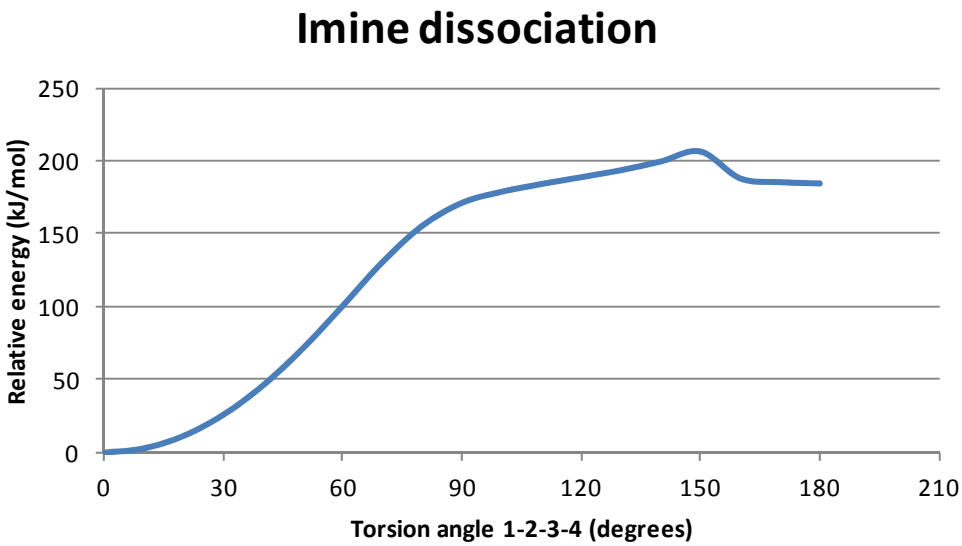

Figure 4-20. Change in energy when rotating torsion angle 1-2-3-4 (**Figure 4-16.**).

The bond dissociation energies were consequently determined by calculating the energy differences of the separately calculated reaction participants in a similar manner to that done for the cyclopalladated complexes (**Scheme 4-3.**).

The identification of the thermodynamically most stable conformations for all the reaction participants was done in a similar manner to that which has been employed for all the molecules so far (**Scheme 4-7.** and **Table 4-10.**). The signature peak frequency, i.e. the $\nu_{C=N}$ absorption band corresponding to the imine (**Table 4-13.**) was also determined.

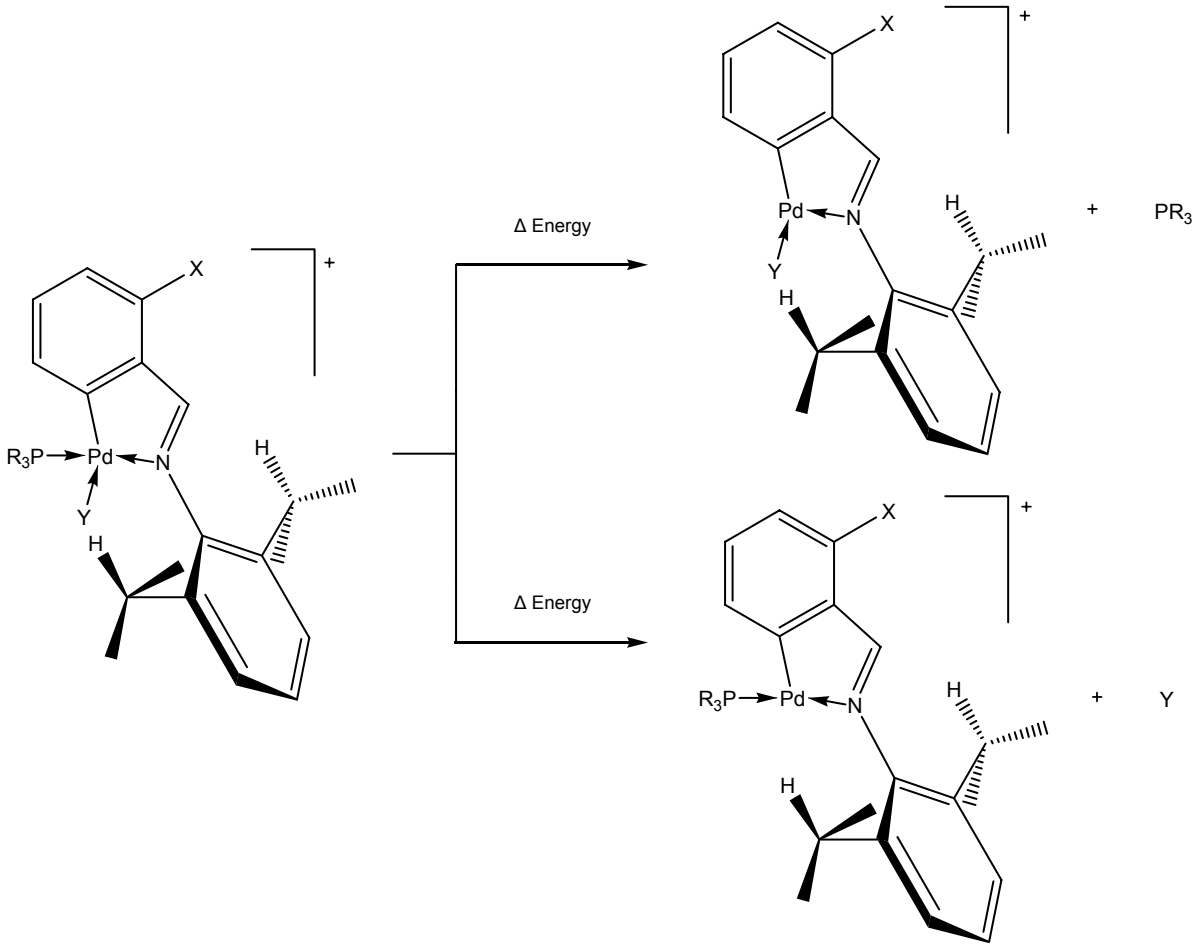

Scheme 4-7. Methodology employed to calculate the bond dissociation energies of the labile ligands of the cationic complexes **C16**, **C18**, **C19**, **C21**, **C23** and **C24** as well as analogous trimethylphosphine and phosphine coordinating complexes thereof (X = Cl, H or CH_3; Y = CH_3CN or py; R = H, CH_3 or Ph).

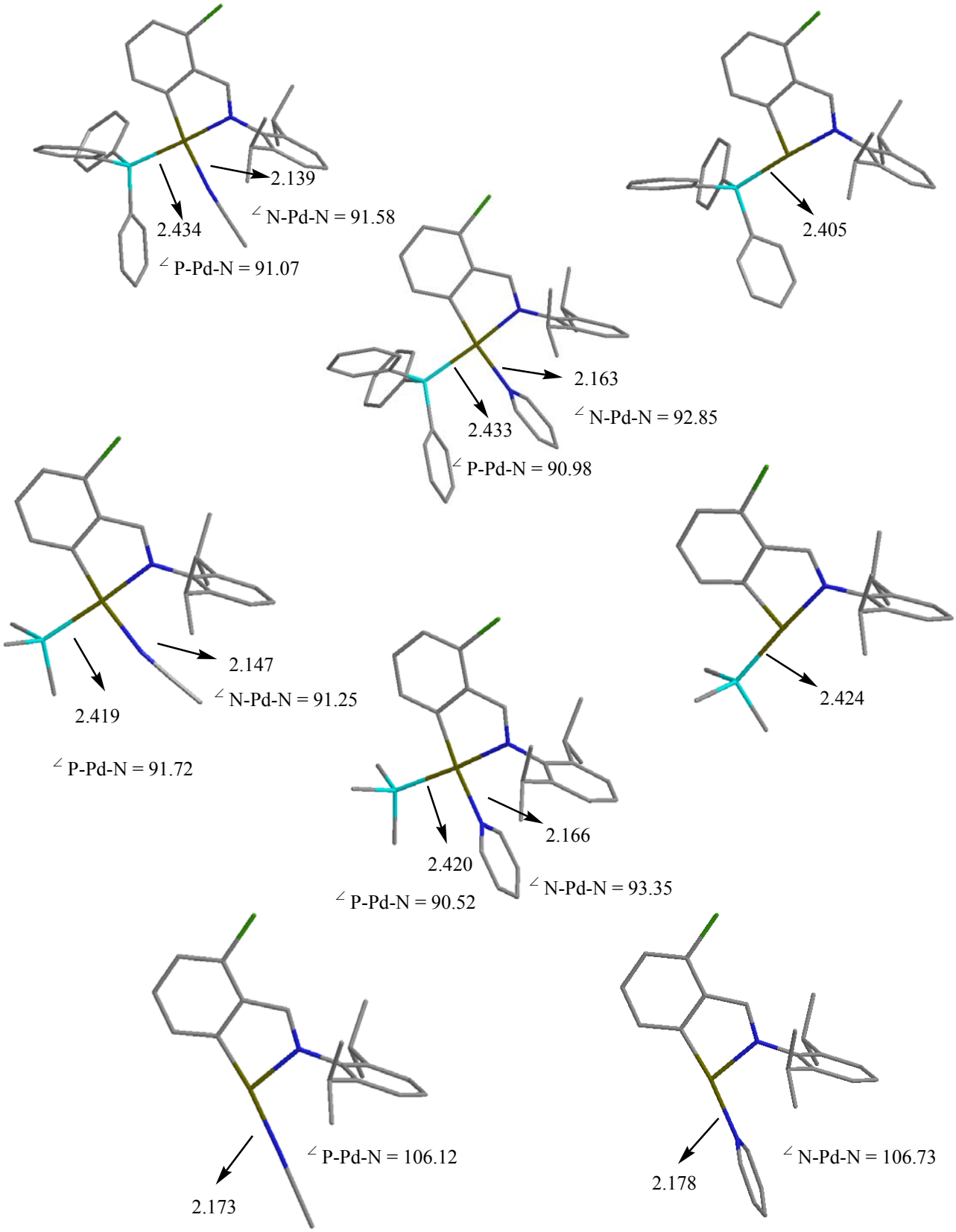

Figure 4-21. Selected geometries of optimised cationic complexes (*ortho*-Cl analogue) and vacant site complexes. Selected structural parameters are given in Å and degrees.

Table 4-10. The bond dissociation energies (BDE's) of coordinating phosphines and donor ligands, acetonitrile or pyridine (Y), of the cationic complexes.[a]

Entry	X	Y	R	Phosphine (kJ/mol)	(Y) (kJ/mol)
1	Cl	CH_3CN	H	126	129
2	H	CH_3CN	H	126	126
3	CH_3	CH_3CN	H	122	123
4	Cl	py	H	124	142
5	H	py	H	123	137
6	CH_3	py	H	119	134
7	Cl	CH_3CN	CH_3	174	122
8	H	CH_3CN	CH_3	172	119
9	CH_3	CH_3CN	CH_3	168	116
10	Cl	py	CH_3	167	131
11	H	py	CH_3	166	127
12	CH_3	py	CH_3	161	123
13 (C16)	Cl	CH_3CN	Ph	177	113
14 (C18)	H	CH_3CN	Ph	174	109
15 (C19)	CH_3	CH_3CN	Ph	169	107
16 (C21)	Cl	py	Ph	169	120
17 (C23)	H	py	Ph	166	116
18 (C24)	CH_3	py	Ph	160	113

[a] Variables X, Y and R as per **Scheme 4-7.**.

The influence of the substituent X on the aromatic ring is discernable but not significant. Its influence on the bond dissociation energies of the various ligands is the same as that for the previously discussed bond dissociation energies of the phosphine ligands for the cyclopalladated neutral complexes (**Scheme 4-1.** and **Table 4-2.**).

The dissociation of the donor ligand to create a vacant coordination site, to generate a potential active catalyst, is favoured above dissociation of the phosphine (**R** = CH_3 or Ph) ligand. The same cannot be said for those complexes bearing phosphine (**R** = H). The use of complexes that include phosphine as a ligand to be employed as a potential catalyst precursor was never regarded in the first place.

With regards to entries **7** – **9** and **10** – **12** (**Table 4-10.**), it is evident that the dissociation of pyridine, as compared to acetonitrile, requires more energy to create a vacant coordination site. The same trend is seen when comparing entries **13** – **15** to **16** – **18**. These trends are directly affected by the relative basicities of the donor ligands. The higher the s-character of a particular orbital, the more strongly electrons are held and shared with greater difficulty. Therefore, the basicity diminishes with change of hybridisation of nitrogen in the order $sp^3 > sp^2 > sp$ (**Figure 4-22.**).

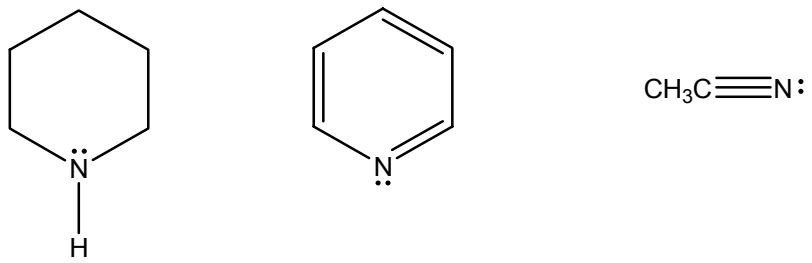

pK_b = 2.88 pK_b = 8.75 pK_b = 24.00

Figure 4-22. The pK_b values of piperidine (left), pyridine (middle) and acetonitrile (right).

The higher basicity of pyridine, as compared to acetonitrile, results in stronger bonding to the palladium metal centre. This means that more energy is required for its dissociation from the metal centre, which is in agreement with the calculated BDE trends.

The relative basicity of the coordinating donor ligand also affects the bond strength of the phosphine (**R** = CH_3 and Ph). When pyridine is the donor ligand, the electron density on the metal centre is greater than in the case of acetonitrile, with the consequence of a weaker bond strength of the phosphine ligand.

The bond dissociation energy calculations were repeated using an alternative method. From the obtained optimised conformations of the cationic complexes, single point calculations were performed on the respective dissociated ligand and vacant cationic complexes respectively taken from the final atomic coordinates of the previously calculated complete cationic complexes.

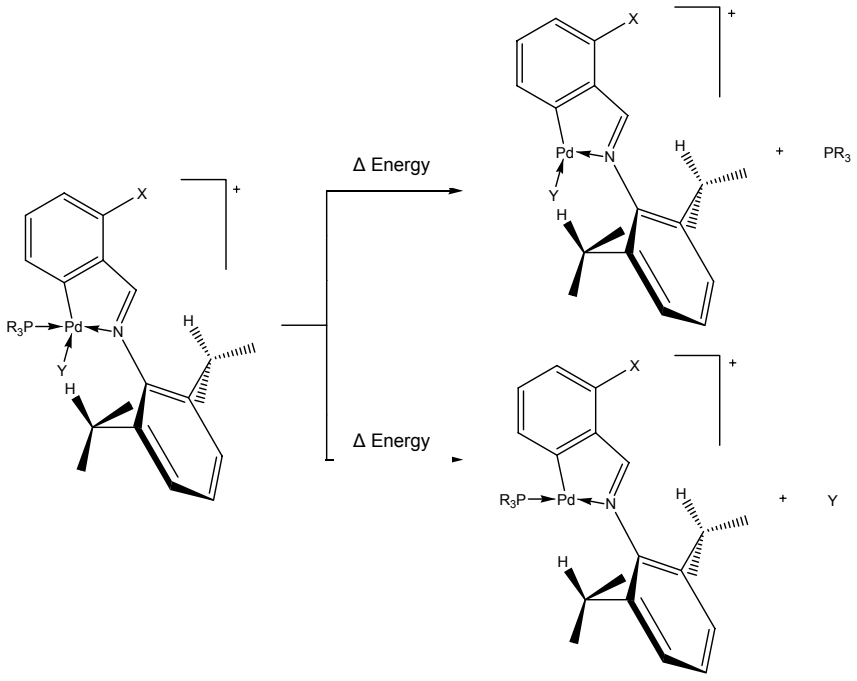

Scheme 4-8. Methodology employed to calculate the bond dissociation energies of the labile ligands. Single point energy calculations based on the final coordinates were used for these calculations (X = Cl, H or CH_3; Y = CH_3CN or py; R = H, CH_3 or Ph).

Table 4-11. The bond dissociation energies (BDE's) of coordinating phosphines and donor ligands, acetonitrile or pyridine (Y), of the cationic complexes using the alternative method.[a]

Entry	X	Y	R	Phosphine (kJ/mol)	(Y) (kJ/mol)
1	Cl	CH_3CN	H	147	137
2	H	CH_3CN	H	146	133
3	CH_3	CH_3CN	H	143	130
4	Cl	py	H	143	154
5	H	py	H	143	149
6	CH_3	py	H	140	146
7	Cl	CH_3CN	CH_3	204	131
8	H	CH_3CN	CH_3	203	127
9	CH_3	CH_3CN	CH_3	199	124
10	Cl	py	CH_3	195	145
11	H	py	CH_3	194	140
12	CH_3	py	CH_3	190	137
13 (C16)	Cl	CH_3CN	Ph	207	125
14 (C18)	H	CH_3CN	Ph	204	122
15 (C19)	CH_3	CH_3CN	Ph	199	119
16 (C21)	Cl	py	Ph	200	141
17 (C23)	H	py	Ph	197	136
18 (C24)	CH_3	py	Ph	192	133

[a] Variables X, Y and R as per **Scheme 4-8.**.

Similar trends are seen for the alternative method. The main discrepancy between the two is that the energies obtained for the alternative method are greater than for the first method. This is to be expected, since the calculated energies are based on systems that are not allowed the opportunity to find their thermodynamically most stable conformation.

The major advantage of the cationic complexes, as compared to the previously discussed neutral complexes to be employed as potential catalyst precursors, is that the generation of a vacant coordination site requires less energy. The potential coordination of an α-olefin is improved using these systems which potentially promotes superior catalytic activity.

The calculated and experimentally obtained results for cationic complexes **C19** and **C24** reveal that the molecular geometries of the optimised energy conformations compare well to the crystallographically determined geometries (**Figure 4-23.** and **Table 4-12.**).

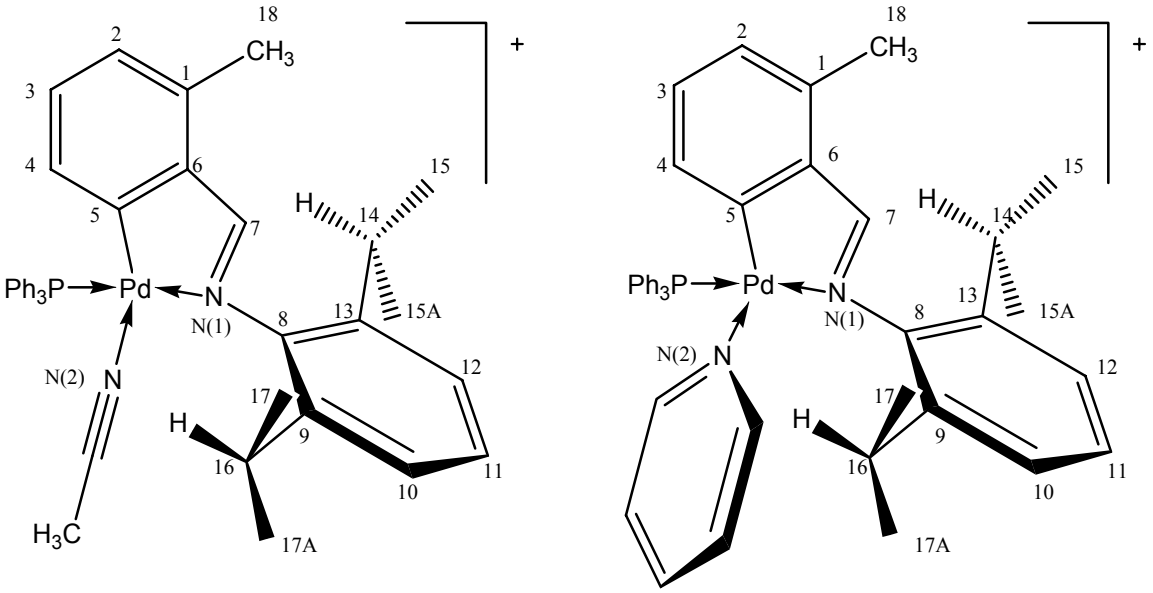

Figure 4-23. Skeletal structures of complexes **C19** (left) and **C24** (right) shown with the numbering schemes.

Table 4-12. Selected bond lengths, bond angles and torsion angles of the DFT and crystallographically determined structures of complex **C19**.[a]

	Calculated	X-Ray			
		A	**B**	**C**	**D**
		Bond lengths (Å)			
Pd-C(5)	2.036	2.000	2.009	1.996	1.998
Pd-N(1)	2.099	2.081	2.077	2.092	2.063
Pd-N(2)	2.148	2.091	2.087	2.095	2.098
Pd-P	2.434	2.274	2.272	2.270	2.273
C(7)-N(1)	1.310	1.285	1.287	1.287	1.290
C(8)-N(1)	1.449	1.438	1.443	1.440	1.444
C(1)-C(18)	1.520	1.515	1.515	1.506	1.509
		Bond angles (degrees)			
N(1)-Pd-N(2)	91.73	89.47	88.94	89.14	89.85
N(2)-Pd-P	91.07	93.64	94.22	93.93	93.46
P-Pd-C(5)	96.23	94.99	95.18	95.79	95.66
C(5)-Pd-N(1)	80.99	81.36	81.36	81.28	81.13
		Torsion angles (degrees)			
C(8)-C(13)-C(14)-C(15)	-108.43	-110.96	-109.08	-112.53	-111.11
C(8)-C(9)-C(16)-C(17)	99.90	103.90	101.91	109.43	108.41

[a] Atom labelling as per numbering scheme (**Figure 4-23.**)

Table 4-13. Selected bond lengths, bond angles and torsion angles of the DFT and crystallographically determined structures of complex **C24**.[a]

	Calculated	**X-Ray**
	Bond lengths (Å)	
Pd-C(5)	2.051	2.024
Pd-N(1)	2.116	2.103
Pd-N(2)	2.171	2.126
Pd-P	2.434	2.275
C(7)-N(1)	1.311	1.281
C(8)-N(1)	1.453	1.433
C(1)-C(18)	1.520	1.507
	Bond angles (degrees)	
N(1)-Pd-N(2)	92.79	91.02
N(2)-Pd-P	91.02	92.09
P-Pd-C(5)	95.32	96.64
C(5)-Pd-N(1)	80.87	80.80
	Torsion angles (degrees)	
C(8)-C(13)-C(14)-C(15)	94.71	99.28
C(8)-C(9)-C(16)-C(17)	-91.08	-83.67

[a] Atom labelling as per numbering scheme (**Figure 4-23.**)

The double-bond character of the imine bond in the cationic complexes is similar to that of the neutral complexes (**Table 4-13.**). The same conclusions were derived from previously

discussed FT-IR spectral and single crystal diffraction analyses in **Chapter 3** (**3.3.1** and **3.3.2**).

Table 4-14. The $\nu_{C=N}$ absorption band frequencies corresponding to the imine of cationic complexes **C21**, **C23**, **C24**, **C26**, **C28** and **C29** in cm^{-1}.[a]

X	Computational		Experimental	
	Y = CH_3CN	Y = py	Y = CH_3CN	Y = py
Cl	1646	1644	1612	1614
H	1647	1646	1616	1612
CH_3	1642	1642	1604	1607

[a] Variables X and Y as per **Scheme 4-7.**.

4.3 Conclusions

The calculated $\nu_{C=N}$ absorption bands, which corresponds to the imine, of the thermodynamically most stable conformations, are consistent with the experimentally obtained $\nu_{C=N}$ absorption bands for all compounds. The calculated five-membered chelate product, complex **C4**, which forms via C_{aryl}-H bond activation is thermodynamically more stable than the six-membered chelate product, complex **C4i**, which would form via C_{allyl}-H bond activation. The formation of non-cyclopalladated complexes bearing two trimethylphosphine ligands is energetically favourable and the formation of non-cyclopalladated complexes bearing two triphenylphosphine ligands is unfavourable. Predictive calculations indicate that triphenylphosphine is not basic enough to displace the imine nitrogen to generate non-cyclopalladated complexes.

Bond dissociation energy calculations confirm that the dissociation of pyridine, as compared to acetonitrile, requires more energy to create a vacant coordination site. This trend is directly affected by the relative basicities of the donor ligands. Calculations reveal that when pyridine is the donor ligand, the electron density on the metal centre is greater than in the case of acetonitrile, with the consequence of a weaker bond strength of the phosphine ligand.

The calculated and crystallographically obtained results for complexes **C9**, **C14**, **C19** and **C24** reveals that the molecular geometries of the optimised energy conformations compare well to the crystallographically determined geometries.

4.4 Computational details

Gaussian 03[5] and Gaussian 09[6] were used to fully optimise all the structures reported in this thesis at the DFT level using the B3LYP functional.[7,8] Among a variety of DFT functionals, it is generally accepted that the most popular B3LYP performs well for transition metal molecular systems. All structures were optimised and characterised as minimum energy states using the LanL2DZ basis set.[9] The identification of minima was done according to default convergence criteria (Max Force = 0.000450, RMS Force = 0.000300, Max Displacement = 0.001800 and RMS Displacement = 0.001200) and frequencies were calculated to ensure that there is no imaginary frequency.

Throughout the computational studies, only the *ortho*-Cl, *ortho*-H and *ortho*-CH_3 analogues, for a particular complex, were optimised. The studies were limited to these three analogues only due to time constraints and so that trends regarding the electron-

releasing/withdrawing properties of the substituent on a particular system could be recognised.

References

1. Y. Boutadla, D. L. Davies, S. A. Macgregor and A. I. Poblador-Bahamonde, *Dalton Trans.*, 2009, 5820.

2. A. J. Swarts, Mononuclear and Multinuclear Palladacycles as Catalyst Precursors, *M.Sc. Thesis*, Stellenbosch University, 2011.

3. N. Mungwe, The Synthesis of the Cyclometallated Palladium Complexes and their Applications in Olefin Oligomerisation and in Phenylacetylene Oligomerisation/ Polymerisation, *M.Sc. Thesis*, University of the Western Cape, 2007.

4. R. C. Bush and R. J. Angelici, *Inorg. Chem*., 1988, **27**, 681.

5. M. J. Frisch, G. W. Trucks, H. B. Schlegel, G. E. Scuseria, M. A. Robb, J. R. Cheeseman, J. A. Montgomery, Jr., T. Vreven, K. N. Kudin, J. C. Burant, J. M. Millam, S. S. Iyengar, J. Tomasi, V. Barone, B. Mennucci, M. Cossi, G. Scalmani, N. Rega, G. A. Petersson, H. Nakatsuji, M. Hada, M. Ehara, K. Toyota, R. Fukuda, J. Hasegawa, M. Ishida, T. Nakajima, Y. Honda, O. Kitao, H. Nakai, M. Klene, X. Li, J. E. Knox, H. P. Hratchian, J. B. Cross, C. Adamo, J. Jaramillo, R. Gomperts, R. E. Stratmann, O. Yazyev, A. J. Austin, R. Cammi, C. Pomelli, J. W. Ochterski, P. Y. Ayala, K. Morokuma, G. A. Voth, P. Salvador, J. J. Dannenberg, V. G. Zakrzewski, S. Dapprich, A. D. Daniels, M. C. Strain, O. Farkas, D. K. Malick, A. D. Rabuck, K. Raghavachari, J. B. Foresman, J. V. Ortiz, Q. Cui, A. G. Baboul, S. Clifford, J. Cioslowski, B. B. Stefanov, G. Liu, A. Liashenko, P. Piskorz, I. Komaromi, R. L.

Martin, D. J. Fox, T. Keith, M. A. Al-Laham, C. Y. Peng, A. Nanayakkara, M. Challacombe, P. M. W. Gill, B. Johnson, W. Chen, M.W. Wong, C. Gonzalez and J.A. Pople, *Gaussian 03, Revision B.05*, Gaussian, Inc., Pittsburgh PA, 2003.

6. M. J. Frisch, G. W. Trucks, H. B. Schlegel, G. E. Scuseria, M. A. Robb, J. R. Cheeseman, G. Scalmani, V. Barone, B. Mennucci, G. A. Petersson, H. Nakatsuji, M. Caricato, X. Li, H. P. Hratchian, A. F. Izmaylov, J. Bloino, G. Zheng, J. L. Sonnenberg, M. Hada, M. Ehara, K. Toyota, R. Fukuda, J. Hasegawa, M. Ishida, T. Nakajima, Y. Honda, O. Kitao, H. Nakai, T. Vreven, J. A. Montgomery, Jr., J. E. Peralta, F. Ogliaro, M. Bearpark, J. J. Heyd, E. Brothers, K. N. Kudin, V. N. Staroverov, R. Kobayashi, J. Normand, K. Raghavachari, A. Rendell, J. C. Burant, S. S. Iyengar, J. Tomasi, M. Cossi, N. Rega, J. M. Millam, M. Klene, J. E. Knox, J. B. Cross, V. Bakken, C. Adamo, J. Jaramillo, R. Gomperts, R. E. Stratmann, O. Yazyev, A. J. Austin, R. Cammi, C. Pomelli, J. W. Ochterski, R. L. Martin, K. Morokuma, V. G. Zakrzewski, G. A. Voth, P. Salvador, J. J. Dannenberg, S. Dapprich, A. D. Daniels, O. Farkas, J. B. Foresman, J. V. Ortiz, J. Cioslowski and D. J. Fox, *Gaussian 09, Revision A.02*, Gaussian, Inc., Wallingford CT, 2009.

7. C. T. Lee, W. T. Yang and R. G. Parr, *Phys. Rev. B*, 1988, **37**, 785.

8. A. D. J. Becke, *J. Chem. Phys*., 1993, **98**, 5648.

9. P. J. Hay and W. R. Wadt, *J. Chem. Phys*., 1985, **82**, 299.

Chapter 5

Conclusions and future work

The Schiff base condensation, C_{aryl}-H bond activation and the subsequent cleavage reactions, as described in this thesis, are suitable synthetic methodologies for the preparation of Schiff base imine ligands **L1 – L5**, μ-Cl binuclear cyclopalladated complexes **C1 – C5**, mononuclear, neutral, cyclopalladated complexes **C6 – C10** and mononuclear, neutral, non-cyclopalladated complexes **C11 – C15** respectively. The various analytical techniques that were employed to characterise the compounds were successful and complement each other well.

Single crystal X-ray diffraction analysis of neutral complexes **C9** and **C14** reveals that the geometry of the palladium atom is distorted square planar when a member of a cyclopalladated system and only slightly distorted square planar when a member of a non-cyclopalladated system.

The chloride abstraction reaction of the neutral cyclopalladated complexes **C6 – C10** and the non-cyclopalladated complexes **C11 – C15** using sodium tetrakis [3,5-*bis*(trifluoromethyl)phenyl] borate is a suitable synthetic methodology for the preparation of cyclopalladated cationic complexes **C16 – C25**, **C26 – C30** and the non-cyclopalladated cationic complex **C31**.

The higher basicity of pyridine as compared to acetonitrile results in a greater degree of electron delocalisation in the palladacycle when coordinated as a donor ligand. The formation of the non-cyclopalladated cationic complex **C31** reveals that trimethylphosphine is more basic than the imine nitrogen of the Schiff base ligand.

The calculated $\nu_{C=N}$ absorption bands, which corresponds to the imine, of the thermodynamically most stable conformations, are consistent with the experimentally obtained $\nu_{C=N}$ absorption bands for all compounds. The calculated five-membered chelate product, complex **C4**, which forms via C_{aryl}-H bond activation is thermodynamically more stable than the six-membered chelate product, complex **C4i**, which would form via C_{allyl}-H bond activation. The formation of non-cyclopalladated complexes bearing two trimethylphosphine ligands is energetically favourable and the formation of non-cyclopalladated complexes bearing two triphenylphosphine ligands is unfavourable. Predictive calculations indicate that triphenylphosphine is not basic enough to displace the imine nitrogen to generate non-cyclopalladated complexes.

Bond dissociation energy calculations confirm that the dissociation of pyridine, as compared to acetonitrile, requires more energy to create a vacant coordination site. This trend is directly affected by the relative basicities of the donor ligands. Calculations indicate that when pyridine is the donor ligand, the electron density on the metal centre is greater than in the case of acetonitrile, with the consequence of a weaker bond strength of the phosphine ligand.

The research that has been presented in this thesis shows promise for further expansion and development to enhance our knowledge regarding the behaviour of palladacycles. Firstly, the employment of analogous aniline starting materials for the Schiff-base condensation reaction could be used to modify the steric properties of the resulting palladium complexes. Alternatively, the properties of the prepared compounds can be modified by employing alternative phosphines for the cleavage of the μ-Cl binuclear cyclopalladated complexes.

The application of the palladacycle complexes that were prepared in this project as catalyst precursors for carbon-carbon bond formation reactions such as in the Heck- and/or

Suzuki-type reactions should be investigated. If the compounds display potential as catalyst precursors, then a theoretical study of the mechanism of the catalytic cycle can be investigated. Further employment of the compounds as catalyst precursors for ethylene oligomerisation reactions could also be studied.

Experimental and computational studies relating to the design and synthesis of the abovementioned palladium complexes and their subsequent performance as catalyst precursors for a variety of carbon-carbon bond formation and ethylene oligomerisation reactions will provide us with a finer understanding regarding the behaviour of palladacycles.